UAB
Universitat Autònoma de Barcelona

PROTEOMICS ANALYSIS OF MOLECULAR FEATURES IN DOWN SYNDROME, SPORADIC AND AUTOSOMAL DOMINANT ALZHEIMER'S DISEASE

Mitchell Martá-Ariza

Universitat Autònoma de Barcelona
School for Doctoral Studies, Doctoral Program in Neuroscience
Institut de Neurociències de la UAB

PROTEOMICS ANALYSIS OF MOLECULAR FEATURES IN DOWN SYNDROME, SPORADIC AND AUTOSOMAL DOMINANT ALZHEIMER'S DISEASE

By Mitchell Martá-Ariza

A dissertation submitted in partial fulfillment of the requirements for the Doctor of Philosophy degree.

Center for Cognitive Neurology, Department of Neurology, NYU Grossman School of Medicine.
Institut de Neurociències de la UAB.

Thesis Directors:

Dr. Thomas Wisniewski

Dr. Alberto Lleó Bisa

Dr. Juan Fortea Ormaechea

UAB Universitat Autònoma de Barcelona Escola de Doctorat INc Institut de Neurociències UAB NYU Grossman School of Medicine

1. ACKNOWLEDGMENTS

I want to express my most sincere gratitude to Dr. Thomas Wisniewski for opening the doors of his laboratory back in 2014 to a young Colombian with a fresh undergraduate degree and full of dreams, hopes and aspirations. Thank you, Tom, for introducing me to the fascinating field of neurodegeneration and Alzheimer's disease, and to a world-class, state-of-the-art laboratory in such a prestigious institution as NYU Grossman School of Medicine. I appreciate from the bottom of my heart all the opportunities I have been given, all the work we have done, the publications we have put out there, and all the conferences I have been able to attend. Beyond the science and the tremendous positive impact on my academic and professional career, I want to thank you for being so kind, generous, and patient, and for sharing your wisdom with me. I have the privilege for being part of your team, and it will always be a part of me.

I want to deeply thank Dr. Alberto Lleó and Dr. Juan Fortea for all your knowledge, advice, help and patience throughout this journey. I cannot express enough my gratitude for supporting me when I started my Doctoral studies, even when you did not know much about me, but believed in me and helped me take on a PhD. I am truly happy I had the chance to meet you and to be a mentee and collaborator in such wonderful research.

I want to thank to the School of Doctoral studies, the Coordination of the Doctoral Program in Neuroscience and the Institut de Neurociències at the Universitat Autònoma de Barcelona. Thanks to Dr. Alfredo Miñano Molina, Dr. Gemma Guillazo-Blanch, my review committee Dr. Arnaldo Parra Damas, Dr. Mar Hernández-Guillamon and Dr. Elisenda Sanz, and to Nuria Vergara Alarcón.

I would like to thank my thesis defense committee, Dr. Christopher William, Dr. Ann-Charlotte Granholm and Dr. Sònia Sirisi, for their support and insightful feedback, which further enhanced the quality of this thesis.

I cannot express in words all my gratitude for the Wisniewski lab, to all my colleagues that have become friends, advisors, mentors and have inscribed their names in my heart. *Ludo*, I could write a chapter describing how incredibly happy I

am to have met such an amazing person. You are exemplary as a friend, a colleague, a professional, and you are the kindest human being I have met. Thank you for your support, your friendship, and for being there even (especially) in the roughest times. *Dominique*, you are a wonderful scientist and a wonderful person. I admire your hard work, your compromise and professionalism, and the high standards imprinted in everything you do. Although I have known you for several years now, to this day I am still impressed by how you are able to achieve so much, so quickly and efficiently. I wish I had at least half of your skill. *Fernando*, you are the first person from this group that I met, and I cannot thank you enough for seeing a future and potential on me —even if it was through a skype meeting. You were key to me being here today, and I appreciate all the knowledge and wisdom you have shared with me over the years. Thank you for your kindness and for lending a hand as I got accustomed to this competitive environment and to this city that I love. *Eleanor,* I want to thank you for being my mentor as well, from the early days after I arrived at Tom's lab when we shared that secluded space where the LCM microscope was located, back when you were giving rise to the powerful approach that now shaped my PhD work. You are an exemplary researcher and an incredible person, and I am very happy I had the chance to work closely with you.

I would like to thank all the core facilities at NYU Grossman School of Medicine, including the Proteomics Laboratory, the Experimental Pathology Research Laboratory, and the Center for Biospecimen Research and Development, for all their help, advice, and technologies. I particularly want to thank *Beatrix "Trixi" Ueberheide* and *Evgeny Kanshin* for their vast help in proteomics—this thesis came to life thanks to you! I appreciate your advice and this fruitful collaboration that has produced (and will produce even more) wonderful data and has helped close the gap in our knowledge about Alzheimer's and neurodegeneration.

I want to thank all the wonderful people I had the opportunity to meet at Dr. Wisniewski's lab and who are now part of my life: *Frances*, you were a staple of the Wisniewski lab, and I deeply admire your values, your hard work, and commitment. Thank you for being so nice to me. *Geoffrey*, thank you for your friendship and for helping me when I had just started this adventure called "PhD." *Manon*, thank you for sharing your expertise with me, for your advice, for all the lessons, and for helping

me without hesitation. *Nina*, thank you for being a great lab partner, an amazing friend, and for all the good times we have shared. *Henrieta*, you are an incredible scientist that has achieved so much, and your awesomeness is just topped by your kindness. I also thank all your team, former and current members, for all their help, support, and laughs throughout all these years. I extend my sincere gratitude to all the past and current members of the Division of Cognitive Neurology.

From the bottom of my heart, I want to thank my beautiful wife, *Jenny*. I would be lost without you, and I would have given up so many times already. You are my cornerstone. You give meaning to every one of my days. There are no words and not enough pages to thank you for everything you mean to me and for everything you have done in my life. I love you, and I deeply admire you.

To all my family, I love you with all my heart! Doy gracias infinitas por la familia que me ha tocado, doy gracias a Dios por cada uno de ustedes. *Mamá* y *Papá*, yo no sería el hombre que soy de no ser por ustedes, y no estaría aquí si no fuera por la inconmesurable dedicación y el amor incondicional que me han dado. No tengo forma como agradecerles todo lo que han hecho por mí. Ustedes son un ejemplo de Fortaleza, amor, esfuerzo, nobleza, humildad y constante entrega. Espero seguir haciéndolos sentir muy orgullosos. Los amo muchísimo.

Haku, you are the purest creature that could ever exist. You have been my loyal companion through the good and bad days. Thank you for your unconditional love.

Table of Contents

2. SUMMARY

Down syndrome (DS) is the most common chromosomal abnormality, resulting from the triplication of chromosome 21 (Hsa21). Advances in medical care have significantly extended life expectancy in this population, but Alzheimer's disease (AD) has emerged as the leading cause of mortality, affecting over 90% of individuals with DS by the seventh decade of life. The strong association between DS and AD is driven by the triplication of the amyloid precursor protein (*APP*) gene, resulting in the overproduction of amyloid-β (Aβ) and early formation of amyloid plaques. By age 40, nearly all individuals with DS exhibit AD pathological hallmarks, including Aβ deposits and neurofibrillary tangles composed of hyperphosphorylated Tau. These neuropathological features closely resemble those of early-onset (EOAD), late-onset (LOAD), and autosomal dominant forms of AD (ADAD), although DS is also characterized by distinct neurodevelopmental and immune alterations that may influence disease progression.

DS has played a central role in shaping the amyloid hypothesis of AD, beginning with early studies that identified Aβ in DS brain vasculature and demonstrated its homology to Aβ found in LOAD. Subsequent identification of *APP* mutations on Hsa21 causing ADAD further established a shared pathogenic mechanism of Aβ altered homeostasis across AD subtypes. Despite these shared features, DSAD also presents unique biological characteristics including differences in brain development, immune function, and biochemical profiles that raise questions about the extent to which underlying mechanisms in DS align with other forms of AD. Given the predictability of symptom onset in DS, similar to that of ADAD, DS offers a valuable model for studying AD pathogenesis and progression.

Proteomics is a powerful tool for advancing our understanding of AD biology, offering direct insight into changes in protein abundance and interactions across tissues and disease stages. While proteomic studies of LOAD and ADAD have revealed widespread alterations in pathways beyond Aβ and Tau, including immune responses, synaptic function, and mitochondrial metabolism, fewer studies have applied this approach to DSAD. Integrating proteomic data from brain tissue and

cerebrospinal fluid allows for a comprehensive analysis of disease-relevant processes and molecular signatures in DS, EOAD, LOAD, and ADAD.

The brain proteomics study characterized the Aβ plaque and surrounding non-plaque tissue proteomes in individuals with DS, EOAD, LOAD and age-matched controls using unbiased localized proteomics. Across all groups, a core set of plaque-associated proteins was identified, with overlapping protein networks related to APP metabolism, immune responses, and lysosomal function. Comparative analysis revealed that DS has a strong similarity to EOAD and LOAD in plaque composition but more divergent patterns in non-plaque tissue. DS non-plaque proteome exhibited specific alterations in extracellular matrix and chromatin-associated proteins, pointing to unique molecular differences between DS and AD subtypes.

We analyzed cerebrospinal fluid (CSF) proteomics from a large cohort of individuals with DS to investigate the progression of AD neuropathology and to compare proteomic alterations with those observed in LOAD and ADAD. While many protein changes were shared across groups, individuals with DS exhibited earlier and more pronounced alterations in immune-related proteins, extracellular matrix pathways, and markers of blood–brain barrier dysfunction. These changes emerged prior to detectable Aβ or tau pathology, suggesting they may be linked to trisomy 21 and contribute to AD risk in DS. Additionally, DS cases showed earlier signs of axonal and white matter pathology and cerebral amyloid angiopathy (CAA) compared to ADAD. These findings highlight distinct molecular features of AD in DS with implications for early intervention and tailored treatment strategies.

The studies presented in this thesis demonstrate that while AD in Down syndrome shares core molecular features with other forms of AD, it also exhibits distinct proteomic alterations linked to the genetic and developmental context of trisomy 21. The findings underscore the value of DS for studying early disease mechanisms and highlight the utility of proteomics for identifying molecular signatures of neurodegeneration. This thesis advances our understanding of shared and divergent pathways across AD subtypes, providing a framework for future efforts to identify stage-specific biomarkers and targeted therapies for AD.

3. LIST OF ABBREVIATIONS

ABCA1	ATP-binding cassette transporter A1
ABCA7	ATP-binding cassette transporter A7
ACH	Amyloid cascade hypothesis
ACh	Acetylcholine
AChE	Acetylcholinesterase
ACTC–DS	Alzheimer's Clinical Trials Consortium–Down Syndrome
AD	Alzheimer's disease
ADAD	Autosomal dominant Alzheimer's disease
ADNC	AD neuropathological changes
AICD	APP intracellular domain
AP-MS	Affinity purification-mass spectrometry
APOE	Apolipoprotein E
APP	Amyloid precursor protein
Aβ	Amyloid-β
BACE1	β site cleaving enzyme 1
BACE2	β secretase 2
BIN1	Bridging integrator 1
CA1 and CA2	Cornu ammonis 1 and 2
CAA	Cerebral amyloid angiopathy
CERAD	The consortium to establish a registry for Alzheimer's disease
CHD	Congenital heart disease
CHI3L1	Chitinase-3 like-protein-1
CNP	2′,3′-cyclic nucleotide phosphodiesterase
CNS	Central nervous system
CREB	cAMP response element-binding protein
CSF	Cerebrospinal fluid
CTFα	C-terminal APP fragment of 83 amino acids
CTFβ	C-terminal APP fragment of 99 amino acids
DAM	Disease-associated microglia
DS	Down syndrome

DSAD	Down syndrome-associated Alzheimer's disease
DSCR	Down syndrome critical region
DYRK1A	Dual-specificity tyrosine phosphorylated and regulated kinase 1A
ECM	Extra-cellular matrix
EOAD	Early-onset Alzheimer's disease
FFPE	Formalin-fixed and Paraffin-embedded
GFAP	Glial fibrillary acidic protein
GSK3β	Glycogen synthase kinase 3 beta
GWAS	Genome wide association studies
HpSp	Hippocampal sparing
Hsa21	Human chromosome 21
IL-1β	Interleukin-1 beta
LC-MS	Liquid Chromatography-Mass Spectrometry
lncRNA	Long non-coding RNA
LOAD	Late-onset Alzheimer's disease
LP	Limbic predominant
LTD	Long-term depression
LTP	Long-term potentiation
MAP	Microtubule associated protein
MBP	Myelin basic protein
MCI	Mild cognitive impairment
mGluR5	Metabotropic glutamate receptor 5
miRNA	Micro RNA
MOG	Myelin oligodendrocyte glycoprotein
MTBR	Microtubule-binding pseudo-repeat
NCL	Neuronal ceroid lipofuscinosis
ncRNA	Non-coding RNA
NfL	Neurofilament light
NFT	Neurofibrillary tangle
NIA-AA	National Institute on Aging and Alzheimer's Association
NLR	NOD-like receptor
NOD	Nucleotide-binding oligomerization domain

PET	Positron emission tomography
PHF	Paired helical filaments
PICALM	Phosphatidylinositol binding clathrin assembly protein
PLP	Proteolipid protein
PrP^C	Prion protein C
PSEN1	Presenilin 1
PSEN2	Presenilin 2
pT217	Tau phosphorylated at threonine 217
pTau	Phosphorylated Tau protein
PVALB	Parvalbumin
RAGE	Receptor for advanced glycation end products
RNAseq	RNA sequencing
ROS	Reactive oxygen species
rpAD	Rapidly progressive Alzheimer's disease
sAPPα	Soluble APP α
sAPPβ	soluble APP β
SMOC1	SPARC-related modular calcium-binding protein 1
SNP	Single nucleotide polymorphism
SOD1	Superoxide dismutase 1
SORL1	Sortilin related receptor L
SYNJ1	Synaptojanin 1
TLR	Toll-like receptor
TNFα	Tumor necrosis factor-alpha
TREM2	Triggering receptor expressed on myeloid cells 2
WES	Whole Exome Sequencing
WGS	Whole Genome Sequencing

4. INTRODUCTION

4.1. Alzheimer's Disease

4.1.1. Brief History of Alzheimer's Disease Research

The first reference to the neurodegenerative disorder now known as Alzheimer's disease was made approximately 118 years ago, when Alöis Alzheimer described the cognitive symptoms followed by *post-mortem* findings of a 51-year-old woman at the Frankfurt am Main asylum in Germany[1]. Briefly, Alzheimer observed symptoms including confusion, disorientation, delusions, and rapid memory loss. After her death, neuropathological examination of her brain revealed widespread atrophy. Bielschowsky's silver staining technique showed what he described as disintegrating cells and tangles of fibrils where neurons were located, along with "minute miliary foci distributed in the cortex", now recognized as amyloid plaques[1].

A few years later, Emil Kraepelin coined the term "Alzheimer's disease" (AD) in his *Handbook of Psychiatry*, crediting the work of Alöis Alzheimer[2]. In 1966 and 1968, Gary Blessed, Bernard Tomlinson, and Martin Roth published foundational studies that correlated clinical features of the disease, evaluated using standardized cognitive tests, with cortical senile plaque counts[3,4]. A pivotal moment came in 1976 when Robert Katzman published an editorial in *Archives of Neurology*, proposing that AD was the fourth leading cause of death among the elderly. This drew increased attention from the National Institutes of Health in the U.S. and the broader public[2,5].

The 1960s and 1970s also saw significant advances in the biochemical characterization of AD neuropathology. Researchers used biochemical fractionation and electron microscopy to isolate and describe the disease's hallmark features in detail. Pioneers such as Robert Terry, Michael Kidd, Khalid Iqbal, and Henryk Wisniewski provided critical insights into the structure and distribution of senile plaques and paired helical filaments[6-8]. In the following decade, efforts to isolate the

proteins involved in AD pathology paved the way for modern molecular research. George Glenner and Caine Wong isolated a 4.2 kDa protein from human brain tissues with severe cerebrovascular amyloidosis[9]. This amyloid fibril-derived peptide was proposed as both a diagnostic tool for the development of monoclonal antibodies and a path to understanding AD neuropathology. Later, in 1985, Colin Masters and colleagues purified a 4 kDa polypeptide from amyloid plaque cores in the brains of individuals with AD and Down syndrome, naming it the *A4* peptide[10]. A groundbreaking discovery took place in 1987 with the identification of the peptide *A4*, later known as amyloid-β (Aβ), as the major subunit of the amyloid fibrils involved in AD in Down syndrome and non-DS[11]. Four independent groups put DS in the spotlight of AD research by localizing the *APP* gene sequence in the proximal portion of the long arm of chromosome 21[11]. Subsequent studies elucidated the metabolic pathways involved in the production of Aβ peptide (reviewed by Karran and De Strooper[12]).

These discoveries laid the groundwork for the development of the “amyloid cascade hypothesis” (ACH), which placed Aβ at the center of AD pathogenesis. Most notably, John Hardy and Gerald Higgins proposed in 1992 that Aβ accumulation was the primary cause of the disease, with neurofibrillary tangles, cell loss, vascular damage, and dementia occurring as downstream effects[13]. While the ACH is supported by extensive human genetic evidence (as discussed in section **4.1.4.1.**), several observations have led some researchers to challenge and reassess the hypothesis. These include failures of many anti-Aβ immunotherapies, the presence of plaques in cognitively normal individuals, and a weak correlation between Aβ burden and cognitive decline[14,15]. However, the recent success and FDA and EMA approval of two anti-Aβ therapies (Lecanemab and Donanemab) have greatly strengthened the ACH[16,17]. Furthermore, post-mortem studies from rare cases of partial trisomy of chromosome 21 (explained in **section 4.2.2**) without *APP* overexpression support the association between increased *APP* gene dosage and AD neuropathology[11].

4.1.2. Clinical Features of Alzheimer's Disease

4.1.2.1. AD continuum and clinical manifestation of AD dementia

Dementia caused by AD is considerably heterogeneous in the development and progression of symptoms as well as the clinical decline in people with AD[18]. Despite this variability, the National Institute on Aging and Alzheimer's Association (NIA-AA) recognizes certain features of probable AD dementia. The most common is the *amnestic presentation*, characterized by impaired learning and difficulty recalling recently acquired information[19]. Less typical presentations of the disease include non-amnestic AD, characterized by deficits in language, visuospatial skills and executive function[18,19]. AD follows a continuum that begins with the appearance of disease-specific biomarkers in asymptomatic individuals and progresses to structural and functional brain changes, eventually leading to profound impairments in cognition and daily function[20,21]. The duration of each stage within this continuum varies and is influenced by several factors, including age, sex, and genetic predispositions[22].

In 2018, the NIA-AA research framework introduced a numerical clinical staging system to classify individuals within the pathophysiological phase of the AD continuum[23]. This framework, largely maintained in the recent revision, incorporates advances in fluid and imaging biomarkers together with assessments of cognitive and psychological function. The earliest phase of the continuum is now defined as stage 0, which includes individuals with genetically determined AD, such as autosomal dominant AD or Down syndrome-associated AD, who are clinically asymptomatic and biomarker negative (**Table 1**)[21].

The early stages of the AD continuum are characterized by an asymptomatic phase commonly referred as *preclinical AD*, often spanning decades before a clinical diagnosis is possible[24]. As cognitive decline begins to emerge but does not yet significantly interfere with everyday functioning, individuals enter a stage known as prodromal AD[25,26]. People in the prodromal stage demonstrate lower-than-expected performance in one or more cognitive domains relative to their age and education

yet maintain independence in daily activities[25]. The dementia stages of the continuum involve greater cognitive and functional impairment, ultimately resulting in complete dependence for basic tasks[21]. Importantly, in people with Down syndrome (DS), baseline intellectual disability may limit independence even at stage 0, so decline from individual baseline is a more appropriate indicator of disease progression[21].

The numerical staging framework for AD progression applies broadly to the general population. In individuals with DS, the staging follows a similar conceptual model but may manifest at different ages. Plasma amyloid changes appear early, followed by alterations in memory and biomarkers of tauopathy and neurodegeneration, including NfL. These are later accompanied by impairments in executive and visuomotor function, and eventually by changes in neuroinflammatory markers[27]. Dementia in DS arises within a context of altered cognitive abilities, requiring assessment of baseline function and developmental patterns[27,28]. Structural MRI studies show reduced volumes in the prefrontal cortex, hippocampus and cerebellum before AD onset[28]. Cognitive batteries such as the Arizona Cognitive Test Battery and the Cambridge Cognition offer critical insight into AD progression in individuals with DS, and inform interventions aimed at modifying developmental trajectories across the lifespan and in clinical trials[21,28-31]. Consideration must also be given to the cognitive variability among individuals with DS, which affects test outcomes and the suitability of these assessments across different ages and stages of AD.

4.1.2.2. Diagnosis of AD and Alzheimer's dementia

Alzheimer's disease is a biological entity, while dementia due to AD represents its clinical manifestation. Therefore, diagnosis integrates both biological and clinical assessments. Clinically, diagnosis relies on assessing cognitive impairment through structured interviews and neuropsychological evaluations[19]. However, as emphasized by the "Revised criteria for diagnosis and staging of AD" in 2024, AD is also a biological entity that must be defined independently of clinical symptoms[21]. The diagnosis of probable Alzheimer's disease in living patients relies on the use of biomarkers, which are now categorized according to the 2024 NIA-AA criteria into three broad groups: core biomarkers of AD neuropathologic change (ADNPC), non-

specific biomarkers involved in AD pathogenesis but also shared with other brain diseases, and biomarkers of common non-AD copathologies. Core biomarkers include the A (amyloid beta) and T (tau) categories, which have been further refined into subgroups based on timing and type of measurement, with fluid and imaging markers no longer assumed to be interchangeable. Non-core biomarkers include those of neurodegeneration (N), inflammation/immune mechanisms (I), vascular brain injury (V), and alpha-synucleinopathy (S), reflecting the frequent presence of copathologies in older adults[21].

Among these, the core biomarkers, including amyloid positron emission tomography (PET), can identify intermediate to high levels of AD neuropathologic change with substantial confidence in symptomatic individuals, in alignment with neuropathologic assessments[21,32]. Although PET is less sensitive than neuropathologic examination and PET-based staging is not fully equivalent to autopsy-based staging, PET has clear prognostic value[21]. However, it is important to note that amyloid accumulation can also be observed in cognitively normal individuals who may never develop dementia, a factor that should be taken into account when interpreting PET results in asymptomatic populations[28,30,33,34].

Biomarker-based approaches have greatly advanced the diagnosis of AD by enabling detection of its biological signature *in vivo*. Although standardization of assays and further refinement for preclinical detection are still needed, current methods are reliable for differential diagnosis at the prodromal AD stage and continue to improve in sensitivity[21]. *Post-mortem* confirmation of amyloid plaques and neurofibrillary tangles remains the traditional gold standard[35], but biomarker-based criteria now provide a robust framework for diagnosis and staging across the disease continuum.

4.1.3. Neuropathological Features of AD

The hallmark neuropathological features of AD include the extracellular accumulation of Aβ peptide in amyloid plaques, such as diffuse and neuritic (also called *senile*) plaques, and the intraneuronal accumulation of hyperphosphorylated Tau protein (pTau) in NFTs (**Figure 1**)[35,36]. In addition to Aβ plaques and NFTs, a distinct lesion known as cerebral amyloid angiopathy (CAA) is commonly observed.

CAA is characterized by the deposition of Aβ peptides in the walls of blood vessels within the leptomeninges and cerebral cortex[35]. While these vascular Aβ deposits may not initially disrupt vascular function, severe involvement can lead to spontaneous vessel rupture, resulting in cerebral hemorrhages that may be fatal[35]. Other lesions include granulovacuolar degeneration, particularly in pyramidal neurons of the cornu ammonis (CA1 and CA2) regions of the hippocampus[35], and the less frequently observed Hirano bodies, which are rodlike eosinophilic neuronal inclusions[35].

Table 1. *NIA-AA Numerical Clinical Staging for People on the AD Continuum.*

Stage 0. Asymptomatic, deterministic gene*
Biomarkers are within normal range and there is no evidence of clinical symptoms. Genetically determined, including ADAD and DSAD. These individuals have the disease from birth, prior to the onset of brain physiological or clinical changes.
Stage 1. Asymptomatic, biomarker evidence only
Cognitive tests are within normal / expected range. There is no evidence of recent cognitive decline or new symptoms.
Stage 2. Transitional decline: mild detectable change, minimal impact on daily function
Performance remains within expected range. Subtle decline from baseline over the past 1 to 3 years and persisted for at least 6 months. Cognitive testing shows mild decline, accompanied by recent changes in mood, anxiety or motivation not explained by life events. Daily functioning remains fully independent with no or minimal impact.
Stage 3. Cognitive impairment with early functional impact
Objective cognitive tests performance is within impaired or abnormal range. Evidence of decline from baseline, documented by an observer or by change of longitudinal cognitive testing. Individual performs daily activities independently, but cognitive difficulties are detectable while performing tasks.
Stage 4. Dementia with mild functional impairment
Progressive cognitive and mild functional impairment on instrumental daily activities, while retaining independence on basic tasks.
Stage 5. Dementia with moderate functional impairment
Progressive cognitive and moderate functional impairment on basic daily activities, requiring assistance.
Stage 6. Dementia with severe functional impairment
Progressive cognitive and functional impairment. Individual is completely dependent for basic daily activities.

** People with Down syndrome may not be fully independent even at stage 0 due to the underlying intellectual disability. Therefore, decline in functional independence from a baseline would be a more appropriate stage indicator. Table adapted from Jack Jr. and colleagues[21].*

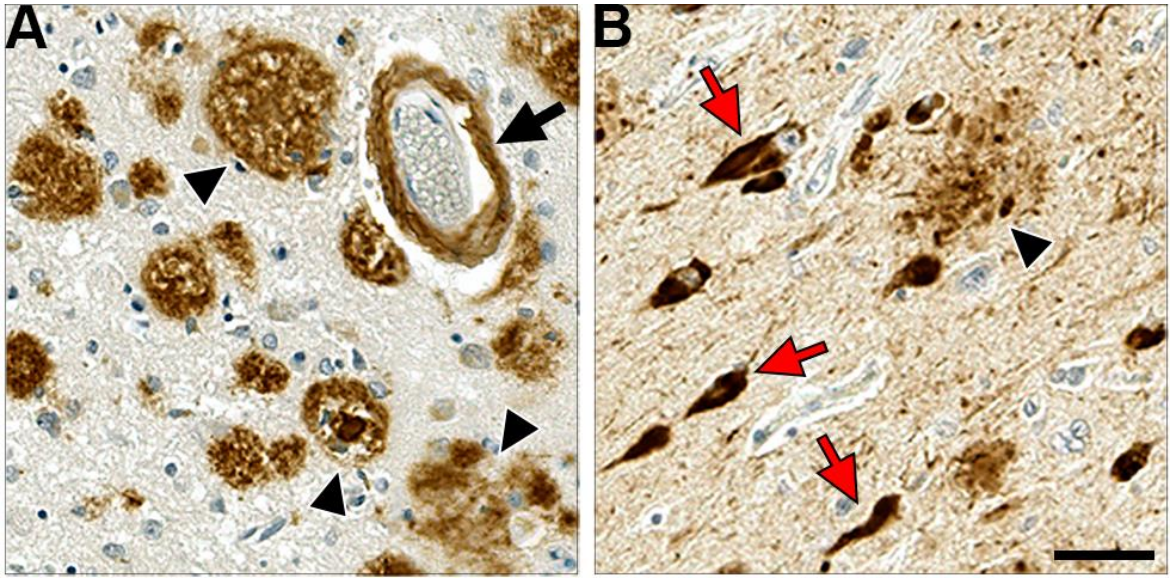

Figure 1. Neuropathological hallmarks of AD. A. *Immunostaining for Aβ peptide using anti-Aβ 4G8 on a DSAD case. Arrowheads indicate Aβ plaques (diffuse, classic cored, and dense "cotton-wool") and the arrow shows vascular Aβ deposition.* ***B.*** *Immunostaining for phosphorylated Tau using PHF-1 on a DSAD case. Red arrows show NFTs and the black arrowhead depicts a neuritic plaque. Scale bar = 50 µm. Unpublished images by Martá-Ariza.*

4.1.3.1. Amyloid-β pathology

The type I transmembrane amyloid precursor protein (APP), encoded by the *APP* gene on human chromosome 21, generates the Aβ peptide through sequential proteolytic cleavages[37]. APP is predominantly expressed by neurons, and previous studies suggest that it plays a role in regulating synaptic transmission and plasticity[38-40]. The most studied APP processing mechanisms occur via two distinct pathways known as *non-amyloidogenic* and *amyloidogenic* (**Figure 2**)[41,42]. However, most recently the η-secretase pathway has been described[43].

In the non-amyloidogenic pathway, APP is first cleaved within the Aβ domain by α-secretase, resulting in the release of the soluble APP ectodomain sAPPα into the extracellular space[44,45]. The remaining membrane-bound C-terminal fragment of 83 amino acids (C83 or CTFα) is subsequently cleaved by γ-secretase, producing a small extracellular fragment known as p3 and releasing the APP intracellular domain (AICD) into the cytoplasm[44,45].

In contrast, the amyloidogenic pathway begins with cleavage by β-secretase, which generates a smaller soluble ectodomain, sAPPβ, released extracellularly[44,45]. This processing leaves a membrane-associated C-terminal fragment of 99 amino acids

(CTFβ), which is subsequently cleaved by γ-secretase, resulting in the release of the Aβ peptide into the extracellular space and the AICD into the cytoplasm [44,45]. The soluble Aβ can undergo a conformational transition into β-sheet–rich structures, which aggregate into soluble oligomers and subsequently precipitate to form amyloid plaques[46].

A variety of Aβ peptides are produced following γ-secretase cleavage in the amyloidogenic pathway. Among these, $A\beta_{1-42}$ is the most commonly found in plaques, while the more soluble $A\beta_{1-40}$ is primarily associated with the cerebral vasculature[47].

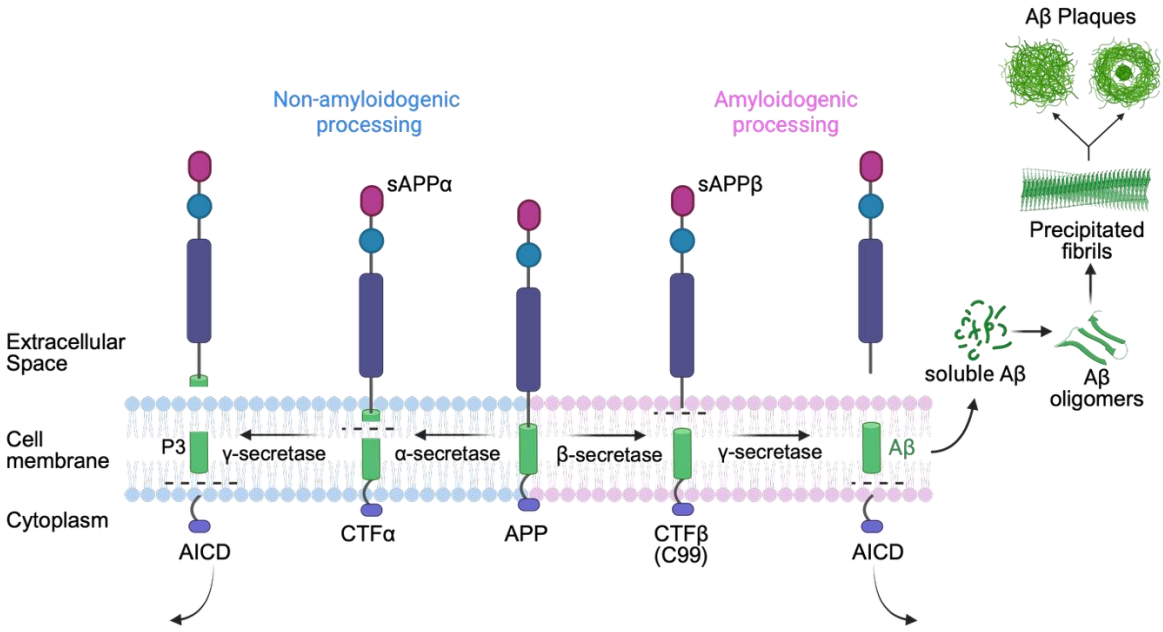

Figure 2. APP Processing Pathways. *The amyloid precursor protein (APP) can be processed via two main pathways. In the non-amyloidogenic pathway, APP is initially cleaved by α-secretase, generating a soluble extracellular fragment (sAPPα) and a C-terminal fragment of 83 amino acids (CTFα) bound to the membrane. CTFα is subsequently cleaved by γ-secretase, producing a p3 fragment and the APP intracellular domain (AICD). In the amyloidogenic pathway, β-secretase cleaves APP to release sAPPβ and generate a 99-amino-acid C-terminal fragment (CTFβ), posteriorly cleaved by γ-secretase to release AICD and the Aβ peptide. Aβ may undergo a conformational shift to β-sheet–rich oligomers that aggregate into fibrils and deposit as amyloid plaques. Figure created with BioRender, adapted from Azargoonjahromi, 2024[44].*

In addition to the amyloidogenic and non-amyloidogenic pathways, APP can also undergo η-secretase processing. This cleavage occurs N-terminal to the β- and α-

secretase sites, generating a C-terminal fragment (CTF-η) and a soluble ectodomain (sAPP-η). CTF-η can then be further processed by BACE1 or ADAM10 to release soluble Aη-β or Aη-α peptides, respectively, while sAPP-α/β may also serve as precursors for Aη generation. Unlike Aβ, these peptides do not extend to the γ-secretase site, making them distinct from previously described N-terminally extended Aβ variants. MT5-MMP has been identified as one enzyme with η-secretase activity, though other proteases may contribute. Importantly, Aη processing occurs under physiological conditions in mouse and human brains as well as CSF, and Aη-α in particular has been shown to impair synaptic plasticity, suggesting that dysregulation of this pathway may contribute to AD pathology[43].

4.1.3.1.1 Morphology of Aβ plaques

Aβ deposits have been classified based on their morphological and physicochemical properties as revealed by histochemical methods[48]. These classification efforts have helped distinguish early from advanced pathological stages, map regional and temporal plaque distribution, and enhance our understanding of disease pathogenesis.

A common distinction in Aβ extracellular aggregates is between *diffuse* and *fibrillar* deposits. Diffuse plaques appear in immunostaining as loosely organized structures with irregular, poorly defined borders. They lack a dense core and associated degenerating neurites and are typically negative for Congo red and Thioflavin S, dyes that bind to β-sheet structures[49,50]. Variants such as *cotton-wool* and *lake-like* plaques have also been described[48,51,52]. Diffuse plaques are often found in the neocortex of cognitively normal elderly individuals and may represent early stages in the maturation of more structured Aβ deposits[53-57]. Diffuse plaques are frequently observed in individuals with DS, even observed before the age of 20 (see **section 4.2.2.1**)[58,59].

In contrast, fibrillar plaques are positive for Congo red and thioflavin S, in addition to immunostaining with anti-Aβ antibodies[48,60]. Terms such as *stellate*, *primitive*, *classic (dense-core)*, and *compact* plaques were introduced to distinguish these β-sheet-rich structures from diffuse plaques[61]. Further classifications differentiate between *compact* and *cored* plaques[56,62]. Notably, *neuritic plaques*, a subset of

fibrillar plaques containing dystrophic neurites and glial elements, correlate with clinical severity in AD[63].

More recently, a plaque subtype called *coarse-grained plaques* has been described in both early- and late-onset AD (EOAD and LOAD), though more frequently in EOAD[64]. These plaques are prominent in the frontal and parietal cortices and show strong immunoreactivity for markers of neuroinflammation and vascular pathology[64,65]. A related subtype, termed *bird-nest plaques*, has been identified in Down syndrome brains with AD pathology[66]. These findings point to distinct clinicopathological features among Aβ plaque types and contribute to the understanding of AD mechanisms.

4.1.3.1.2 Cerebral amyloid angiopathy

Cerebral amyloid angiopathy (CAA) is defined by the deposition of Aβ in the brain vasculature. While commonly co-occurring with AD pathology, CAA can also appear independently[67-70]. This vascular involvement is frequently associated with cortical microinfarcts and recurrent hemorrhages, and increased CAA severity is linked to the progression of AD clinical symptoms[70,71]. Aβ deposits in CAA typically form a spiral pattern with a patchy distribution, often located adventitial rather than medially in larger arterioles, and predominantly composed of the more soluble $A\beta_{1-40}$[67].

CAA is classified into two types: *Type 1* involves Aβ deposition in cortical capillaries, whereas *Type 2* lacks capillary involvement[67,72]. CAA progression follows a distinct spatial pattern from parenchymal Aβ pathology. Initially, Aβ accumulates in the leptomeningeal and neocortical vessels, then spreading to allocortical and midbrain vessels, and finally reaching the basal ganglia, thalamus, and lower brainstem[73].

In DS, the presence of CAA is nearly ubiquitous in adulthood, consistent with APP triplication. While rare before age 40, it becomes a prominent feature in older individuals with DS (see **section 4.2.2.1**)[74]. In DS, a high frequency of Type 1 involvement is observed, often extending beyond the neocortex to cerebellum, basal ganglia, midbrain, and thalamus. Cerebellar CAA is as frequent and severe as neocortical CAA, a pattern more pronounced than in sporadic cases. Despite this widespread and severe vascular pathology, hemorrhagic complications such as

lobar intracerebral hemorrhage are relatively infrequent, suggesting additional modifying mechanisms[75]. Furthermore, CAA in DS has been associated with distinctive glial iron pathology and vascular calcification, likely reflecting chronic hypoperfusion. Collectively, these features indicate that while the distribution of CAA in DS resembles the stereotyped progression seen in sporadic disease, its severity and pattern are unique, with implications for both pathophysiology and treatment response[75].

4.1.3.2. Tau pathology

Tau is a microtubule associated protein (MAP) primarily expressed in neurons. Tau is encoded by the *MAPT* gene, which generates a total of 6 Tau isoforms because of alternate splicing of exons 2, 3 and 10[76,77]. Under physiological conditions, it plays essential roles in axonal transport and growth, microtubule stabilization, and neuronal polarization, among other functions[78,79]. Tau undergoes several post-translational modifications, including hyperphosphorylation, acetylation, N-glycosylation and truncation[78,80]. Among these, hyperphosphorylation is considered a major factor in the formation of pathological Tau, which can be detected in the brain decades before the onset of clinical symptoms through the presence of phosphorylated pre-tangles and neuropil threads[80-83].

In AD, Tau pathology is primarily observed in the soma, dystrophic axons and dendrites, and in association with neuritic plaques (**Figure 1B**)[62,80]. The dystrophic neurites are abnormally distended neuron cell processes displaying the paired helical filaments (PHF) morphology[55]. The dystrophic neurites contain neurofilament proteins, lysosomal bodies and other vesicles, suggesting the alteration of cytoskeleton and the transport and protein degradation machineries, which contribute to the AD neurodegenerative process[60].

Recent advances in cryo-EM have shown that the molecular conformation of Tau filaments is conserved across different etiological forms of AD[84,85]. Specifically, PHFs and straight filaments in ADAD, late-onset AD (LOAD), and Down syndrome-associated AD (DSAD) share an identical fold, distinguishing them from the structurally distinct Tau folds described in primary tauopathies such as chronic traumatic encephalopathy, subacute sclerosing panencephalitis, or amyotrophic

lateral sclerosis/parkinsonism-dementia complex[85]. This conserved conformation is also present in DS, indicating that Aβ-driven mechanisms, rather than disease-specific environments, underlie the structural features of tau filaments[84,85].

4.1.3.3. Distribution patterns of Aβ and Tau pathologies

The neuropathological hallmarks of AD follow a relatively predictable spatial and temporal distribution across the brain, enabling both the pathological diagnosis of AD and staging of the disease[57,86,87]. Thal and colleagues described the progression of Aβ plaque pathology in five phases (**Figure 3A**). In Phase 1, early deposits, primarily diffuse plaques, are restricted to the neocortex. Phase 2 involves the extension of Aβ plaques to limbic regions, including the entorhinal cortex, subiculum, amygdala, and cingulate gyrus. By Phase 3, plaque pathology reaches subcortical structures such as the basal ganglia and thalamus. In Phase 4, additional regions including the midbrain, pons, and medulla oblongata become involved. Finally, Phase 5 is defined by Aβ accumulation in the cerebellar cortex[57,88].

The staging of NFT pathology was first proposed by Braak and colleagues in 1991, based on Gallyas silver staining of 100 µm thick sections[86]. The staging method was later revised in 2006 to accommodate conventionally thin sections (5–15 µm), suitable for immunohistochemistry using the AT8 antibody, which detects Tau hyperphosphorylated at serine 202 and threonine 205[81,89]. According to this framework, pTau pathology begins in the transentorhinal region of the hippocampal formation (Stage I) and then extends to the subiculum within the pyramidal cell layer (Stage II). These initial stages are referred to as the transentorhinal stages. As the disease progresses, NFT accumulation spreads to the CA1 region of the hippocampus in Stage III, and by Stage IV, it involves the full hippocampal pyramidal layer, including CA1 to CA4, and the adjacent inferior temporal cortex. These two stages are known as the limbic stages, reflecting the profound impact of Tau pathology on hippocampal circuitry. In the final stages, Tau pathology reaches the isocortex, with Stage V involving the peristriate area of the occipital cortex, and Stage VI showing intraneuronal aggregates in the striate cortex. These two stages are known as the “isocortical stages” (**Figure 3B**). Braak staging shows a strong

correlation with clinical symptoms: stages I–II are generally associated with a preclinical or asymptomatic phase, while stages V–VI are strongly linked to cognitive impairment and clinical dementia[81,86,88].

Neuritic plaques offer insight into the interaction between Aβ and Tau pathologies. These deposits encapsulate lysosomes, axonally transported proteins, such as APP and BACE1, dystrophic neurites, and various aggregated Tau species[48,88]. The consortium to establish a registry for Alzheimer's disease (CERAD) developed a staging framework for neuritic plaques staging based on Thioflavin S or silver staining methods to quantify the density in multiple neocortical areas[63].

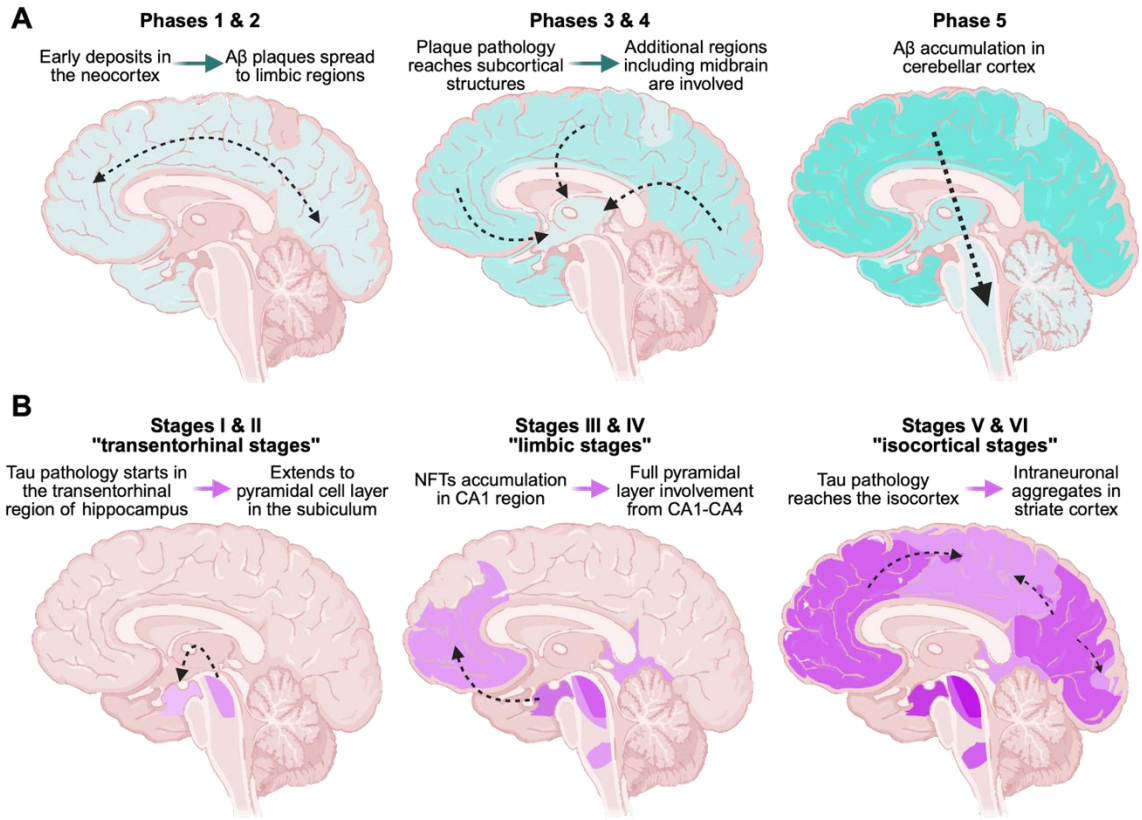

Figure 3.Temporal and anatomical distribution of Aβ and Tau pathology. *Accumulation of Aβ and pTau misfolded proteins follows a characteristic predictable pattern.* ***A.*** *Aβ spread progression based on Thal phases.* ***B.*** *Tau pathology staging proposed by Braak and colleagues. Figure created with BioRender, adapted from Jucker & Walker, 2011[90].*

4.1.3.3.1 "ABC" scoring of AD neuropathology

The NIA-AA proposed a standardized framework for assessing Alzheimer's disease neuropathologic changes (ADNC), incorporating three components: (A) the Aβ pathology score, based on Thal phases, (B) the neurofibrillary tangle score, based

on Braak staging, and (C) the neuritic plaque score, based on CERAD guidelines[32]. Each component is rated from 0 to 3 and reported as “A0, B0, C0” to reflect the presence and extent of pathology. The overall ADNC severity is classified as “not present,” “low,” “intermediate,” or “high.” High scores in all three categories strongly correlate with clinical dementia, and both high and intermediate levels of ADNC are considered sufficient to explain cognitive symptoms in AD[32,88].

4.1.3.4. Synaptic loss

Synapses are specialized compartments for information transfer within neuronal networks and serve as primary sites for memory formation[91-93]. Although both neurons and synapses are progressively lost in AD, early memory deficits are more closely associated with synapse loss than with neuronal death or the accumulation of Aβ plaques and Tau aggregates[91]. Early studies demonstrated a strong correlation between synaptic loss and cognitive decline[94,95]. Post-mortem analyses of AD brain tissue and studies in murine models have shown that oligomeric forms of Aβ and Tau accumulate at synaptic sites[96-98]. Increasing evidence indicates that the soluble forms of Aβ and Tau, rather than plaques and NFTs, exert direct synaptotoxic effects by disrupting calcium influx and depleting synaptic vesicle proteins such as synaptotagmin, synaptogyrin 3, and synaptophysin at presynaptic terminals[99]. It has been suggested that Aβ and pathogenic Tau forms can be propagated through synapses early in pathogenesis, and Tau pathology may spread through the brain in a trans-synaptic fashion[99,100].

4.1.4. Pathogenesis of AD

The presence of amyloid plaques and NFTs remains the defining hallmark for the diagnosis of AD. While the Aβ peptide and pathological forms of Tau play central roles in AD pathogenesis, the definitive cause of the disease remains unresolved[101]. Over the years, several hypotheses have been proposed to explain AD pathogenesis, including the amyloid cascade hypothesis, the Tau hypothesis, and the cholinergic hypothesis. Additional mechanisms have also been implicated, such as neuroinflammation, vascular dysfunction, oxidative stress, mitochondrial impairment, metabolic dysregulation, and protein misfolding[101,102]. Recent

therapeutic advances, most notably the monoclonal antibodies aducanumab, lecanemab and donanemab, have shown great efficacy in clearing Aβ and robust albeit modest slowing cognitive decline[102]. While these therapies represent important disease-modifying progress, they also highlight that Aβ and tau pathologies, although central to AD, are not sufficient on their own to explain the full spectrum of disease etiology and clinical manifestations.

4.1.4.1. The amyloid cascade hypothesis

The ACH, first proposed by Hardy and Higgins in 1992 and later revised in 2016, has served as the primary theoretical framework for understanding the pathogenesis of AD[13,103]. This linear neuron-centric model posits that the pathological process is initiated by the accumulation of Aβ, which sequentially leads to Tau pathology, synaptic dysfunction, inflammation, neuronal loss, and ultimately, dementia[104]. The most compelling evidence supporting the ACH in humans includes the identification of Aβ as the main constituent of amyloid plaques, as well as genetic studies demonstrating that mutations in the *APP* gene, or other genes involved in its processing such as presenilin 1 (*PSEN1*) and presenilin 2 (*PSEN2*), cause early-onset familial Alzheimer's disease, or autosomal dominant AD (ADAD) [103]. Further support comes from individuals with Down syndrome (DS), in whom trisomy of chromosome 21 results in the overexpression of APP, leading to Aβ accumulation. A significant proportion of individuals with DS eventually develop the clinical and pathological features of AD[74,103]. In addition, the protective *APP* mutation A673T, known as the "Icelandic mutation", significantly downregulates β-cleavage, thus attenuating the production of Aβ and reducing amyloid pathology[105,106].

In summary, the ACH proposes that Aβ peptides, particularly $A\beta_{1-42}$, accumulate in the brain either due to genetic mutations associated with familial AD or through sporadic mechanisms such as impaired Aβ clearance. Accumulation of Aβ monomers lead to toxic Aβ oligomers, which progressively deposit as diffuse plaques. These deposits trigger a glial response and initiate inflammatory processes that disrupt neuronal homeostasis and promote Tau hyperphosphorylation and tangle formation. This cascade ultimately results in widespread synaptic and

neuronal dysfunction and loss, which underlies the cognitive decline observed in AD (**Figure 4**)[103].

Despite its foundational role in AD research, the ACH has faced skepticism, largely due to past clinical trial failures[107]. Recent positive results with lecanemab and donanemab reaffirm the critical role of Aβ in AD pathology[108]. Additionally, the detection of amyloid in cognitively normal older adults highlights its long preclinical phase, emphasizing that both therapeutic response and disease progression must be understood within a temporal framework.

4.1.4.1. Tau hypothesis

Hyperphosphorylated Tau is the main component of NFTs, whose spatial and temporal distribution shows a strong correlation with the clinical progression of AD[80-83]. Tau is encoded by the *MAPT* gene, and alternative splicing in exons 2, 3 and 10 generates 6 Tau isoforms (**Figure 5A**). The isoforms produced through variation in the C-terminal microtubule-binding pseudo-repeat (MTBR) domain are relevant as those generate the 3R and 4R forms depending on the number of microtubule-binding repeats[109]. These regions are critical for microtubule attachment and directly influence microtubule dynamics[109].

Isoforms 3R and 4R are usually expressed in a 1:1 ratio, but multiple studies have shown that altered *MAPT* expression leads to an imbalance in 3R and 4R ratios in various tauopathies such as Pick's disease or progressive supranuclear palsy[110]. It remains debated whether the overall 3R:4R isoform ratio is altered in AD. Nevertheless, several studies suggest an increased expression of 4R in brain regions vulnerable to the disease[110].

Although native Tau is relatively resistant to aggregation, the presence of two hexapeptide motifs in the MTBR domain denominated PHF6 (residues 306–311) and PHF6* (residues 317–335) promote β-sheet formation and facilitates aggregation, even in the absence of external stimuli[109,111]. Post-translational modifications and mutations, such as P301L, further enhance Tau propensity to aggregation.

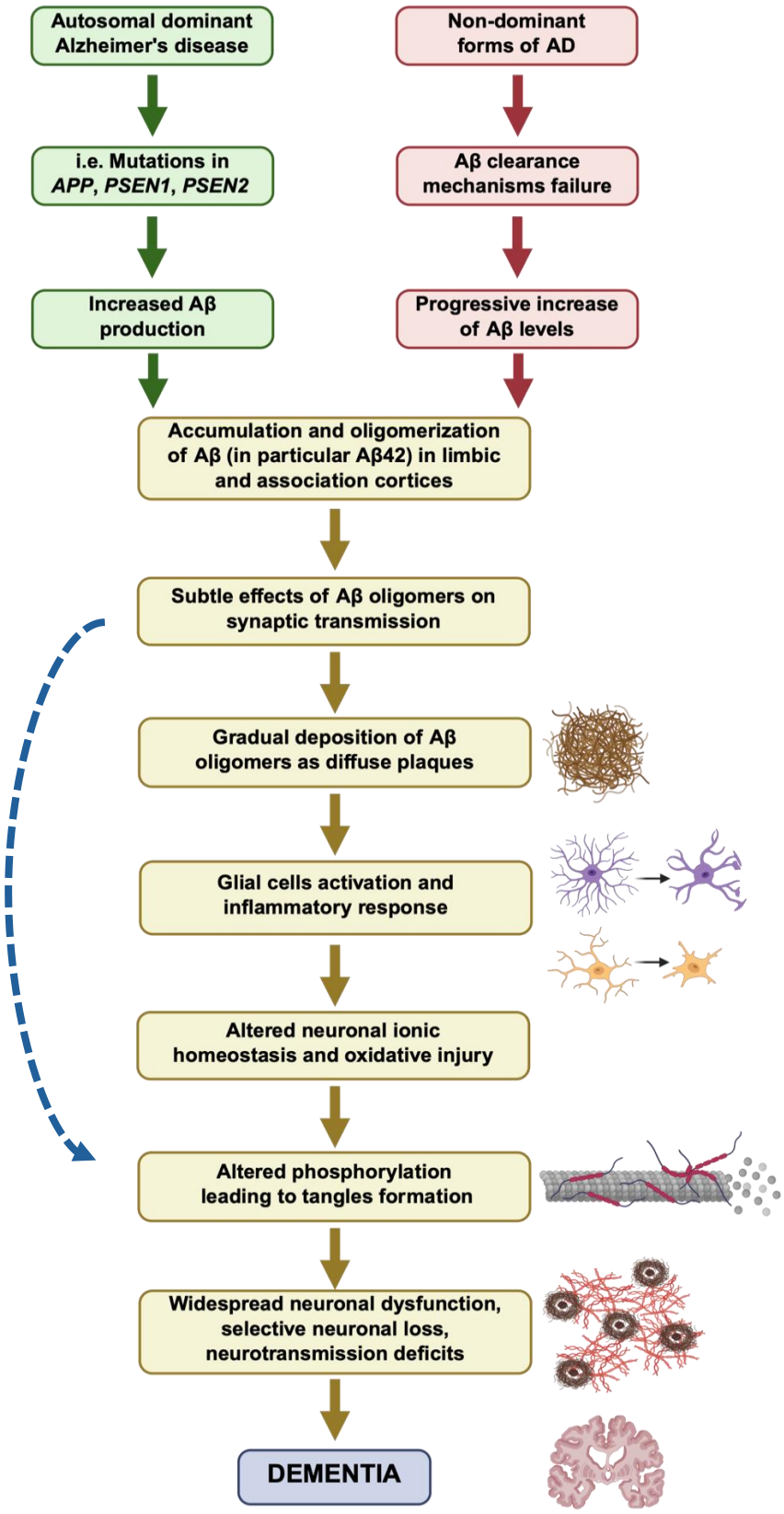

Figure 4. Major pathogenic events leading to AD as proposed by the ACH. *Blue arrow indicates that Aβ oligomers may directly injure synapses and neurites. Image created in Biorender, modified from Selkoe & Hardy*[103].

Tau protein contains 85 putative phosphorylation sites (45 serine, 35 threonine and 5 tyrosine)[111]. Under normal physiological conditions, Tau is phosphorylated in a tightly regulated manner[112]. However, during AD pathogenesis, this regulation becomes disrupted due to an imbalance in kinase and phosphatase activity, leading to Tau hyperphosphorylation[102,113]. As a result, Tau exhibits reduced affinity for microtubules and detaches from them, causing cytoskeleton destabilization. The detached pTau undergoes conformational changes into β-sheet rich structures, forming oligomers that aggregate into PHF and eventually NFTs (**Figure 5B**) [46,111,114]. These aggregates are a defining feature of tauopathies and are used as pathological indicators of disease stage in AD[111,115].

Hyperphosphorylated Tau contributes to neurodegeneration through multiple mechanisms, including impaired axonal transport and synaptic function, disruption of the cellular stress response, and the promotion of neuroinflammation[116]. Pathological Tau may also facilitate disease progression by propagating toxic species across synapses, where they induce aggregation of monomeric Tau in recipient neurons, leading to the formation of new oligomers[100,116].

4.1.4.2. The Cholinergic hypothesis

The cholinergic hypothesis, originally proposed in 1982 to explain age-related memory dysfunction[117], suggests that dysfunction of the neurons containing acetylcholine (ACh) substantially contributes to the cognitive decline observed in individuals with AD[118]. This hypothesis emerged following early studies of AD pathogenesis that identified damage in the basal forebrain projections, which appeared to correlate with cognitive impairment[118].

ACh is an excitatory neurotransmitter involved in learning and memory processes[119]. It is synthesized from choline and acetyl coenzyme A by acetylcholine transferase, then transported into synaptic vesicles by a specialized acetylcholine transporter. Upon arrival of a neural signal, ACh is released into the synaptic cleft, where it binds to nicotinic and muscarinic receptors on the postsynaptic neuron. Any remaining ACh is degraded by acetylcholinesterase (AChE) and reabsorbed by the presynaptic neuron[102].

In AD, the loss of cholinergic neurons is thought to be related to nerve growth factor-dependent nutritional depletion[102]. Clinical data showed a significant reduction of cholinergic neurons and a pronounced deficiency in acetylcholine transferase activity in AD patients[119]. In conjunction with the neurotoxic effects of Aβ, this decline leads to reduced ACh levels, which impairs learning, memory, sleep cycle regulation, and motor function[102]. Further support for the cholinergic hypothesis comes from studies in animal models and human cases using anticholinergic agents, such as muscarinic and nicotinic antagonists, which have demonstrated impaired working and spatial memory across various behavioral paradigms[118]. This hypothesis paved the way for the development of symptomatic treatments for AD, including AChE inhibitors such as donepezil, rivastigmine, and galantamine[102].

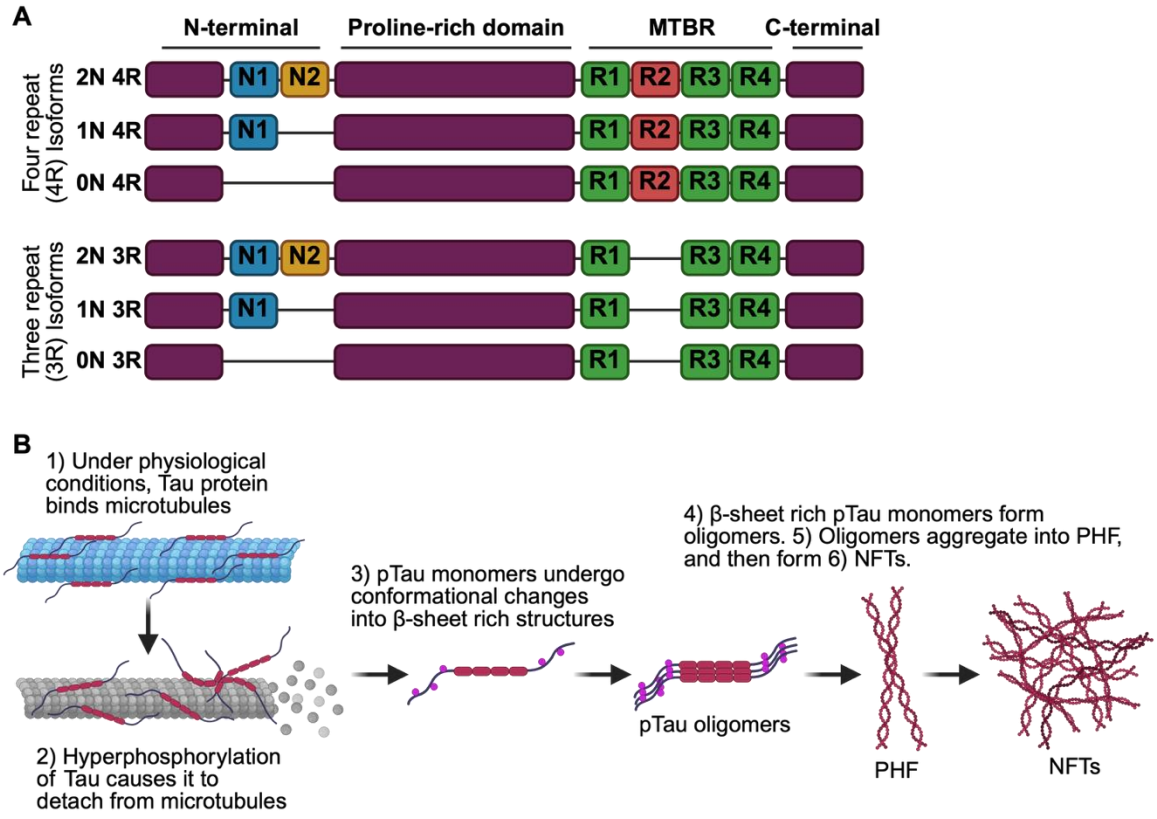

Figure 5. Human Tau isoforms and Tau protein conformational changes in AD. A. *MAPT gene alternative splicing figure shows N-terminal amino acid sequences excluded from exons 2 and 3 and microtubule binding domain (MTBR) alternative splicing of exon 10 resulting in 3R or 4R Tau isoforms. Image created in BioRender, Panel A based on Guo and colleagues, 2017[111].*

4.1.4.3. Neuroinflammation and the cellular phase of AD

Mounting evidence indicates that mechanisms beyond Aβ and Tau pathology contribute to AD pathogenesis and progression. Neuroinflammation, defined by the release of pro- and anti-inflammatory cytokines in the CNS under pathological conditions, has emerged as a cardinal feature of the disease[120,121]. Neuroinflammation was initially considered a secondary response to the pathogenic cascade triggered by Aβ and NFT deposition. However, growing evidence indicates that it also acts as a causal factor in AD development, with immune system alterations occurring even before the onset of clinical symptoms[122]. Even before Aβ was fully characterized, early studies reported the presence of immunoglobulins and complement components within neuritic plaques, highlighting the involvement of immune processes in AD[123]. Recent findings highlight glial cells as active contributors to AD pathophysiology[124,125]. Astrocytes and microglia, in particular, play central roles in neuroinflammatory processes[122]. Reactive astrocytes and activated microglia are commonly associated with neuritic plaques, suggesting that Aβ and pTau may serve as triggers for their activation[55].

4.1.4.3.1 Role of Microglia in AD pathogenesis

Microglia play a central role in the immune response and help shape AD progression. Microglia are resident macrophages of the CNS[120]. Under physiological conditions, they participate in synaptic pruning, neuronal apoptosis, maintenance of synaptic plasticity, and immune surveillance[126]. In AD, microglia activates in response to neurotoxic peptides and protein aggregates[126]. This activation is characterized by morphological changes, including a shift toward an enlarged soma with shorter processes and less ramifications[127,128].

Aβ can bind to pattern recognition receptors such as receptor for advanced glycation end products (RAGE), Toll-like receptors (TLR), and nucleotide-binding oligomerization domain (NOD) like-receptors (NLRs)[125]. Studies in AD mouse models suggest that TLR4 is involved in the upregulation of tumor necrosis factor-alpha (TNFα), interleukin-1 beta (IL-1β), IL-10 and IL-17 as well as in the clearance of Aβ deposits[129,130]. *In vitro* studies showed the capacity of RAGE to bind $A\beta_{1\text{-}40}$ and

$A\beta_{1-42}$, and possibly mediates the interaction of Aβ and endothelial cells and neurons triggering oxidative stress, and with microglia resulting in cell activation and release of cytokines[131]. Aβ peptides can also activate NLRs like NLRP3, facilitating the formation of the inflammasome complex, maturation of IL-1β, thus triggering an inflammatory response[132]. Microglia release ROS in addition to proinflammatory cytokines including IL-1β, IL-6, TNFα, thereby contributing to oxidative stress[110]. They also promote astrocyte reactivity by secreting IL-1α, TNF, and C1q, both *in vitro* and *in vivo*[133].

However, transcriptomic studies have shown that microglial activation extends beyond morphological changes. Mouse models of AD suggest a gradual shift from a homeostatic state to a disease-associated state[126,134]. During this transition, microglia downregulate homeostatic genes including TMEM119, CX_3CR1 and P2RY12, while upregulating the expression of multiple pro- and anti-inflammatory molecules[120,134]. RNA sequencing of microglia isolated from human AD brain tissues revealed subpopulations defined by the expression of disease-associated genes previously identified in transgenic AD mice[134,135].

An essential gene in the shift from a homeostatic to activated microglial state is the triggering receptor expressed on myeloid cells 2 (*TREM2*), specific alleles of which are associated with an increased risk of LOAD of approximately 3- to 5- fold[136,137]. Whole-genome expression profiling of AD brain tissue identified TYROBP, the gene encoding the *TREM2* receptor, as a central regulator of a microglia-specific immune module, reinforcing the relevance of *TREM2* signaling in AD[138]. Microglia establish spatial associations with Aβ and pTau, and frequently cluster around amyloid plaques[120,139]. In murine models, *TREM2* is essential for enabling microglia to form a barrier around Aβ and regulate plaque deposition[139,140]. These plaque-associated microglia show high immunoreactivity for activation markers such as MHCII and COX2, as well as cytokines including IL-1, MCP-1, MIP-1α, IL-1β, TNFα, and IL-6[141].

4.1.4.3.2 Role of Astrocytes in AD pathogenesis

Astrocytes are the most abundant neural stem cell-derived glial cell type in the CNS[142-144]. Astrocytes provide trophic, structural and metabolic support to neurons

and interact with other brain cell types in the brain, including microglia[145,146]. Astrocytes also contribute to synapse formation and maintenance, neurotransmitter reuptake and recycling, and help preserve the integrity of the blood-brain barrier[144].

In response to injury or disease, astrocytes become reactive, undergoing changes in morphology, gene expression, and their capacity to maintain brain homeostasis[145]. Mouse studies identified two activation states, A1 and A2, analogous to M1 and M2 macrophages[133]. A1 astrocytes exhibit neurotoxic features *in vitro*, whereas the A2 show neuroprotective activity[133]. However, reactive astrocytes represent a heterogeneous population, broadly classified by their induction in response to acute injury, infection or inflammation, or disease pathology[145]. A shared characteristic among these subtypes is that they arise in response to external stimuli. However, the binary classifications such as A1 or A2 or neurotoxic vs. neuroprotective fall short to capture the multiple changes astrocytes undergo in disease[147]. The assessment of multiple functional and molecular parameters together with the astrocytes impact on pathology are necessary for a better classification[147].

A large spatiotemporal transcriptomics study using frozen human AD brain tissue revealed significant regional and temporal differences in astrocyte gene expression, which may help explain region-specific vulnerability to AD[148]. Certain astrocyte clusters show upregulation of genes involved in cell death, oxidative stress, lipid storage, fatty acid oxidation, and inflammation[124]. It has also been suggested that reactive astrocytes exert neurotoxic effects through the release of saturated long-chain free fatty acids and phosphatidylcholine[149].

Multiple studies support a crosstalk mechanism between astrocytes, microglia, and neurons that promotes neurodegeneration in AD, reinforcing prior findings that microglia influence astrocyte behavior in response to pathology[133]. Aβ peptides can activate NF-κB signaling in astrocytes, triggering the release of complement component C3, which binds to C3a receptors on neurons and microglia, leading to synaptic and neuronal dysfunction and microglial activation[150,151].

4.1.4.3.3 Role of Oligodendrocytes in AD pathogenesis

Oligodendrocytes are responsible for producing myelin in the central nervous system[152,153]. Oligodendrocytes wrap axons in a spiral configuration using their own membranes to enable efficient electrical signal conduction and provide metabolic support to axons[154,155]. Myelin is composed of lipids and proteins, including myelin basic protein (MBP), myelin oligodendrocyte glycoprotein (MOG), proteolipid protein (PLP), and 2′,3′-cyclic nucleotide phosphodiesterase (CNP)[155-158].

Although oligodendrocytes remain relatively understudied in AD, early observations suggested a connection between neuronal vulnerability and myelination. In 1996, Braak and Braak noted that the progression of NFTs in AD mirrors myelogenesis in reverse[159]. Early magnetic resonance imaging studies revealed extensive myelin breakdown in AD patients, which exceeds that observed in normal aging[160]. More recent studies have shown microstructural changes in white matter detectable by MRI and increased white matter hyperintensities observed in ADAD, which correlate with cognitive decline[161]. Additionally, Aβ plaque deposition has been linked to oligodendrocyte loss and focal demyelination in the cortical grey matter of transgenic AD mouse models, contributing to impaired cortical processing and dystrophic neurite formation[162-164].

Mouse models overexpressing PLP exhibit late-onset myelin degeneration and subsequent axonal pathology[165]. In transgenic mice with myelin abnormalities and deficient mature T and B lymphocytes, researchers observed secondary inflammation distinguished by CD8+ T-cell infiltration and microgliosis[165]. Myelin lipid turnover generates lymphocyte chemoattractants typically degraded by peroxisomes; failure to degrade these inflammatory molecules due to abnormal turnover may promote neuroinflammation[166].

Recent transcriptomic and proteomic studies have further demonstrated the role of oligodendrocytes and myelin pathology in AD progression, revealing significant transcriptional changes and altered protein expression[167-172]. Proteomic techniques, such as subcellular proximity labeling with antibody recognition, have uncovered disrupted signaling at the axon-myelin interface involving lipid metabolism,

axonogenesis, and Aβ production, while levels of important myelin proteins such as PLP1, CNP, and MBP remain largely unchanged[173].

A spatial transcriptomics study by Sadick and colleagues identified five oligodendrocyte clusters based on transcriptional signatures related to glial cell development, cholesterol metabolism, antigen presentation, and innate immune pathways[124]. In AD samples, these clusters showed downregulation of pathways crucial for synaptic support, amino acid and fatty acid metabolism, and myelination. Some clusters also exhibited reduced expression of enzymes like stearoyl-CoA desaturase (SCD) and phosphodiesterases (PDEs), indicating impaired lipid synthesis and myelin production[124].

Oligodendrocytes can also transition to a disease-associated state that has also been recognized in other neurodegenerative disorders[174-177]. This phenotype emerges after microglia adopt the DAM state and following the accumulation of amyloid plaques[176,177]. Disease-associated oligodendrocytes are characterized by upregulation of the serine protease inhibitor *SERPINA3N* and the complement component *C4b*[176]. Although the roles of these genes in the oligodendrocyte disease phenotype remain unclear, it has been speculated that they may exert protective effects against T cell-induced cytotoxicity[178].

4.1.4.4. Synapse structure and dysfunction in AD

Synapses can exert either excitatory or inhibitory effects on the target cell. In the CNS, glutamate is the most common excitatory neurotransmitter, while gamma-aminobutyric acid (GABA) is the predominant inhibitory neurotransmitter in the adult brain[179]. Excitatory synapses typically form in small dendritic protrusions called spines, allowing them to be separated from the main dendritic shaft and become highly specialized. In contrast, inhibitory synapses usually form directly on the dendritic shaft or the neuronal soma, although there are exceptions to this pattern. Once formed, synaptic connections remain dynamic; they can strengthen with increased activity or shrink and be lost when activity decreases. This phenomenon, known as synaptic plasticity, is fundamental for cognitive functions such as learning and memory[91,179].

Given the critical role of synapses in normal brain physiology, synaptic loss is a common feature of several neurodegenerative diseases. In AD, synaptic degeneration correlates strongly with cognitive decline (as seen in **section 4.1.3.4**)[99,179]. In AD mouse models, oligomeric Aβ has been shown to accumulate at excitatory synapses, and the amyloid plaque-associated protein Clusterin (also known as ApoJ) has been detected in synapses from human AD brain tissues[96,98]. Soluble hyperphosphorylated Tau oligomers have also been found in synapses in *post-mortem* AD brain samples [180,181].

Oligomeric Aβ induces excitotoxicity at the pre-synaptic terminal by increasing Ca^{2+} influx and forming membrane pores that further enhance calcium entry. Misfolded Tau at the pre-synapse contributes to the loss of synaptic vesicle proteins such as synaptotagmin, synaptogyrin 3, and synaptophysin, leading to depletion of the synaptic vesicle pool[182-184]. Mitochondrial dysfunction and elevated ROS production occur in both pre- and post-synaptic compartments. At the post-synapse, soluble Aβ binds to receptors including prion protein C (PrP^C) and metabotropic glutamate receptor 5 (mGluR5), leading to activation of Fyn, which in turn triggers IP3 signaling, enhances eEF2 activity, and promotes Tau phosphorylation[185,186]. Aβ also interacts with NMDARs, causing Ca^{2+} influx, suppression of the transcription factor CREB, and disinhibition of GSK3β, which together impair long-term potentiation (LTP) and enhance long-term depression (LTD)[187-189]. These events contribute to synapse deterioration. Additionally, Aβ binding to TMEM97 disrupts calcium homeostasis, while intracellular calcium release is further promoted through activation of IP3 and ryanodine receptors[190,191].

4.1.4.5. Genetic risk factors for AD

Age remains as the strongest risk factor for developing AD, although other contributors such as diabetes type 2, traumatic brain injury and obesity have been identified, along with protective influences like higher educational level, bilingualism, and regular physical activity[192,193]. In addition to these factors, recent genomic research has identified multiple of genes implicated in the pathogenesis of AD[194]. Genetic predisposition plays a major role in AD onset and progression, not only in autosomal dominant forms but also in sporadic cases[110]. A study comparing twins

estimated AD heritability to range between 58% and 79%, with the variation possibly explained by environmental factors unique to each individual[195].

4.1.4.5.1 Autosomal dominant AD

Autosomal dominant AD is a rare form of Alzheimer's, accounting for less than 1% of all cases[196]. It results from mutations in the *APP*, *PSEN1*, and *PSEN2* genes, which typically exhibit full penetrance and a conserved age of onset[197-200]. *PSEN1* and *PSEN2*, encoding presenilin 1 and 2, are part of the γ-secretase complex and contribute to abnormal Aβ production by altering the Aβ42/Aβ40 ratio[194,201]. Mutations at the β-secretase cleavage site of *APP*, such as the E682K or "Leuven" mutation, shift APP processing toward the amyloidogenic pathway, increasing Aβ1-42 levels and the Aβ42/Aβ40 ratio[202]. Other *APP* mutations, including the Dutch, Flemish, Italian, and Arctic variants, are associated with early-onset CAA without increasing overall Aβ production[203]. Additionally, rare variants in *APP*, *PSEN1* and *PSEN2* have been identified in LOAD families and may influence disease risk or modify the age of onset[204].

4.1.4.5.2 Apolipoprotein E

Apolipoprotein E (*APOE*) gene is a well-established genetic risk factor for AD. *APOE* polymorphisms are the most significant genetic modifiers of LOAD, with the ε4 allele increasing risk and the ε2 allele providing a protective effect[205-209]. ApoE is a 299-amino acid glycoprotein expressed in several tissues, with the highest levels found in the liver and the brain[206]. In the CNS, ApoE is mainly produced by astrocytes and, albeit less prominently, by microglia; neurons can express it under certain conditions, although at much lower levels[210,211].

Under physiological conditions, astrocytes secrete ApoE as HDL-like particles[211-213]. ApoE lipidation is mediated by the ATP-binding cassette transporter A1 (ABCA1)[214,215]. ApoE-containing lipoproteins are then internalized by neurons through receptors, with the low-density lipoprotein receptor (LDLR) being important for regulating brain ApoE levels[206,209,216-218]. In addition to lipid transport, ApoE isoforms influence synaptic integrity and plasticity, glucose metabolism, and cerebrovascular function in the brain[209].

Post-mortem studies in AD brains have found a strong correlation between intraneuronal Aβ accumulation and the APOE ε4 allele[219]. Evidence suggests that ApoE interacts physically with Aβ, potentially influencing its conformational change into β-sheet-rich aggregates[220,221]. The ε4 isoform is linked to increased amyloid plaque deposition, while ε2 is associated with reduced plaque burden[222-224]. Biomarker studies using cerebrospinal fluid (CSF) and neuroimaging have consistently shown that *APOE* ε4 is associated with greater Aβ deposition across healthy older adults, individuals with mild cognitive impairment (MCI), and AD patients[225-228]. *APOE* ε4 carriers not only begin accumulating Aβ earlier than non-carriers but also exhibit a faster rate of Aβ accumulation over time, even after adjusting for baseline pathology levels[207].

4.1.4.5.3 Other genetic factors

Approximately 95% of all reported AD cases worldwide are sporadic, with the majority corresponding to LOAD[229]. Genome-wide association studies (GWAS) have identified additional genetic risk factors that contribute to AD susceptibility[192,194]. These genes influence the development and age of onset of LOAD. and are involved in pathways such as cholesterol metabolism, immune response, endo-lysosomal function, and vesicle-mediated transport[192,195].

In addition to *APOE*, two notable genes related to cholesterol metabolism and AD risk are *CLU* and *ABCA7*[192,194]. *CLU*, located on chromosome 8, encodes clusterin (also known as ApoJ), a protein involved in lipid transport, complement regulation, and endocrine secretion, and has also been linked to Aβ clearance[192,194]. Elevated plasma levels of CLU have been proposed as a marker of brain atrophy and disease severity[230,231]. Clusterin may contribute to AD pathogenesis by modulating immune responses or interfering with neurodegeneration-associated repair mechanisms[232]. *ABCA7* is expressed in hippocampal CA1 neurons and at much higher levels in microglia[233]. ABCA7 regulates lipid efflux into lipoprotein particles, stimulates cholesterol release, modulates APP processing, and supports the phagocytic clearance of apoptotic cells[234-237]. ABCA7-deficient mice show increased Aβ deposition, supporting its role in Aβ homeostasis[238].

As discussed in **section 4.1.4.3**, neuroinflammation is central to AD pathogenesis. Complement receptor 1 (*CR1*) encodes for the CR1 protein, which is a component of the complement response cascade[194]. The single nucleotide polymorphism (SNP) rs381836 in *CR1* has been linked to increased LOAD risk in *APOE* ε4 carriers and to elevated levels of neuritic plaques[239]. *CD33,* a gene expressed in myeloid cells and microglia, is involved in anti-inflammatory signaling, cell adhesion, and clathrin-independent endocytosis[240]. Increased expression of CD33-positive microglia correlates with insoluble Aβ1-42 levels and plaque burden in AD brains[241].

Among AD-associated genes, *TREM2* is considered one of the most significant after *APOE*. Variants such as R47H and R62H have been associated with a substantially increased risk of developing AD[136,137]. TREM2 activation initiates phosphorylation cascades involving proteins and lipids, leading to calcium mobilization, cytoskeletal remodeling, mTOR and MAPK pathway activation, and enhanced energy metabolism[242]. In AD mouse models, TREM2 deficiency impairs microglial response, resulting in inadequate formation of protective barriers around amyloid plaques and increased Aβ accumulation[139,243]. TREM2 is also essential for the phagocytic clearance of Aβ and plays a fundamental role in the transition of microglia toward the DAM phenotype[134,244].

Genes implicated in endocytosis have also been associated with AD risk. *BIN1* encodes bridging integrator 1, a protein involved in clathrin-mediated endocytosis, vesicle trafficking, immune responses, apoptosis, calcium homeostasis, and indirectly in cholesterol metabolism[192]. Two *BIN1* SNPs have been linked to increased LOAD risk, and another variant correlates with elevated tau burden[245,246]. *PICALM* encodes a protein involved in clathrin assembly and is mainly expressed in neurons[194]. Deficiency of PICALM alters iron metabolism and affects APP processing. PICALM co-localizes with APP, and its disruption impairs APP trafficking and increases plaque formation in mouse models[247]. *SORL1*, which encodes the sortilin-related receptor, regulates vesicle trafficking from the plasma membrane to the Golgi-endoplasmic reticulum and mediates APP recycling through endocytic pathways[194,248]. Mice lacking *SORL1* exhibit increased Aβ levels, and reduced *SORL1* mRNA expression has been reported in AD brains[249,250].

Other gene variants have also been linked to AD, though their roles remain unclear. Some of these are involved in immune-related pathways (*HLA-DRB5*, *HLA-DRB1*, *INPP5D*), immune and synaptic functions (*MEF2C*), cell migration and synaptic signaling (*PTK2B*), cytoskeletal function and axonal transport (*CELF1*, *NME8*, *CSS4*), and tau metabolism (*CASS4*, *FERMT2*)[192,251]. Further research is needed to understand the functions of these genes under both normal and pathological conditions.

4.1.5. Subtypes of AD

As discussed so far, the complexity of AD pathophysiology reflects the heterogeneous nature of the disease. Variability in age of onset, symptom presentation, neuropathological patterns, and the genetic landscape of risk and resilience factors has led researchers to propose the existence of biological subtypes that may account for this heterogeneity. Several approaches have been developed to classify AD into subtypes based on clinical features, neuropathological characteristics, imaging profiles, and molecular signatures.

4.1.5.1. Classification of AD based on age at onset

As described in **section 4.1.5.1**, the most common form of AD is sporadic LOAD. Typical LOAD is characterized by substantial hippocampal volume loss and enlargement of the temporal horn, which contribute to the prominent memory dysfunction observed in these cases[252,253]. However, other AD presentations show predominant cognitive impairments in language, executive function, motor skills, or visuospatial abilities rather than memory. This alternative manifestation usually occurs at a younger age, with onset arbitrarily defined as before 65 years old, and is referred to as early-onset AD (EOAD)[254]. Studies have shown that EOAD is often associated with greater dysfunction in fronto-parietal regions compared to the temporal lobe[255,256]. Non-amnestic presentation is more common than LOAD, and together with a frequently preserved hippocampal volume, EOAD can be misdiagnosed[257]. While both EOAD and LOAD share Aβ plaque deposition, EOAD exhibits a higher burden of NFTs and neuritic plaques in the frontal and parietal lobes compared to LOAD[258,259].

4.1.5.2. Classification of AD based on neuropathological features

Closely related to age of onset, AD can also be categorized as typical or atypical based on the topography of neuropathological hallmarks, particularly NFTs. Within the atypical presentations, which are more often seen in EOAD, Murray and colleagues identified the subtypes hippocampal sparing (HpSp) and limbic predominant (LP) AD[258]. HpSp exhibits increased NFT density in the association and motor cortices, larger hippocampal volumes, and higher neuronal counts in the CA1 region. Clinically, HpSp is associated with early onset, shorter disease duration, and rapid progression, often presenting with focal cortical syndromes such as progressive aphasia, posterior cortical atrophy, or a frontotemporal dementia variant[258]. In contrast, LP shows severe hippocampal atrophy and NFT accumulation in allocortical regions, with some isocortical involvement, alongside the presence of senile plaques. LP also more frequently presents TDP-43 pathology compared to HpSp[258]. Another described subtype, minimal atrophy AD, displays little to no gray matter atrophy, a slower disease progression, and an intermediate age at symptom onset. It is characterized by a relatively low burden of Tau pathology, increased Aβ deposition, and a higher incidence of small-vessel disease[260].

4.1.5.3. Classification of AD based on the rate of progression

Some individuals with AD experience an unusually fast progression of symptoms, independent of age at onset, sex, or general cognitive function[261,262]. Rapidly progressive AD (rpAD) is defined by survival of three years or less after diagnosis, with a median survival of 7 to 10 months. These patients show rapid cognitive decline, often leading to misdiagnosis as Creutzfeldt-Jakob disease[263]. rpAD typically occurs without autosomal mutations and shares neuropathological features with typical sporadic AD[264]. However, distinct conformational properties of Aβ1-42 have been observed in rpAD, including less-stable conformers that fragment more easily in the presence of denaturants. This instability facilitates faster replication and

propagation, resembling prion-like behavior[265]. Proteomic analyses of amyloid plaques from rpAD and LOAD brain tissues revealed different protein compositions. rpAD plaques were enriched with neuronal proteins, particularly synaptic and cytoskeletal, while LOAD plaques contained more astrocytic proteins. These differences suggest distinct underlying mechanisms between rpAD and the more typical sporadic AD[264].

4.1.5.4. Classification of AD based on genetics

AD can also be classified according to the presence of genetic variants, particularly mutations in specific genes, as discussed in **section 4.1.4.5.1**, ADAD is defined by mutations in the *APP*, *PSEN1*, or *PSEN2* genes and typically presents before the age of 65 years[196,266]. FAD follows a Mendelian inheritance pattern and most pedigrees exhibit nearly 100% penetrance[267]. Approximately 80% of identified ADAD mutations occur in *PSEN1*, 15% in *APP*, and the remaining in *PSEN2*[268]. The clinical and pathological features of FAD closely resemble those of LOAD, with the primary difference being the earlier onset and inherited nature of the disease[267]. Other genetically determined form of AD is Down syndrome (DS), primarily caused by triplication of the *APP* gene on chromosome 21, which serves as the basis for the a well-established association between DS and AD, (see section **4.2.2.**)[74,269].

4.2. Down syndrome

DS is the most prevalent chromosomal abnormality, resulting from the partial or complete triplication of human chromosome 21 (Hsa21), with an estimated worldwide incidence of 1 in 700 to 1,000 live births[270-272]. First described by Langdon Down in 1866, the condition was identified based on characteristic physical traits and intellectual disability, and recognized as a congenital defect[273]. In 1959, research groups led by Lejeune, Gautier, and Turpin in France, and Jacobs, Baikie, Court Brown, and Strong in Scotland, independently identified trisomy 21 as the chromosomal basis of Down syndrome[274,275].

Individuals with DS typically exhibit learning and attention deficits, working memory impairment, and delayed motor and language development[276]. Early research linked

the intellectual disability in DS to delayed brain maturation and reduced brain volume, particularly in the temporal and frontal lobes, which are smaller in individuals with DS compared to healthy controls[277,278]. DS affects multiple organ systems, most notably the musculoskeletal, neurological, and cardiovascular systems (**Figure 6**)[271]. Common co-occurring conditions include congenital heart disease, present in approximately 60% of individuals; vision and hearing problems, affecting 72%; gastrointestinal issues (61%); respiratory complications (45%); and feeding difficulties (33%)[279]. Additionally, interconnected conditions such as obesity, sleep apnea, and diabetes are frequently observed in this population[280]. Interestingly, individuals with Down syndrome have a reduced risk of certain cancers, particularly solid tumors, as well as a lower incidence of atherosclerosis[281]. Despite the fact that these phenotypes are linked to the trisomy of Hsa21, there is considerable variability in their expression, and the underlying genetic mechanisms are not yet fully understood[281].

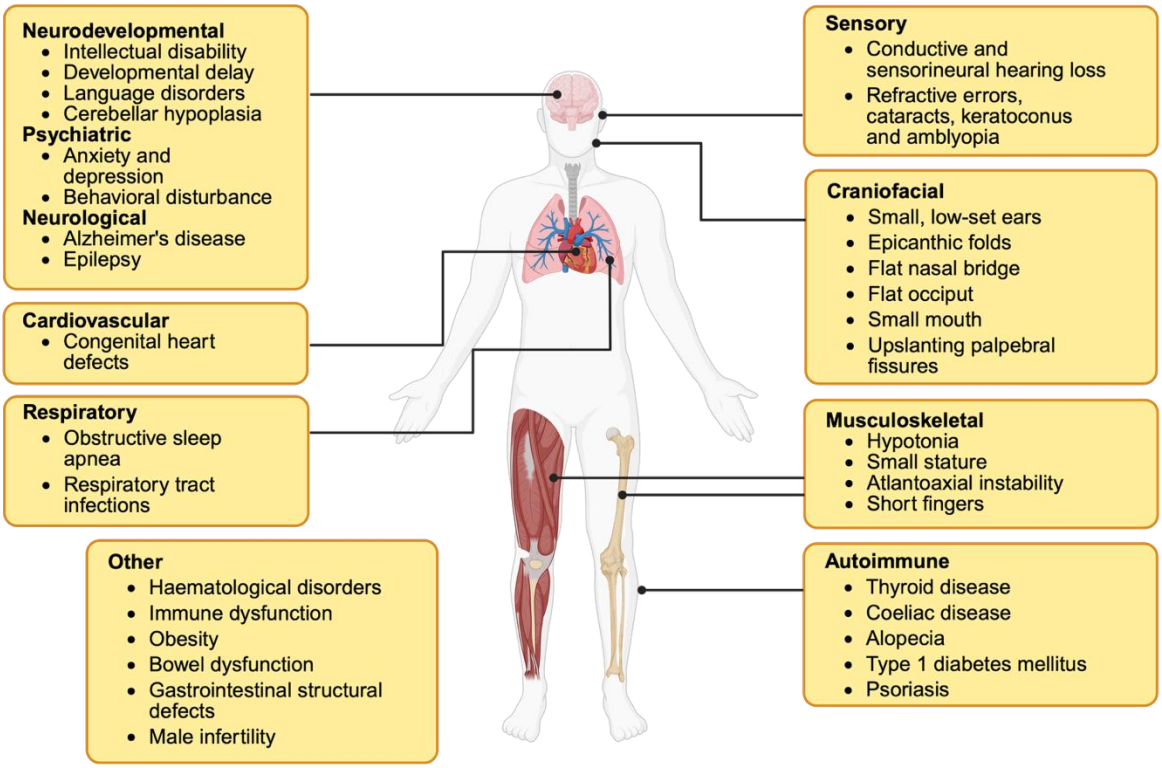

Figure 6. Co-occurring conditions in DS. *Individuals with trisomy 21 exhibit a characteristic set of features affecting multiple body systems, though presentation varies. Common traits include short stature, short fingers, hypotonia, and distinctive facial features such as epicanthic folds, flat nasal bridge, small ears and mouth, and up-slanting palpebral fissures. Congenital heart defects are frequent. People with DS also have increased risk of hypothyroidism, sleep apnea, epilepsy, hearing and vision issues, haematological disorders like leukemia, recurrent*

infections, anxiety, and early-onset Alzheimer disease. Figure created in BioRender, based on Antonarakis et al. 2020[271].

4.2.1. Genetic features of Down syndrome

There are three chromosomal alterations that can lead to Down syndrome: nondisjunction (complete trisomy 21), mosaicism, and translocation. Nondisjunction is the most common, accounting for approximately 96% of all cases, and occurs when chromosomes fail to segregate properly during meiosis, resulting in gametes with an extra copy of Hsa21[280,282]. Mosaicism is rare, representing 2 to 4% of cases, and involves individuals with a mixture of trisomic and euploid cell lines[280,282,283]. Translocation, also present in 2 to 4% of cases, is a structural abnormality in which the long arm of Hsa21 attaches to another chromosome, most commonly chromosome 14 or 22[280,282,283].

Hsa21 is the smallest human chromosome, carrying an estimated of 234 protein-coding genes[270]. The short arm of Hsa21 primarily contains repetitive DNA sequences and is therefore unlikely to contribute significantly to the phenotype observed in DS[284]. Despite its size, it is among the richest chromosomes in genes encoding long non-coding RNAs (lncRNAs), although it contains relatively few micro-RNA (miRNA) and other non-coding RNA (ncRNA) genes[270]. Overall, Hsa21 is one of the poorest chromosomes in terms of functional DNA elements per megabase, which has led to speculation that this may partly explain the postnatal viability of trisomy 21[270].

Compared to the rest of the genome, Hsa21 is significantly enriched in genes related to cytoskeletal structure and vesicle function or trafficking[285,286]. Pathway analysis has identified cytoskeleton organization and synaptic transmission as significant terms among the downregulated genes on Hsa21, suggesting potential synaptic deficits[286]. Previous studies have implicated cytoskeletal proteins in the development of neurological disorders, including Alzheimer's disease[287,288]. Notably, dysregulation of Hsa21 cytoskeletal genes has been observed in adult but not fetal DS brains[286].

Hsa21 also includes genes encoding transcription factors, which may contribute to the heterogeneous phenotypes observed in DS due to their regulatory roles over

other genes[285]. For instance, RUNX1 has been implicated in the increased risk of leukemia[289,290], while BACH1 and ERG are thought to be involved in AD[285].

4.2.1.1. Two hypotheses to explain DS phenotype

Two main hypotheses seek to explain the DS phenotype. The gene-dosage effect or imbalance hypothesis suggests that the presence of a third copy of chromosome 21 leads to a 1.5-fold increase in the expression of many genes located on this chromosome, which in turn alters the expression of genes on other chromosomes, disrupts the stoichiometric balance of protein complexes and cellular pathways, and ultimately contributes to the clinical manifestations of DS[291].

On the other hand, the amplified developmental instability or altered homeostasis hypothesis proposes that trisomy 21 causes a global disturbance in cellular regulatory networks, leading to increased vulnerability to environmental and genetic perturbations. This model emphasizes that the overexpression of trisomic genes disrupts the capacity of cells, tissues and organs to maintain developmental and physiological stability, which may help explain the wide variability in phenotypes observed among individuals with DS[292-294].

Pioneer exponents of the altered homeostasis hypothesis sought to explain both the shared characteristics of different aneuploidies and the observation that some phenotypic traits of DS also occur in the general population, albeit at much lower frequencies[293,294]. In this view, components of developmental systems that are less stable in the general population become more frequently and severely impaired in individuals with trisomy[294]. However, this hypothesis was later challenged by evidence showing that trisomies 13, 18, and 21 have distinct and non-overlapping clinical features. For example, trisomy 13 is frequently associated with renal abnormalities that are rarely seen in DS, while AD pathology is a hallmark of DS and not typically observed in the other trisomies[293].

Initial gene mapping studies of Hsa21 led to the hypothesis that overexpression of specific genes on this chromosome could account for DS phenotypes, including genes such as the proto-oncogene *ETS2*, implicated in congenital heart disease,

and *GART*, involved in purine metabolism[295,296]. These findings also contributed to the formulation of the Down syndrome critical region (DSCR) concept[296].

DSCR emerged from analyses of individuals with partial trisomy 21. It was initially proposed that the distal segment of the long arm of Hsa21 (21q22) contained the essential loci responsible for the DS phenotype[297]. However, conflicting findings from different studies, including a report of a child with DS carrying a partial tetrasomy of the short arm and proximal long arm of Hsa21, challenged the notion of a minimal critical region capable of explaining all DS features[297]. Pelleri and colleagues later analyzed 125 cases of partial trisomy 21 and proposed a highly restricted DSCR (HR-DSCR) of only 34 kb located at 21q22.13[298].

Nevertheless, subsequent studies have demonstrated that genes on Hsa21 are not consistently overexpressed, and that the corresponding proteins are not significantly more abundant in DS compared to controls. Moreover, there is limited evidence for gene-dosage compensation at the transcriptional or steady-state RNA levels[299-301]. Murine models have shown that the DS phenotype cannot be fully explained by this region alone and Transcriptomic and proteomic studies have further demonstrated that the functional consequences of gene triplication are complex and extend beyond the DSCR, casting doubt on its sufficiency in accounting for the full spectrum of DS features[299,302-304].

4.2.2. Down syndrome and Alzheimer's disease

Advancements in medical care for individuals with DS over recent decades have significantly increased life expectancy, now exceeding 60 years (**Figure 7**)[305-307]. As a result, this aging population shows a higher prevalence of age-related co-occurring conditions, including AD[308]. Nearly all individuals with DS exhibit neuropathological features of early-onset AD by age 40, and between 88% and nearly 100% of those over 60 years old develop AD-related dementia, which is currently the leading cause of death in this population[309]. There is a common assumption that the age at onset of dementia varies widely among individuals[74,310-313]. However, despite a shared genetic predisposition, dementia rarely occurs before the age of 40, and the onset and severity of clinical dementia resembles the patterns

observed in ADAD[314]. In this context, researchers often use the concept of estimated year to onset (EYO), which aligns an individual's age relative to the expected age of symptom onset. This allows comparisons across individuals who share a genetic predisposition but differ in the timing of clinical manifestation[315,316].

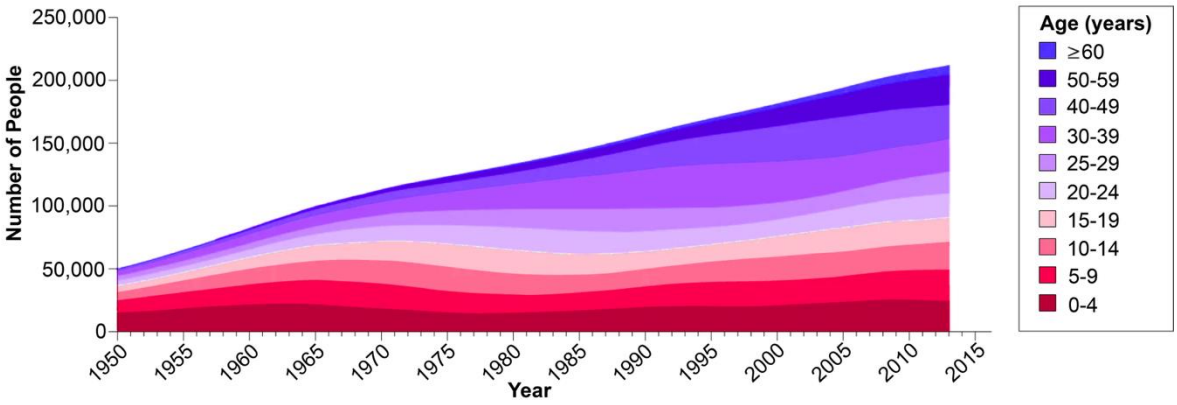

Figure 7. Prevalence of Down syndrome in the U.S. *The graph combines prevalence of DS data between 1950-2010 and data from 2011-2013 in the U.S. Figure modified from Antonarakis et al. 2020[271].*

The strong association between DS and AD is primarily attributed to the triplication of the *APP* gene on Hsa21[9,317,318]. Two reported cases involving individuals aged 78 and 65 with partial trisomy 21 and clinical features of DS, but only two copies of the *APP* gene, showed neither biomarker nor clinical signs of AD. These findings support the notion that *APP* triplication is both necessary and sufficient to drive EOAD in DS[74,317,319]. Consequently, DS is considered a genetically determined form of AD, akin to ADAD[320].

4.2.2.1. AD neuropathology in DS

The hallmark neuropathological lesions of AD exhibit a similar appearance and distribution in DS compared to the sporadic and autosomal dominant forms of the disease[74]. Intracellular Aβ disrupts endosomal dynamics and morphology. Aβ has been reported in enlarged endosomes and lysosomes as early as 28 weeks of gestation[321,322]. Electron microscopy studies later revealed that endosomes are not necessarily larger, but instead more numerous and clustered, which appear as enlarged endosomes under conventional light microscopy[323]. Aβ accumulation within endosomes can induce mitochondrial dysfunction and lead to oxidative damage[324]. Diffuse amyloid plaques become detectable as early as adolescence, followed by a steep accumulation of dense and neuritic plaques by age 40[58,59].

Although the general patterns of AD pathology are comparable across subtypes, individuals with DS show greater accumulation of Aβ plaques and NFTs in the hippocampal region than those with EOAD and LOAD[59,86,325]. The earliest pathological changes, such as diffuse plaques, are not directly detectable through biomarkers, but likely contribute to the pseudo-normal CSF Aβ levels observed in young adults. Notably, changes in CSF Aβ and Tau can be detected roughly a decade before these alterations become evident through PET imaging (**Figure 8**)[74].

Diffuse amyloid plaques composed predominantly of $A\beta_{1-42}$ have been observed before the age of 20 in individuals with DS[58], suggesting that these diffuse deposits precede the formation of cortical neuritic plaques. $A\beta_{1-42}$ plaques are more prevalent than $A\beta_{1-40}$ across all age groups[58,326]. Diffuse $A\beta_{1-42}$ deposits have also been identified in the cerebellum and striatum as early as age 30, while fibrillar plaques are rarely found in these regions even in older individuals, indicating a region-specific progression of plaque pathology[327]. Aβ undergoes various post-translational modifications, including isomerization, racemization and oxidation[328-330].

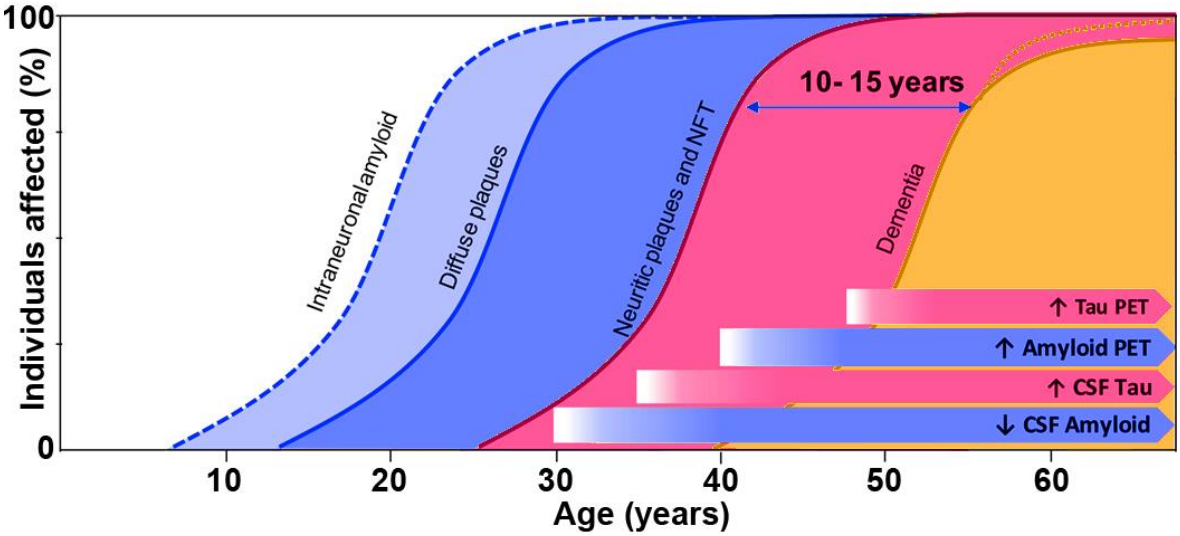

Figure 8. Progressive accumulation of AD neuropathology across the lifespan in DS. *Accumulation of intraneuronal Aβ starts in the first decade of life (blue dotted line). Extracellular diffuse deposits are observed in teenagers and after 30 years of age. The pathology progresses with the accumulation of neuritic plaques and appearance of NFTs in the fourth decade. In vivo biomarkers for Aβ and Tau can be detected between 30 and 40 years of age, almost a decade before PET biomarkers are detectable. Figure modified from Fortea et al. 2021[74].*

Prior evidence suggests increased levels of pyroglutamate-3 Aβ in the plasma of older individuals with DS compared to non-DS individuals with and without developmental disabilities, along with pyroglutamate-11 Aβ in plaque cores and vascular Aβ in DS[331-333]. More recently, elevated levels of phosphorylated and

pyroglutamate Aβ species have been reported in amyloid plaques from DS brains compared to EOAD[334].

While vascular pathologies such as atherosclerosis, arteriolosclerosis, and hypertension are uncommon in individuals with DS[71], CAA is more frequent and severe in DS than in both early-onset and sporadic forms of AD (explained in **section 4.1.3.1.2**)[71,311,335]. Nonetheless, the severity of CAA in DS does not appear to be associated with the presence of the apoE4 isoform, despite its known correlation with CAA in EOAD[335].

Early Tau neuropathology has been observed in the outer molecular layer of the hippocampus in individuals with DS between 30 and 40 years of age, followed by the formation of NFTs in the CA1 and subiculum regions, along with neuronal loss in the entorhinal cortex[336]. While NFTs in DS follow a distribution pattern similar to that of AD, NFT density is notably higher in DS brains[337]. The exacerbated Tau pathology in DS may be influenced by the overexpression of the dual-specificity tyrosine-phosphorylation-regulated kinase 1A (*DYRK1A*) gene and the regulator of calcineurin-1 (*RCAN1* or calcipressin 1) gene, both located on Hsa21[338,339]. These genes encode proteins that modulate Tau phosphorylation (as further discussed in **section 4.2.2.2**).

4.2.2.2. Pathogenesis of AD in DS

4.2.2.2.1 Genes of Interest for AD in DS

The primary link between AD and DS is the triplication of *APP*. However, Hsa21 harbors other genes of interest implicated in AD pathology, such as S100β, *DYRK1A*, *SOD1*, *BACE2* among others (**Figure 9**)[313,339-342].

DYRK1A phosphorylates Tau and enhances its suitability for subsequent phosphorylation by GSK3β. Additionally, DYRK1A phosphorylates alternate splicing factors, leading to an increased 3R:4R Tau isoform ratio, which is associated with neurodegeneration. Supporting these findings, individuals with DS aged 30-40 years and older show a greater number of DYRK1A-positive and 3R Tau-positive NFTs compared to those with sporadic AD[339].

RCAN1 is elevated in the hippocampus and cerebral cortex in AD brains. By inhibiting calcineurin, RCAN1 may promote Tau phosphorylation through reduced phosphatase activity and increased GSK3β levels[338,343]. Some evidence also suggests that $A\beta_{1-42}$ upregulates both RCAN1 and DYRK1A[344,345].

Superoxide dismutase 1 (SOD1) plays a critical role in cellular antioxidant defense by catalyzing the dismutation of O_2^- to O_2 and H_2O_2, which is further converted to water by catalase and glutathione peroxidase[346]. Triplication of SOD1 disrupts the balance among these enzymes, resulting in the accumulation of H_2O_2[347].

Two Hsa21 genes, β secretase 2 (*BACE2*) and Synaptojanin 1 (*SYNJ1*), have been implicated in Aβ processing and clearance. BACE2 is an aspartyl protease capable of cleaving APP at the β site, generating Aβ peptide[348]. However, some evidence suggests BACE2 could function as an alternative α-secretase, and Sun and colleagues demonstrated that BACE2 can also cleave APP at a θ-site between residues 671 and 672, thereby preventing Aβ production[349-351]. SYNJ1 is a phosphoinositide phosphatase upregulated in DS brains, and is involved in endocytosis, endosomal trafficking and synaptic vesicle recycling[352].

SYNJ1 dysfunction has been linked to AD neurodegeneration, potentially by inducing endosomal abnormalities, and it shows a strong correlation with Aβ levels in DS[353]. Protein S100β is a neurite growth-promoting factor derived from astrocytes[354]. S100β levels are elevated in neural progenitor cells in individuals with DS[355,356] and are significantly increased in AD brains, primarily due to astrocyte activation in response to amyloid plaques[357].

In addition, Hsa21 contains four genes encoding interferon receptors *IFNAR1*, *IFNAR2*, *IFNGR2* and *IL10RB*[358]. Their triplication results in sustained activation of the interferon (IFN) pathway, which can drive microglial activation and contribute to neurotoxicity[359].

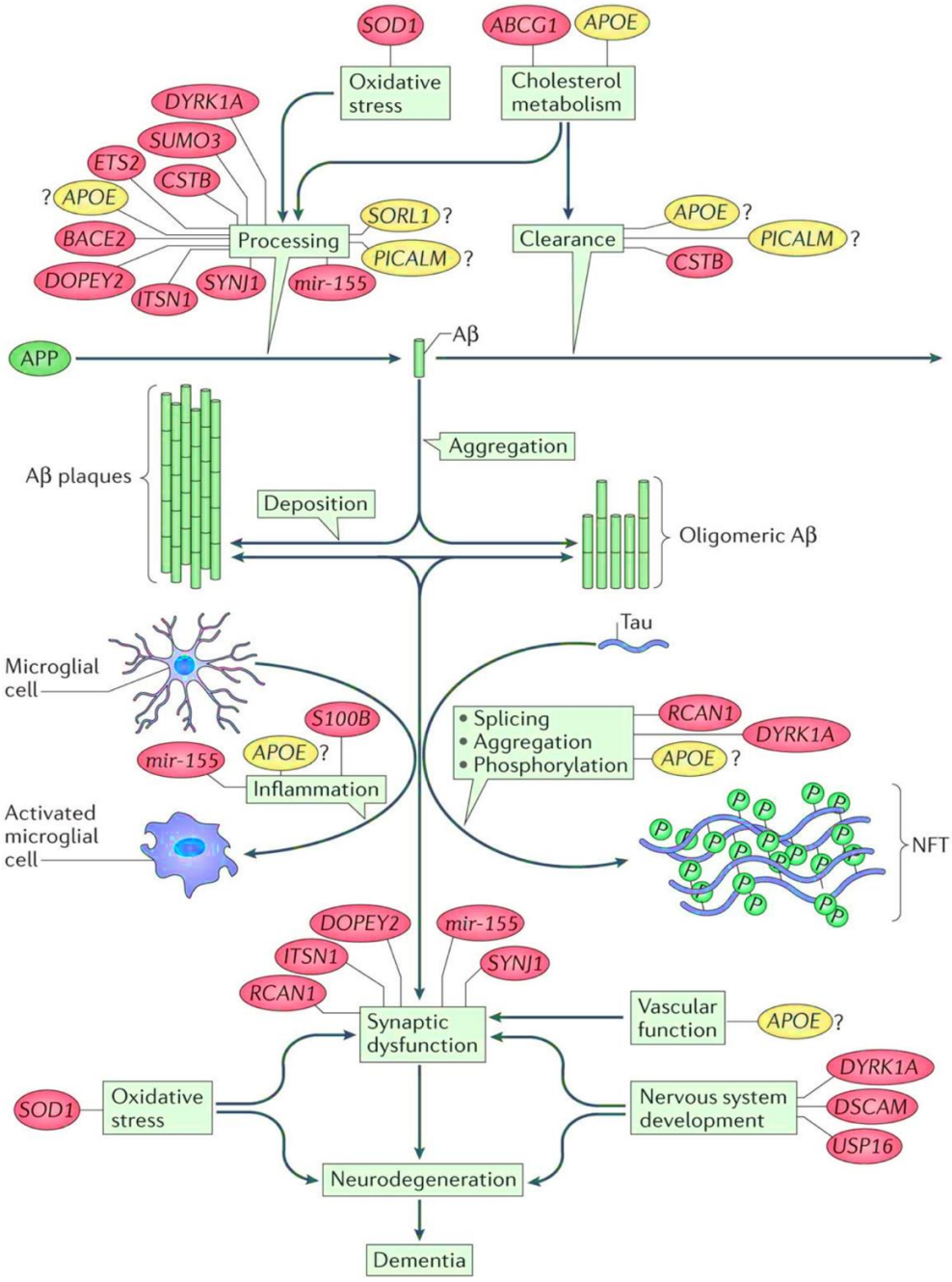

Figure 9. Potential mechanisms of AD pathogenesis in DS and associated genes. *Several genes may modulate relevant processes for AD in DS, including non-Hsa21 genes (indicated in yellow) such as APOE, PICALM, SORL1 related to cholesterol metabolism, APP processing and endo-lysosomal pathways. Multiple Hsa21 genes (indicated in red) are involved in APP and cholesterol metabolism, oxidative stress, synaptic function and inflammation. However, the importance of these genes and precise mechanisms remain to be studied. Figure adapted from Wiseman et al. 2015[360].*

4.2.2.2.2 Neuroinflammation in DS with AD

Section **4.1.4.3** described how neuroinflammation is a main component in the pathogenesis of AD. Immune response and neuroinflammation have been linked to

the clearance of Aβ deposits as well as to the exacerbation of amyloid plaques and Tau pathology[331]. Several genes in Hsa21 are triplicated in people with DS and play critical roles in neuroinflammatory processes (**Table 2**)[361].

As most of the genes from Hsa21 related to neuroinflammation are associated with the pro-inflammatory response observed in macrophages with phenotype M1, it was hypothesized that DS would exhibit an exacerbated M1 inflammatory response[361]. However, subsequent studies by Wilcock and colleagues using brain tissue samples from individuals with DS, DSAD and sporadic AD showed that DS cases under 40 years of age exhibited a bias toward M1/M2b phenotypes, whereas older DSAD cases showed a distinct M2b profile. This phenotype, typically associated with the presence of immune complexes, was rarely observed in sporadic AD, highlighting mechanistic differences in the neuroinflammatory process between DSAD and sporadic AD[362].

Table 2. *Genes of interest for neuroinflammation located in Hsa21.*

Gene	Protein Name	Function
CXADR	Coxsackie virus and adenovirus receptor	Activation of JNK and p38-MAPK pathways leading to production of M1 cytokines.
ADAMTS1	ADAM metalloproteinase with thrombospondin type 1 motif, 1	Secreted protease degrades extracellular matrix (ECM) proteoglycans and is induced by IL-1*β*
ADAMTS5	ADAM metalloproteinase with thrombospondin type 1 motif, 5	Secreted protease degrades ECM proteoglycans and is induced by IL-1*β* and TGF*β*.
TIAM1	T-cell lymphoma invasion and metastasis 1	Necessary for cytokine-mediated generation of oxidative species through NADPH oxidase.
IFNAR2	Interferon (alpha, beta, and omega) receptor 2	Activates JAK/STAT-mediated pathway in response to IFN*α*/*β*.
IFNAR1	Interferon (alpha, beta, and omega) receptor 1	Activates JAK/STAT-mediated pathway in response to IFN*α*/*β*.

IFNGR2	Interferon gamma receptor 2	Activates JAK/STAT-mediated pathway in response to IFN*γ*.
RIPK4	Receptor-interacting serine-threonine kinase 4	Necessary for signaling through TNFR1
CBS	Cystathione-beta-synthase	Participates in the production of hydrogen sulfide (H_2S); which regulates inflammation
S100B	S100 calcium binding protein B	Secreted by astrocytes in response to IL-1*β* and cyclic AMP
PRMT2	Protein arginine methyltransferase 2	Regulates JAK/STAT pathway by the methylation of arginine

Table adapted from Wilcock 2012[361].

Microglial cells undergo morphological changes in response to AD pathology, showing increased frequencies of amoeboid and rod-like shapes, along with reduced ramified microglia, compared to LOAD[363,364]. These rod-like microglia are associated with Tau pathology and are found in proximity to dystrophic axons[363]. Interestingly, such rod-like microglia have been observed in transgenic murine models of Tau pathology but not in Aβ mouse models[363,365,366]. In DSAD, there is also an increased expression of microglial markers associated with activation and phagocytosis, such as CD64 and CD86, compared to LOAD[362]. Flores-Aguilar and colleagues described the dynamic course of neuroinflammation in DS across the lifespan[363]. Fetal and neonatal brains show IL-1–positive microglia, reactive astrocytes, and oxidative stress, while young adults display elevated proinflammatory cytokines such as IL-1, IL-6, and IL-8[363]. In older adults, cytokine levels shift, with reductions in VEGF-A, IFNγ, TNFα, and IL-12p40, indicating immune decline similar to LOAD[363]. Other mediators, including IL-10 and TREM2, follow biphasic patterns across age, suggesting stage-specific effects on microglial function[363]. Microglial morphology in children and young adults show changes consistent with intermediate activation states, which progress in older adults to fully activated and dystrophic microglia with enlarged somas and shortened processes, consistent with chronic inflammation leading to exhaustion and degeneration[363].

4.2.2.2.3 Endo-lysosomal pathways in DSAD

Secretory and endosomal machinery are central to AD neuropathology in DS. The degradation of ubiquitinated cargo relies on the proper formation and function of the endo-lysosomal system, which can be disrupted by impaired lysosomal acidification, inactivation of cathepsin D, and altered hydrolase activity[367]. Rab GTPase rab5 acts as a master regulator of endocytosis, cycling between an inactive GDP-bound and an active GTP-bound state[368]. Maturation of endosomes involves the conversion from rab5- to rab7-positive vesicles, marking the transition to late endosomes. This process is mediated by GTP-bound rab5 through signaling mechanisms that lead to rab7 recruitment and activation, followed by rab5 inactivation[369-371].

Brains from individuals with DS and DSAD show morphological abnormalities in late endosomes, including clustering, which is one of the earliest alterations observed in AD and DS, not observed in normally aged brains[321]. Analyses of CA1 neurons have demonstrated upregulation of rab5 and rab7 GTPases, suggesting impaired coordination between these two regulators[372]. One mechanism underlying endosomal dysfunction involves the CTFβ fragment produced during the amyloidogenic processing of APP by the β site cleaving enzyme 1 (BACE1), which occurs primarily in endosomes[373]. CTFβ can bind to APPL1, causing hyperactivation of rab5 and slowing endosomal transport, impairing endosomal maturation and reducing neuronal support[374,375].

Further evidence from *in vitro* studies in fibroblasts from individuals with DS and murine models of DS shows that modest overexpression of endogenous APP is sufficient to induce lysosomal disruption, with elevated CTFβ levels being the most likely cause[376]. Lysosomal acidification is essential for its functions, particularly proteolysis, axonal cargo transport, and signaling[377,378]. Studies using AD mouse models and fibroblasts derived from individuals with DS have revealed lysosomal de-acidification as a prominent feature of endo-lysosomal dysfunction[375].

Additionally, as mentioned, genome-wide association studies (GWAS) have identified AD risk polymorphisms in genes encoding PICALM, BIN1, SORL1 and CD2AP, all of which directly regulate the endo-lysosomal pathway[194].

4.2.2.2.4 Oligodendrocytes and white matter defects in DSAD

As described in section **4.1.4.3.3**, oligodendrocytes are active contributors to AD neuropathology, transitioning to a disease-associated state characterized by both loss of function and gain of toxic properties[379]. A comprehensive transcriptomic study using post-mortem brain tissue samples from individuals with DS, spanning mid-fetal development to adulthood, revealed substantial dysregulation of genes involved in oligodendrocyte differentiation and myelination[380]. Histological analysis further demonstrated a reduction in overall myelinated fiber density and decreased structural complexity in myelinated axonal patterns compared to control brains[380]. Ultrastructural imaging in a DS mouse model also showed a lower number of small-bore myelinated axons and thinner myelin sheaths in white matter[380]. Additionally, Aβ aggregates have been observed in the white matter of the frontal cortex in individuals with DS, where they exhibit cytotoxic effects on oligodendrocytes[381,382].

In individuals with DS at the MCI stage, altered white matter integrity has been detected in late-myelinating fiber bundles within commissural and limbic pathways, suggesting early white matter dysfunction during AD progression[383]. In dementia, these alterations become more widespread, affecting cortico-cortical association pathways as seen in sporadic AD[383,384]. Changes in white matter microstructure, particularly in frontal lobe circuitry, may underlie cognitive impairment that precedes cortical atrophy in DSAD[385].

4.2.3. Advancing Alzheimer's research through the study of Down syndrome

As discussed in the preceding sections, there is substantial overlap between the neuropathological features of AD in individuals with DS and those observed in other forms of AD, including EOAD and LOAD, suggesting the presence of common pathogenic mechanisms. Aβ accumulates in extracellular plaques and within blood vessel walls, although amyloid deposition begins decades earlier in DS compared to LOAD[386]. NFTs appear later, with the hippocampus, entorhinal cortex, and

neocortex as the most affected regions[387]. The distribution of Aβ plaques and NFTs is similar in DS and AD, though with greater density in DS[337].

Early research into DS neuropathology played a critical role in shaping the amyloid hypothesis. Glenner and Wong isolated the Aβ peptide from the brain vasculature of individuals with DS and demonstrated its similarity to the Aβ found in LOAD brains, providing an early link between Hsa21 and AD pathology[313]. Subsequently, *APP* mutations on Hsa21 that increase $A\beta_{1-42}$ levels were identified in cases of ADAD, supporting a common mechanism of Aβ dysregulation across LOAD, ADAD, and DSAD[197,388].

In addition to these classical hallmarks, individuals with DSAD exhibit neuroinflammatory changes that correlate with cognitive decline, mirroring those seen in AD[361]. Similarly, the endo-lysosomal network, is disrupted early in DS[194,374,375,389]. White matter alterations due to dysfunctional oligodendrocytes are also observed in both DS and non-DS AD cases[124,380,383].

Research on DSAD provides insight into LOAD mechanisms by advancing our understanding of AD neurobiology and supporting the identification of biomarkers linked to cognitive decline and disease progression. The extremely high prevalence of AD in this population presents a unique opportunity to explore strategies for slowing, halting, or preventing the disease. Moreover, the high incidence of AD among adults with DS, together with the possibility of identifying individuals with trisomy 21 at or before birth, highlights the potential for implementing early interventions or preventive approaches during preclinical stages[386,390].

4.2.3.1. Clinical trials for DSAD

No individuals with DS have been included in passive immunization trials against Aβ that led to US Food and Drug Administration approval of treatments. Because DS requires different cognitive outcome measures and has higher prevalence of CAA compared to sporadic AD, current recommendations advise against the use of approved disease-modifying therapies in DSAD[391]. Several clinical trials through the Alzheimer's Clinical Trials Consortium–Down Syndrome (ACTC–DS) are now testing treatments targeting Aβ pathology in this population. These include ABATE, a phase 1b/2 trial of the anti-Aβ active immunotherapy ACI-24.060 in prodromal

sporadic AD and DSAD; Hero, a phase 1b trial of the antisense oligonucleotide ION269 targeting the *APP* gene; and ALADDIN, a phase 4 trial evaluating the safety and tolerability of donanemab[391]. Future ACTC–DS studies linked to the Trial Ready Cohort–Down Syndrome are planned to explore *APP* silencing with siRNA technologies as well as non-pharmacological interventions[391].

Recent clinical trials targeting immune dysregulation in Down syndrome have shown promising results. A Phase II trial of the JAK1/3 inhibitor tofacitinib in individuals with DS demonstrated good safety and preliminary efficacy, with improvements in autoimmune skin conditions and reductions in interferon signaling, inflammatory cytokines and autoantibodies[392]. These findings support the potential of immunomodulatory therapies in addressing the underlying inflammatory burden associated with DS-related Alzheimer's disease.

4.3. Use of proteomics approaches for the study of AD

AD is a heterogeneous, multifaceted disorder with complex causes influenced by a combination of genetic, environmental, and lifestyle factors (reviewed in sections **4.1.2** to **4.1.4**). The diagnosis of AD is confirmed *post-mortem* by the presence of Aβ plaques and NFTs[393]. Early evidence and most recent findings suggest that AD neuropathology extends beyond Aβ and Tau proteins[334,394]. Additional associated processes to the Aβ and Tau neuropathology are neuroinflammation, endo-lysosomal pathways alteration, white matter and synaptic dysfunction, and progressive neuronal loss, ultimately leading to cognitive decline[395]. Evidence from imaging and biomarker studies indicates that the disease process begins approximately two decades before clinical symptoms emerge, suggesting a prolonged preclinical phase[28].

Despite considerable research, key aspects of AD pathogenesis remain unclear. It is still unknown the causal factors of AD, what mechanisms drive the accumulation of Aβ and Tau pathology, what factors lead to cognitive decline, or why disease progression varies so widely among individuals. The same questions apply to DSAD; despite the gene dosage effect of *APP* and subsequent impact in amyloid

pathology, there are hidden factors that result in an atypical pathological progression of AD until the 30's in people with DS, and the clinical manifestations of AD emerge decades after the onset of pathological events, which begin as early as childhood (see section **4.2**).

Addressing these gaps is essential for advancing therapeutic strategies and identifying reliable biomarkers. The urgent need for new treatments is underscored by the high failure rate of AD clinical trials and the limited number of therapies that can modify disease progression[395]. This lack of success has been attributed to several challenges, including the initiation of treatment too late in the disease course, incorrect therapeutic targets, and limitations in the relevance of animal models that do not accurately reflect the human form of AD[396,397].

Research on AD pathogenesis has often employed hypothesis-driven approaches focusing on specific proteins[395]. This strategy has led to major findings including the identification of Aβ as the main component of plaques[9,10], Tau as the major component of NFTs[83], and ApoE as the strongest risk factor for LOAD[221,398]. However, by focusing on predetermined targets, this method limits the discovery of novel proteins and restricts a broader understanding of protein alterations in AD.

4.3.1. Unbiased high throughput approaches for the analysis of AD

More recently, several studies aiming to understand AD pathogenesis have employed *hypothesis-free* high-throughput techniques known as "omics" approaches. These include genome-wide association studies (GWAS), whole-genome sequencing (WGS), and whole-exome sequencing (WES) for genomics; RNA sequencing (RNAseq) and microarray analysis for transcriptomics; and Liquid Chromatography-Mass Spectrometry (LC-MS) for proteomics analysis, among other strategies[395].

A pioneer AD GWAS study by Coon and colleagues identified *APOE* as a major risk factor for LOAD, followed by two large-scale GWAS that uncovered *CLU*, *PICALM*, and *CR1* as additional genetic risk factors for AD[246,399,400]. WGS efforts further led

to the discovery of two fundamental AD-associated genes, *TREM2* and *BIN1*[137,401,402].

Large-scale RNAseq studies using *post-mortem* AD brain tissues from the Mayo Clinic Brain Bank, the Religious Orders Study and Memory and Aging Project (ROSMAP) and Mount Sinai School of Medicine (MSSM) identified critical mechanisms in AD pathogenesis. These included the downregulation of myelination networks, dysregulation of the cell cycle, and the identification of *INPPL1* and *PLXNB1* as genes associated with Aβ levels[403,404]. Building on these findings, Morabito and collaborators integrated bulk RNAseq data from these three cohorts with epigenetic datasets and their own single-nucleus RNAseq data to generate a more comprehensive view of genome-wide changes in AD[405]. Their study revealed that pathways related to calcium signaling, ubiquitination, and mitochondrial function are neuron specific. Moreover, microglial clusters were highly enriched in genes linked to increased AD risk, a pattern not observed in other tauopathies, underscoring the relevance of the combined presence of Aβ and Tau pathology in AD[405].

While genomics and transcriptomics have uncovered important genetic risk factors for AD, these approaches have inherent limitations. They often fail to capture post-translational protein modifications, the functional impact of risk-associated genes, and susceptibility loci located in non-coding regions. Furthermore, proteomics studies have demonstrated alterations at the protein level that are not reflected in transcriptomic data [170,406].

4.3.2. Proteomics approaches for AD research

Proteomics studies of human AD brain tissues using mass spectrometry (MS) are crucial to complement genomic approaches, as proteins and the metabolic pathways they regulate often represent the final effectors of genetic and environmental risk in AD[170,395]. In the past, MS-based proteomics was limited by technical constraints, offering less comprehensive analyte coverage compared to genomics methods[170,395]. However, recent advances in proteomics technologies, including more accessible and refined instruments, expanded protein databases, and improved bioinformatic tools, have enhanced the ability to extract accurate

information from raw MS data[168]. Bottom-up proteomics offers several advantages including enabling the simultaneous quantification of thousands of proteins from microscopic samples, detects post-translational modifications such as phosphorylation and ubiquitination that are implicated in AD pathogenesis, and maintains an unbiased approach that facilitates the discovery of novel proteins involved in the disease[395].

4.3.2.1. Proteomics using bulk tissue homogenates

Most proteomic studies of human AD brain tissue have examined protein changes in bulk samples, typically comparing AD cases to age-matched cognitively normal individuals and focusing on a single vulnerable brain region. Several large-scale studies have identified consistently altered proteins across cohorts, supporting their relevance to AD pathogenesis[170,406-413]. Some of the most comprehensive analyses have compared protein expression in advanced AD, preclinical AD, and age-matched controls using frontal cortex samples. These studies have revealed hundreds of protein alterations across disease stages, with changes increasing progressively with AD severity, indicating that disease progression involves a growing number of dysregulated pathways contributing to physiological dysfunction and cognitive decline[170,406,409,412]. Main pathways identified include anti-inflammatory glial responses and altered RNA binding and splicing at preclinical stages, followed by progressive disruption of synaptic function and synaptogenesis, and a pronounced inflammatory response in later stages marked by elevated astrocytic and microglial proteins, aligning with the extent of neuropathology.

4.3.2.2. CSF proteomics

CSF is the most accessible biofluid to study the molecular complexity of neurodegenerative diseases *in vivo*[414]. MS-based proteomics have enabled large-scale screening of biofluids through both unbiased and targeted approaches to expand our understanding of AD mechanisms and facilitate biomarker discovery[415]. In addition, affinity-based technologies such as Olink and SomaScan are increasingly employed for proteomic analysis of CSF. Olink uses DNA-tagged, target-specific antibodies to enable relative protein quantification through sequencing after antibody binding[416]. SomaScan employs target-specific DNA-

based aptamers, with relative protein levels quantified via next-generation sequencing[417].

De Geus and colleagues compiled CSF proteomics studies utilizing MS- and affinity-based methods, identifying 1448 differentially enriched proteins between AD and controls[415]. Among these, 32 proteins showed the highest overlap across studies, including SPARC-related modular calcium-binding protein 1 (SMOC1) and chitinase-3 like-protein-1 (CHI3L1), which are recognized markers of AD[418,419]. Clustering and functional enrichment analyses revealed upregulation of pathways related to glycolytic metabolism, glutathione metabolism, and the 14-3-3 protein family, which has also been reported to be altered in AD brain tissue[415]. Overall, these findings highlight CSF proteins that are consistently reported in AD, some of which have also been identified in brain tissue, underscoring their potential as novel biomarkers[415].

4.3.2.3. Localized proteomics to study neuropathological features of AD

Localized proteomics strategies targeting disease-associated pathological features or specific cell populations offer valuable insights into mechanisms relevant to AD pathogenesis, both in comparison with controls and across different subtypes of the disease. In this approach, Aβ plaques, NFTs, CAA or vulnerable cell types are microdissected from human brain tissue sections and analyzed by MS[420,421]. Importantly, this method is compatible with formalin-fixed and paraffin-embedded (FFPE) tissues, which constitute a major source of human brain specimens in biobanks worldwide, particularly from autopsy collections. This compatibility increases the feasibility of conducting studies on human tissues, including rare cases[395]. Additionally, localized proteomics can be performed using microscopic amounts of tissue (approximately 2 mm^2), while still enabling the identification of over a thousand proteins[395].

This approach has led to the identification of hundreds of proteins within amyloid plaques, including COL25A1, which is more abundant than Aβ itself, as well as numerous proteins not previously linked to AD pathology[264,334,422,423]. Studies using localized proteomics have also revealed significant differences in the protein

composition of Aβ plaques between rpAD and LOAD, and have identified the protein signature of EOAD, LOAD, and DS plaques[264,334,423]. Furthermore, over 500 proteins have been identified in NFTs, including several novel components not previously associated with Tau pathology[424]. Most recently, the proteome of CAA was characterized in AD, MCI, and age-matched control cases, revealing significant protein differences among groups and alterations in pathways related to the extracellular matrix. Notably, the protein SEMA3G was identified as a CAA-specific marker and validated by immunohistochemistry[70].

4.3.2.4. Affinity purification-MS for the analysis of Aβ and Tau interactomes

Affinity purification followed by mass spectrometry (MS) enables the isolation of a protein of interest, such as Aβ or Tau, along with its interacting partners, using specific antibodies. These co-isolated proteins are then identified by MS, providing an unbiased and comprehensive profile of the interactome relevant to Aβ or Tau pathology in AD[395]. This strategy contributes to a better understanding of AD pathogenesis and can support the discovery of novel biomarkers or therapeutic targets.

Ayyadevara and colleagues applied this method to isolate aggregated Aβ complexes from human brain tissue using a non-specific Aβ antibody that also recognizes full-length APP. To improve specificity, their proteomic analysis focused only on the insoluble fraction, under the assumption that it would be enriched in proteins associated with insoluble Aβ aggregates[425]. Another study used monomeric and oligomeric $A\beta_{1-42}$ bound to beads to pull down interacting proteins from AD brain samples[426]. Together, these studies identified over 100 Aβ-interacting proteins, with a preference for binding to oligomeric forms rather than monomers. Despite these advances, Aβ interactome studies remain limited, largely due to the lack of antibodies that selectively recognize Aβ without cross-reacting with APP[395].

Several studies have examined the Tau interactome in human brain tissues and identified protein interactions specific to Tau isoforms, as well as potential therapeutic candidates to mitigate Tau toxicity[425,427]. However, the use of antibodies against total Tau in these studies limited their ability to distinguish between

physiological and pathological interactions. To address this, Drummond and collaborators investigated the interactome of phosphorylated Tau (pTau) using the PHF-1 antibody, which specifically recognizes paired helical filaments[424]. This approach revealed 75 pTau interactors, including 29 previously known to associate with pTau, 34 previously associated only with total Tau, and 12 novel proteins not formerly linked to Tau or pTau[424].

Two recent studies extended this work by characterizing pTau interactors across different *APOE* haplotypes[428,429]. One study used the PHF-1 antibody and identified 80 interactors in *APOE*ε3/ε3 and 68 in *APOE*ε4/ε4 AD cases. Interactors in *APOE*ε3/ε3 brains were primarily associated with the nucleoplasm and RNA processing, while those in *APOE*ε4/ε4 brains were more linked to synaptic compartments and cellular transport[429]. The second study focused on Tau phosphorylated at threonine 217 (pT217), an early marker of AD pathology, and identified 23 interactors, including SQSTM1, a known pTau-binding protein. Notably, five subunits of the CTLH E3 ubiquitin ligase complex, previously unlinked to AD, were among the interactors. Although more proteins interacted with pT217 in *APOE*ε3/ε3 cases than in ε4/ε4, CTLH subunits were common to both genotypes[428].

5. SPECIFIC AIMS

5.1. Biological Question

Understanding the molecular mechanisms that drive Alzheimer's disease (AD) remains a major challenge in neurodegenerative research. Although the accumulation of Aβ plaques and Tau neurofibrillary tangles defines the pathology, the processes that lead to their formation and the ways they vary among etiological subtypes of AD, such as early-onset AD (EOAD), late-onset AD (LOAD), and Down syndrome with Alzheimer's disease (DSAD), are not fully understood. Individuals with DS develop AD with near-universal penetrance mainly due to the triplication of the *APP* gene[74]. The prevalence of DSAD increases with age and, at comparable estimated years to symptom onset, exceeds that of autosomal dominant inherited forms of AD. Individuals with DS also exhibit a more homogeneous, age-dependent pathology than those with LOAD, making AD in people with DS is a compelling opportunity to investigate disease pathophysiology and progression[74,308,390,430].

An overarching biological question addressed in this thesis is how DSAD compares to other forms of AD at the proteomic level. Specifically, **to what extent do the molecular features of DSAD resemble or diverge from those of EOAD, LOAD and ADAD?** Mass spectrometry-based proteomics provides a direct approach to characterize disease-relevant proteins and pathways in human tissues and fluids. Through comparative analysis of Aβ plaque proteomes and CSF proteomics, this work aimed to characterize shared and distinct molecular signatures across AD subtypes and improve our understanding of the mechanisms that underlie disease progression.

To further investigate molecular mechanisms in DSAD, this thesis includes findings that lay the groundwork for future studies of the Aβ interactome. Using an affinity purification–mass spectrometry approach previously applied to the pTau interactome[429], this strategy will examine Aβ-interacting proteins in DSAD, providing

a complementary path to identify disease-relevant pathways beyond global proteomic profiling.

5.2. Research Objectives

1. To characterize and compare the protein composition of Aβ plaques in DS, EOAD, and LOAD using unbiased localized proteomics.

   Article 1: *Comparison of the Amyloid Plaque Proteome in Down Syndrome, Early-Onset Alzheimer's Disease and Late-Onset Alzheimer's Disease*.

   PMID: 39825890; DOI: 10.1007/s00401-025-02844-z

   Article 2: *The amyloid plaque proteome in early onset Alzheimer's disease and Down syndrome*.
   PMID: 35418158; DOI: 10.1186/s40478-022-01356-1

2. To evaluate proteomics changes in CSF of individuals with DS and to compare the findings with ADAD and LOAD.

   Article 3: *Proteomic analysis of Down syndrome cerebrospinal fluid compared to late-onset and autosomal dominant Alzheimer´s disease*.

   PMID: 40595720; DOI: 10.1038/s41467-025-61054-z

6. RESULTS

6.1. Unbiased localized proteomics for the characterization of Aβ plaques in DS and AD.

Article 1: Comparison of the amyloid plaque proteome in Down syndrome, early-onset Alzheimer's disease, and late-onset Alzheimer's disease.

Article 2: The amyloid plaque proteome in early onset Alzheimer's disease and Down syndrome.

Acta Neuropathologica (2025) 149:9
https://doi.org/10.1007/s00401-025-02844-z

ORIGINAL PAPER

Comparison of the amyloid plaque proteome in Down syndrome, early-onset Alzheimer's disease, and late-onset Alzheimer's disease

Mitchell Martá-Ariza[1,2,3] · Dominique F. Leitner[1,2,4] · Evgeny Kanshin[5,6] · Jianina Suazo[1,2] · Ana Giusti Pedrosa[7] · Manon Thierry[1,2] · Edward B. Lee[8] · Orrin Devinsky[1,4] · Eleanor Drummond[2,9] · Juan Fortea[10,11,12] · Alberto Lleó[10,11] · Beatrix Ueberheide[1,5,6] · Thomas Wisniewski[1,2,13,14]

Received: 8 November 2024 / Revised: 2 January 2025 / Accepted: 4 January 2025

Abstract

Down syndrome (DS) is strongly associated with Alzheimer's disease (AD) due to *APP* overexpression, exhibiting Amyloid-β (Aβ) and Tau pathology similar to early-onset (EOAD) and late-onset AD (LOAD). We evaluated the Aβ plaque proteome of DS, EOAD, and LOAD using unbiased localized proteomics on post-mortem paraffin-embedded tissues from four cohorts ($n = 20$/group): DS (59.8 ± 4.99 y/o), EOAD (63 ± 4.07 y/o), LOAD (82.1 ± 6.37 y/o), and controls (66.4 ± 13.04). We identified differentially abundant proteins when comparing Aβ plaques and neighboring non-plaque tissue (FDR < 5%, fold-change > 1.5) in DS ($n = 132$), EOAD ($n = 192$), and LOAD ($n = 128$), with 43 plaque-associated proteins shared across all groups. Positive correlations were observed between plaque-associated proteins in DS and EOAD ($R^2 = .77$), DS and LOAD ($R^2 = .73$), and EOAD and LOAD ($R^2 = .67$). Top gene ontology biological processes (GOBP) included lysosomal transport ($p = 1.29 \times 10^{-5}$) for DS, immune system regulation ($p = 4.33 \times 10^{-5}$) for EOAD, and lysosome organization ($p = 0.029$) for LOAD. Protein networks revealed a plaque-associated protein signature involving APP metabolism, immune response, and lysosomal functions. In DS, EOAD, and LOAD non-plaque vs. control tissue, we identified 263, 269, and 301 differentially abundant proteins, with 65 altered proteins shared across all cohorts. Non-plaque proteins in DS showed modest correlations with EOAD ($R^2 = .59$) and LOAD ($R^2 = .33$) compared to the correlation between EOAD and LOAD ($R^2 = .79$). Top GOBP term for all groups was chromatin remodeling ($p < 0.001$), with additional terms for DS including extracellular matrix, and protein–DNA complexes and gene expression regulation for EOAD and LOAD. Our study reveals key functional characteristics of the amyloid plaque proteome in DS, compared to EOAD and LOAD, highlighting shared pathways in endo/lysosomal functions and immune responses. The non-plaque proteome revealed distinct alterations in ECM and chromatin structure, underscoring unique differences between DS and AD subtypes. Our findings enhance our understanding of AD pathogenesis and identify potential biomarkers and therapeutic targets.

Keywords Down syndrome · Alzheimer's disease · Proteomics · Amyloid-β · Neuropathology

Introduction

Down syndrome (DS) is the most prevalent chromosomal abnormality, characterized by the partial or complete triplication of chromosome 21 (Hsa21) [3, 24]. DS is strongly associated with Alzheimer's disease (AD) due to the triplication of the amyloid-β precursor protein (*APP*) gene in Hsa21 [30, 39, 41]. Hsa21 also contains other genes of interest for AD, such as S100β (associated with astrocytes), *DYRK1A* (encodes for a kinase that phosphorylates Tau), and *SOD1* and *BACE2* (related to oxidative stress) [40, 91, 93, 127, 129], which may play a role in AD in addition to *APP*. By age 40, virtually, all individuals with DS exhibit AD pathological hallmarks, including extracellular amyloid-β (Aβ) accumulation and neurofibrillary tangles formed by hyperphosphorylated Tau [31, 102, 130]. Brain atrophy and elevated cerebrospinal fluid and plasma levels of Aβ42 and neurofilament light, respectively, have been observed in people with DS [36]. These neuropathological features are qualitatively similar to other AD forms, such as early (EOAD) and late-onset AD (LOAD) [2, 36].

Earlier investigations and most recent findings suggest that AD neuropathology extends beyond Aβ and Tau proteins [31, 81], implicating hundreds of associated proteins

Extended author information available on the last page of the article

Published online: 18 January 2025

in biological dysfunctions, such as synaptic transmission, immune response, mitochondrial metabolism, and oxidative stress [16, 25, 55]. Proteomic comparisons between DS and EOAD Aβ plaques reveal common proteins enriched in both conditions, although differences in protein abundance have been observed [31]. Despite recent progress, the molecular mechanisms of AD remain elusive, particularly regarding common pathophysiological mechanisms across AD subtypes and the specifics of AD neuropathogenesis in DS. Individuals with DS develop AD neuropathology earlier than the general AD population, with Aβ and Tau accumulation patterns mirroring those in AD [53]. However, the extent to which the protein composition in DS pathological lesions aligns with other AD subtypes remains uncertain [23]. Identifying gene–phenotype associations in DS is also challenging due to multiple triplicated genes [2]. Given these complexities, DS is particularly relevant as an AD model, due to the universal prevalence of DS with AD pathology with increasing age, compared to the other autosomal dominant inherited forms of AD and the more homogeneous, age-dependent pathology compared to LOAD [2, 37, 50, 109].

In light of these findings, this study aimed to characterize the proteomic differences among AD subtypes. In particular, we examined the Aβ plaque proteome in DS, EOAD, and LOAD, expanding on prior DS and EOAD comparisons [31]. Our analysis revealed a substantial similarity of proteins enriched in Aβ plaques across all experimental groups, providing new evidence about the Aβ plaque-protein composition of individuals with DS in direct comparison with EOAD and LOAD. The proteomes also shared functional associations, thus revealing a consistent plaque-protein signature in DS, EOAD, and LOAD. Despite the enrichment of similar plaque proteins in all cohorts, we observed subtle differences in the proteome composition, characterized by variations in protein abundance in each group. Corresponding observations were made in the proteomic composition of DS, EOAD, and LOAD non-plaque tissue compared to controls. These insights may contribute to identifying novel therapeutic targets or biomarkers tailored to the specific features of different AD subtypes.

Methods

Human brain tissue

Post-mortem formalin-fixed and paraffin-embedded (FFPE) brain tissues from DS, EOAD, LOAD, and cognitive normal age-matched controls ($n = 20$ brain cases for each cohort) were obtained from the National Institutes of Health NeuroBioBank (Maryland and Mt. Sinai brain banks), UK Brain Bank Network (South West Dementia brain bank), IDIBAPS Biobank from Barcelona, University of Pennsylvania and NYU Grossman School of Medicine, including autopsy tissues from NYU Alzheimer's Disease Research Center (ADRC), Center for Biospecimen Research and Development (CBRD)/Department of Pathology and the North American SUDEP Registry (NASR) at NYU Comprehensive Epilepsy Center (CEC). FFPE tissue blocks containing hippocampus and surrounding entorhinal and temporal cortex were used for the present study as it contains a high amount of amyloid pathology. The cases were assessed by the brain repositories to confirm advanced AD, by ABC neuropathological score [12, 84, 117]. Further details about the cases are included in Table 1 and detailed case history is provided in Supp. Table. 1. Cases lacking information about α-synuclein and TDP-43 were stained by CBRD and assessed in the laboratory. Inclusion criteria for all cases included tissue formalin fixation below 3 years. We tolerated cases with TDP-43 (DS = 2, EOAD = 2, LOAD = 1) or α-synuclein (DS = 7, EOAD = 2, LOAD = 1) inclusions to increase the number of cases, as these co-pathologies are common in the elderly population. We performed one-way ANOVA analysis followed by post hoc Tukey's multiple

Table 1 Case history summary

Group	Cases	Mean age at death (years)*	Sex	Mean PMI (hours)*	Neuropathology	*APOE* genotype
Down syndrome	20	59.8 ± 4.99	7 F/13 M	17.95 ± 11.71	Equivalent to A3, B3, C3 score or Braak V-VI, Thal 5	ε3/ε3: 13, ε4/ε4: 2, ε3/ε4: 3, ε2/ε4: 1
EOAD	20	63 ± 4.07	5 F/15 M	27.47 ± 12.76	Equivalent to A3, B3, C3 score or Braak V-VI, Thal 4	ε3/ε3: 10, ε4/ε4: 3, ε3/ε4: 5, ε2/ε3: 2
LOAD	20	# 82.1 ± 6.37	10 F/10 M	33.22 ± 19.19	A3, B3, C3 or Braak VI	ε3/ε3: 6, ε4/ε4: 3, ε3/ε4: 7, ε2/ε3: 2, ε2/ε4: 2
Control	20	66.4 ± 13.04	9 F/11 M	59.50 ± 27.30	≤ A1, B1, C1	N/A

*Mean age at death and mean PMI ± Standard deviation. #Significant differences by one-way ANOVA

comparison test to evaluate age differences among the cohorts and multiple variable linear regression to determine the influence of clinical traits age and sex in the proteomics results.

APOE genotyping

APOE genotyping was conducted for the cases where this information was not provided by the brain banks, following a previously established protocol [31]. Briefly, DNA extraction from FFPE tissue scrolls was performed using the QIAamp DNA FFPE Advanced UNG Kit (Qiagen, cat. 56,704) as indicated by the manufacturer. Two end-point PCRs were carried out using custom primers (forward primer 5′ AGGCCTACAAATCGGAACTGG 3′; reverse primer 5′ CCTGTTCCACCAGGGGC 3′; Sigma). After the initial PCR, DNA purification from the agarose gel was accomplished using the QIAquick Gel Extraction Kit (Qiagen, cat. 28,704), following the manufacturer's protocol. Subsequently, the gel-purified DNA was used for the second end-point PCR, followed by Sanger sequencing and sequence analysis using SnapGene 5.3.1 software.

Immunohistochemistry for Aβ and pTau

FFPE 8 µm tissue sections that contain the hippocampus and adjacent temporal cortex were collected on glass slides. Sections underwent chromogenic immunohistochemistry for total Aβ (Aβ 17–24 clone 4G8, 1:1000, BioLegend, cat. 800,710) and Tau pathology (PHF-1, 1:200, in house developed mouse monoclonal antibody provided by Dr. Peter Davies, Albert Einstein University, NY, USA [45]). Sections were deparaffinized and rehydrated through a brief series of xylene and ethanol washes. Antigen retrieval methods performed include a 7-min treatment of 88% formic acid followed by heat-induced citrate buffer treatment (10 mM sodium citrate, 0.05% Tween-20; pH 6). Endogenous peroxidase was quenched with 0.3% H_2O_2 solution for 20 min. Sections were blocked with 10% normal goat serum, followed by an overnight incubation with the primary antibody diluted in 4% normal goat serum. Sections were incubated for 1 h at room temperature with the appropriate secondary antibody (biotinylated HRP mouse IgG, 1:1000, Vector, cat. BA-2000). Staining signal was amplified using VECTASTAIN Avidin–Biotin Complex (ABC) kit (Vector, cat. PK6100) for 30 min. The chromogen DAB was used to visualize the pathology. Sections were counterstained with hematoxylin and coverslipped using the appropriate mounting media. Aβ and Tau quantities were quantified from whole slide scans at 20X magnification using a Leica Aperio Versa 8 microscope. Five regions of interest (ROIs) in the temporal cortex and hippocampus (CA1, CA2, CA3) were used to calculate the percent positive pixel area. We used a custom macro based on the 'Positive Pixel Count' algorithm in ImageScope v.12.4.3.5008, with a modification to the 'Color saturation threshold' = 0 and the 'Upper limit of intensity for weak-positive pixels' (Iwp high) = 190. Statistical differences between experimental groups were evaluated using one-way ANOVA followed by Tukey's post hoc multiple comparisons test in GraphPad Prism v 9.5.1. Data are shown as mean ± standard error of the mean (SEM).

Laser-capture microdissection

Unbiased localized proteomics was performed using the method outlined in Fig. 1a. FFPE tissues were cut into 8 µm sections from autopsy hippocampal and adjacent entorhinal and temporal cortex tissues onto laser-capture microdissection (LCM) compatible PET membrane slides (Leica, cat. 11,505,151). Amyloid-β deposits were visualized by immunohistochemistry using the pan-Aβ 4G8 antibody (1:1000, BioLegend, cat. 800,710), using the chromogen 3,3-diaminobenzidine (DAB, Thermo Scientific, cat. 34,065) reaction. Classic cored, neuritic and dense Aβ plaques were targeted (not diffuse or cotton-wool plaques) in gray matter of the hippocampal formation, and the adjacent subiculum and entorhinal cortex, as well as from the gray matter of the temporal cortex, in regions distant from the hippocampus, for a more homogeneous analysis, using LCM to dissect a total area of 2 mm^2 and the same area for neighboring non-plaque tissue (Fig. 1b–c), at 10X magnification with a LMD6500 microscope equipped with a UV laser (Leica). We avoided diffuse amyloid aggregates in all the cases used to maintain sample consistency. Microdissected samples were centrifuged for 2 min at 14,000 g and stored at − 80 °C. We also microdissected adjacent tissue free of plaques from the same microscopic field of views that contained microdissected amyloid plaques, but at a sufficient distance from plaques to ensure that plaque-associated tissue was not collected (Fig. 1c). These samples are henceforth referred to as 'non-plaque'. In addition, analogous non-plaque tissue from control cases was selected from matching hippocampal and temporal cortex regions as those used in DS, EOAD, and LOAD, denoted as 'Control non-plaque'. The schematic diagrams for the figure were generated using BioRender.com.

Label-free quantitative mass spectrometry (MS) proteomics

The extraction and digestion of proteins from Laser-Capture Microdissection (LCM) excised plaque and non-plaque tissue samples were performed using the SPEED sample prep workflow [28]. Briefly, tissue sections were incubated in 10 µl of LC–MS grade formic acid (FA) for 5 min at 73 °C. The FA was then neutralized by a tenfold dilution with 2 M TRIS containing 10 mM Tris (2-carboxyethyl) phosphine

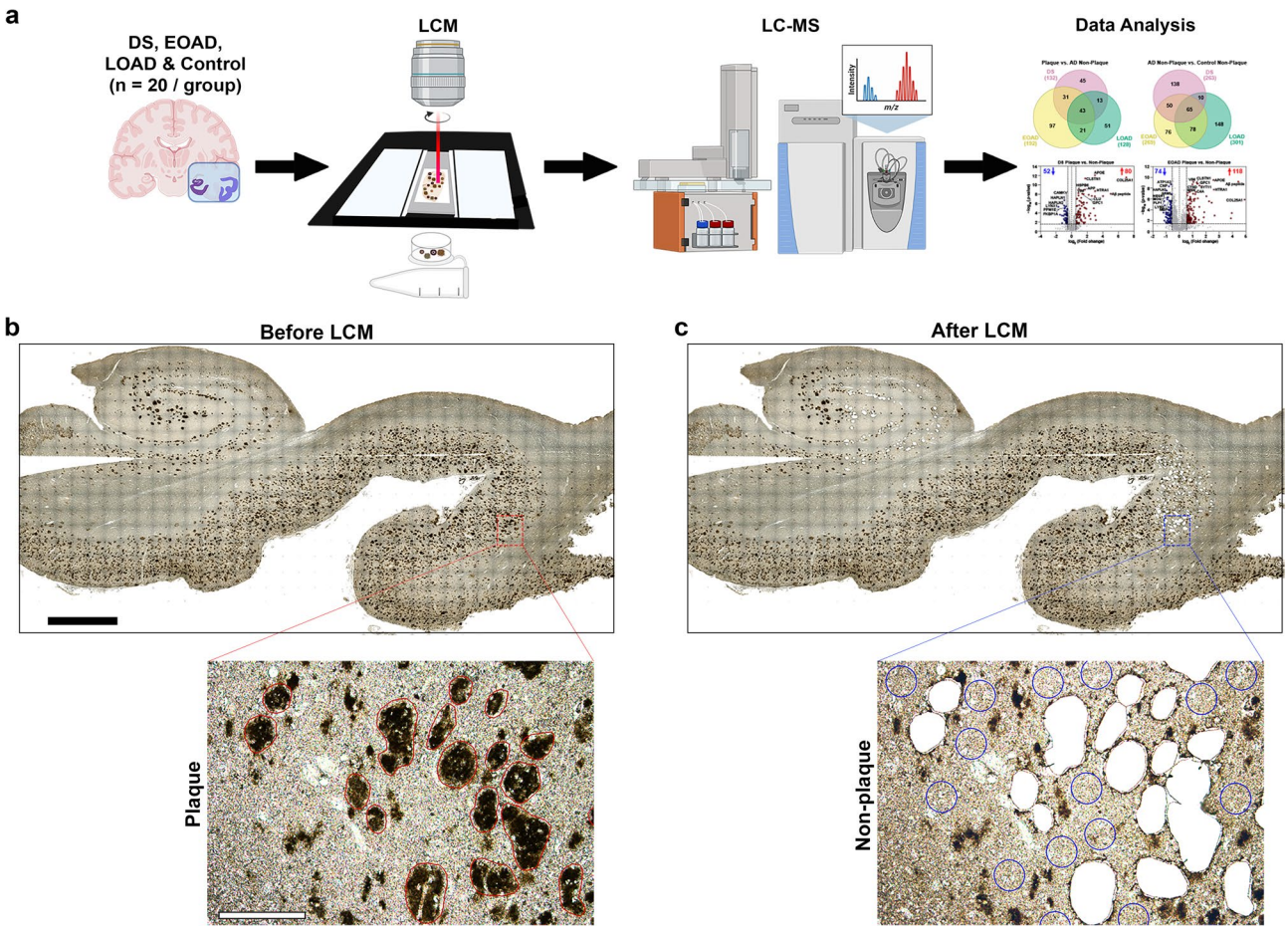

Fig. 1 Schematic of the localized proteomics protocol. **a** Laser-capture microdissection of 2 mm^2 total area of amyloid-β plaques from hippocampus and adjacent temporal cortex from FFPE autopsy brain tissue from control, DS, EOAD, and LOAD ($n = 20$ cases/experimental group). Amyloid plaque proteins were quantified by label-free mass spectrometry and posteriorly analyzed. **b–c** Microphotographs of a typical brain tissue section immunolabeled against Aβ illustrate the precise microdissection of amyloid plaques before (**b**) and after LCM (**c**). 2 mm (black bar, top) and 200 µm (white bar, bottom)

(TCEP) and 20 mM chloroacetic acid (CAA), followed by an incubation at 90 °C for 1 h. For enzymatic digestion, samples were diluted sixfold with water containing 0.2 µg of sequencing-grade trypsin. Digestion was carried out overnight at 37 °C and halted by acidification to 2% TFA.

Liquid chromatography–tandem mass spectrometry (LC–MS/MS) was performed online on an Evosep One LC using a Dr. Maisch ReproSil-Pur 120 C18 AQ analytical column (1.9-µm bead, 150 µm ID, 15 cm long). Peptides were gradient eluted from the column directly into an Orbitrap HF-X mass spectrometer using the 88-min extended Evosep method (SPD15) at a flow rate of 220 nl/min. The mass spectrometer was operated in data-independent acquisition (DIA) mode, acquiring MS/MS fragmentation across 22 m/z windows after every MS full-scan event.

High-resolution full MS spectra were acquired with a resolution of 120,000, an Automatic Gain Control (AGC) target of 3e6, a maximum ion injection time of 60 ms, and a scan range of 350–165 m/z. Following each full MS scan, 22 data-independent higher-energy collisional dissociation (HCD) MS/MS scans were acquired at a resolution of 30,000, an AGC target of 3e6, and a stepped normalized collision energy (NCE) of 22.5, 25, and 27.5.

Proteomics computational analysis

The analysis of the MS data was conducted utilizing the Spectronaut software (https://biognosys.com/shop/spectronaut), searching in direct-DIA mode (w/o experimental spectral library) against the *Homo Sapiens* UniProt database (http://www.uniprot.org/) combined with a list of common laboratory contaminants. The integrated search engine Pulsar was employed for the database search. The enzyme specificity was configured to trypsin, allowing for up to two missed cleavages during the search process. The search also included oxidation of methionine as a variable modification,

and carbamidomethylation of cysteines as a fixed modification. The false discovery rate (FDR) for identification of peptide, protein, and site was limited to 1%. Quantification was performed on the MS/MS level, utilizing the three most intense fragment ions per precursor. Independent quantification of Aβ was manually curated and incorporated into the search results, consistent with previous studies [31, 71, 106]. The intensity of Aβ was quantified by integrating the area under the curve for the peptide LVFFAEDVGSNK, which corresponds to amino acids 17–28 of Aβ. This peptide does not differentiate between cleaved or full-length sequences but shows strong enrichment and correlation with Aβ pathology [31, 49, 72, 106]. Data were log-transformed and normalized using median intensity across all samples. For subsequent data analysis, the Perseus [119], R environment (http://www.r-project.org/), or GraphPad Prism were used for statistical computing and graphical representation.

Proteomics statistical analyses

The protein expression matrix ($n = 2080$) was filtered to remove common laboratory contaminants, non-human proteins, and those proteins observed in less than half of all the four groups evaluated ($n = 1995$). For principal component analysis (PCA), missing values were imputed from the normal distribution with a width of 0.3 and a downshift of 1.8 (relative to measured protein intensity distribution) using Perseus v 1.6.14.0 [119]. We performed paired *t* tests to evaluate the amyloid plaques enrichment in relation to the non-plaque tissue adjacent to the amyloid plaques. In addition, we performed unpaired *t* tests to compare the protein enrichment of non-plaques from DS, EOAD, and LOAD compared to control tissue samples. Proteins were deemed significantly altered if they had a false discovery rate (FDR) below 5% (permutation-based FDR with 250 data randomizations). We further filtered the significant proteins based on the fold-change (FC) difference > 1.5 fold between the groups. The proteins of interest common to each pairwise comparison from 'plaques vs. non-plaque' and 'non-plaque vs. control non-plaque' tissue were evaluated by Venn diagrams generated from InteractiVenn [54]. Pearson's correlation analysis between DS, EOAD, and LOAD differentially abundant proteins identified in the pairwise comparisons were evaluated using GraphPad Prism v 9.5.1. For this analysis, we considered proteins that were significantly altered in at least one of the groups and had an FC > 1.5, on a given correlation.

Mapping protein-coding genes to human chromosomes

Genes coding for the proteins identified in the study were mapped to their respective chromosomes in R using the function 'mapIds' from the *Annotation DBI* package v 1.62.2 with the genome-wide annotation for human, org.Hs.eg.db v 3.17.0. Percentage of significantly altered proteins was calculated by dividing the number of significant proteins per each chromosome by the total number of proteins mapped to the respective chromosome. Location for each protein-coding gene in the chromosome 21 (*Homo sapiens* autosome 21, or Hsa21) was determined using the UCSC Human Genome Browser [68].

Gene Ontology functional annotation

Gene Ontology (GO) enrichment analysis was performed in R using the function *enrichGO* from the package *clusterProfiler* v 4.8.2, with the genome-wide annotation for human, org.Hs.eg.db v 3.17.0. GO terms were filtered to an FDR < 0.05 using the Benjamini–Hochberg method [9]. Isoform labels were excluded from Uniprot accession IDs for GO functional annotation. Duplicate proteins were removed, and the resulting list comprising 1980 proteins lacking isoforms was utilized as the background dataset. Functional annotation was focused on GO biological process (GO BP) and GO cellular component (GO CC). Heavily redundant GO terms were reduced using the *simplify* function from clusterProfiler, with a cutoff of 0.7. Top ten significantly enriched GO terms for highly abundant proteins in 'plaques vs. non-plaque' and 'non-plaque vs. control non-plaque' for each experimental group were selected using the adjusted *p* value ($-\text{Log}_{10}$ adj. *p* value) and compared using heatmaps generated in GraphPad Prism.

Protein–protein interaction networks

Protein–protein interaction (PPI) networks were made in Cytoscape v 3.10.0 using 'STRING: protein query' (STRING v 11.5 database [114]) with a (high) confidence score of 0.7. Networks reflect functional and physical protein associations for the differentially abundant proteins in DS, EOAD, and LOAD. Node size of the networks indicate the adjusted *p* value ($-\log_{10}$ [*p* value]) from the *t* tests and node color indicates fold-change ($\log_2$ [FC]). Disconnected nodes were not depicted in the final network. Dotted-line colored boxes highlight proteins clustered by function similarity.

Comparison with previous AD proteomics studies in human brain

Our data were compared to previous proteomic studies using the NeuroPro database (v1.12; https://neuropro.biomedical.hosting/) [4]. NeuroPro is a combined analysis of differentially enriched proteins found in human AD brain tissues identified in 38 published proteomics studies (at the time of use for this study, February 2024). NeuroPro database was

filtered to include only proteins found in advanced AD proteomics studies (AD and AD/C). Alternatively, we applied a second filter to advanced AD to include proteomics studies in 'plaques' only. Protein lists obtained after filtering the NeuroPro database were manually curated to address current 'obsolete deleted', 'merged' or 'demerged' UniProt accession IDs. We performed a manual curation of NeuroPro protein lists to provide an accurate comparison between the proteins identified in previous proteomics studies and our present study. The UniProt accession IDs and gene IDs from the proteins we identified in the current study were matched to the IDs from the NeuroPro to identify proteins that have not been previously associated with human AD and amyloid plaque proteomics.

Additionally, as the NeuroPro database does not include DS proteomics data, we compared our current DS plaque dataset with our previous DS plaque proteomics study [31]. We identified the common proteins using the whole data matrix of both studies, by comparing the Uniprot Accession ID and the Gene ID, to account for any identifier differences. Then, we identified the significantly altered proteins in each study; for our dataset, we defined significantly altered proteins by FDR ≤ 5% and a fold-change ≥ 1.5. In our previous study, significantly altered proteins were defined by $p < 0.05$ and a fold-change ≥ 1.5. For the comparison, we included the significantly abundant and significantly decreased plaque proteins. We evaluated common significant proteins from the datasets using Venn diagrams generated from InteractiVenn [54]. In addition, we performed Pearson's correlation analysis between datasets using GraphPad Prism v 9.5.1. For the correlation analysis, we considered proteins that were significantly altered in at least one of the datasets.

Validation of proteins of interest

The proteins chloride voltage-gated channel 6 (CLCN6) and the Tripeptidyl peptidase I (TPP1, also known as CLN2), which are enriched in Aβ plaques, were validated using immunohistochemistry (IHC). CLCN6 was selected due to its significantly high abundance in DS plaques, limited evidence of its presence in plaques and about its role in AD, and its previously described function in the central nervous system [13, 92]. TPP1 was selected as another lysosomal protein, which has been described in the previous human proteomics studies to be associated to Aβ plaques, but it has not been validated by IHC. For immunolabeling, 8 µm serial sections adjacent to those used for proteomic analysis were deparaffinized and rehydrated. Sections from six cases in each cohort were subjected to antigen retrieval in a microwave, using Tris–EDTA buffer (pH 9, Proteintech), diluted 1X for CLCN6, and sodium citrate buffer pH 6, followed by formic acid treatment for TPP1. Primary antibodies against CLCN6 (1:350, Thermo Scientific, cat. OSC00147W-100UL), TPP1 (1:100, Sigma-Aldrich, cat. HPA037709-100UL), and the pan-Aβ 4G8 antibody (1:1000) were incubated overnight, followed by Alexa Fluor 488 and 647 secondary antibodies (Thermo Scientific). Additionally, we performed a co-staining using MAP2 (1:200, BD Biosciences, cat. 556,320) and CLCN6 to assess cell specificity of CLCN6 expression. Whole-slide scans were acquired at 20X magnification using a Leica Aperio Versa 8 microscope.

For CLCN6 quantification, ten regions of interest (ROIs) from the same anatomical areas used for LCM were analyzed using a custom macro in ImageJ 1.54f. Briefly, a mask was generated to delineate the plaques area in the field of view, which was then applied to the CLCN6 channel to measure fluorescence intensity (total fluorescence = Integrated Density—[Area measured * Background mean gray value]) or the area occupied by CLCN6-positive objects using the "Measure" function. CLCN6-positive area was normalized to the total area of the plaques. Non-plaque CLCN6 area and fluorescence were measured by modifying the macro, where plaque ROIs were first subtracted from the CLCN6 channel before proceeding with the previously described quantification method. Significant differences were assessed using paired t tests (for comparisons between plaque and non-plaque tissue within the same case) or unpaired t tests (for comparisons between control non-plaque tissue and non-plaque tissue from DS, EOAD, or LOAD), with analyses performed using GraphPad Prism.

TPP1 was quantified using QuPath v 0.5.1. Briefly, 10 regions of interest (ROIs) were manually annotated from the gray matter of the hippocampal formation and temporal cortex. Aβ plaques were annotated using a pixel classifier, with a Gaussian prefilter, smoothing sigma of 2, and a threshold of 30. Objects below 350 μm^2 were filtered out from the final annotations. Non-plaque adjacent tissue was selected using the same classifier, but ignoring pixels above threshold and assigning the remaining pixels detected to the class "Non-plaques". TPP1-positive objects were annotated using a similar pixel classifier, with smoothing sigma of 1.5 and a threshold of 26. Objects below 20 μm^2 were filtered out for the final annotations. Density of protein TPP1 was calculated for positive immunolabeling inside plaques and for presence of TPP1 in the non-plaque region, using the formula TPP1 density = (sum of TPP1 areas/sum of plaques area) × 100. T tests' statistical analyses were performed in GraphPad Prism.

Weighted gene correlation network analysis

We used the *WGCNA* package (version 1.72.1) in the R environment to conduct a Weighted Gene Correlation Network Analysis adapted from the WGCNA framework [137] to investigate protein expression correlations. First, the curated protein expression matrix from the proteomics

analysis ($n = 1995$) underwent quality control to identify samples with excessive missing values. The networks were then constructed using the *blockwiseModules* function for each cohort (DS, EOAD, and LOAD), creating separate networks for Aβ plaques and non-plaque tissue within each cohort. The networks were constructed as "signed networks" with the topological overlap matrix (TOM) also set to "signed". *TOMdenom* parameter was specified as "mean" to facilitate the capture of tightly connected protein groups within the network. The soft-thresholding power was set to 9 for DS Plaques and 10 for non-plaques, 7 for EOAD plaques and 11 for non-plaques, and 18 for LOAD plaques and 14 for LOAD non-plaque dataset. Additional parameters included a minimum module size of 10, a mergeCutHeight of 0.07 to merge highly similar modules more stringently, and a deepSplit value of 4 to facilitate finer differentiation of modules. A minimum intramodular connectivity (kME) of 0.3 was required for proteins to remain in a given module, with a reassignment threshold of 0.05 allowing minor reallocation of proteins to more appropriate modules if necessary. The biweight midcorrelation method (bicor) was used as the primary correlation measure, with a fallback to Pearson correlation for outlier adjustment where necessary (maxPOutliers = 0.1). Numeric module labels were employed for consistency, and to reduce the complexity of module visualization, the pamRespectsDendro option was set to FALSE.

After running the *blockwiseModules* function, we used the *signedKME* function within the WGCNA package to perform an iterative module cleanup to refine the module assignments in the protein correlation networks, as previously described [63]. The iterative cleanup process involved creating a bicor correlation table to assess the relationship between each protein and the respective module eigenproteins, referred to as kME. Initially, proteins with an intramodular kME below 0.30 were removed. The reassignment process consisted of reallocating proteins in the gray module (those not assigned to any module) to any module with a maximum kME greater than 0.30 and reassigning proteins whose intramodular kME was more than 0.10 below their maximum kME relative to any other module. This procedure continued iteratively until the minimum kME of the proteins in a module was above the threshold of 0.30 and the difference between the maximum kME and the intramodular kME was less than 0.1, or up to 30 iterations if module reassignment criteria were not met. After each reassignment, the module eigenproteins and the kME table were recalculated using the *moduleEigengenes* and *signedKME* functions, ensuring that all module assignments remained valid and appropriately ranked. Ultimately, this cleanup procedure reinforced the reliability of the module structure by systematically refining the assignments of proteins to their respective modules based on kME values.

After the iterative module cleanup was performed, correlations between module eigenproteins (MEs) and clinical variables (*APOE* genotype, age, Sex, co-pathologies, and Aβ and pTau levels) were calculated and plotted in a heatmap using the *labeledHeatmap* function of the WGCNA package. Subsequently, GO enrichment analysis was performed for each of the correlation networks using the function *enrichGO* from the package *clusterProfiler*, filtering GO terms to an FDR < 0.05 using the Benjamini–Hochberg method followed by the *simplify* function with a cutoff of 0.7 to remove heavily redundant terms.

Results

Amyloid-β and Tau pathologies are significantly increased in DS

AD pathology was assessed using the Braak and Thal staging or equivalent ABC score, for all cases used for proteomics analysis (Table 1, detailed case history in Supp. Table 1). Age was significantly different ($p < 0.0001$) in the LOAD cohort in comparison to the other experimental groups. However, we included eight controls ≤ 65 years old and the remaining 12 cases ≥ 65 to compensate for the age gap between EOAD and LOAD (Supp. Table 1). In addition, multiple variable linear regression analysis showed that age ($p = 0.97$) and sex ($p = 0.45$) did not contribute significantly to the differences observed in the proteomics analysis (Supp. Table 2).

Assessment of the regional distribution of Aβ and Tau pathology (Supp. Figure 1a, b) in all cases showed that Aβ levels in hippocampal and temporal regions were similar in DS and EOAD. However, Aβ quantities in DS were significantly higher ($p = 0.013$) compared to LOAD (Supp. Figure 1c). PHF-1 immunoreactive Tau pathology was significantly higher in DS compared to EOAD and LOAD ($p = 0.0002$ and $p < 0.0001$, respectively) (Supp. Figure 1d). Aβ and Tau pathology were not significantly different between EOAD and LOAD (Supp. Figure 1c–d). These results suggest an exacerbated Aβ and Tau pathology in DS despite the advanced stage of AD for all the cases in the cohorts evaluated.

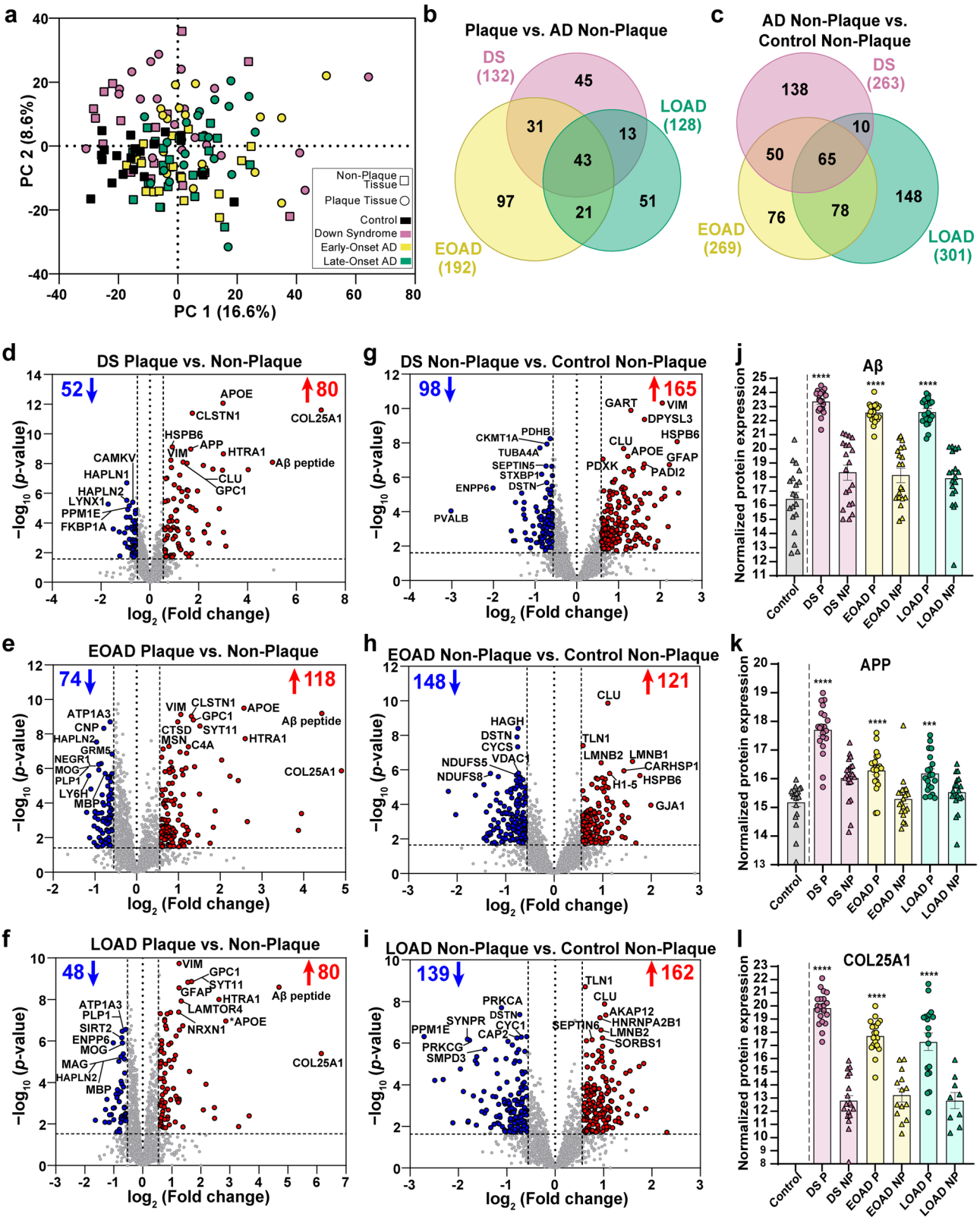
a
PC 2 (8.6%)
PC 1 (16.6%)
Non-Plaque Tissue
Plaque Tissue
Control
Down Syndrome
Early-Onset AD
Late-Onset AD
b
Plaque vs. AD Non-Plaque
DS (132)
LOAD (128)
EOAD (192)
45
31
13
43
97
21
51
c
AD Non-Plaque vs. Control Non-Plaque
DS (263)
EOAD (269)
LOAD (301)
138
10
50
65
148
76
78
d
DS Plaque vs. Non-Plaque
52
80
APOE
CLSTN1
COL25A1
HSPB6
APP
VIM
HTRA1
Aβ peptide
CAMKV
HAPLN1
CLU
GPC1
HAPLN2
LYNX1
PPM1E
FKBP1A
−log10 (p-value)
log2 (Fold change)
g
DS Non-Plaque vs. Control Non-Plaque
98
165
GART
VIM
DPYSL3
HSPB6
CKMT1A
PDHB
TUBA4A
CLU
APOE
GFAP
SEPTIN5
PDXK
PADI2
STXBP1
ENPP6
DSTN
PVALB
e
EOAD Plaque vs. Non-Plaque
74
118
ATP1A3
VIM
CLSTN1
GPC1
APOE
Aβ peptide
CNP
CTSD
SYT11
HAPLN2
MSN
HTRA1
C4A
GRM5
NEGR1
COL25A1
MOG
PLP1
LY6H
MBP
h
EOAD Non-Plaque vs. Control Non-Plaque
148
121
CLU
HAGH
DSTN
CYCS
TLN1
LMNB2
LMNB1
CARHSP1
NDUFS5
VDAC1
NDUFS8
HSPB6
H1-5
GJA1
f
LOAD Plaque vs. Non-Plaque
48
80
VIM
GPC1
SYT11
GFAP
HTRA1
Aβ peptide
ATP1A3
LAMTOR4
PLP1
*APOE
SIRT2
NRXN1
ENPP6
MOG
COL25A1
MAG
HAPLN2
MBP
i
LOAD Non-Plaque vs. Control Non-Plaque
139
162
TLN1
CLU
PRKCA
AKAP12
DSTN
SYNPR
CYC1
SEPTIN6
HNRNPA2B1
PPM1E
CAP2
LMNB2
PRKCG
SORBS1
SMPD3
j
Aβ
Normalized protein expression
Control
DS P
DS NP
EOAD P
EOAD NP
LOAD P
LOAD NP
k
APP
l
COL25A1

◂**Fig. 2** Principal component analysis (PCA) and differential protein expression in Aβ plaques and non-plaque tissue. **a** PCA shows the distribution of the $n = 20$ cases per each experimental group, with minimal segregation. **b** Venn diagram of differentially abundant Aβ plaque proteins shows 43 common proteins for all the AD subtypes evaluated, 45 for DS, 97 for EOAD, and 51 for LOAD. **c** Venn diagram of differentially abundant non-plaque proteins depicts 138 proteins in DS, 76 proteins in EOAD, 148 proteins in LOAD, and 65 common proteins for all AD subtypes. **d–f** Volcano plots indicate differentially expressed proteins (enriched in red, decreased in blue) in Aβ plaques compared to non-plaque tissue in DS (132 proteins, **d**), EOAD (192 proteins, **e**) and LOAD (128 proteins, **f**). **g–i** Volcano plots depict differentially expressed proteins in DS non-plaque tissue compared to controls (263 proteins, **g**), EOAD non-plaques (269 proteins, **h**), and LOAD non-plaques (301 proteins, **i**). **j–l** Normalized protein expression obtained from the label-free quantitative mass spectrometry proteomics of Aβ peptide (**j**), APP protein (**k**), and COL25A1 (**l**). Significance was determined using a student's two-tailed *t* test (FDR < 5%, fold-change > 1.5). *P* values are indicated based on the pairwise comparisons. *** $p < 0.001$, **** $p < 0.0001$. Error bars indicate standard error of the mean (SEM). Significant pairwise comparisons are indicated for those analyses that were performed, and controls are shown as reference

Protein abundance in amyloid plaques and non-plaque tissue varies across DS, EOAD, and LOAD

Aβ plaque pairwise comparisons

Protein differential expression in Aβ plaques and adjacent AD non-plaque tissue was evaluated using LFQ-MS in the microdissected hippocampus and temporal cortex (Fig. 1). LFQ-MS identified 1995 proteins (Supp. Tables 3–4), detected in at least 50% of the cases in any of the groups. PCA showed minimal segregation by groups (DS, EOAD, LOAD, or control) or by sample type (plaques and non-plaque tissue).

We identified 132 differentially abundant proteins in DS Aβ plaques compared to DS non-plaque tissue (Fig. 2b, d), 192 proteins in EOAD plaques vs. EOAD non-plaques (Fig. 2b, e), and 128 proteins in LOAD plaques vs. LOAD non-plaque tissue (FDR ≤ 5%, FC ≥ 1.5) (Fig. 2b, f). From these sets of proteins, 43 were shared between the three cohorts. We found 45 proteins with differential enrichment in plaques in DS, 97 proteins in EOAD, and 51 proteins in LOAD (Fig. 2b), indicating that enrichment of some proteins in Aβ plaques is variable in each experimental group. We observed a consistent enrichment of AD associated proteins such as the Aβ specific peptide LVFFAEDVGSNK (sequence corresponds to amino acids 17–28 of APP, Fig. 2d–f, j). This peptide does not discriminate between cleaved or full-length sequences. However, previous findings have shown a strong correlation to Aβ pathology [31, 49, 106]. We also identified previously detected amyloid plaque proteins, such as HTRA1, GPC1, VIM, APOE, CLSTN1, and SYT11 within the top ten most significant proteins across groups (Table 2). As expected, APP was within the top ten significantly abundant proteins in DS amyloid plaques (Fig. 2d) and was also significantly enriched in amyloid plaques in EOAD and LOAD (Fig. 2k). The plaque-protein COL25A1 [collagen alpha-1(XXV) chain, also known as CLAC-P] was the most abundant protein in amyloid plaques in all experimental groups, showing more enrichment in plaques than the Aβ peptide (Fig. 2d–f, l). Interestingly, COL25A1 was below mass spectrometry detection threshold in all control tissues (Fig. 2l), suggesting that this protein is highly correlated to Aβ plaque pathology. COL25A1 was increased 129.5-fold in DS, 29.9-fold in EOAD and 71-fold in LOAD (Table 2). In addition, COL25A1 was within the top ten significant proteins only in DS (Table 2). Hyaluronan and proteoglycan link protein 2 (HAPLN2, also known as Bral1) was within the most significant proteins decreased in plaques in the three cohorts studied. In addition, we observed decreased plaque-protein levels of oligodendrocyte proteins. MOG was significantly decreased in all groups, and MAG and MBP were significantly decreased in EOAD and LOAD amyloid plaques, respectively (Supp. Table 3). MAG and MBP levels were also decreased in plaques in DS, although it did not meet our significance criteria. The glucose transport facilitator SLC2A3 (also known as GLUT3) was decreased in amyloid plaques in all groups, yet it was significant only in EOAD and LOAD (Table 2). Overall, we observed similar proteins altered in Aβ plaques in all groups evaluated. However, most of the proteins show different abundance levels in plaques of DS, EOAD, and LOAD, accounting for the differences observed among groups.

AD non-plaque tissue pairwise comparisons

We identified 263 differentially expressed proteins in DS non-plaque tissue compared to control non-plaque tissue (Fig. 2c, g), 269 proteins in EOAD non-plaque tissue vs. control non-plaque tissue (Fig. 2c, h), and 301 significantly altered proteins in LOAD non-plaque tissue vs. control non-plaque tissue (Fig. 2c, i). We identified 65 altered non-plaque proteins compared to control tissue that were common between all cohorts evaluated (Fig. 2c). We also observed 138 proteins with differential enrichment levels in DS non-plaque tissue, 76 proteins in EOAD, and 148 proteins in LOAD (Fig. 2c). Notably, we identified among the top ten enriched proteins in DS non-plaque tissue CLU, VIM, HSPB6, and SYNM (Supp. Table 5), which we also found enriched in amyloid plaques in all disease groups. CLU was consistently enriched in non-plaque tissue in the three groups evaluated when compared to control tissue (Supp. Table 5). VIM and HSPB6 were also among the most enriched proteins in EOAD non-plaque tissue (Supp. Table 5). Conversely, we identified the actin-binding protein destrin (DSTN) as the only

Table 2 Top 20 significant proteins in Down syndrome, and early-onset and late-onset AD for 'plaque vs. non-plaque' pairwise comparisons

Down syndrome—Plaque vs Non-plaque						
Uniprot Accession ID	Gene name	Name	*p* value	Fold Change	Change in EOAD	Change in LOAD
Increased						
Q9BXS0	COL25A1	Collagen alpha-1(XXV) chain	2.51E-12	129.5	↑	↑
	Aβ		8.16E-09	32.5	↑	↑
Q92743	HTRA1	Serine protease HTRA1	2.24E-09	8.1	↑	↑
P02649	APOE	Apolipoprotein E	8.6E-13	8.0	↑	↑
O94985	CLSTN1	Calsyntenin-1	4.12E-12	3.3	↑	↑
P05067	APP	Amyloid-beta precursor protein	1.07E-09	3.2	↑	↑
P35052	GPC1	Glypican-1	9.46E-09	2.9	↑	↑
P10909	CLU	Clusterin	7.95E-09	2.6	↑	↑
O14558	HSPB6	Heat shock protein beta-6	7.59E-10	1.9	↑	↑
P08670	VIM	Vimentin	6.01E-09	1.8	↑	↑
Decreased						
P0DP58	LYNX1	Ly-6/neurotoxin-like protein 1	5.39E-06	3.3	↓	↓
P42677	RPS27	40S ribosomal protein S27	4.11E-05	1.9	↓	
Q9GZV7	HAPLN2	Hyaluronan and proteoglycan link protein 2	3E-06	1.9	↓	↓
P10915	HAPLN1	Hyaluronan and proteoglycan link protein 1	2.03E-07	1.9	↓	↓
P62942	FKBP1A	Peptidyl-prolyl cis–trans isomerase FKBP1A	1.26E-05	1.9	↓	
Q8WY54	PPM1E	Protein phosphatase 1E	7.22E-06	1.8		↓
P13987	CD59	CD59 glycoprotein	4.05E-05	1.8		↓
Q8NCB2	CAMKV	CaM kinase-like vesicle-associated protein	4.01E-06	1.6		
O75363	BCAS1	Breast carcinoma-amplified sequence 1	1.48E-05	1.5	↓	↓
Q9H9H5	MAP6D1	MAP6 domain-containing protein 1	2.36E-05	1.5	↓	
Early-onset AD—Plaque vs Non-plaque						
Uniprot Accession ID	Gene name	Name	*p* value	Fold Change	Change in DS	Change in LOAD
Increased						
	Aβ		6.43E-10	21.6	↑	↑
Q92743	HTRA1	Serine protease HTRA1	1.84E-08	6.0	↑	↑
P02649	APOE	Apolipoprotein E	3.18E-10	5.9	↑	↑
Q9BT88	SYT11	Synaptotagmin-11	3.45E-09	2.9	↑	↑
P35052	GPC1	Glypican-1	1.51E-09	2.6	↑	↑
O94985	CLSTN1	Calsyntenin-1	9.36E-10	2.5	↑	↑
P0C0L4	C4A	Complement C4-A	5.49E-08	2.4	↑	↑
P08670	VIM	Vimentin	7.4E-10	2.1	↑	↑
P07339	CTSD	Cathepsin D	1.97E-09	2.0	↑	↑
P26038	MSN	Moesin	5.16E-08	1.7		↑
Decreased						
O94772	LY6H	Lymphocyte antigen 6H	2.55E-06	2.2		↓
Q9GZV7	HAPLN2	Hyaluronan and proteoglycan link protein 2	2.88E-08	1.9	↓	↓
Q16653	MOG	Myelin-oligodendrocyte glycoprotein	5.84E-07	1.9	↓	↓
P60201	PLP1	Myelin proteolipid protein	1.18E-06	1.9	↓	↓
Q7Z3B1	NEGR1	Neuronal growth regulator 1	5.09E-07	1.8		
P09543	CNP	2',3'-cyclic-nucleotide 3'-phosphodiesterase	4.73E-09	1.7		
P02686	MBP	Myelin basic protein	1.97E-06	1.7		↓

Table 2 (continued)

Early-onset AD—Plaque vs Non-plaque						
Uniprot Accession ID	Gene name	Name	*p* value	Fold Change	Change in DS	Change in LOAD
P13637	ATP1A3	Sodium/potassium-transporting ATPase subunit alpha-3	1.95E-09	1.6		↓
P11169	SLC2A3	Solute carrier family 2, facilitated glucose transporter member 3	1.97E-06	1.5		↓
P41594	GRM5	Metabotropic glutamate receptor 5	1.45E-07	1.5		↓
Late-onset AD—Plaque vs Non-plaque						
Uniprot Accession ID	Gene name	Name	*p* value	Fold change	Change in DS	Change in EOAD
Increased						
	Aβ		2.55E-09	25.8	↑	↑
Q92743	HTRA1	Serine protease HTRA1	9.94E-09	6.2	↑	↑
P35052	GPC1	Glypican-1	1.39E-09	3.2	↑	↑
Q9BT88	SYT11	Synaptotagmin-11	1.5E-09	2.9	↑	↑
Q0VGL1	LAMTOR4	Regulator complex protein LAMTOR4	1.19E-08	2.5	↑	↑
P14136	GFAP	Glial fibrillary acidic protein	2.78E-09	2.4		↑
P08670	VIM	Vimentin	1.87E-10	2.4	↑	↑
Q9ULB1	NRXN1	Neurexin-1	4.05E-08	2.4	↑	↑
Q9UM22	EPDR1	Mammalian ependymin-related protein 1	4.23E-08	1.9	↑	↑
P55084	HADHB	Trifunctional enzyme subunit beta, mitochondrial	4.83E-08	1.5		
Decreased						
Q6UWR7	ENPP6	Glycerophosphocholine cholinephosphodiesterase ENPP6	1.23E-06	2.0	↓	↓
O75363	BCAS1	Breast carcinoma-amplified sequence 1	9.47E-06	1.8	↓	↓
Q9GZV7	HAPLN2	Hyaluronan and proteoglycan link protein 2	5.75E-06	1.7	↓	↓
Q8IXJ6	SIRT2	NAD-dependent protein deacetylase sirtuin-2	7.07E-07	1.7		↓
P60201	PLP1	Myelin proteolipid protein	3.38E-07	1.6	↓	↓
Q16653	MOG	Myelin-oligodendrocyte glycoprotein	1.25E-06	1.6	↓	↓
P20916	MAG	Myelin-associated glycoprotein	4.16E-06	1.6		↓
P02686	MBP	Myelin basic protein	7.42E-06	1.6		↓
P11169	SLC2A3	Solute carrier family 2, facilitated glucose transporter member 3	3.52E-05	1.5		↓
P13637	ATP1A3	Sodium/potassium-transporting ATPase subunit alpha-3	2.8E-07	1.5		↓

protein among the top ten significantly decreased proteins in non-plaque tissue from DS, EOAD, and LOAD cohorts compared to controls (Supp. Table 5). We also observed that parvalbumin (PVALB) was the most decreased protein in DS non-plaque tissue compared with controls (Fig. 2g), whereas the levels of PVALB in EOAD and LOAD were not significantly different from controls (Supp. Table 4). Our proteomics findings in non-plaque tissue showed that there were more differences in protein levels in non-plaque tissue between groups, in comparison to the more consistent protein levels in plaques, highlighting the largely similar plaque proteome between AD subtypes despite differences in baseline, non-plaque-protein expression.

Amyloid plaque proteomes of DS, EOAD, and LOAD are highly correlated

We performed correlation analyses to compare the proteomes of Aβ plaques and non-plaque tissues in DS, EOAD, and LOAD. Proteins included in the correlations were significant and FC > 1.5 at least in one of the groups evaluated. For amyloid plaques, there was a positive correlation between

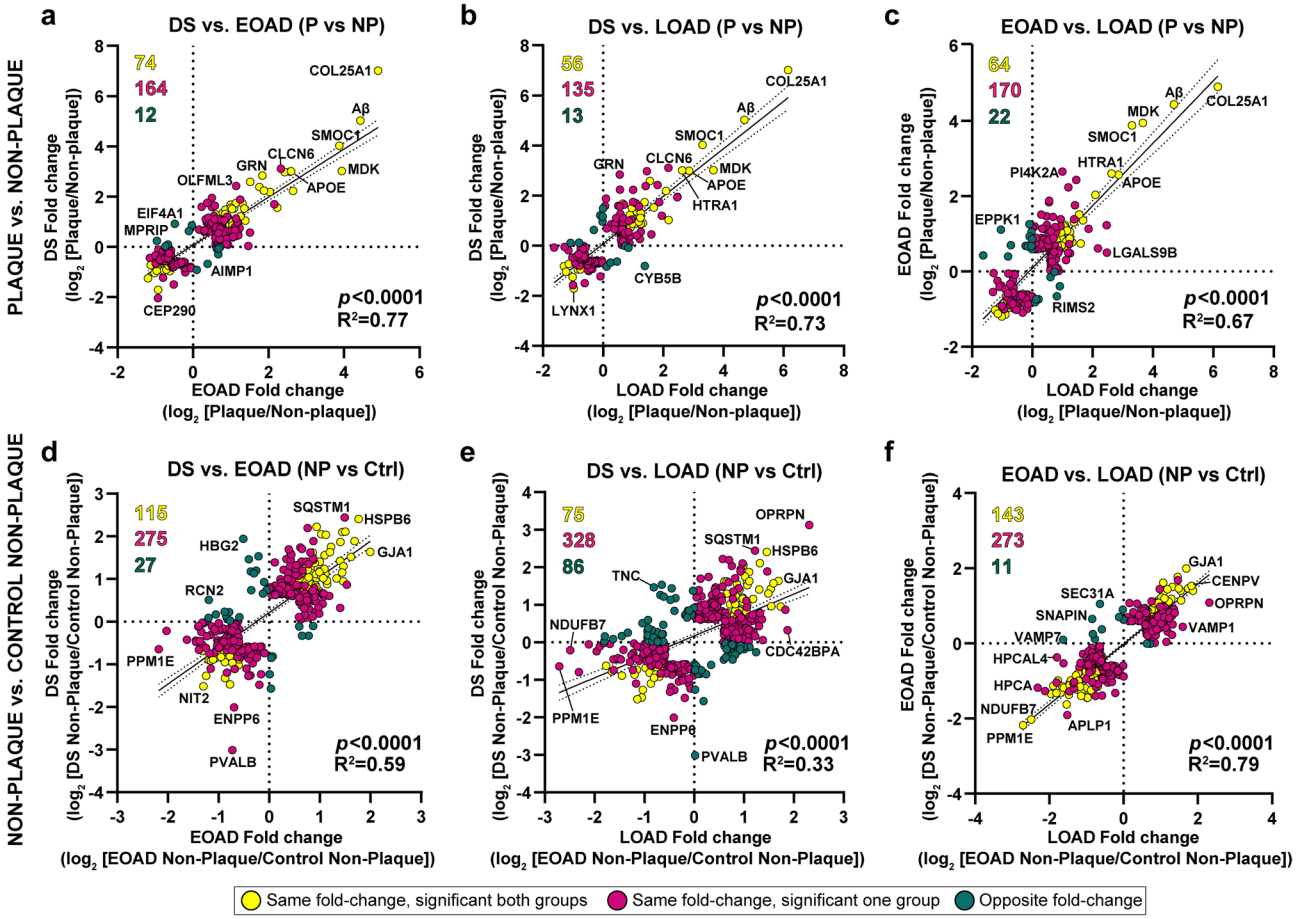

Fig. 3 Correlation analyses of differentially abundant proteins in Aβ plaques and non-plaque tissue. **a–c** Correlation analyses for significant proteins in Aβ plaques vs non-plaque tissue and **d–f** DS, EOAD and LOAD non-plaque vs control non-plaque tissue. Yellow dots represent proteins changing in the same direction (highly abundant or less abundant proteins in both groups evaluated) and that are significant for both groups compared. Magenta dots represent proteins changing in the same direction, but are significant only in one of the groups evaluated. Green dots represent proteins changing in opposite direction (i.e., abundant in one group and less abundant in the other group evaluated). Numbers are colored to match the dots. Proteins were selected for the correlation analysis if they were significant at least in one of the groups compared and its fold-change > 1.5. We observed a positive correlation between DS vs. EOAD **a** ($p < 0.0001$, $R^2 = 0.77$, **b** DS vs. LOAD ($p < 0.0001$, $R^2 = 0.73$) and **c** EOAD vs. LOAD ($p < 0.0001$, $R^2 = 0.67$). There is also a positive correlation when comparing non-plaque proteins in **d** DS vs. EOAD ($p < 0.0001$, $R^2 = 0.59$) and **e** DS vs. LOAD ($p < 0.0001$, $R^2 = 0.33$). **h.** Correlation between EOAD and LOAD non-plaque proteins ($p < 0.0001$, $R^2 = 0.79$)

DS and EOAD ($R^2 = 0.77$, $p < 0.0001$). We observed 65.5% (164/250) of the proteins changing in the same direction (i.e., fold-change for a protein is positive or negative in both groups), where 29.6% (74/250) of the proteins were significantly altered in DS and EOAD plaques (Fig. 3a). We only observed 4.8% (12/250) of the proteins changing in different directions (i.e., fold-change for a protein is positive in one group and negative in the other) (Fig. 3a). DS and LOAD plaque proteomes also correlated positively ($R^2 = 0.73$, $p < 0.0001$), with 66.2% (135/204) of the proteins with same fold-change direction and 27.5% (56/204) of the proteins significantly altered in both groups (Fig. 3b). Similar to DS and EOAD, only 6.3% (13/204) of the proteins were changing in opposite direction (Fig. 3b). There was also a positive correlation between EOAD and LOAD differentially abundant plaque proteins ($R^2 = 0.67$, $p < 0.0001$), similar to what we observed between DS vs. the AD subtypes evaluated. We identified 66.4% (234/256) of the proteins changing in the same direction, and 25% (64/256) of the proteins were significant in both groups (Fig. 3c). The proteins changing in opposite direction accounted for 8.6% (22/256) of the total (Fig. 3c). Our analysis shows high similarity among the proteins altered in Aβ plaques vs. non-plaques of DS, EOAD, and LOAD, with the majority of the proteins changing in the same direction.

Correlation analyses of DS, EOAD, and LOAD non-plaque differentially abundant proteins showed positive correlations between DS and EOAD ($R^2 = 0.59$, $p < 0.0001$)

and a weaker correlation between DS and LOAD ($R^2 = 0.33$, $p < 0.0001$) (Fig. 3d–e). We observed 65.9% (275/417) of the proteins changing in the same direction in DS and EOAD Aβ plaques, where 27.6% (115/417) of the proteins were significantly altered in both groups. We observed 6.5% (27/417) of proteins changing in the opposite direction (Fig. 3d). Similarly, 67.1% (328/489) of the proteins in DS and LOAD were changing in the same direction (Fig. 3e). We observed that 15.3% (75/489) of the proteins were significant in both groups, whereas 17.6% (86/489) of proteins had opposite fold changes (Fig. 3e). Moreover, we observed a higher positive correlation between EOAD vs. LOAD non-plaque proteomes ($R^2 = 0.79$, $p < 0.0001$), with 63.9% (273/427) of the proteins were changing in the same direction, with 33.5% (143/427) being also significant in both groups (Fig. 3f). Only 2.6% (11/427) of the proteins were changing in opposite directions (Fig. 3f). Overall, we observed a similar 'amyloid plaques protein signature' across the experimental groups. Nonetheless, correlations of the non-plaque tissue proteomes suggest a higher similarity between EOAD and LOAD differentially enriched proteins in comparison to DS.

Protein-coding genes present in Hsa21 are not associated with protein enrichment in Aβ plaques

We performed chromosomal mapping of significantly altered proteins identified through proteomic analysis across all human chromosomes using the UCSC Human Genome Browser to evaluate the distribution of these proteins across DS, EOAD, and LOAD. Supplemental Figure 2 illustrates the percentage of significantly altered proteins for each group. The overall percentage of proteins from each chromosome was below 20%, and no single chromosome exhibited a markedly overrepresented protein expression pattern. This suggests that proteins from all chromosomes, not just Hsa21, contribute to the molecular differences observed in both DS and AD.

Of the 1995 proteins identified in this study, 22 were from Hsa21 (Fig. 4). We compared these proteins with those reported in a previous DS plaque proteomics study [31], identifying a total of 26 Hsa21 proteins between the two studies. A significant portion, 69.2% (18/26), of these proteins were shared between the current and previous studies (Fig. 4). Among the proteins identified, APP was significantly altered in Aβ plaques in all cohorts (Fig. 4). GART was significantly abundant in LOAD and DS non-plaque tissue (Fig. 4a, c), and PCP4 was differentially expressed in LOAD and EOAD non-plaque tissue (Fig. 4a, b). CXADR was differentially expressed in EOAD amyloid plaques (Fig. 4b). APP was also significantly enriched in DS non-plaque tissue (FDR < 0.05, Fig. 4a). NCAM2, CBR1, CBR3, PDXK, CSTB, and COL6A1 were

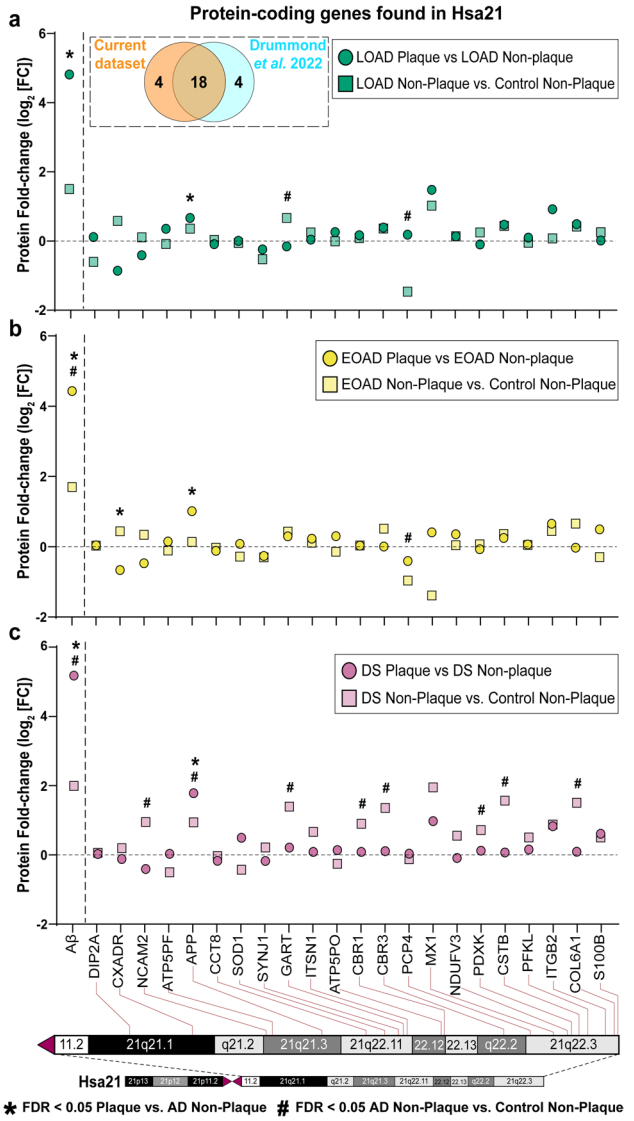

Fig. 4 Mapping protein-coding genes to chromosome 21 (Hsa21). **a** Dashed box contains Venn diagram of proteins from genes in Hsa21 identified in the current study vs. Drummond et al. 2022, [31]. **a–c** The figure depicts fold-change (Log_2 FC) of the 22 Hsa21 genes whose corresponding protein products were found in Aβ plaques (circles) or neighboring non-plaque tissue (squares) in LOAD (**a**) EOAD (**b**) and DS (**c**). Paired two-tailed *t* tests (plaques vs. non-plaques) or unpaired two-tailed *t* tests (non-plaques vs. control) with permutation correction at a 5% FDR are indicated. Aβ peptide is shown as reference

significantly enriched in DS non-plaque tissue (Fig. 4a). Taken together, these results along with the chromosomal mapping of all significantly altered proteins suggest that Hsa21 triplication does not necessarily lead to the enrichment of those gene products in Aβ plaques or in the surrounding non-plaque tissue.

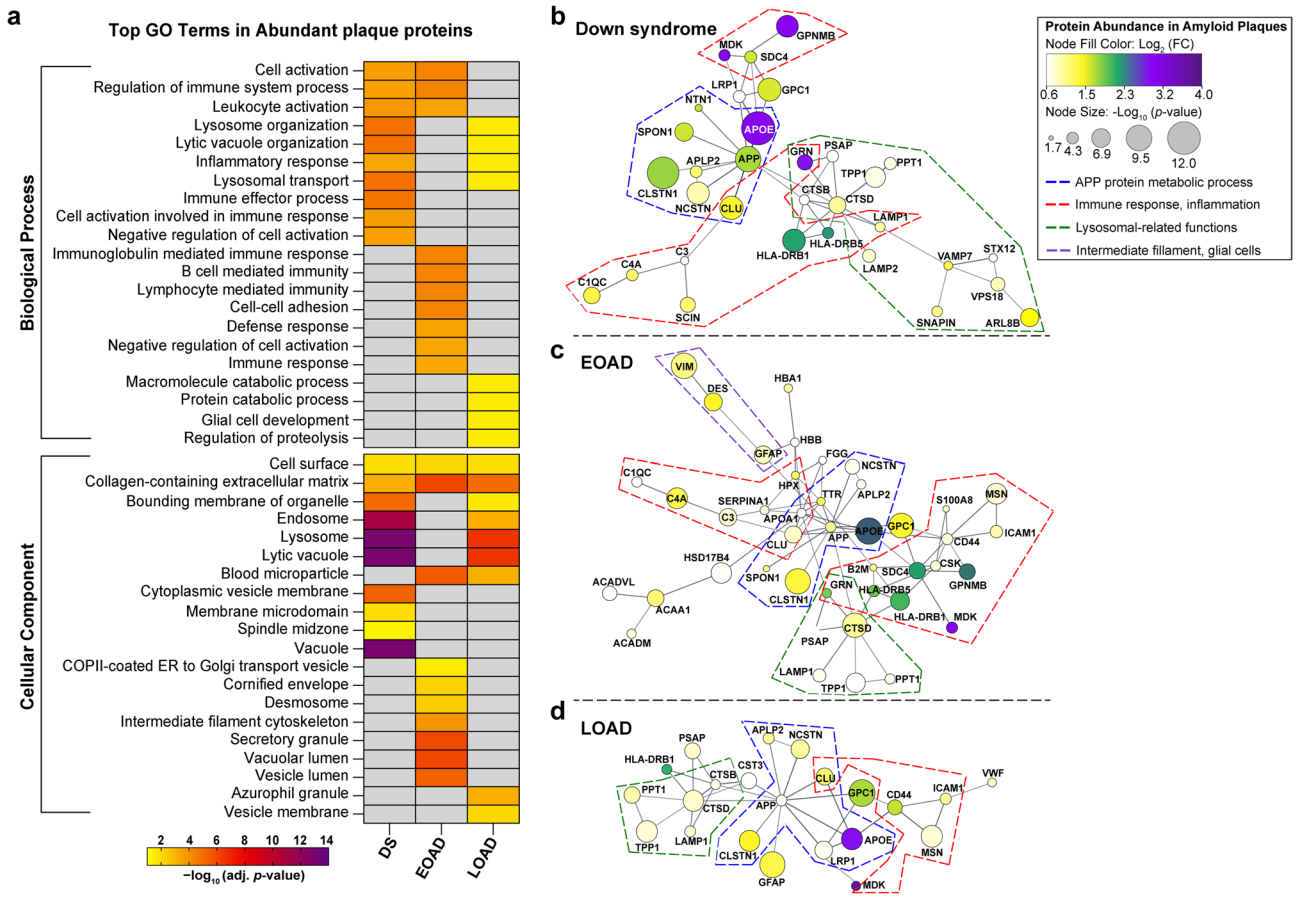

Fig. 5 Gene ontology annotation and protein–protein interaction networks of significantly abundant proteins in Aβ plaques. **a** GO terms heatmap depicts top ten enriched BP and CC GO terms for significantly abundant Aβ plaque proteins in DS, EOAD, and LOAD. Color indicates the adjusted p value < 0.05 (− Log_{10} [adj. p value]). **b–d** Protein networks (PPI Enrichment $p = 1 \times 10^{-16}$) show functional and physical amyloid plaques protein associations in DS (**b**), EOAD (**c**) and LOAD (**d**). Node color indicates fold-change ($\log_2$ [FC]) and node size depicts adjusted p value (-$\log_{10}$ [p value]) from the student's two-tailed t test. Disconnected nodes are not shown in the network. Colored dotted lines highlight groups of proteins based on functions/pathways observed in the GO terms; blue: APP protein metabolic process, red: immune response and inflammation, green: lysosomal-related functions, and purple: intermediate filament proteins, glial cells. GO terms annotation was performed using R package *clusterProfiler* v 4.8.2. PPI networks were created in Cytoscape v 3.10.0 using STRING database v 11.5

Aβ plaque-protein signature is related to APP processing, immunity, and lysosomes

Aβ plaques functional analyses

We identified functional associations for the significantly abundant proteins in Aβ plaques and AD non-plaque tissue by performing 'GO enrichment analysis' (FDR < 0.05, Supp. Tables 6–13). Top enriched biological process (BP) GO terms in DS included lytic vacuole organization, lysosome organization, and lysosomal transport (for the three terms, $p = 1.29 \times 10^{-5}$, Fig. 5a, Supp. Table 6). We also identified terms cell activation ($p = 0.00024$), regulation of immune system process ($p = 0.00027$), and leukocyte activation ($p = 0.00016$), which were also observed in EOAD (Fig. 5a). For cellular component (CC), we identified as the top terms vacuole, lysosome, lytic vacuole ($p = 9.56 \times 10^{-14}$), and endosome ($p = 9.71 \times 10^{-14}$, Fig. 5a, Supp. Table 10), similarly as BP GO terms. In contrast, EOAD most enriched BP terms were regulation of immune system process, B-cell-mediated immunity, immunoglobulin-mediated immune response, and lymphocyte-mediated immunity ($p = 4.33 \times 10^{-5}$, Fig. 5a, Supp. Table 6). Top CC GO terms in EOAD were secretory granule ($p = 1.13 \times 10^{-6}$), vacuolar lumen, and collagen-containing extracellular matrix (both $p = 8.75 \times 10^{-7}$, Fig. 5a, Supp. Table 10). LOAD also showed BP GO terms related to lysosomes as observed in DS, yet with a lower significance. For instance, we identified lysosomal transport and organization and lytic vacuole organization ($p = 0.0288$ Fig. 5a, Supp. Table 6). CC GO terms included lysosome and lytic vacuoles ($p = 2.47 \times 10^{-7}$), collagen-containing extracellular matrix ($p = 9.41 \times 10^{-6}$),

and endosome ($p = 0.00063$) (Fig. 5a, Supp. Table 10), highlighting functional similarities of plaque-associated proteins between DS and LOAD.

We also evaluated the physical and functional protein interactions of significantly abundant proteins in Aβ plaques, using Cytoscape and the STRING database (Fig. 5b–d). The networks for amyloid plaque proteins for all the cohorts evaluated showed a significant degree of protein–protein interactions (PPI enrichment $p = 1 \times 10^{-16}$). We observed a consistent group of proteins in all forms of AD evaluated, which were grouped based on functional enrichment (Fig. 5b–d). For instance, we identified proteins related to APP and Aβ metabolism (APP, APOE, CLU, CLSTN1, NCSTN, APLP2, and SPON1), immune response and inflammation (HLA-DRB1, HLA-DRB5, C1QC, C4A, and C3 consistent in DS and EOAD; CD44, ICAM1, and MSN in EOAD and LOAD), and lysosomal-related functions (PPT1, TPP1, LAMP1, PSAP, and CTSD). APOE was highly abundant in Aβ plaques in DS and LOAD (Fig. 5b, d) compared to EOAD, being the most significant in DS (Fig. 5b) in comparison to EOAD and LOAD. We also identified a group of glial-related proteins in EOAD network, namely VIM, DES, and GFAP (Fig. 5c). Overall, our findings suggest a similar plaque-protein signature in the three groups, which were functionally associated mainly to APP and Aβ processing, immunity-related responses, and lysosomal functions.

In addition, an analysis of the ten most abundant proteins (ranked by FC) differentially enriched in Aβ plaques in DS, EOAD, or LOAD further showed the relationship of Aβ plaque-associated proteins with lysosomal and immune-related functions (Supp. Table 14). According to the GO annotation, we found that the significantly enriched amyloid plaque proteins in DS predominantly relate to endo/lysosomal functions, including CLCN6, ATG9A, and VAMP7 (Fig. 6, Supp. Table 14). Oligodendrocyte protein MOG was significantly decreased in plaques for all cohorts, but

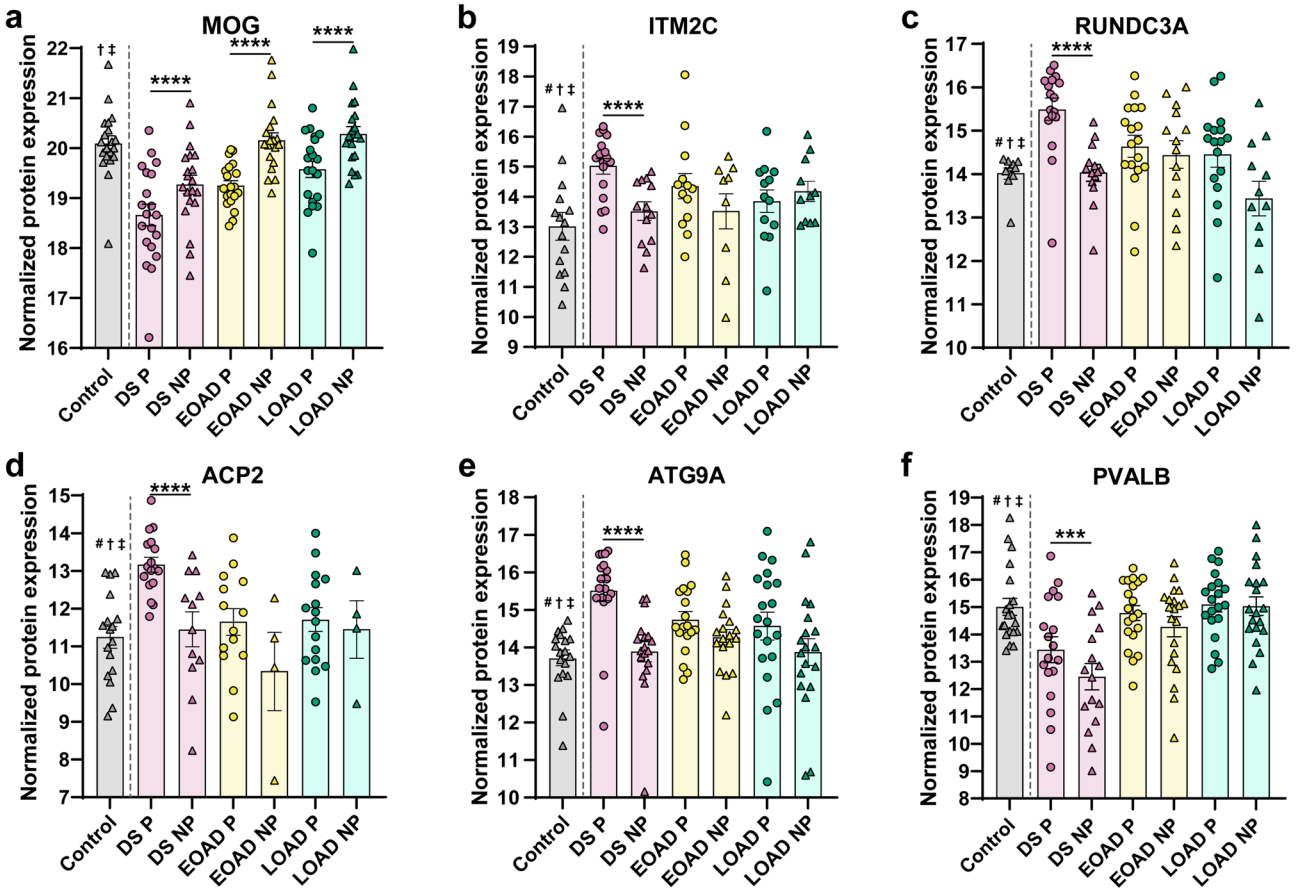

Fig. 6 Enriched Aβ plaque proteins of interest in DS compared with EOAD and LOAD. (**a–f**) Normalized protein expression obtained from the label-free quantitative mass spectrometry proteomics of abundant Aβ plaque proteins of interest in DS. Proteins are shown by order of decreasing significance. Proteins of interest were defined as significant (FDR < 5%, fold-change > 1.5) only in DS and also have known or predicted roles in AD and DS. Pairwise comparisons p values are indicated. * $p < 0.05$, **** $p < 0.0001$. Error bars indicate standard error of the mean (SEM). Significant pairwise comparisons are indicated for those analyses that were performed, controls are shown as reference. Additional symbols on top of the control bar indicate that the given protein is not significantly abundant in non-plaque AD tissue compared to controls in # DS, † EOAD, and ‡ LOAD, respectively

fold-change suggests an increased reduction in DS (Supp. Table 3, Fig. 6a) in comparison to the other groups. We identified protein ITM2C, which is involved in Aβ peptide production [29] (Fig. 6b). We also observed proteins with functions linked to presynaptic signaling and axon guidance, namely, RUNDC3A and NTN1 [60, 104] (Fig. 6). The calcium-binding protein and marker of inhibitory neurons PVALB was significantly enriched in DS plaques but was unaltered in EOAD and LOAD (Fig. 6f). In contrast, we observed that Aβ plaque proteins significantly abundant in EOAD are mostly related to immune response, immunoglobulin-mediated immune response (S100A7, HPX, and IL36G), as well as vacuole lumen and secretory vesicles related (GGH, TTR). The protein EPPK1 is linked to cytoskeletal organization functions such epithelial cell proliferation and intermediate filament organization (Supp. Table 14). In LOAD, we observed a series of proteins involved in bounding membrane of organelle, collagen-containing extracellular matrix, and vesicle membrane (CYB5B, VWF and PTPRN2). Although we did not observe particular association with GO terms, other amyloid plaque LOAD proteins, including TIMM8A, ACSS3, and SFXN5 (linked to mitochondrial functions) [89, 133, 138], THUMPD1 and RPS7 (related to RNA-binding activity and ribosomes) [14, 128] and NRXN2 (protein–protein interactions at the synapses) [76] were identified (Supp. Table 14). These observations support our findings in the GO functional enrichment and protein interaction networks, providing evidence that some of the most abundant proteins in DS plaques are primarily linked to lysosomal pathways.

Non-plaque tissue functional analyses

GO terms for abundant non-plaque proteins showed chromatin remodeling as the top BP term for all experimental groups (DS $p = 0.00128$, EOAD $p = 5.79 \times 10^{-9}$, LOAD $p = 1.69 \times 10^{-10}$, Supp. Figure 3a, Supp. Table 8). Importantly, top BP GO terms in DS were associated with integrin-mediated signaling, extracellular structure, and extracellular matrix organization ($p = 0.00684$, Supp. Figure 3a, Supp. Table 8). In contrast, EOAD and LOAD top BP GO terms included protein–DNA complex assembly ($p = 4.74 \times 10^{-6}$ and $p = 1.14 \times 10^{-8}$, respectively), regulation of gene expression (EOAD $p = 5.08 \times 10^{-5}$, LOAD $p = 1.68 \times 10^{-8}$), and nucleosome assembly (EOAD $p = 4.74 \times 10^{-6}$, LOAD $p = 3.25 \times 10^{-8}$) (Supp. Figure 3a, Supp. Table 8). Top CC GO terms for DS were collagen-containing extracellular matrix, which was also observed in EOAD and LOAD, external encapsulating structure, and extracellular matrix ($p = 3.52 \times 10^{-8}$, Supp. Figure 3a, Supp. Table 12). Top CC GO term for EOAD was nucleosome ($p = 4.44 \times 10^{-6}$), which was also identified in DS and LOAD. Other EOAD top CC GO terms were DNA packaging complex ($p = 8.01 \times 10^{-6}$) and protein–DNA complex ($p = 2.23 \times 10^{-5}$) (Supp. Figure 3a, Supp. Table 12). In a similar fashion, LOAD top CC GO terms were DNA packaging complex, protein–DNA complex (both $p = 3.78 \times 10^{-14}$), and nucleosome ($p = 1.71 \times 10^{-12}$) (Supp. Figure 3a, Supp. Table 12).

We also created protein interaction networks of non-plaque tissue DS, EOAD, and LOAD proteomes, which showed a highly significant degree of protein–protein interactions (PPI enrichment $p = 1 \times 10^{-16}$, Supp. Figure 3b–d). We observed groups of RNA-binding proteins, such as SRSF4, eukaryotic initiation factors (eIF4), and the heterogeneous nuclear ribonucleoproteins (hnRNP) protein family, primarily in EOAD and LOAD networks (Supp. Figure 3c, d). We also observed a set of intermediate filament and glial proteins, such as GFAP, AQP4, DES, VIM, ALDH1L1, and GART (Supp. Figure 3b–d). Additionally, there were groups of histone proteins related to the nucleosome, such as H2A, H2B, and H1 protein families (Supp. Figure 3b–d). Particularly, the DS protein interaction network exhibited a set of collagens, laminins, cell adhesion proteins, proteoglycans, and heparin sulfate proteins (Supp. Figure 3b) as well as proteasome and chaperone proteins also involved in regulation of gene expression, including SQSTM1, PSMB4, PSMD4, and HSPB6 (Supp. Figure 3b). Our findings highlight a pivotal role of extracellular matrix (ECM) and structural components in DS besides the proteins associated to Aβ plaque pathology.

Comparative analysis with previous human AD proteomics and identification of novel plaque proteins

We compared the differentially abundant proteins found in Aβ plaques and AD non-plaque tissue with previous human AD proteomics studies compiled in the NeuroPro database [4]. We observed that 77.7% of altered proteins identified in amyloid plaques in our study were also identified in previous AD plaque proteomics studies (Fig. 7a). From the 301 significantly altered plaque proteins that we identified in the present study, 13.6% have not been found in previous plaque proteomics studies, but only reported as significantly altered in bulk brain tissue proteomics studies (Fig. 7a). Similarly, 85.2% of the proteins we identified in the non-plaque tissue have been described in previous plaque and bulk tissue proteomics studies, whereas 10.9% have been identified in bulk human brain tissue but not in plaque proteomics studies (Fig. 7a). Interestingly, we identified in our study 34 proteins that have not been described previously in any human AD proteomics study, either in plaques or in bulk tissue (Fig. 7a, Supp. Table 15–16).

In DS specifically, we identified seven amyloid plaque proteins and eight non-plaque tissue proteins significantly

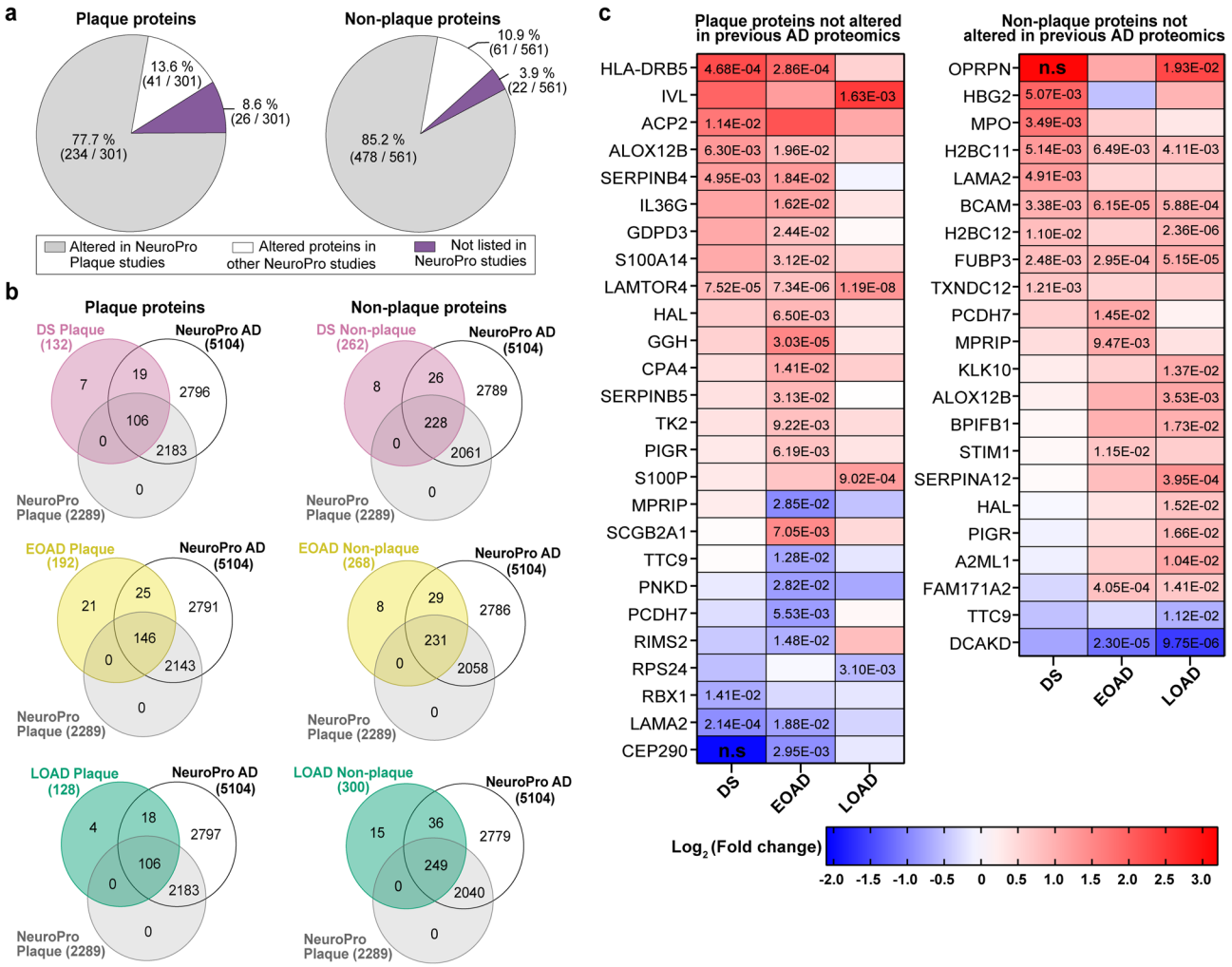

Fig. 7 Comparison of protein changes with previous advanced AD proteomics studies. **a** Altered proteins identified in the current study were compared with proteins found altered in previous AD proteomics compiled in NeuroPro [4] (v1.12; https://neuropro.biomedical.hosting/). Pie charts show that 77.7% (234/301) of altered plaque proteins in the present study have been identified in previous AD plaque proteomics studies (gray). 13.6% (41/301) of the proteins have been seen only in bulk tissue proteomics studies (white), and 8.6% (26/301) of the altered proteins observed in the current study have not been described in previous AD proteomics (purple). In a similar fashion, 85.2% (478/561) proteins altered in AD non-plaque tissue have been observed in AD plaque proteomics, 10.9% (61/561) only in bulk tissue proteomics, and 3.9% (22/561) have not been described in previous AD proteomics studies. **b** Venn diagrams illustrate the altered proteins identified in Aβ plaques and AD non-plaque tissue for each AD subtype evaluated, in comparison to the 5104 altered proteins in advanced AD registered in NeuroPro database. **c** Heatmaps depicting the fold-change (Log_2 [FC]) of the plaque and AD non-plaque altered proteins identified in the present study that have not been described in previous AD proteomics. Numbers in the cells represent the significance (FDR < 0.05) values observed in the pairwise comparisons, n.s represent no significant differences regardless of the fold-change

altered in our study, which have not been found in past AD brain tissue proteomics studies (Fig. 7b, Supp. Table 17). Similarly, we identified in EOAD 21 significantly altered proteins in plaque and eight in non-plaque tissue, which have not been described previously (Fig. 7b, Supp. Table 17). In the case of LOAD, we observed four significantly altered proteins in amyloid plaques and 15 in non-plaque tissue that have not been identified in previous AD plaques or bulk brain tissue proteomics studies (Fig. 7b, Supp. Table 17). From this group of proteins, LAMTOR4 (late endosomal/lysosomal adaptor and MAPK and MTOR activator 4) was significantly enriched in Aβ plaques in all the cohorts analyzed (Fig. 7c). The proteins HLA-DRB5, ALOX12B, and SERPINB4 were significantly enriched in DS and EOAD amyloid plaques (Fig. 7c). In contrast, LAMA2 was significantly decreased in DS and EOAD amyloid plaques (Fig. 7c). On the other hand, we observed the histone protein H2BC11, the basal cell adhesion protein BCAM, and the DNA-binding protein FUBP3 significantly enriched in non-plaque tissue in DS, EOAD, and LOAD (Fig. 7c). The protein centrosomal protein of 290 kDa (CEP290) showed a marked decrease in DS Aβ plaques compared

to DS non-plaque tissue; however, it was detected in few cases of the 20 evaluated in that cohort (Supp. Table. 3), reason why it did not reach FDR < 0.05 (Fig. 7c). The protein FAM171A2 was significantly enriched only in EOAD and LOAD, contrary to the protein DCAKD that was significantly decreased in EOAD and LOAD non-plaque tissue (Fig. 7c). Overall, our proteomics findings are consistent with previous proteomics studies. Notably, our comparative analysis allowed us to identify novel proteins in AD human proteomics.

Validation of the Aβ plaques protein signature in DS and novel plaque proteins in human DS proteomics

The NeuroPro database is a powerful tool to investigate proteomic changes in AD human brains. However, by the time of writing this article, the database does not include DS proteomics data. Therefore, we compared our DS amyloid plaques proteomics findings with our previous study (Drummond et al., 2022 [31]) where unbiased localized proteomics was used to interrogate the DS amyloid plaques proteome. In the study led by Drummond and colleagues, any Aβ plaque detected by IHC was sampled regardless of plaque morphology. We observed 2522 proteins between both DS plaque proteomics datasets, comprised of 1981 proteins in the present study and 2258 proteins in our previous work (excluding isoforms). We observed 68.1% (1717/2522) of proteins overlapping between both studies, with a total of 228 significantly altered plaque proteins in either dataset. Among these, 21.9% (50/228) were common to both studies (Fig. 8a). Particularly, 36% (82/228) of the significantly altered proteins in the present study were not significant in Drummond et al., and conversely, 42.1% (96/228) of the proteins identified in the previous study were not detected in the current dataset (Fig. 8a, Supp. Table 18). This variance may reflect differences in statistical thresholds and increased sample size, providing higher power in this study to identify more plaque-enriched proteins in DS with greater confidence. For instance, 35 proteins that were significantly enriched proteins detected in the Drummond study but not significant in ours were nonetheless observed in our dataset, with many showing increased abundance trends that nearly reached significance. In addition, from the proteins that were different between both studies (Fig. 8a), only 12 had a different direction of change, suggesting that most of the differences observed between the datasets are due to the differential stringency applied and the number of samples. Despite these differences, we observed a significant positive correlation between the Aβ plaque proteomes of the DS cohorts ($p < 0.0001$, $R^2 = 0.60$, Fig. 8b). In fact, the 50 common proteins between both studies were changing in the same direction (48 enriched and 2 decreased in plaques, Fig. 8b). Within these set of amyloid plaque

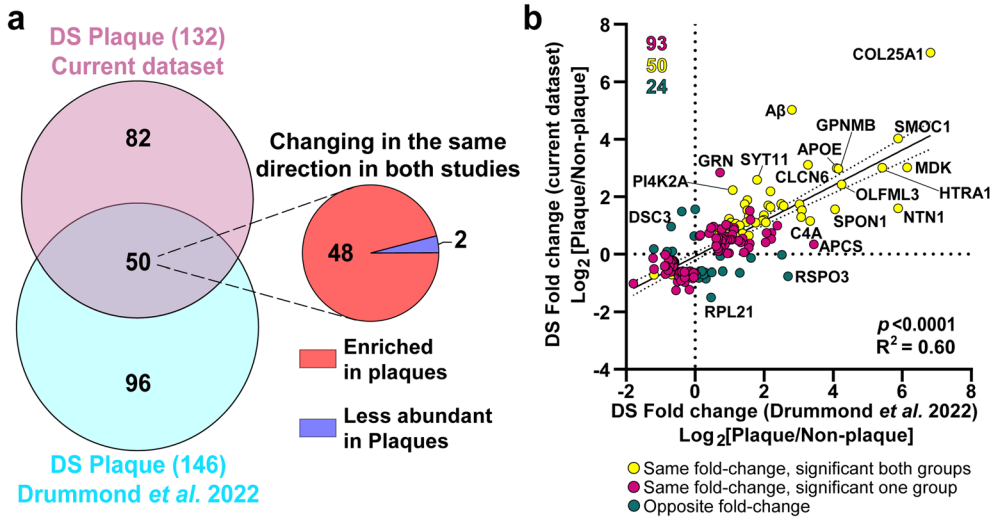

Fig. 8 Comparison of protein changes between the DS plaques localized proteomics studies. **a** Venn diagram depicts differentially abundant proteins identified in the current study and the previous DS plaque proteomics study (Drummond et al. 2022, [31]). We identified 132 significantly altered proteins compared to 146 identified previously. From the 50 common proteins identified, 48 were enriched in Aβ plaques and 2 proteins were less abundant in both studies. **b** Correlation analysis between differentially abundant proteins in the current study and previous DS localized proteomics. Yellow dots represent significant proteins changing in the same direction (highly abundant or less abundant proteins in both groups evaluated) in both groups compared. Magenta dots represent proteins changing in the same direction, but are significant only in one of the groups evaluated. Green dots represent proteins changing in opposite direction (i.e., abundant in one group and less abundant in the other group evaluated). There was a significant positive correlation ($p < 0.0001$, $R^2 = 0.60$) between the two datasets

proteins, we identified Aβ peptide, APP, COL25A1, and a set of previously described plaque proteins, such as APOE, SMOC1, CLU, C3, and CLCN6 among others (extended data in Supp. Table 18), thus validating a plaque-protein signature also observed in DS Aβ pathology. Interestingly, from the seven novel DS plaque proteins regarding the NeuroPro database (Supp. Table 17), only ACP2 was also observed in the previous DS plaque proteomics study (Supp. Table 18). Our study is consistent with previous similar proteomics studies on AD brains, and further expanded the proteins present at these pathological lesions.

Validation of CLCN6 and TPP1 in Aβ plaques by immunohistochemistry

We performed immunofluorescence to validate the late endosome protein CLCN6, as it emerged as the most abundant plaque protein among the top ten significantly altered proteins in DS Aβ plaques (Supp. Table 14). Previously, CLCN6 was identified within plaques solely through our

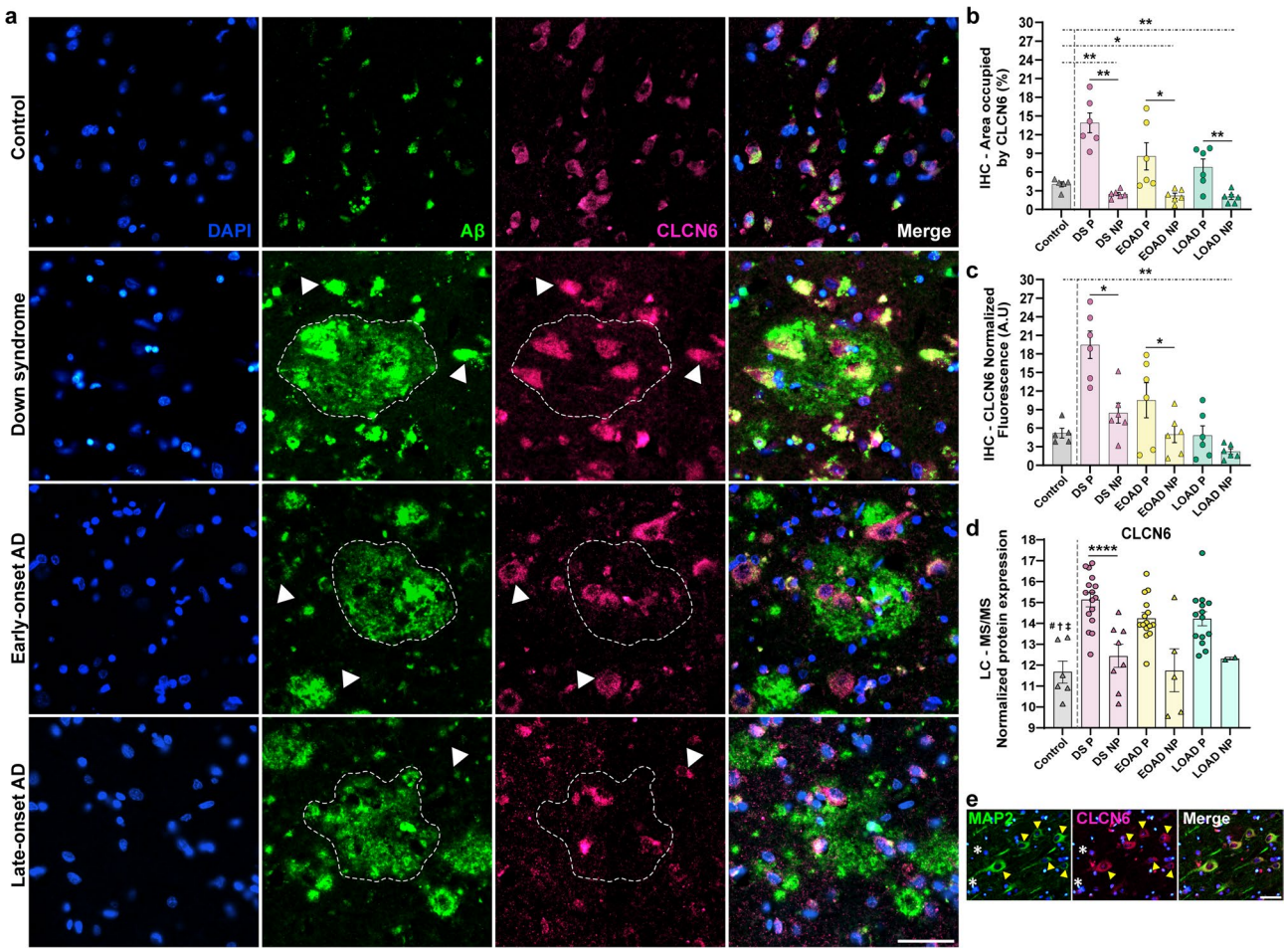

Fig. 9 Immunohistochemical validation of CLCN6 protein in human brain tissues. **a** Immunohistochemistry of Aβ and CLCN6 in control, DS, EOAD, and LOAD. Dotted line represents the plaque in CLCN6 panel. White arrowheads depict positive CLCN6 cells surrounding Aβ plaques. Merge panel shows intracellular colocalization of CLCN6 and Aβ. Scale bar 50 µm. **b** Bar graph showing normalized area occupied by CLCN6 and **c** normalized CLCN6 fluorescence, corresponding to plaque and non-plaque tissue. Paired two-tailed *t tests* indicate statistical differences between Plaque vs non-plaque tissue samples, whereas unpaired two-tailed *t tests* were performed to compare control non-plaque samples vs DS, EOAD, and LOAD non-plaque samples. For panels B and C, $n=6$ cases. **d** Normalized protein expression of CLCN6 obtained from the label-free quantitative mass spectrometry proteomics. **e** Immunohistochemistry of neuronal protein MAP2 and CLCN6 in DS tissue away from plaques. Yellow arrowheads depict co-staining of MAP2 and CLCN6. White asterisks show small unidentified cells negative for MAP2 and positive for CLCN6. Scale bar 50 µm. Pairwise comparisons p values are indicated. * $p<0.05$, ** $p<0.01$, **** $p<0.0001$. Error bars indicate standard error of the mean (SEM). Significant pairwise comparisons are indicated for those analyses that were performed, controls are shown as reference. Additional symbols on top of the control bar indicate that the given protein is not significantly abundant in non-plaque AD tissue compared to controls in # DS, † EOAD and ‡ LOAD, respectively

proteomics study [31], without histochemical evidence of its presence in Aβ plaques. Immunofluorescence staining showed CLCN6 localized in the cytoplasm of cells adjacent to intracellular 4G8 anti-Aβ-positive staining (Fig. 9a). Within plaques, Aβ appears to encapsulate CLCN6 + cells, with the highest intracellular colocalization between CLCN6 and Aβ. Moreover, CLCN6 + /4G8 + cells were observed on the periphery of amyloid plaques, suggesting a potential role for CLCN6 + cells in either releasing Aβ species into plaques or participating in a phagocytic process (Fig. 9a).

Quantification of CLCN6 fluorescence and area, normalized by plaque area, showed a significant increase in Aβ plaques in DS, EOAD, and LOAD compared to non-plaque tissue (Fig. 9b–c). Interestingly, CLCN6 area was significantly reduced in non-plaque tissue across all cohorts relative to control non-plaque tissue (Fig. 9b–c). These histochemical results are consistent with trends observed in the proteomic data (Fig. 9d). Further co-staining with MAP2 indicated that most CLCN6 + cells are neurons, with a minority of smaller MAP2- cells also displaying CLCN6 staining (Fig. 9e). Overall, these findings suggest that CLCN6 may be involved in storing and transporting Aβ, which could be released extracellularly in the AD pathogenic context, contributing to amyloid plaque formation.

TPP1 is a lysosomal protein that was identified in previous human proteomics [4, 31], but has not been characterized in Aβ plaques by immunohistochemistry. Our validation revealed a distinctive punctate expression pattern common of lysosomal-associated proteins. These bright puncta were consistently observed both within Aβ plaques and in the surrounding non-plaque regions (Fig. 10a). In addition to the punctate signal, TPP1 expression appeared to be widespread and highly abundant throughout the tissues, with immunoreactivity present diffusely in the cytoplasmic regions of presumably neurons and glial cells (Fig. 10a). We observed TPP1-positive staining in Aβ plaques, with a pattern suggesting that the protein is not directly colocalized with Aβ. Instead, TPP1 appears to occupy spaces within the plaques

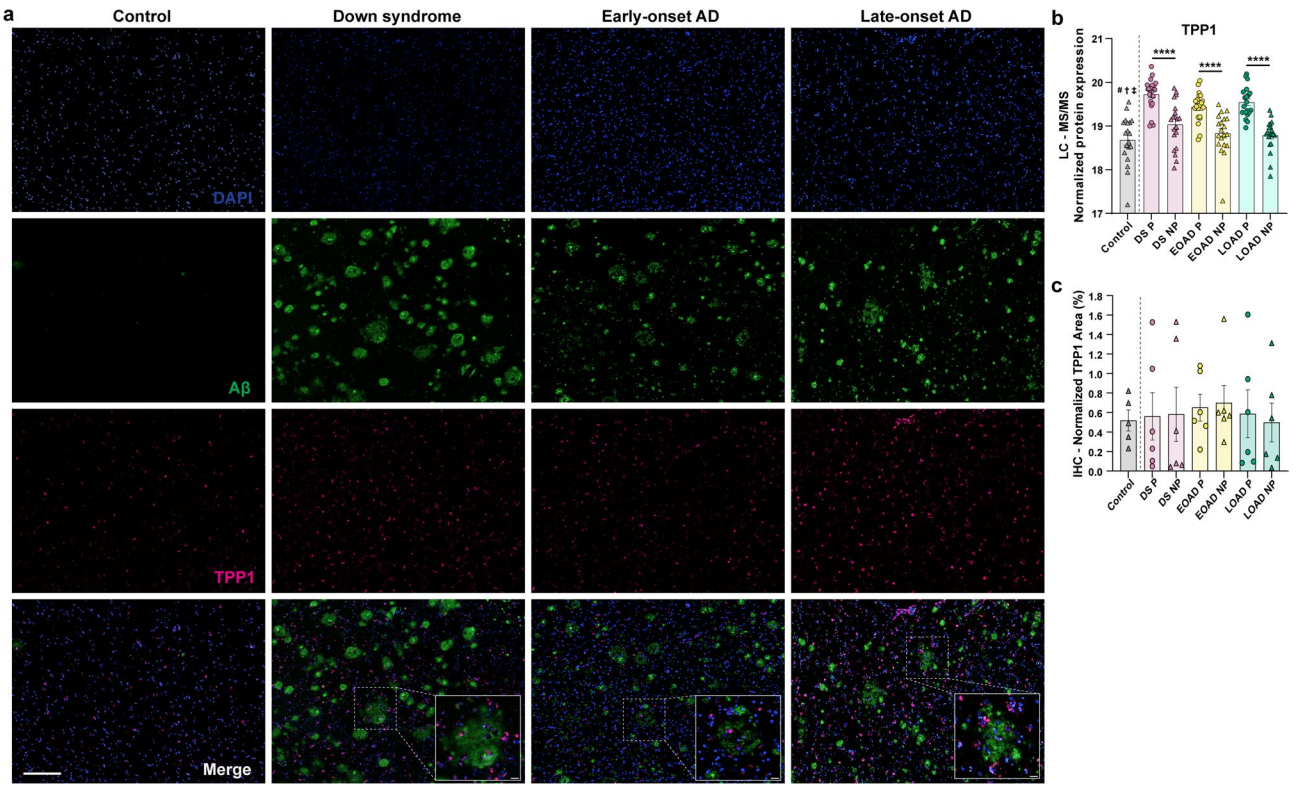

Fig. 10 Immunohistochemical validation of TPP1 protein in human brain tissues. **a** Immunohistochemistry of Aβ and TPP1 in control, DS, EOAD, and LOAD. Bottom panel, dotted lines highlight TPP1-positive immunolabeling embedded in Aβ plaques for DS, EOAD, and LOAD. Scale bar 200 µm and 20 µm for plaque zoom panels. **b** Normalized protein expression of TPP1 obtained from the label-free quantitative mass spectrometry proteomics. Pairwise comparisons *p* values are indicated. **** $p < 0.0001$. Significant pairwise comparisons are indicated for those analyses that were performed, controls are shown as reference. Additional symbols on top of the control bar indicate that the given protein is not significantly abundant in non-plaque AD tissue compared to controls in # DS, † EOAD, and ‡ LOAD, respectively. **c** Bar graph showing normalized TPP1 area, corresponding to plaque and non-plaque tissue. No statistical differences between plaque vs non-plaque tissue samples were found. For panels C, $n = 6$ cases. Error bars indicate standard error of the mean (SEM)

that are less densely packed with amyloid or is embedded within denser amyloid aggregates while remaining distinguishable (bottom panel Fig. 10a.). Our proteomics analysis showed that TPP1 is significantly enriched in plaques of DS, EOAD, and LOAD (Fig. 10b). However, the enrichment of TPP1 in amyloid plaques is low (fold-change of 1.62 in DS, 1.51 in EOAD, and 1.69 in LOAD; Supp. Table 3). We did not observe significant differences in TPP1 levels by IHC (Fig. 10c). Notably, the density and intensity of TPP1 staining within plaques were qualitatively similar to those in the non-plaque areas, consistent with proteomic findings indicating subtle enrichment of TPP1 in plaques. Overall, our observations suggest that TPP1 is not exclusively localized to plaques but is instead distributed throughout the brain parenchyma.

Correlation of protein changes to clinical traits

WGCNA allowed us to identify correlations between clusters of co-expressing proteins with clinical traits, including *APOE* genotype, sex, age, TDP-43 and α-synuclein copathologies, and Aβ and pTau pathology regional levels. Top GO BP and CC annotations associated with each module are presented (FDR < 0.05), with additional information about module sizes and extended functional annotation provided in the supplementary tables 19 to 26. Notably, Module 1 from DS plaques, containing multiple highly abundant plaque proteins (e.g., CLCN6, MDK, ITM2C, ARL8B, and C1QC), correlated significantly only with pTau levels ($R = 0.5$, $p = 0.024$) (Supp. Figure 4). In EOAD, we observed negative correlations between *APOE* 3 and 4 genotypes, as well as between *APOE* and age. Functional annotation indicated that modules correlated with *APOE* genotype are related to synaptic signaling and mitochondrial metabolic processes (Supp. Figure 5). Additionally, Module 5, including astrocytic proteins DES, VIM, GFAP, GJA1, and ALDH1L1, was positively correlated with *APOE3* and negatively correlated with *APOE4* ($R = 0.54$, $p = 0.014$ and $R = -0.52$, $p = 0.02$), underscoring astrocytes relevance in AD neuropathology (Supp. Figure 5). On the other hand, LOAD plaques co-expression networks revealed a significant correlation between Module 58, functionally associated with the axonal myelin sheath and containing multiple oligodendrocyte proteins (MOG, MBP, MAG, CNP, HAPLN2, and PLP1), and Aβ neuropathology ($R = -0.51$, $p = 0.021$) (Supp. Figure 6). In addition, Module 30, comprising proteins COL25A1, C3, and fibrinogens (FGA, FGB, FGG), was positively correlated with *APOE4* and Tau ($R = 0.45$, $p = 0.048$ and $R = 0.56$, $p = 0.01$, respectively), and negatively correlated with age ($R = -0.63$, $p = 0.011$) (Supp. Figure 6), suggesting potential age-dependent alterations in some of the proteins associated with module 30. Age correlated significantly with multiple modules in all cohorts, but it is noteworthy that the LOAD cohort is inherently older than DS and EOAD.

In non-plaque tissue co-expression networks, modules 15, 29, and 44 in DS non-plaques showed opposing correlations with *APOE3* and *APOE4* (Supp. Figure 7), with Module 15 also associated with "Cytoplasmic translation" and "Ribosomal subunit" functions. EOAD non-plaque networks showed the most modules significantly correlated with *APOE* genotype (Supp. Figure 8). Functional enrichment included terms related to neuron differentiation, axon structure, presynapse, cytoskeletal organization, and GTPase regulation in modules negatively correlated with *APOE4* (Supp. Figure 8). Module 55 was negatively correlated with *APOE4* and positively with Tau ($R = -0.57$, $p = 0.085$ and $R = 0.5$, $p = 0.025$) (Supp. Figure 8), and included proteins C3 and fibrinogens (FGA, FGB, FGG), similar to Module 30 in LOAD plaques. This observation suggests that common proteins may have distinct roles in AD pathology across subtypes. LOAD non-plaque correlation networks showed a few modules significantly correlated with *APOE4* genotype, similarly as LOAD plaques correlations (Supp. Figure 9). In particular, Module 23 was associated with "response to unfolded protein," comprising multiple heat shock proteins, such as HSPE1, HSPD1, HSPA8, HSPA9, and HSP90AA1 (Supp. Figure 9). Overall, our WGCNA analysis revealed that each cohort evaluated has distinct clusters of co-expressing proteins that correlate with clinical variables, such as *APOE* genotype, pTau, and Aβ pathology, suggesting that AD pathology progresses through different mechanisms in DS, EOAD, and LOAD. The interaction of the multiple proteins identified on each experimental group and clinical traits may inform the development of therapies and biomarkers tailored to each form of AD.

Discussion

We conducted a comparative analysis of Aβ plaque and non-plaque proteomes in individuals with DS, EOAD, and LOAD, identifying 43 proteins consistently altered in Aβ plaques across all cohorts. The Aβ plaque proteomes showed a high degree of correlation among DS and AD subtypes, although certain proteins showed differential abundance across the groups. GO functional enrichment and protein–protein interaction analyses indicated predominant associations of Aβ plaque proteins with APP metabolism, lysosomal functions, and immune responses. Our findings suggest a shared "Aβ plaque protein signature" across the evaluated groups, underscoring a notable similarity between the DS plaque proteome and those of EOAD and LOAD. In contrast, the non-plaque proteome showed group-specific variations in protein abundance, leading to distinct functional associations. These results highlight physiological

differences in the brains of individuals with DS compared to those with EOAD and LOAD.

Our unbiased localized proteomics approach enabled the identification of hundreds of proteins associated with Aβ plaques, including HTRA1, CLU, CLSTN1, GPC1, and VIM, which have been linked to protective roles against Aβ neuropathology or regulation of amyloid production [44, 73, 120, 125]. Additionally, we confirmed the presence of proteins in Aβ plaques that are less studied in the context of AD, such as CLCN6, ARL8B, TPP1, VAMP7, and SMOC1 [31], suggesting a potential important role for these proteins in AD pathology. We previously demonstrated a strong colocalization of SMOC1 with diffuse and neuritic plaques, with a higher proportion in hippocampus than in neighboring cortex [31]. Most recent findings have shown colocalization of SMOC1 and PDGFRα, indicating that SMOC1 expression is highest in OPCs, as expected from RNAseq datasets [5]. Furthermore, our findings include several previously unreported plaque-enriched proteins in human AD and DS proteomics, expanding on earlier studies. These novel proteins—linked to critical processes in AD pathology and DS, such as lysosomal function (ACP2, LAMTOR4), immune response (HLA-DRB5, IL36G), and ubiquitination (RBX1)—have been implicated in AD through genetic studies [20, 66, 87, 112, 123, 132, 135]. Thus, our results provide evidence supporting these proteins' involvement in AD pathophysiology.

Our network analysis revealed a functional pattern among plaque proteins, with an increased level of predicted protein–protein interactions observed across all experimental groups. Notably, proteins such as NTN1, NCSTN, SPON1, and CLSTN1 were present in all cohorts and have known associations with APP/Aβ processing [32, 47, 48, 77, 88, 94, 105, 111, 120, 134]. While APP metabolism is well recognized in AD, with the APP gene located on chromosome 21 [65], these APP-related proteins remain understudied in DS. Our proteomics data also highlighted the presence of immune and inflammation-related proteins, including C1QC, C4A, C3, MDK, CLU, HLA-DRB1, and HLA-DRB5. These proteins clustered near the APP node in the protein networks, suggesting potential interactions with Aβ. This observation aligns with prior studies linking complement proteins, CLU, and MDK to senile plaques [22, 74, 81]. Specifically, murine studies indicate that CLU may contribute to neurotoxicity and fibrillar Aβ deposition [26]. Conversely, MDK has been shown to bind Aβ, with transgenic mouse studies indicating a reduction in Aβ deposition, although the underlying mechanisms remain unclear [85]. Co-expression network analysis in murine AD models and human AD brain samples showed strong association of MDK with Aβ plaques and cerebrovascular amyloid (CAA), and suggest an increase in both parenchymal amyloid plaques and CAA, suggesting that MDK directly impacts amyloid deposition [74]. Furthermore, studies using AD mouse models suggest that complement proteins may contribute to synapse loss, dystrophic neurite formation, and increased Aβ aggregation, potentially through microglia–astrocyte crosstalk in response to amyloid pathology (reviewed by Batista and colleagues [7, 35, 56, 107, 131]). Additionally, our findings reveal the enrichment of HLA-DRB1 and the novel plaque-protein HLA-DRB5 in Aβ plaques. Previous single-cell transcriptomic studies of human AD prefrontal cortex have correlated HLA-DRB1 and HLA-DRB5 expression in microglia with AD pathology [80, 124], although the mechanisms of HLA proteins in Aβ neuropathology remain largely unknown.

Our Aβ plaques proteomics data highlighted the enrichment of multiple proteins associated with the endo/lysosomal pathway, supporting prior findings that lysosomal dysfunction is a fundamental mechanism in AD [17, 42, 86, 116]. We identified TPP1, PPT1, LAMP1, ARL8B, and confirmed VAMP7, previously identified as a novel amyloid plaque protein [31], which are involved in lysosomal trafficking, vesicle fusion and protein degradation [1, 100, 121]. ARL8B is associated with Niemann–Pick disease type C [99]. ARL8B also may have a neuroprotective role against amyloid pathology [46]. In addition, we showed that ARL8B is associated with plaques, specifically to areas that were not brightly stained for Aβ. In addition, we identified ARL8B expression in a subset of reactive plaque-associated astrocytes [31]. ARL8B has also been detected in cerebrospinal fluid of AD patients compared to controls and Huntington's disease patients, indicating that ARL8B altered levels are AD-specific [10]. LAMP1 has been found enriched in Aβ plaques, and studies using AD murine models have shown that LAMP1-plaque-associated protein is particularly increased in axons [43] and dystrophic neurites [108]. Additionally, there is an enrichment of LAMP1 in reactive microglia within senile plaques, which has been implicated in amyloid removal [6].

TPP1 is a lysosomal matrix protein and is ubiquitously expressed in the human brain [15]. TPP1 has been shown to destabilize Aβ through endoproteolytic cleavage [110], and deficiencies in TPP1, together with PPT1, are linked to the neurodegenerative lysosomal storage disease neuronal ceroid lipofuscinosis (NCL) [59]. TPP1 has been identified in previous human proteomics studies [4, 31], but our current work is the first to provide a preliminary characterization of its role in the context of AD plaque pathology. Label-free mass spectrometry is a highly sensitive technique, which explains our observation of a subtle but significant enrichment of TPP1 in plaques, despite that we did not have evidence of the same pattern in our histochemistry. Although our preliminary validation of TPP1 did not reveal significant differences between Aβ plaques and non-plaque tissue, we observed a punctate expression pattern throughout the brain parenchyma, with notable association to Aβ plaques. These findings are similar to

observations of other lysosomal proteins, such as ARL8B [31], LAMP1 [52], cathepsin D and lipofuscin [18], and CLCN6, which associate with plaques but do not directly colocalize with Aβ. This suggests that TPP1 may not interact directly with Aβ but is instead localized to small pockets within amyloid plaques where Aβ is either absent or undergoing degradation.

CLCN6 is predominantly expressed in neurons within the central and peripheral nervous systems and is localized in the late endosomes of neuronal cell bodies [92]. Our proteomics and immunohistochemical analyses confirmed the presence of CLCN6 in the neuronal cytoplasm, specifically surrounding intracellular Aβ, and revealed its enrichment in amyloid plaques compared to non-plaque tissue. Notably, CLCN6 has not been studied previously in the context of AD or DS, highlighting the novelty of these findings. Previous studies have demonstrated that CLCN6 disruption leads to lysosomal storage disease with behavioral abnormalities, resembling neuronal ceroid lipofuscinosis (NCL) [92, 95]. This pathology may be linked to a CLCN6 mutation impairing late endosome acidification, thereby compromising protein degradation and the autophagosomal pathway, which is a defect associated with late-onset NCL [103]. Late endosomes play a critical role in forming intraluminal vesicles and serve as reservoirs for sorting ubiquitinated proteins destined for lysosomal degradation. Disruption of CLCN6 may therefore impede the degradation of key proteins such as TDP-43 and Tau, potentially contributing to intracellular protein accumulation and drawing parallels with other neurodegenerative disorders [57, 103]. Additionally, our WGCNA analysis in DS plaques highlighted a co-expression network module, including CLCN6 and other highly abundant plaque proteins, associated with Tau neuropathology levels. Altogether, our data suggest that CLCN6 may play a substantial role in the aggregation of neurotoxic proteins associated with AD neuropathology through its function in the endo/lysosomal pathway.

A closer examination of the most significant functional associations in the DS Aβ plaque proteome elucidated a substantial enrichment of lysosomal-related GO terms, followed by those linked to the immune system and cell activation. Both lysosomal and immune processes are integral to AD pathophysiology [42, 69, 70, 81, 113, 116, 126]. Strong evidence suggests that endo/lysosomal alterations in DS are associated with APP and the βCTF fragment produced after BACE-1 cleavage of APP, potentially explaining early changes in DS [19, 58, 61, 62]. Increased systemic inflammation, possibly exacerbated by Aβ accumulation, is also evident in individuals with DS [34, 75]. Interestingly, the functional associations observed in the DS plaque proteome appear to be a combination of those found in EOAD and LOAD, further highlighting the Aβ plaque proteome similarity across cohorts.

Significant plaque proteins were enriched across all cohorts, with some proteins specifically enriched in certain groups. This may help understand AD pathogenesis and the unique mechanisms in DS and AD subtypes. Interestingly, COL25A1 (CLAC-P) was the most enriched protein in plaques, especially in DS compared to EOAD and LOAD. Previous studies in mice suggested that CLAC, derived from COL25A1, is crucial in converting diffuse Aβ deposits into senile plaques [51, 118]. This finding may partially account for the heightened amyloid pathology observed in DS. Moreover, previous research has shown that the interaction between CLAC and Aβ is determined by negatively charged residues in the central region [64]. Given recent discoveries about Aβ filaments in DS and Aβ fibril variation in different AD subtypes, structural differences in Aβ fibrils may result in unique interactions with COL25A1 [33, 97]. Further investigation is required to comprehend the binding affinity of COL25A1 in DS and other forms of AD. However, our previous study indicated similar levels of COL25A1 in DS and EOAD plaques [31]. It is plausible that the observed differences between our current and past studies are due to technical factors, such as sample preparation, data acquisition, and cohort size [98].

Our proteomics analysis revealed a significant reduction of oligodendrocyte proteins, including HAPLN2, PLP1, MOG, MAG, MBP, and BCAS1, within Aβ plaques and also in the non-plaque proteome across all cohorts compared to controls. Additionally, WGCNA analysis identified a co-expression module of these oligodendrocytic proteins that negatively correlates with Aβ neuropathology, suggesting that Aβ accumulation may impact oligodendrocyte function and myelin stability. Previous studies in the AD murine model 5xFAD reported loss of myelin-associated lipids and disruption of the myelin sheath associated with Aβ plaques in the brain parenchyma [67]. Zhan and colleagues provided evidence, using superior temporal gyrus of human AD brains, of increased levels of degraded MBP protein and colocalization with $A\beta_{42}$ in the plaque cores and also aggregated adjacent to the plaques [136]. Due to the interaction between MBP and $A\beta_{42}$, the authors suggest that degraded MBP and other damaged myelin components may have a role in plaque development [136]. These findings indicate that oligodendrocyte disruption may worsen neurodegeneration in the context of Aβ pathology and highlight a potential therapeutic target. A study in rhesus monkeys linked myelin degeneration to normal aging and cognitive decline [11]. Recent studies using transgenic mice and human AD tissues have shown that myelin defects promote Aβ plaque formation and cause transcriptional changes in oligodendrocytes seen in AD and other degenerative diseases [27, 101]. Given that individuals with DS often exhibit age-associated disorders earlier than euploid individuals [38], myelin damage may be an early characteristic in DS, potentially

exacerbating amyloid pathology. Further studies are warranted to understand how oligodendrocytes are impacted in DS and AD.

The analysis of the non-plaque tissue proteome in DS, EOAD, and LOAD highlighted two primary altered components in AD: the ECM and chromatin structure. In the DS non-plaque proteome, we observed a cluster of ECM-related proteins, which was not evident in EOAD and LOAD but suggested by functional annotation analysis. Early studies using human AD brain samples showed ECM proteins (collagen, laminin, and HSPG) colocalizing with neuritic plaques [90]. Subsequent findings in transgenic mice and human AD brain samples indicated increased mRNA levels of collagen-type VI proteins proportional to APP and Aβ expression, suggesting protective roles against Aβ neurotoxicity [21]. Our data indicate that the ECM in DS is more significantly affected compared to EOAD and LOAD. Recent studies using trisomy 21 iPSCs at different stages of neuronal induction suggested aberrant ECM pathways and increased cell–cell adhesion, affecting neural development [79, 83]. Proteomics studies of human AD brain tissues correlated cell–ECM interaction pathways and matrisome components with AD neuropathological and cognitive traits [63], and ECM components were observed in pre-clinical AD cases, suggesting early ECM alterations in AD. These observations support a more significant and earlier alteration of ECM proteins in DS, possibly exacerbated by AD neuropathology. Additionally, proteins linked to chromatin structure were consistently altered in non-plaque tissue in all groups, most prominently in LOAD and EOAD. Our observations align with previous research suggesting structural changes in chromatin accessibility and altered gene expression in AD [8, 78, 115, 122]. Studies using murine models of DS and trisomy 21 iPSCs have shown reduced global transcription activity and changes resembling those in senescent cells, such as chromosomal introversion, nuclear lamina disruption, and altered chromatin accessibility [82, 96]. This evidence may explain the differences observed in the protein interaction networks and functional annotation analyses between the non-plaque proteomes of DS and the AD subtypes studied.

While our study sheds light on the molecular mechanisms behind Aβ plaque pathology in DS and various forms of AD, it is essential to recognize certain limitations. Bottom–up proteomics identifies proteins from detected peptides, reflecting only the trypsin-digestible proteome. Proteins are assembled as the smallest set explaining all observed peptides, with specific proteoforms reported only if unique peptides are detected. Despite this limitation, bottom–up proteomics offers higher sensitivity than other methods and avoids the need for pre-selecting protein targets, making label-free mass spectrometry ideal for discovery proteomics. Our findings highlight significant proteome changes, providing a foundation for future hypothesis generation and further investigation into the mechanisms driving these protein alterations. However, future studies should use additional validation and characterization methods for candidate proteins, which could further substantiate our findings, such as evaluation by two-dimensional (2D) electrophoresis and Western blotting, in addition to immunohistochemistry. These top–down proteomic technologies will be helpful for quantifying the levels of specific proteins, thereby complementing the discovery-based approach of bottom–up proteomics and providing a more comprehensive view of protein isoforms and post-translational modifications.

Our analysis was also restricted to classic cored plaques and dense aggregates from DS and AD cases primarily at advanced disease stages, constraining our conclusions to an 'end-point' proteome profile. Nonetheless, we identified notable neuropathological distinctions between DS and other cohorts, potentially associated with observed proteomic alterations in plaque and non-plaque tissues. Future studies targeting different morphological types of plaques (i.e., diffuse or cotton-wool plaques) would be interesting. Our analysis was also limited to vulnerable brain regions in AD. Future investigations should encompass broader age ranges and include more detailed analysis of brain subregions, such as those within the hippocampus, entorhinal cortex, and adjacent temporal cortex. This approach could help create a more detailed 'proteomics landscape' of AD neuropathology, enhancing our understanding of disease progression and resilience mechanisms. Furthermore, membrane proteins, particularly integral membrane proteins, are often underrepresented in proteomics studies due to detection challenges. Finally, while our research is unbiased, it remains susceptible to variability arising from unknown genetic factors in each case. Subsequent research endeavors should integrate genetic details such as familial AD mutations and other known genetic variables, and expand on the sampling for *APOE* genotypes, to gain deeper insights into their impact on AD.

Conclusions

Our study provides novel insights into the amyloid plaque proteome of DS, highlighting key functional aspects and contrasting them with EOAD and LOAD. We observed a notable similarity among the plaque proteomes of DS, EOAD, and LOAD, with predominant associations of plaque proteins with endo/lysosomal pathways, immunity, and APP metabolism. Specifically, the identification of CLCN6 underscores its potential role in AD pathology through its involvement in the endo/lysosomal pathway and warrants further investigation as a potential therapeutic target. The analysis of the non-plaque proteome revealed significant differential

alterations in ECM and chromatin structure, emphasizing the nuanced differences between DS, EOAD, and LOAD. Our unbiased proteomics approach not only identifies enriched plaque proteins but also suggests potential therapeutic targets or biomarkers for AD, offering promising avenues for future research and clinical applications.

Supplementary Information The online version contains supplementary material available at https://doi.org/10.1007/s00401-025-02844-z.

Acknowledgements The authors wish to thank Jenny R Diaz for her valuable advice in writing the manuscript and Ludovic Debure for his technical assistance with this project. The authors also want to thank Dr. Eric Dammer for his valuable insights regarding weighted correlation network analysis for proteomics. Human post-mortem tissue was obtained from the NIH NeuroBioBank, the South West Dementia Brain Bank, University of Bristol, UK, member of the Brains for Dementia Research (BDR) Network, IDIBAPS Biobank from Barcelona, University of Pennsylvania, and NYU Grossman School of Medicine. The authors extend our gratitude to the families, clinicians, medical examiners, and coroners for their participation in this research.

Author contributions TW, MMA, and ED contributed to the conception and design of the research framework. MMA, EK, JS, AGP, and BU contributed to data collection. MMA, EK, and DL performed statistical analyses. MMA, DL, ED, JF, AL, and TW contributed to the interpretation of the data. MMA wrote the first draft of the manuscript. All authors contributed to the writing, critical review and editing of the manuscript. TW and EBL obtained funding.

Funding This manuscript was supported by NIH grants R01AG087280, P30AG066512 and P01AG060882 (to TW), and P30AG072979 (to EBL). The NYULH Center for Biospecimen Research and Development, Histology and Immunohistochemistry Laboratory (RRID:SCR_018304) is supported in part by the Laura and Isaac Perlmutter Cancer Center Support under Grant No. NIH/NCI P30CA016087. This study was also funded by the Instituto de Salud Carlos III (Ministerio de Asuntos Económicos y Transformación Digital, Gobierno de España) through the projects INT21/00073, PI20/01473 and PI23/01786 to J.F.) and the Centro de Investigación Biomédica en Red sobre Enfermedades Neurodegenerativas Program 1, partly jointly funded by Fondo Europeo de Desarrollo Regional, Unión Europea, Una Manera de Hacer Europa, and cofunded by the European Regional Development Fund/European Social Fund (ERDF/ESF), 'A way to make Europe'/'Investing in your future'. This work was also supported by the National Institutes of Health grants (R01 AG056850; R21 AG056974, R01 AG061566, R01 AG081394 and R61AG066543) to J.F. It was also supported by Fundación Tatiana Pérez de Guzmán el Bueno (IIBSP-DOW-2020-151 to J.F.) and Horizon 2020–Research and Innovation Framework Programme from the European Union (H2020-SC1-BHC-2018-2020 to J.F.).

Data availability The resulting mass spectrometry raw data are accessible on the MassIVE server (https://massive.ucsd.edu/) under MassIVE ID: MSV000094800. All data analyzed during this study are included in this published article and its supplementary information files.

Declarations

Conflict of interest J.F. reported receiving personal fees for service on the advisory boards, adjudication committees or speaker honoraria from AC Immune, Adamed, Alzheon, Biogen, Eisai, Esteve, Fujirebio, Ionis, Laboratorios Carnot, Life Molecular Imaging, Lilly, Lundbeck, Novo Nordisk, Perha, Roche, Zambón and outside the submitted work. J.F. reports holding a patent for markers of synaptopathy in neurodegenerative disease (licensed to ADx, EPI8382175.0).

References

1. Aladeokin AC, Akiyama T, Kimura A, Kimura Y, Takahashi-Jitsuki A, Nakamura H et al (2019) Network-guided analysis of hippocampal proteome identifies novel proteins that colocalize with Abeta in a mice model of early-stage Alzheimer's disease. Neurobiol Dis. https://doi.org/10.1016/j.nbd.2019.104603
2. Aldecoa I, Barroeta I, Carroll SL, Fortea J, Gilmore A, Ginsberg SD et al (2024) Down Syndrome biobank consortium: a perspective. Alzheimers Dement. https://doi.org/10.1002/alz.13692
3. Antonarakis SE, Skotko BG, Rafii MS, Strydom A, Pape SE, Bianchi DW et al (2020) Down syndrome. Nat Rev Dis Primers 6:9. https://doi.org/10.1038/s41572-019-0143-7
4. Askenazi M, Kavanagh T, Pires G, Ueberheide B, Wisniewski T, Drummond E (2023) Compilation of reported protein changes in the brain in Alzheimer's disease. Nat Commun 14:4466. https://doi.org/10.1038/s41467-023-40208-x
5. Balcomb K, Johnston C, Kavanagh T, Leitner D, Schneider J, Halliday G et al (2024) SMOC1 colocalizes with Alzheimer's disease neuropathology and delays Abeta aggregation. Acta Neuropathol 148:72. https://doi.org/10.1007/s00401-024-02819-6
6. Barrachina M, Maes T, Buesa C, Ferrer I (2006) Lysosome-associated membrane protein 1 (LAMP-1) in Alzheimer's disease. Neuropathol Appl Neurobiol 32:505–516. https://doi.org/10.1111/j.1365-2990.2006.00756.x
7. Batista AF, Khan KA, Papavergi MT, Lemere CA (2024) The importance of complement-mediated immune signaling in Alzheimer's disease pathogenesis. Int J Mol Sci. https://doi.org/10.3390/ijms25020817
8. Bendl J, Hauberg ME, Girdhar K, Im E, Vicari JM, Rahman S et al (2022) The three-dimensional landscape of cortical chromatin accessibility in Alzheimer's disease. Nat Neurosci 25:1366–1378. https://doi.org/10.1038/s41593-022-01166-7
9. Benjamini Y, Hochberg Y (2018) Controlling the false discovery rate: a practical and powerful approach to multiple testing. J Roy Stat Soc: Ser B (Methodol) 57:289–300. https://doi.org/10.1111/j.2517-6161.1995.tb02031.x
10. Boeddrich A, Haenig C, Neuendorf N, Blanc E, Ivanov A, Kirchner M et al (2023) A proteomics analysis of 5xFAD mouse brain regions reveals the lysosome-associated protein Arl8b as a candidate biomarker for Alzheimer's disease. Genome Med 15:50. https://doi.org/10.1186/s13073-023-01206-2
11. Bowley MP, Cabral H, Rosene DL, Peters A (2010) Age changes in myelinated nerve fibers of the cingulate bundle and corpus callosum in the rhesus monkey. J Comp Neurol 518:3046–3064. https://doi.org/10.1002/cne.22379
12. Braak H, Braak E (1991) Neuropathological stageing of Alzheimer-related changes. Acta Neuropathol 82:239–259. https://doi.org/10.1007/BF00308809
13. Brandt S, Jentsch TJ (1995) ClC-6 and ClC-7 are two novel broadly expressed members of the CLC chloride channel family. FEBS Lett 377:15–20. https://doi.org/10.1016/0014-5793(95)01298-2
14. Broly M, Polevoda BV, Awayda KM, Tong N, Lentini J, Besnard T et al (2022) THUMPD1 bi-allelic variants cause loss of tRNA acetylation and a syndromic neurodevelopmental disorder. Am J Hum Genet 109:587–600. https://doi.org/10.1016/j.ajhg.2022.02.001
15. Carcel-Trullols J, Kovacs AD, Pearce DA (2015) Cell biology of the NCL proteins: What they do and don't do. Biochim Biophys

Acta 1852:2242–2255. https://doi.org/10.1016/j.bbadis.2015.04.027
16. Castrillo JI, Lista S, Hampel H, Ritchie CW (2018) Systems biology methods for Alzheimer's disease research toward molecular signatures, subtypes, and stages and precision medicine: application in cohort studies and trials. Methods Mol Biol 1750:31–66. https://doi.org/10.1007/978-1-4939-7704-8_3
17. Cataldo AM, Barnett JL, Berman SA, Li J, Quarless S, Bursztajn S et al (1995) Gene expression and cellular content of cathepsin D in Alzheimer's disease brain: evidence for early up-regulation of the endosomal-lysosomal system. Neuron 14:671–680. https://doi.org/10.1016/0896-6273(95)90324-0
18. Cataldo AM, Hamilton DJ, Nixon RA (1994) Lysosomal abnormalities in degenerating neurons link neuronal compromise to senile plaque development in Alzheimer disease. Brain Res 640:68–80. https://doi.org/10.1016/0006-8993(94)91858-9
19. Cataldo AM, Peterhoff CM, Troncoso JC, Gomez-Isla T, Hyman BT, Nixon RA (2000) Endocytic pathway abnormalities precede amyloid beta deposition in sporadic Alzheimer's disease and Down syndrome: differential effects of APOE genotype and presenilin mutations. Am J Pathol 157:277–286. https://doi.org/10.1016/s0002-9440(10)64538-5
20. Chen Y, Neve RL, Liu H (2012) Neddylation dysfunction in Alzheimer's disease. J Cell Mol Med 16:2583–2591. https://doi.org/10.1111/j.1582-4934.2012.01604.x
21. Cheng JS, Dubal DB, Kim DH, Legleiter J, Cheng IH, Yu GQ et al (2009) Collagen VI protects neurons against Abeta toxicity. Nat Neurosci 12:119–121. https://doi.org/10.1038/nn.2240
22. Choi-Miura NH, Ihara Y, Fukuchi K, Takeda M, Nakano Y, Tobe T et al (1992) SP-40,40 is a constituent of Alzheimer's amyloid. Acta Neuropathol 83:260–264. https://doi.org/10.1007/BF00296787
23. Davidson YS, Robinson A, Prasher VP, Mann DMA (2018) The age of onset and evolution of Braak tangle stage and Thal amyloid pathology of Alzheimer's disease in individuals with Down syndrome. Acta Neuropathol Commun 6:56. https://doi.org/10.1186/s40478-018-0559-4
24. de Graaf G, Buckley F, Skotko BG (2017) Estimation of the number of people with Down syndrome in the United States. Genet Med 19:439–447. https://doi.org/10.1038/gim.2016.127
25. De Strooper B, Karran E (2016) The cellular phase of Alzheimer's Disease. Cell 164:603–615. https://doi.org/10.1016/j.cell.2015.12.056
26. DeMattos RB, O'Dell MA, Parsadanian M, Taylor JW, Harmony JA, Bales KR et al (2002) Clusterin promotes amyloid plaque formation and is critical for neuritic toxicity in a mouse model of Alzheimer's disease. Proc Natl Acad Sci U S A 99:10843–10848. https://doi.org/10.1073/pnas.162228299
27. Depp C, Sun T, Sasmita AO, Spieth L, Berghoff SA, Nazarenko T et al (2023) Myelin dysfunction drives amyloid-beta deposition in models of Alzheimer's disease. Nature 618:349–357. https://doi.org/10.1038/s41586-023-06120-6
28. Doellinger J, Schneider A, Hoeller M, Lasch P (2020) Sample preparation by easy extraction and digestion (SPEED): a universal, rapid, and detergent-free protocol for proteomics based on acid extraction. Mol Cell Proteomics 19:209–222. https://doi.org/10.1074/mcp.TIR119.001616
29. Dolfe L, Tambaro S, Tigro H, Del Campo M, Hoozemans JJM, Wiehager B et al (2018) The Bri2 and Bri3 BRICHOS domains interact differently with Abeta(42) and Alzheimer Amyloid Plaques. J Alzheimers Dis Rep 2:27–39. https://doi.org/10.3233/ADR-170051
30. Doran E, Keator D, Head E, Phelan MJ, Kim R, Totoiu M et al (2017) Down Syndrome, partial trisomy 21, and absence of Alzheimer's disease: the role of APP. J Alzheimers Dis 56:459–470. https://doi.org/10.3233/JAD-160836
31. Drummond E, Kavanagh T, Pires G, Marta-Ariza M, Kanshin E, Nayak S et al (2022) The amyloid plaque proteome in early onset Alzheimer's disease and Down syndrome. Acta Neuropathol Commun 10:53. https://doi.org/10.1186/s40478-022-01356-1
32. Edbauer D, Winkler E, Regula JT, Pesold B, Steiner H, Haass C (2003) Reconstitution of gamma-secretase activity. Nat Cell Biol 5:486–488. https://doi.org/10.1038/ncb960
33. Fernandez A, Hoq MR, Hallinan GI, Li D, Bharath SR, Vago FS et al (2024) Cryo-EM structures of amyloid-beta and tau filaments in Down syndrome. Nat Struct Mol Biol. https://doi.org/10.1038/s41594-024-01252-3
34. Flores-Aguilar L, Iulita MF, Kovecses O, Torres MD, Levi SM, Zhang Y et al (2020) Evolution of neuroinflammation across the lifespan of individuals with Down syndrome. Brain 143:3653–3671. https://doi.org/10.1093/brain/awaa326
35. Fonseca MI, Zhou J, Botto M, Tenner AJ (2004) Absence of C1q leads to less neuropathology in transgenic mouse models of Alzheimer's disease. J Neurosci 24:6457–6465. https://doi.org/10.1523/JNEUROSCI.0901-04.2004
36. Fortea J, Vilaplana E, Carmona-Iragui M, Benejam B, Videla L, Barroeta I et al (2020) Clinical and biomarker changes of Alzheimer's disease in adults with Down syndrome: a cross-sectional study. Lancet 395:1988–1997. https://doi.org/10.1016/S0140-6736(20)30689-9
37. Fortea J, Zaman SH, Hartley S, Rafii MS, Head E, Carmona-Iragui M (2021) Alzheimer's disease associated with Down syndrome: a genetic form of dementia. Lancet Neurol 20:930–942. https://doi.org/10.1016/S1474-4422(21)00245-3
38. Franceschi C, Garagnani P, Gensous N, Bacalini MG, Conte M, Salvioli S (2019) Accelerated bio-cognitive aging in Down syndrome: state of the art and possible deceleration strategies. Aging Cell. https://doi.org/10.1111/acel.12903
39. Gardiner K, Davisson M (2000) The sequence of human chromosome 21 and implications for research into Down syndrome. Genome Biol 1(reviews0002):0001. https://doi.org/10.1186/gb-2000-1-2-reviews0002
40. Glenner GG, Wong CW (1984) Alzheimer's disease and Down's syndrome: sharing of a unique cerebrovascular amyloid fibril protein. Biochem Biophys Res Commun 122:1131–1135. https://doi.org/10.1016/0006-291x(84)91209-9
41. Glenner GG, Wong CW (1984) Alzheimer's disease: initial report of the purification and characterization of a novel cerebrovascular amyloid protein. Biochem Biophys Res Commun 120:885–890. https://doi.org/10.1016/s0006-291x(84)80190-4
42. Gouras GK, Tsai J, Naslund J, Vincent B, Edgar M, Checler F et al (2000) Intraneuronal Abeta42 accumulation in human brain. Am J Pathol 156:15–20. https://doi.org/10.1016/s0002-9440(10)64700-1
43. Gowrishankar S, Yuan P, Wu Y, Schrag M, Paradise S, Grutzendler J et al (2015) Massive accumulation of luminal protease-deficient axonal lysosomes at Alzheimer's disease amyloid plaques. Proc Natl Acad Sci U S A 112:E3699-3708. https://doi.org/10.1073/pnas.1510329112
44. Grau S, Baldi A, Bussani R, Tian X, Stefanescu R, Przybylski M et al (2005) Implications of the serine protease HtrA1 in amyloid precursor protein processing. Proc Natl Acad Sci U S A 102:6021–6026. https://doi.org/10.1073/pnas.0501823102
45. Greenberg SG, Davies P, Schein JD, Binder LI (1992) Hydrofluoric acid-treated tau PHF proteins display the same biochemical properties as normal tau. J Biol Chem 267:564–569
46. Griffin EF, Yan X, Caldwell KA, Caldwell GA (2018) Distinct functional roles of Vps41-mediated neuroprotection in Alzheimer's and Parkinson's disease models of neurodegeneration. Hum Mol Genet 27:4176–4193. https://doi.org/10.1093/hmg/ddy308

47. Haass C, Schlossmacher MG, Hung AY, Vigo-Pelfrey C, Mellon A, Ostaszewski BL et al (1992) Amyloid beta-peptide is produced by cultured cells during normal metabolism. Nature 359:322–325. https://doi.org/10.1038/359322a0
48. Hafez DM, Huang JY, Richardson JC, Masliah E, Peterson DA, Marr RA (2012) F-spondin gene transfer improves memory performance and reduces amyloid-beta levels in mice. Neuroscience 223:465–472. https://doi.org/10.1016/j.neuroscience.2012.07.038
49. Handa T, Sasaki H, Takao M, Tano M, Uchida Y (2022) Proteomics-based investigation of cerebrovascular molecular mechanisms in cerebral amyloid angiopathy by the FFPE-LMD-PCT-SWATH method. Fluids Barriers CNS 19:56. https://doi.org/10.1186/s12987-022-00351-x
50. Hartley D, Blumenthal T, Carrillo M, DiPaolo G, Esralew L, Gardiner K et al (2015) Down syndrome and Alzheimer's Disease: common pathways, common goals. Alzheimers Dement 11:700–709
51. Hashimoto T, Fujii D, Naka Y, Kashiwagi-Hakozaki M, Matsuo Y, Matsuura Y et al (2020) Collagenous Alzheimer amyloid plaque component impacts on the compaction of amyloid-beta plaques. Acta Neuropathol Commun 8:212. https://doi.org/10.1186/s40478-020-01075-5
52. Hassiotis S, Manavis J, Blumbergs PC, Hattersley KJ, Carosi JM, Kamei M et al (2018) Lysosomal LAMP1 immunoreactivity exists in both diffuse and neuritic amyloid plaques in the human hippocampus. Eur J Neurosci 47:1043–1053. https://doi.org/10.1111/ejn.13913
53. Head E, Lott IT, Wilcock DM, Lemere CA (2016) Aging in Down syndrome and the development of Alzheimer's disease neuropathology. Curr Alzheimer Res 13:18–29. https://doi.org/10.2174/1567205012666151020114607
54. Heberle H, Meirelles GV, da Silva FR, Telles GP, Minghim R (2015) InteractiVenn: a web-based tool for the analysis of sets through Venn diagrams. BMC Bioinformatics 16:169. https://doi.org/10.1186/s12859-015-0611-3
55. Higginbotham L, Ping L, Dammer EB, Duong DM, Zhou M, Gearing M et al (2020) Integrated proteomics reveals brain-based cerebrospinal fluid biomarkers in asymptomatic and symptomatic Alzheimer's disease. Sci Adv. https://doi.org/10.1126/sciadv.aaz9360
56. Hong S, Beja-Glasser VF, Nfonoyim BM, Frouin A, Li S, Ramakrishnan S et al (2016) Complement and microglia mediate early synapse loss in Alzheimer mouse models. Science 352:712–716. https://doi.org/10.1126/science.aad8373
57. Hu YB, Dammer EB, Ren RJ, Wang G (2015) The endosomal-lysosomal system: from acidification and cargo sorting to neurodegeneration. Transl Neurodegener 4:18. https://doi.org/10.1186/s40035-015-0041-1
58. Im E, Jiang Y, Stavrides PH, Darji S, Erdjument-Bromage H, Neubert TA et al (2023) Lysosomal dysfunction in Down syndrome and Alzheimer mouse models is caused by v-ATPase inhibition by Tyr(682)-phosphorylated APP betaCTF. Sci Adv. https://doi.org/10.1126/sciadv.adg1925
59. Itagaki R, Endo M, Yanagisawa H, Hossain MA, Akiyama K, Yaginuma K et al (2018) Characteristics of PPT1 and TPP1 enzymes in neuronal ceroid lipofuscinosis (NCL) 1 and 2 by dried blood spots (DBS) and leukocytes and their application to newborn screening. Mol Genet Metab 124:64–70. https://doi.org/10.1016/j.ymgme.2018.03.007
60. Janoueix-Lerosey I, Pasheva E, de Tand MF, Tavitian A, de Gunzburg J (1998) Identification of a specific effector of the small GTP-binding protein Rap2. Eur J Biochem 252:290–298. https://doi.org/10.1046/j.1432-1327.1998.2520290.x
61. Jiang Y, Mullaney KA, Peterhoff CM, Che S, Schmidt SD, Boyer-Boiteau A et al (2010) Alzheimer's-related endosome dysfunction in Down syndrome is Abeta-independent but requires APP and is reversed by BACE-1 inhibition. Proc Natl Acad Sci U S A 107:1630–1635. https://doi.org/10.1073/pnas.0908953107
62. Jiang Y, Sato Y, Im E, Berg M, Bordi M, Darji S et al (2019) Lysosomal dysfunction in Down syndrome Is APP-dependent and mediated by APP-betaCTF (C99). J Neurosci 39:5255–5268. https://doi.org/10.1523/JNEUROSCI.0578-19.2019
63. Johnson ECB, Carter EK, Dammer EB, Duong DM, Gerasimov ES, Liu Y et al (2022) Large-scale deep multi-layer analysis of Alzheimer's disease brain reveals strong proteomic disease-related changes not observed at the RNA level. Nat Neurosci 25:213–225. https://doi.org/10.1038/s41593-021-00999-y
64. Kakuyama H, Soderberg L, Horigome K, Winblad B, Dahlqvist C, Naslund J et al (2005) CLAC binds to aggregated Abeta and Abeta fragments, and attenuates fibril elongation. Biochemistry 44:15602–15609. https://doi.org/10.1021/bi051263e
65. Kang J, Lemaire HG, Unterbeck A, Salbaum JM, Masters CL, Grzeschik KH et al (1987) The precursor of Alzheimer's disease amyloid A4 protein resembles a cell-surface receptor. Nature 325:733–736. https://doi.org/10.1038/325733a0
66. Karlsson IK, Ploner A, Wang Y, Gatz M, Pedersen NL, Hagg S (2023) Leukocyte DNA methylation in Alzheimer s disease associated genes: replication of findings from neuronal cells. Epigenetics 18:2158285. https://doi.org/10.1080/15592294.2022.2158285
67. Kaya I, Jennische E, Lange S, Tarik Baykal A, Malmberg P, Fletcher JS (2020) Brain region-specific amyloid plaque-associated myelin lipid loss, APOE deposition and disruption of the myelin sheath in familial Alzheimer's disease mice. J Neurochem 154:84–98. https://doi.org/10.1111/jnc.14999
68. Kent WJ, Sugnet CW, Furey TS, Roskin KM, Pringle TH, Zahler AM et al (2002) The human genome browser at UCSC. Genome Res 12:996–1006. https://doi.org/10.1101/gr.229102
69. Kinney JW, Bemiller SM, Murtishaw AS, Leisgang AM, Salazar AM, Lamb BT (2018) Inflammation as a central mechanism in Alzheimer's disease. Alzheimers Dement (N Y) 4:575–590. https://doi.org/10.1016/j.trci.2018.06.014
70. Krance SH, Wu CY, Chan ACY, Kwong S, Song BX, Xiong LY et al (2022) Endosomal-lysosomal and autophagy pathway in Alzheimer's Disease: a systematic review and meta-analysis. J Alzheimers Dis 88:1279–1292. https://doi.org/10.3233/JAD-220360
71. Leitner D, Kavanagh T, Kanshin E, Balcomb K, Pires G, Thierry M et al (2024) Differences in the cerebral amyloid angiopathy proteome in Alzheimer's disease and mild cognitive impairment. Acta Neuropathol 148:9. https://doi.org/10.1007/s00401-024-02767-1
72. Leitner D, Pires G, Kavanagh T, Kanshin E, Askenazi M, Ueberheide B et al (2024) Similar brain proteomic signatures in Alzheimer's disease and epilepsy. Acta Neuropathol 147:27. https://doi.org/10.1007/s00401-024-02683-4
73. Levin EC, Acharya NK, Sedeyn JC, Venkataraman V, D'Andrea MR, Wang HY et al (2009) Neuronal expression of vimentin in the Alzheimer's disease brain may be part of a generalized dendritic damage-response mechanism. Brain Res 1298:194–207. https://doi.org/10.1016/j.brainres.2009.08.072
74. Levites Y, Dammer EB, Ran Y, Tsering W, Duong D, Abreha M et al (2024) Integrative proteomics identifies a conserved Abeta amyloid responsome, novel plaque proteins, and pathology modifiers in Alzheimer's disease. Cell Rep Med. https://doi.org/10.1016/j.xcrm.2024.101669
75. Licastro F, Chiappelli M, Ruscica M, Carnelli V, Corsi MM (2005) Altered cytokine and acute phase response protein levels in the blood of children with Downs syndrome: relationship with dementia of Alzheimer's type. Int J Immunopathol

Pharmacol 18:165–172. https://doi.org/10.1177/039463200501800117
76. Lin PY, Chen LY, Jiang M, Trotter JH, Seigneur E, Sudhof TC (2023) Neurexin-2: an inhibitory neurexin that restricts excitatory synapse formation in the hippocampus. Sci Adv. https://doi.org/10.1126/sciadv.add8856
77. Lourenco FC, Galvan V, Fombonne J, Corset V, Llambi F, Muller U et al (2009) Netrin-1 interacts with amyloid precursor protein and regulates amyloid-beta production. Cell Death Differ 16:655–663. https://doi.org/10.1038/cdd.2008.191
78. Lukiw WJ, Crapper McLachlan DR (1990) Chromatin structure and gene expression in Alzheimer's disease. Brain Res Mol Brain Res 7:227–233. https://doi.org/10.1016/0169-328x(90)90032-9
79. Martinez JL, Piciw JG, Crockett M, Sorci IA, Makwana N, Sirois CL et al (2024) Transcriptional consequences of trisomy 21 on neural induction. Front Cell Neurosci 18:1341141. https://doi.org/10.3389/fncel.2024.1341141
80. Mathys H, Davila-Velderrain J, Peng Z, Gao F, Mohammadi S, Young JZ et al (2019) Single-cell transcriptomic analysis of Alzheimer's disease. Nature 570:332–337. https://doi.org/10.1038/s41586-019-1195-2
81. McGeer PL, Klegeris A, Walker DG, Yasuhara O, McGeer EG (1994) Pathological proteins in senile plaques. Tohoku J Exp Med 174:269–277. https://doi.org/10.1620/tjem.174.269
82. Meharena HS, Marco A, Dileep V, Lockshin ER, Akatsu GY, Mullahoo J et al (2022) Down-syndrome-induced senescence disrupts the nuclear architecture of neural progenitors. Cell Stem Cell 29(116–130):e117. https://doi.org/10.1016/j.stem.2021.12.002
83. Mollo N, Aurilia M, Scognamiglio R, Zerillo L, Cicatiello R, Bonfiglio F et al (2022) Overexpression of the Hsa21 Transcription Factor RUNX1 Modulates the Extracellular Matrix in Trisomy 21 Cells. Front Genet. https://doi.org/10.3389/fgene.2022.824922
84. Montine TJ, Phelps CH, Beach TG, Bigio EH, Cairns NJ, Dickson DW et al (2012) National Institute on Aging-Alzheimer's Association guidelines for the neuropathologic assessment of Alzheimer's disease: a practical approach. Acta Neuropathol 123:1–11. https://doi.org/10.1007/s00401-011-0910-3
85. Muramatsu H, Yokoi K, Chen L, Ichihara-Tanaka K, Kimura T, Muramatsu T (2011) Midkine as a factor to counteract the deposition of amyloid beta-peptide plaques: in vitro analysis and examination in knockout mice. Int Arch Med 4:1. https://doi.org/10.1186/1755-7682-4-1
86. Nixon RA (2017) Amyloid precursor protein and endosomal-lysosomal dysfunction in Alzheimer's disease: inseparable partners in a multifactorial disease. FASEB J 31:2729–2743. https://doi.org/10.1096/fj.201700359
87. Novikova G, Kapoor M, Tcw J, Abud EM, Efthymiou AG, Chen SX et al (2021) Integration of Alzheimer's disease genetics and myeloid genomics identifies disease risk regulatory elements and genes. Nat Commun 12:1610. https://doi.org/10.1038/s41467-021-21823-y
88. Park SY, Kang JY, Lee T, Nam D, Jeon CJ, Kim JB (2020) SPON1 can reduce amyloid beta and reverse cognitive impairment and memory dysfunction in Alzheimer's Disease mouse model. Cells. https://doi.org/10.3390/cells9051275
89. Paschen SA, Rothbauer U, Kaldi K, Bauer MF, Neupert W, Brunner M (2000) The role of the TIM8-13 complex in the import of Tim23 into mitochondria. EMBO J 19:6392–6400. https://doi.org/10.1093/emboj/19.23.6392
90. Perlmutter LS, Barron E, Saperia D, Chui HC (1991) Association between vascular basement membrane components and the lesions of Alzheimer's disease. J Neurosci Res 30:673–681. https://doi.org/10.1002/jnr.490300411
91. Perluigi M, Butterfield DA (2012) Oxidative stress and Down syndrome: a route toward Alzheimer-like dementia. Curr Gerontol Geriatr Res. https://doi.org/10.1155/2012/724904
92. Poet M, Kornak U, Schweizer M, Zdebik AA, Scheel O, Hoelter S et al (2006) Lysosomal storage disease upon disruption of the neuronal chloride transport protein ClC-6. Proc Natl Acad Sci U S A 103:13854–13859. https://doi.org/10.1073/pnas.0606137103
93. Potter H, Granic A, Caneus J (2016) Role of trisomy 21 mosaicism in sporadic and familial Alzheimer's disease. Curr Alzheimer Res 13:7–17. https://doi.org/10.2174/1567205013011512071006 16
94. Prasher VP, Farrer MJ, Kessling AM, Fisher EM, West RJ, Barber PC et al (1998) Molecular mapping of Alzheimer-type dementia in Down's syndrome. Ann Neurol 43:380–383. https://doi.org/10.1002/ana.410430316
95. Pressey SN, O'Donnell KJ, Stauber T, Fuhrmann JC, Tyynela J, Jentsch TJ et al (2010) Distinct neuropathologic phenotypes after disrupting the chloride transport proteins ClC-6 or ClC-7/Ostm1. J Neuropathol Exp Neurol 69:1228–1246. https://doi.org/10.1097/NEN.0b013e3181ffe742
96. Puente-Bedia A, Berciano MT, Tapia O, Martinez-Cue C, Lafarga M, Rueda N (2021) Nuclear Reorganization in Hippocampal Granule Cell Neurons from a Mouse Model of Down Syndrome: Changes in Chromatin Configuration. Int J Mol Sci, Nucleoli and Cajal Bodies. https://doi.org/10.3390/ijms22031259
97. Qiang W, Yau WM, Lu JX, Collinge J, Tycko R (2017) Structural variation in amyloid-beta fibrils from Alzheimer's disease clinical subtypes. Nature 541:217–221. https://doi.org/10.1038/nature20814
98. Rahman MM, Lendel C (2021) Extracellular protein components of amyloid plaques and their roles in Alzheimer's disease pathology. Mol Neurodegener 16:59. https://doi.org/10.1186/s13024-021-00465-0
99. Roney JC, Li S, Farfel-Becker T, Huang N, Sun T, Xie Y et al (2021) Lipid-mediated motor-adaptor sequestration impairs axonal lysosome delivery leading to autophagic stress and dystrophy in Niemann-Pick type C. Dev Cell 56(1452–1468):e1458. https://doi.org/10.1016/j.devcel.2021.03.032
100. Rosa-Ferreira C, Munro S (2011) Arl8 and SKIP act together to link lysosomes to kinesin-1. Dev Cell 21:1171–1178. https://doi.org/10.1016/j.devcel.2011.10.007
101. Sadick JS, O'Dea MR, Hasel P, Dykstra T, Faustin A, Liddelow SA (2022) Astrocytes and oligodendrocytes undergo subtype-specific transcriptional changes in Alzheimer's disease. Neuron 110(1788–1805):e1710. https://doi.org/10.1016/j.neuron.2022.03.008
102. Saini F, Dell'Acqua F, Strydom A (2022) Structural connectivity in Down Syndrome and Alzheimer's Disease. Front Neurosci. https://doi.org/10.3389/fnins.2022.908413
103. Sassi C, Capozzo R, Hammer M, Zecca C, Federoff M, Blauwendraat C et al (2021) Exploring dementia and neuronal ceroid lipofuscinosis genes in 100 FTD-like patients from 6 towns and rural villages on the Adriatic Sea cost of Apulia. Sci Rep 11:6353. https://doi.org/10.1038/s41598-021-85494-x
104. Serafini T, Kennedy TE, Galko MJ, Mirzayan C, Jessell TM, Tessier-Lavigne M (1994) The netrins define a family of axon outgrowth-promoting proteins homologous to C. elegans UNC-6. Cell 78:409–424. https://doi.org/10.1016/0092-8674(94)90420-0
105. Seubert P, Vigo-Pelfrey C, Esch F, Lee M, Dovey H, Davis D et al (1992) Isolation and quantification of soluble Alzheimer's beta-peptide from biological fluids. Nature 359:325–327. https://doi.org/10.1038/359325a0
106. Seyfried NT, Dammer EB, Swarup V, Nandakumar D, Duong DM, Yin L et al (2017) A Multi-network Approach Identifies Protein-Specific Co-expression in Asymptomatic and

Symptomatic Alzheimer's Disease. Cell Syst. https://doi.org/10.1016/j.cels.2016.11.006
107. Shah A, Kishore U, Shastri A (2021) Complement system in Alzheimer's disease. Int J Mol Sci. https://doi.org/10.3390/ijms222413647
108. Sharoar MG, Palko S, Ge Y, Saido TC, Yan R (2021) Accumulation of saposin in dystrophic neurites is linked to impaired lysosomal functions in Alzheimer's disease brains. Mol Neurodegener 16:45. https://doi.org/10.1186/s13024-021-00464-1
109. Snyder HM, Bain LJ, Brickman AM, Carrillo MC, Esbensen AJ, Espinosa JM et al (2020) Further understanding the connection between Alzheimer's disease and Down syndrome. Alzheimers Dement 16:1065–1077. https://doi.org/10.1002/alz.12112
110. Sole-Domenech S, Rojas AV, Maisuradze GG, Scheraga HA, Lobel P, Maxfield FR (2018) Lysosomal enzyme tripeptidyl peptidase 1 destabilizes fibrillar Abeta by multiple endoproteolytic cleavages within the beta-sheet domain. Proc Natl Acad Sci U S A 115:1493–1498. https://doi.org/10.1073/pnas.1719808115
111. Spilman PR, Corset V, Gorostiza O, Poksay KS, Galvan V, Zhang J et al (2016) Netrin-1 interrupts amyloid-beta amplification, increases sAbetaPPalpha in vitro and in vivo, and improves cognition in a mouse model of Alzheimer's Disease. J Alzheimers Dis 52:223–242. https://doi.org/10.3233/JAD-151046
112. Sun Y, Zhu J, Zhou D, Canchi S, Wu C, Cox NJ et al (2021) A transcriptome-wide association study of Alzheimer's disease using prediction models of relevant tissues identifies novel candidate susceptibility genes. Genome Med 13:141. https://doi.org/10.1186/s13073-021-00959-y
113. Szabo MP, Mishra S, Knupp A, Young JE (2022) The role of Alzheimer's disease risk genes in endolysosomal pathways. Neurobiol Dis. https://doi.org/10.1016/j.nbd.2021.105576
114. Szklarczyk D, Gable AL, Nastou KC, Lyon D, Kirsch R, Pyysalo S et al (2021) The STRING database in 2021: customizable protein-protein networks, and functional characterization of user-uploaded gene/measurement sets. Nucleic Acids Res 49:D605–D612. https://doi.org/10.1093/nar/gkaa1074
115. Tachiwana H, Dacher M, Maehara K, Harada A, Seto Y, Katayama R et al (2021) Chromatin structure-dependent histone incorporation revealed by a genome-wide deposition assay. Elife. https://doi.org/10.7554/eLife.66290
116. Takahashi RH, Milner TA, Li F, Nam EE, Edgar MA, Yamaguchi H et al (2002) Intraneuronal Alzheimer abeta42 accumulates in multivesicular bodies and is associated with synaptic pathology. Am J Pathol 161:1869–1879. https://doi.org/10.1016/s0002-9440(10)64463-x
117. Thal DR, Rub U, Orantes M, Braak H (2002) Phases of A beta-deposition in the human brain and its relevance for the development of AD. Neurology 58:1791–1800. https://doi.org/10.1212/wnl.58.12.1791
118. Tong Y, Xu Y, Scearce-Levie K, Ptacek LJ, Fu YH (2010) COL25A1 triggers and promotes Alzheimer's disease-like pathology in vivo. Neurogenetics 11:41–52. https://doi.org/10.1007/s10048-009-0201-5
119. Tyanova S, Temu T, Sinitcyn P, Carlson A, Hein MY, Geiger T et al (2016) The Perseus computational platform for comprehensive analysis of (prote)omics data. Nat Methods 13:731–740. https://doi.org/10.1038/nmeth.3901
120. Vagnoni A, Perkinton MS, Gray EH, Francis PT, Noble W, Miller CC (2012) Calsyntenin-1 mediates axonal transport of the amyloid precursor protein and regulates Abeta production. Hum Mol Genet 21:2845–2854. https://doi.org/10.1093/hmg/dds109
121. Vats S, Galli T (2022) Role of SNAREs in unconventional secretion-focus on the VAMP7-dependent secretion. Front Cell Dev Biol. https://doi.org/10.3389/fcell.2022.884020
122. Wang Y, Zhang X, Song Q, Hou Y, Liu J, Sun Y et al (2020) Characterization of the chromatin accessibility in an Alzheimer's disease (AD) mouse model. Alzheimers Res Ther 12:29. https://doi.org/10.1186/s13195-020-00598-2
123. Wang Z, Zhang Q, Lin JR, Jabalameli MR, Mitra J, Nguyen N et al (2021) Deep post-GWAS analysis identifies potential risk genes and risk variants for Alzheimer's disease, providing new insights into its disease mechanisms. Sci Rep 11:20511. https://doi.org/10.1038/s41598-021-99352-3
124. Wang ZX, Wan Q, Xing A (2020) HLA in Alzheimer's Disease: genetic association and possible pathogenic roles. Neuromolecular Med 22:464–473. https://doi.org/10.1007/s12017-020-08612-4
125. Watanabe N, Araki W, Chui DH, Makifuchi T, Ihara Y, Tabira T (2004) Glypican-1 as an Abeta binding HSPG in the human brain: its localization in DIG domains and possible roles in the pathogenesis of Alzheimer's disease. FASEB J 18:1013–1015. https://doi.org/10.1096/fj.03-1040fje
126. Webers A, Heneka MT, Gleeson PA (2020) The role of innate immune responses and neuroinflammation in amyloid accumulation and progression of Alzheimer's disease. Immunol Cell Biol 98:28–41. https://doi.org/10.1111/imcb.12301
127. Wegiel J, Kaczmarski W, Barua M, Kuchna I, Nowicki K, Wang KC et al (2011) Link between DYRK1A overexpression and several-fold enhancement of neurofibrillary degeneration with 3-repeat tau protein in Down syndrome. J Neuropathol Exp Neurol 70:36–50. https://doi.org/10.1097/NEN.0b013e318202bfa1
128. Wen Y, An Z, Qiao B, Zhang C, Zhang Z (2019) RPS7 promotes cell migration through targeting epithelial-mesenchymal transition in prostate cancer. Urol Oncol 37(297):e291-297. https://doi.org/10.1016/j.urolonc.2019.01.011
129. Wiseman FK, Pulford LJ, Barkus C, Liao F, Portelius E, Webb R et al (2018) Trisomy of human chromosome 21 enhances amyloid-beta deposition independently of an extra copy of APP. Brain 141:2457–2474. https://doi.org/10.1093/brain/awy159
130. Wisniewski T, Goni F (2015) Immunotherapeutic approaches for Alzheimer's disease. Neuron 85:1162–1176. https://doi.org/10.1016/j.neuron.2014.12.064
131. Wu T, Dejanovic B, Gandham VD, Gogineni A, Edmonds R, Schauer S et al (2019) Complement C3 is activated in human AD brain and is required for neurodegeneration in mouse models of amyloidosis and tauopathy. Cell Rep. https://doi.org/10.1016/j.celrep.2019.07.060
132. Xue J, Liu J, Geng M, Yue J, He H, Fan J (2021) Identification of potential hub genes of Alzheimer's disease by weighted gene co-expression network analysis. Nan Fang Yi Ke Da Xue Xue Bao 41:1752–1762. https://doi.org/10.12122/j.issn.1673-4254.2021.12.01
133. Yoshimura Y, Araki A, Maruta H, Takahashi Y, Yamashita H (2017) Molecular cloning of rat acss3 and characterization of mammalian propionyl-CoA synthetase in the liver mitochondrial matrix. J Biochem 161:279–289. https://doi.org/10.1093/jb/mvw067
134. Yu G, Nishimura M, Arawaka S, Levitan D, Zhang L, Tandon A et al (2000) Nicastrin modulates presenilin-mediated notch/glp-1 signal transduction and betaAPP processing. Nature 407:48–54. https://doi.org/10.1038/35024009
135. Yu L, Chibnik LB, Srivastava GP, Pochet N, Yang J, Xu J et al (2015) Association of Brain DNA methylation in SORL1, ABCA7, HLA-DRB5, SLC24A4, and BIN1 with pathological diagnosis of Alzheimer disease. JAMA Neurol 72:15–24. https://doi.org/10.1001/jamaneurol.2014.3049
136. Zhan X, Jickling GC, Ander BP, Stamova B, Liu D, Kao PF et al (2015) Myelin basic protein associates with AbetaPP, Abeta1-42, and amyloid plaques in cortex of Alzheimer's disease brain. J Alzheimers Dis 44:1213–1229. https://doi.org/10.3233/JAD-142013

137. Zhang B, Horvath S (2005) A general framework for weighted gene co-expression network analysis. Stat Appl Genet Mol Biol. https://doi.org/10.2202/1544-6115.1128
138. Zhang H, Meng L, Liu Y, Jiang J, He Z, Qin J et al (2023) Sfxn5 regulation of actin polymerization for neutrophil spreading depends on a citrate-cholesterol-PI(4,5)P2 pathway. J Immunol 211:462–473. https://doi.org/10.4049/jimmunol.2200863

Authors and Affiliations

Mitchell Martá-Ariza[1,2,3] · Dominique F. Leitner[1,2,4] · Evgeny Kanshin[5,6] · Jianina Suazo[1,2] · Ana Giusti Pedrosa[7] · Manon Thierry[1,2] · Edward B. Lee[8] · Orrin Devinsky[1,4] · Eleanor Drummond[2,9] · Juan Fortea[10,11,12] · Alberto Lleó[10,11] · Beatrix Ueberheide[1,5,6] · Thomas Wisniewski[1,2,13,14]

✉ Thomas Wisniewski
Thomas.wisniewski@nyulangone.org

1 Department of Neurology, NYU Grossman School of Medicine, New York, NY, USA

2 Center for Cognitive Neurology, NYU Grossman School of Medicine, New York, NY, USA

3 Institut de Neurociències, Universitat Autònoma de Barcelona, Barcelona, Spain

4 Comprehensive Epilepsy Center, Department of Neurology, NYU Langone Health and Grossman School of Medicine, New York, NY, USA

5 Proteomics Laboratory, Division of Advanced Research Technologies, NYU Grossman School of Medicine, New York, NY, USA

6 Department of Biochemistry and Molecular Pharmacology, NYU Grossman School of Medicine, New York, NY, USA

7 Center for Neural Science, New York University, New York, NY, USA

8 Department of Pathology and Laboratory Medicine, Perelman School of Medicine at the University of Pennsylvania, Philadelphia, PA, USA

9 Brain and Mind Centre and School of Medical Sciences, University of Sydney, Camperdown, NSW, Australia

10 Memory Unit, Department of Neurology, Institut de Recerca Sant Pau, Hospital de Sant Pau, Universitat Autònoma de Barcelona, Barcelona, Spain

11 Centro de Investigación Biomédica en Red en Enfermedades Neurodegenerativas (CIBERNED), Madrid, Spain

12 Barcelona Down Medical Center, Fundació Catalana de Síndrome de Down, Barcelona, Spain

13 Department of Pathology, NYU Grossman School of Medicine, New York, NY, USA

14 Department of Psychiatry, NYU Grossman School of Medicine, New York, NY, USA

Drummond *et al.*
Acta Neuropathologica Communications (2022) 10:53
https://doi.org/10.1186/s40478-022-01356-1

Acta Neuropathologica Communications

RESEARCH

Open Access

The amyloid plaque proteome in early onset Alzheimer's disease and Down syndrome

Eleanor Drummond[1,2*], Tomas Kavanagh[1], Geoffrey Pires[2], Mitchell Marta-Ariza[2], Evgeny Kanshin[3], Shruti Nayak[4], Arline Faustin[2], Valentin Berdah[2], Beatrix Ueberheide[2,3,5] and Thomas Wisniewski[2,6*]

Abstract

Amyloid plaques contain many proteins in addition to beta amyloid (Aβ). Previous studies examining plaque-associated proteins have shown these additional proteins are important; they provide insight into the factors that drive amyloid plaque development and are potential biomarkers or therapeutic targets for Alzheimer's disease (AD). The aim of this study was to comprehensively identify proteins that are enriched in amyloid plaques using unbiased proteomics in two subtypes of early onset AD: sporadic early onset AD (EOAD) and Down Syndrome (DS) with AD. We focused our study on early onset AD as the drivers of the more aggressive pathology development in these cases is unknown and it is unclear whether amyloid-plaque enriched proteins differ between subtypes of early onset AD. Amyloid plaques and neighbouring non-plaque tissue were microdissected from human brain sections using laser capture microdissection and label-free LC–MS was used to quantify the proteins present. 48 proteins were consistently enriched in amyloid plaques in EOAD and DS. Many of these proteins were more significantly enriched in amyloid plaques than Aβ. The most enriched proteins in amyloid plaques in both EOAD and DS were: COL25A1, SMOC1, MDK, NTN1, OLFML3 and HTRA1. Endosomal/lysosomal proteins were particularly highly enriched in amyloid plaques. Fluorescent immunohistochemistry was used to validate the enrichment of four proteins in amyloid plaques (moesin, ezrin, ARL8B and SMOC1) and to compare the amount of total Aβ, Aβ40, Aβ42, phosphorylated Aβ, pyroglutamate Aβ species and oligomeric species in EOAD and DS. These studies showed that phosphorylated Aβ, pyroglutamate Aβ species and SMOC1 were significantly higher in DS plaques, while oligomers were significantly higher in EOAD. Overall, we observed that amyloid plaques in EOAD and DS largely contained the same proteins, however the amount of enrichment of some proteins was different in EOAD and DS. Our study highlights the significant enrichment of many proteins in amyloid plaques, many of which may be potential therapeutic targets and/or biomarkers for AD.

Keywords: Alzheimer's disease, Amyloid plaques, Amyloid beta, Proteomics, Early onset, Down syndrome, Mass spectrometry

Introduction

Amyloid plaques are a neuropathological hallmark of Alzheimer's disease and primarily consist of the protein beta amyloid (Aβ). However, it is often overlooked that amyloid plaques also contain hundreds of proteins in addition to Aβ. These include proteins that directly interact with Aβ (e.g. apolipoprotein E [1]), proteins present in microglia and astrocytes that surround and infiltrate plaques, and proteins present in dystrophic neurites (e.g. phosphorylated tau [2], neurofilament proteins [3],

*Correspondence: Eleanor.drummond@sydney.edu.au; Thomas.Wisniewski@nyulangone.org
[1] Brain and Mind Centre and School of Medical Sciences, Faculty of Medicine and Health, University of Sydney, 94 Mallett Street, Camperdown, NSW, Australia
[2] Centre for Cognitive Neurology, Department of Neurology, New York University Grossman School of Medicine, Science Building, Rm 1017, 435 East 30th Street, New York, NY 10016, USA
Full list of author information is available at the end of the article

secernin-1 [4]). Previous studies have shown that many of these plaque proteins have mechanistic roles in AD. For example, proteins that directly interact with Aβ influence Aβ aggregation and therefore mediate amyloid plaque formation [5–7]. The proteins present in plaque-associated glia influence glial function and can mediate pathological glial function [8, 9]. Proteins present in dystrophic neurites provide insight into the factors involved in the formation of dystrophic neurites and neuritic plaques, which correlate better with cognitive impairment than diffuse plaques [10]. Therefore, comprehensively profiling the proteins that are enriched in amyloid plaques would increase our understanding about AD pathogenesis, and possibly identify new biomarkers and/or new therapeutic targets for AD.

Previous studies have typically used immunohistochemistry to identify amyloid plaque proteins. Mass spectrometry-based proteomics is an alternative approach that allows efficient quantification of thousands of amyloid plaque proteins simultaneously. Proteomics also offers additional advantages of allowing discovery of novel plaque proteins due to its unbiased nature and bypassing complications due to antibody sensitivity and specificity issues. Given these significant advantages, we recently developed a localized proteomics approach to analyze the proteome of neuropathological lesions in AD such as plaques and neurofibrillary tangles [11–13].

The significant heterogeneity in the clinical and neuropathological phenotype of AD suggests that multiple subtypes of AD exist. Previous studies have used various approaches to define AD subtypes [14–17]. Some studies have defined AD subtypes by age of onset (e.g. early onset vs late onset), genetics (e.g. apoE2 vs apoE3 vs apoE4 or familial AD vs sporadic AD), by neuropathology phenotype (e.g. limbic predominant vs hippocampal sparing vs typical), by rate of progression (e.g. rapidly progressive AD vs typical AD), or more recently using unbiased 'omics approaches. We recently showed that plaques in rapidly progressive AD had a significantly different proteome than plaques in typical sporadic AD, suggesting that the amyloid plaque proteome is not consistent in all AD subtypes and that these plaque protein differences may contribute to the development of different subtypes of AD [11]. It is currently unclear whether amyloid plaques in other AD subtypes also have significantly different protein composition, or whether these plaque protein differences were unique to rapidly progressive AD.

The aim of this study was to compare the amyloid plaque proteome in two subtypes of early onset AD: sporadic early onset AD (EOAD) and Down Syndrome (DS) with AD. Between 5 and 10% of AD cases are considered early onset [18]. Of these, only approximately 10% are caused by *APP*, *PSEN1* and *PSEN2* mutations. The cause of the remaining ~ 90% of EOAD cases is unknown and these cases are therefore characterized as sporadic EOAD. It is currently unclear if the same molecular mechanisms drive sporadic EOAD cases and late-onset AD [18]. DS with AD is another prevalent subtype of early onset AD. Adults with DS have a very high risk of developing AD, which is thought to be driven by the triplication and consequent overexpression of APP in DS [19]. People with DS develop AD associated neuropathology very early in life. Accumulation of soluble Aβ has been observed in fetuses with DS [20]. Intraneuronal Aβ is present in children as young as 1 year old [21], which is followed by the development of diffuse plaques by the age of approximately 12 years [22, 23]. Mature plaques are commonly present in the 30's and advanced AD neuropathology is present by the 40's [24]. The progressive accumulation of amyloid and tau pathology in DS largely follows a similar pattern to that observed in AD [25], albeit with more plaques in the striatum and thalamus [26] and a higher plaque density overall in DS in comparison to AD [27]. Multiple studies have shown that plaques in DS contain similar post-translationally modified Aβ species as observed in AD, including Aβ phosphorylated at serine 8 and pyroglutamate modified Aβ [23, 28–31], however it is still unknown if plaques in DS have a different protein composition to that in AD.

Here, we show that amyloid plaques in DS and EOAD are enriched in many proteins besides Aβ including a common core group of 48 proteins that are enriched in plaques in both AD subtypes. While similar proteins were enriched in both DS and EOAD, some proteins were enriched to a greater extent in plaques in a particular subtype of AD, providing new evidence that some distinctions in plaque protein composition are present.

Methods

Ethics statement

All procedures were performed under protocols approved by the Institutional Review Board at New York University Alzheimer Disease Center, NY, USA. In all cases, written informed consent for research was obtained from the patient or legal guardian, and the material used had appropriate ethical approval for use in this project. All patients' data and samples were coded and handled according to NIH guidelines to protect patients' identities.

Human tissue samples

N = 5 cases of early onset sporadic Alzheimer's disease (EOAD) and n = 5 cases of DS with Alzheimer's disease were included for proteomic experiments. Inclusion criteria for EOAD included age < 65 years, ABC neuropathological score of A3, B3, C3 [32], no

mutation in *APP*, *PSEN1* or *PSEN2*, tissue formalin fixation time < 6 months. Inclusion criteria for DS cases was ABC neuropathological score of A3, B3, C3, formalin fixation time < 6 months. Formalin fixed paraffin embedded tissue blocks containing the hippocampus and surrounding entorhinal/temporal cortex that were collected and processed as part of routine autopsy procedures were used in this study. This region was selected because it contains a high amount of amyloid pathology in EOAD and in DS with AD. N = 3 cases of EOAD, DS, late onset sporadic AD (LOAD) and cognitively normal, age matched controls were included in immunohistochemistry validation studies. Case specific information for the human tissue samples used in this study is included in Table 1.

APOE genotyping

APOE genotyping was performed on all the cases using either formalin-fixed paraffin embedded (FFPE) or frozen tissue (FT) for the cases where it was available (see Table 1). FT is the preferred tissue for genotyping as the results are more reliable using this source, which is less likely to be affected by DNA contamination; however, FT was available only from five cases. For FFPE tissues, DNA was isolated from six 8 µm brain sections per sample, using the automated system QIAsymphony SP (Qiagen) and the protocol indicated by the manufacturer. Two endpoint PCRs were performed before sequencing. The first endpoint PCR was conducted in a total volume of 25 µl containing 0.2 µM of each custom primer (Forward primer 5′ AGGCCTACAAATCGGAACTGG 3′; reverse primer 5′ CCTGTTCCACCAGGGGC 3′; Sigma), 0.5 mM each dNTP (Thermo Scientific), 2 U GoTaq G2 Hot Start polymerase (Promega), 25 mM $MgCl_2$ solution (Promega) and 4.2 µl Betaine (Sigma). Cycling conditions were at 98 °C for 4 min and 40 cycles at 98 °C/10 s, 63 °C/1 min and 72 °C/1 min 10 s, followed by 72 °C 10 min. All the amplified fragments were resolved on 2% agarose gels, stained with GelRed 10,000X (Biotium) and visualized under UV exposure. DNA was purified from the agarose gel using the Illustra™ GFX™ PCR DNA and Gel Band Purification Kit (Cytiva) as indicated by the manufacturer, and DNA concentration was quantified using nanodrop One (Thermo Scientific). The second endpoint PCR was performed using the purified DNA with the conditions described previously, except for the concentration of the primers, which was reduced to 0.15 µM. Unpurified PCR products were submitted to Genewiz for Sanger sequencing, and the sequences were analyzed using SnapGene 5.3.1 software (Additional File 2). For genotyping using frozen tissue, 25 mg were dissected from the brain section and transferred to a 1.5 ml tube. DNA was isolated using the DNeasy Blood & Tissue kit (Qiagen) following the manufacturer's instructions. A single endpoint PCR was performed in a total volume of 25 µl containing 0.2 µM of each custom primer (Forward

Table 1 Human tissue samples used in this study

Patient ID	Sex	Age at death	*APOE* genotype on FFPE or FT	ABC score	Fixation duration in weeks	Inclusion in proteomics study	Inclusion in IHC studies	Number of plaques micro-dissected	Number of non-plaques micro-dissected
EOAD #1	F	55	ε3/ε3; FFPE	A3, B3, C3	2	Yes	Yes	641	643
EOAD #2	M	62	ε3/ε3; FT	A3, B3, C3	3	Yes	Yes	622	622
EOAD #3	M	63	ε3/ε3; FFPE	A3, B3, C3	2	Yes	Yes	644	648
EOAD #4	M	63	ε4/ε4; FT	A3, B3, C3	3	Yes	Yes	627	627
EOAD #5	F	60	ε3/ε4; FT	A3, B3, C3	3	Yes	Yes	680	680
EOAD #6	M	70	ε3/ε3; FFPE	A3, B3, C3	2		Yes	n/a	n/a
EOAD #7	F	70	ε3/ε3; FFPE	A3, B3, C3	2		Yes	n/a	n/a
DS #1	F	58	ε3/ε3; FFPE	A3, B3, C3	2	Yes	Yes	607	607
DS #2	M	55	ε3/ε4; FFPE	A3, B3, C3	2	Yes	Yes	641	641
DS #3	M	54	ε3/ε3; FFPE	A3, B3, C3	2	Yes	Yes	603	603
DS #4	F	59	ε3/ε3; FFPE	A3, B3, C3	2	Yes	Yes	633	633
DS #5	F	37	ε3/ε3; FFPE	A3, B3, C3	2	Yes	Yes	626	624
LOAD #1	M	76	ε3/ε4; FT	A3, B3, C3	3		Yes	n/a	n/a
LOAD #2	M	77	ε3/ε3; FFPE	A3, B3, C3	3		Yes	n/a	n/a
LOAD #3	F	88	ε3/ε4; FT	A3, B3, C3	2		Yes	n/a	n/a
Control #1	M	59	ε3/ε3; FFPE	A1, B1, C0	3		Yes	n/a	n/a
Control #2	F	77	ε3/ε3; FFPE	A1, B1, C1	2		Yes	n/a	n/a
Control #3	F	71	ε3/ε3; FFPE	A1, B1, C0	2		Yes	n/a	n/a

primer 5′ AGCCCTTCTCCCCGCCTCCCACTGT 3′; reverse primer 5′ CTCCGCCACCTGCTCCTTCAC CTCG 3′; Sigma), 10 µl of DreamTaq Green PCR Master Mix (2X) and 4.2 µl Betaine (Sigma). Cycling conditions were at 98 °C for 4 min and 35 cycles at 98 °C/10 s, 63 °C/45 s and 72 °C/1 min 10 s, followed by 72 °C 10 min. Unpurified PCR products were submitted to Genewiz for Sanger sequencing, and the sequences were analyzed using SnapGene 5.3.1 software.

Immunohistochemistry for Aβ species

8 µm formalin-fixed paraffin embedded tissue sections containing the hippocampus and surrounding cortex underwent fluorescent immunohistochemistry for six different Aβ species: total Aβ (combination of 4G8 [BioLegend; #800701] and 6E10 [BioLegend; #803001]), Aβ40 (in-house developed monoclonal rabbit antibody [33]), Aβ42 (in-house developed monoclonal rabbit antibody [33]), Aβ phosphorylated at serine position 8 (pAβ; in-house developed monoclonal mouse antibody), pyroglutamate modified Aβ (pyro-Aβ; [34]), and the conformational oligomeric antibody TWF9 [35] that recognizes beta-sheet containing oligomeric species including Aβ. Sections were deparaffinized and rehydrated through a series of xylene and ethanol washes. Antigen retrieval was performed by treatment with either 88% formic acid for 7 min followed by boiling in citrate buffer (10 mM sodium citrate, 0.05% Tween-20; pH6) for total Aβ, Aβ42, Aβ40, pyro-Aβ or with citrate buffer alone for pAβ and TWF9. Sections were blocked with 10% normal goat serum, incubated overnight primary antibodies diluted in 4% normal goat serum. Sections were incubated for 2 h at room temperature with appropriate fluorescent secondary antibodies (diluted 1:500, from Jackson ImmunoResearch). Sections were counter stained with Hoechst 33342 (Sigma) and coverslipped (Prolong Diamond, Thermo Fisher Scientific). Whole slide images were generated using a NanoZoomer HT2 (Hamamatsu) slide scanner. Eight 4× magnification images were collected for quantification from the whole slide scans: four containing the cortex, one each of CA1, CA2, CA3 and CA4, which together generated an average percentage staining load per case. Quantification of the percentage staining load was performed using ImageJ by quantifying the number of pixels above a defined staining threshold for each marker. The percentage staining load of total Aβ, Aβ42, Aβ40, phosphorylated Aβ and pyroglutamate Aβ abundance was restricted to staining in amyloid plaques only, while percentage staining load of oligomers refers to levels throughout the cortical grey matter. Significant differences were determined by one-way ANOVA followed by Tukey's multiple comparisons test.

Laser capture microdissection for localized proteomics

Proteomic studies were carried out using the method outlined in Fig. 1. 8 µm sections of formalin-fixed paraffin

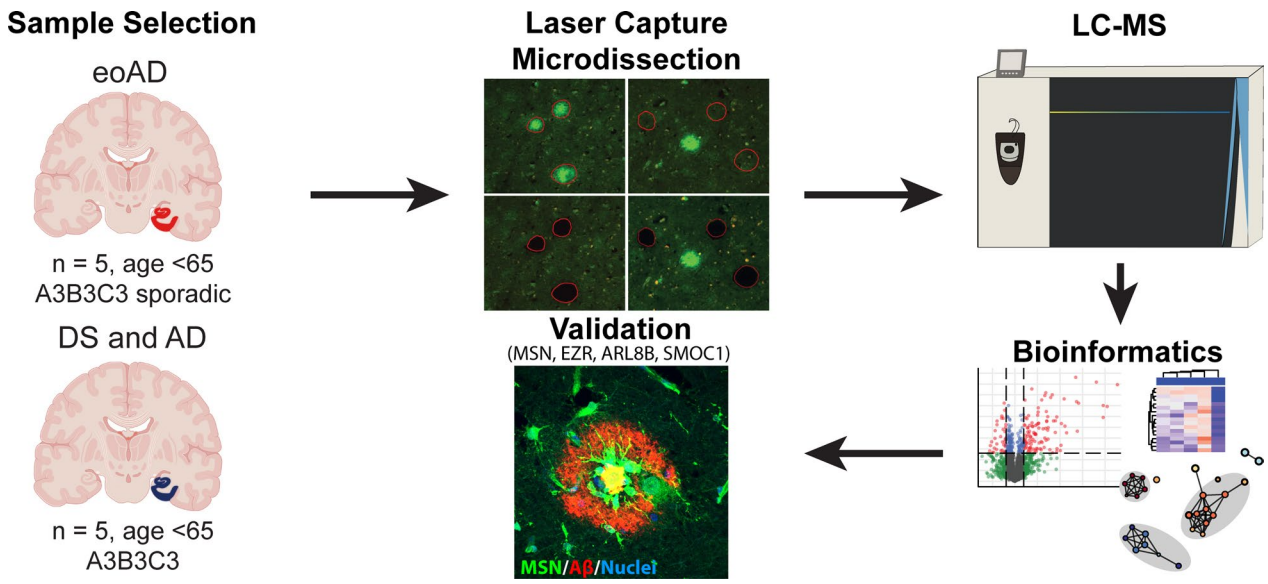

Fig. 1 Schematic of methods used in this study. Formalin fixed paraffin embedded human tissue samples containing the hippocampus were used in this study (n = 5/group; all with advanced AD neuropathology [A3, B3, C3]). Laser capture microdissection was used to microdissect plaques or neighboring non-plaque tissue, LC–MS was used to quantify proteins present in each sample and various bioinformatics approaches were used to identify plaque enriched proteins and pathway or cell-type enrichment. Immunohistochemistry and comparison with previous studies through systematic literature searches was used to validate the enrichment of selected proteins in plaques

embedded tissue were collected onto laser capture microdissection (LCM)-compatible slides and amyloid plaques were visualized using fluorescent immunohistochemistry using a combination of the pan-Aβ antibodies 4G8 (1:4000; BioLegend; #800701) and 6E10 (1:4000; BioLegend; #803001). LCM was performed using a LMD 6500 microscope (Leica) using the method detailed in [11, 36]. 2 mm^2 total area of fluorescently-labelled plaques was microdissected using LCM for each case. 2 mm^2 total area of neighboring non-plaque tissue was also collected for each case. Non-plaque tissue was only selected from the same microscopic field of views that contained microdissected plaques, while remaining sufficiently distant from plaques to ensure that plaque-associated tissue was not collected (Fig. 1). The same number of microdissected regions were collected for plaques and non-plaques for each sample to control for proteomic variation based on the tissue loss associated with microdissection. The inclusion criteria for plaques in this study was any plaque visualized by IHC. There was no restriction based on plaque morphology. Plaques were microdissected from any region present on the hippocampal section, which included hippocampus, entorhinal cortex and temporal cortex. Plaques or non-plaque regions were collected into double distilled water and stored at − 80 °C until sample processing for LC–MS.

Localized proteomics of amyloid plaques

Samples were processed for LC–MS/MS using the formic acid sample preparation method we have previously used to analyze the proteome of amyloid plaques [11, 13, 37]. Tissue underwent secondary deparaffinization using a heating protocol (95 °C for one hour and 65 °C for 2 h and were incubated in 70% LC–MS grade formic acid overnight at room temperature. Samples were sonicated (3 × 3 min), dried using a SpeedVac concentrator, resuspended in 100 mM ammonium bicarbonate and then reduced with Dithiothreitol (20 mM) and alkylated with iodoacetamide (50 mM). Samples were digested with sequencing grade modified trypsin (200 ng; Promega) by gentle agitation overnight at room temperature. Samples were acidified with 0.2% TFA and peptides were desalted using Poros beads. Peptides were eluted off the beads by addition of 40% acetonitrile in 0.5% acetic acid followed by the addition of 80% acetonitrile in 0.5% acetic acid. The organic solvent was removed using a SpeedVac concentrator and the samples were reconstituted in 0.5% acetic acid.

One third of each sample was loaded onto the column using the auto sampler of an EASY-nLC 1200 HPLC (ThermoFisher). The peptides were gradient eluted directly into an Orbitrap Fusion Lumos mass spectrometer using a 145-min gradient. The Orbitrap Fusion Lumos mass spectrometer acquired high resolution full MS spectra with a resolution of 240,000 (at m/z 200), AGC target of 1e6, with a maximum ion time of 50 ms, and scan range of 400–1500 m/z. Following each full MS data-dependent low resolution HCD MS/MS spectra were acquired. All MS/MS spectra were collected using the following instrument parameters: rapid ion trap scan rate, ACG target of 2e4, maximum ion time of 150 ms, one microscan, 0.7 m/z isolation window, fixed first mass of 150 m/z and NCE of 32.

LC–MS data analysis

Protein quantitation was performed using MaxQuant software suite v. 1.6.3.4 [38]. Raw data generated by match between runs. The MS/MS spectra were searched against the SwissProt subset of the Uniprot *H. Sapiens* proteome database (26,186 entries) using the Andromeda search engine [39]. A list of 248 common laboratory contaminants included in MaxQuant, as well as reversed versions of all sequences were also added to the database. The enzyme specificity was set to trypsin with a maximum number of missed cleavages set to 2. Peptide identification was performed with an initial precursor mass deviation up to 7 ppm and a fragment mass deviation of 20 ppm with subsequent nonlinear mass recalibration. Oxidation of methionine and acetylation of protein NTerm were searched as variable modifications and carbamidomethylation of cysteines was searched as a fixed modification. The false discovery rate (FDR) for peptide, protein, and site identification was set to 1% and was calculated using a decoy database approach. The minimum peptide length was set to 7. The option match between runs (1 min time tolerance) was enabled to correlate identification and quantitation results across different runs. Normalization for label-free quantification was performed using MaxLFQ algorithm [38]. Missing values were imputed from normal distribution in Perseus [40] using default parameters. The final protein list was filtered to only include proteins that were present in at least 3 cases in at least one experimental group. An independent quantification for Aβ was manually curated and included in the search results, consistent with previous studies [41]. To do this, the intensity for Aβ was determined by integrating the area under the curve for peptide LVFFAEDVGSNK, which corresponds to amino acids 17–28 of Aβ.

Plaque enriched/depleted proteins were determined as those with a fold change difference between plaques and non-plaques > 1.5 fold and an uncorrected p value of $p < 0.05$ (paired t-test). Fold change difference was selected as the primary determinant of enrichment/depletion in plaques as this correlated best with immunohistochemistry studies, which is the gold standard

approach for identifying plaque enriched proteins. Uncorrected *p*-values were included to provide an indication of variance within a group, however plaque-enriched proteins identified by *p*-values alone did not correlate as well with prior gold-standard immunohistochemistry studies.

Direct comparison of plaque protein levels in DS and EOAD was performed using plaque protein levels that were normalized to the neighboring non-plaque tissue for each individual case. For this, normalized plaque protein levels were calculated as the ratio of protein intensity in plaques:non-plaques for each case. Differences in normalized plaque protein levels between DS and EOAD were identified using an unpaired *t*-test and proteins were deemed significantly different based on a combination of $p < 0.05$ and fold change difference > 1.5.

Data analysis and figure generation

General data manipulations and grouping were performed in R v4.0.2 [42] using the tidyverse v1.3.0 collection of packages. Plots were generated in R with the packages ggplot2 v3.3.2, ggpubr v0.4.0, ggrepel v0.8.2, EnhancedVolcano v1.6.0, VennDiagram v1.6.20, ComplexHeatmap v2.4.3, circlize v0.4.10 and edited in Adobe Illustrator v25.2.3. KEGG pathways and Gene Ontology enrichment analysis was performed in R using the packages enrichplot v1.8.1, DOSE v3.14.0, clusterProfiler 3.16.1, GOSemSim v2.14.2 with terms filtered to an FDR < 0.05. Heatmaps were created with scaled data using the scale function in R. Protein–protein interaction networks and gene ontology cellular compartment annotations were generated in STRING v11.0 [43] and the networks were edited in Cytoscape v3.8.1 and Adobe Illustrator.

Comparison with previous studies

Systematic literature searches were used to identify plaque enriched proteins that have been validated in previous studies. A protein was designated a "known plaque protein" if there was published evidence of enrichment in amyloid plaques in human tissue using immunohistochemistry or mass spectrometry. Additional literature searches were used to determine if a protein was functionally associated with either Aβ or APP in instances where there was no immunohistochemistry evidence of presence in plaques. Key words used in these pubmed searches were: "Alzheimer's and gene ID" or "Alzheimer's and protein name". Plaque enriched proteins identified by mass spectrometry were determined by comparison with Xiong et al. [44], which is the only previous study to identify plaque enriched proteins in comparison to non-plaque regions in human brain tissue using mass spectrometry. Published data from Xiong et al. was filtered to identify plaque-enriched proteins that were identified by at last 2 peptides, had a fold-change difference of > 1.5 fold between plaques and non-plaques for AD versus controls or preclinical AD versus controls and did not include the word "keratin" or "immunoglobulin" in the protein name to make their data comparable with ours. Proteins with an abundance in the bottom 10% in sAD plaques or preclinical plaques were excluded. Uniprot ID was used to match proteins between studies.

Change in brain protein expression in AD versus controls was determined using our in-house developed database—NeuroPro—which combines results from 33 previous studies that used proteomics to identify consistent protein differences between AD and control human brain tissue [11, 12, 41, 44–73].

Validation immunohistochemistry

Proteins were selected for validation studies based on the following criteria: enrichment in both EOAD and DS plaques, protein abundance in the top 50% in amyloid plaques, high fold change enrichment in plaques, appropriate commercial antibody available and limited/no previous evidence of presence in plaques by immunohistochemistry. Based on these criteria the following proteins were selected for immunohistochemistry validation studies: MSN, EZR, SMOC1 and ARL8B. 8 µm formalin-fixed paraffin embedded tissue sections containing the hippocampus and surrounding cortex were used for immunohistochemistry validation studies using the fluorescent immunohistochemistry method described above. Primary antibodies used for these validation studies included: MSN (1:200; Proteintech; #16495-1-AP), EZR (1:100; Thermo Scientific; #QG218841), SMOC1 (1:100; Invitrogen; #PA5-31392), ARL8B (1:200; Invitrogen; #PA5-98885), Aβ (combination of 4G8 [BioLegend; #800701] and 6E10 [BioLegend; #803001], both 1:4000). The combined formic acid and citrate buffer antigen retrieval method (described above) was used for all validation immunohistochemistry studies. 63× images of fluorescent immunohistochemistry were collected using a confocal microscope Zeiss 700 with the ZEN Black 2.3 SP1 acquisition software. ARL8B immunoreactivity in neurons, microglia and astrocytes was tested using the same method as above with the following primary antibodies: GFAP (1:1000; BioLegend; #837201), IBA1 (1:200; Millipore; #MABN92-25UG) and MAP2 (1:300, BD Pharmingen, #556320). A negative control was included in all immunohistochemistry experiments, which consisted of a section of AD hippocampal tissue that underwent the same method with the primary antibody omitted.

The percentage of amyloid plaques co-localized with ARL8B or SMOC1 was quantified using whole slide

fluorescent scans that were collected using the Aperio VERSA digital slide scanner (Leica) with the 10× objective. Images were visualized and analyzed using the software Aperio ImageScope ver. 12.4.3 (Leica). Plaques co-stained with SMOC1 or ARL8B and Aβ or plaques stained only with Aβ in the hippocampal region were manually counted and then the ratio of co-stained plaques versus total plaques was calculated (co-stained plaques/total plaques × 100). The proportion of the plaques was obtained by plotting total number of plaques compared to the plaques co-stained by SMOC1 or ARL8B and Aβ, using the "grouped" layout of GraphPad Prism 8. Significant differences between groups were identified using one-way ANOVA followed by Tukey multiple comparison's analysis, using GraphPad Prism 8 software.

Results

Differences in Aβ species in EOAD and DS

Amyloid plaques in DS and EOAD had similar amounts of total Aβ, Aβ40 and Aβ42 (Fig. 2A). The size of amyloid plaques was similar in DS and EOAD. However, amyloid plaques in DS had significantly higher amounts of both phosphorylated Aβ and pyroglutamate Aβ than EOAD cases (Fig. 2B). Phosphorylated Aβ immunoreactivity was observed both in plaques and in neurons in DS and EOAD. Two main types of intraneuronal staining were observed: staining consistent with presence in neurofibrillary tangles and neurons containing large puncta of phosphorylated Aβ. Phosphorylated Aβ was also observed in dystrophic neurites. While there were significantly increased levels of phosphorylated Aβ in plaques in DS in comparison to EOAD, similar levels of intraneuronal phosphorylated Aβ were observed in DS and EOAD. Pyroglutamate Aβ was observed in amyloid plaques in both DS and EOAD. Significantly more pyroglutamate Aβ was observed in DS in comparison to EOAD (Fig. 2B).

Oligomers were visualized using the pan-oligomeric antibody TWF9, which is a conformational antibody that recognizes Aβ oligomers in addition to other beta sheet containing oligomers [35]. Consistent with previous studies, TWF9 immunoreactivity was observed in neuronal soma. No immunoreactivity was observed within plaques. DS cases had significantly lower levels

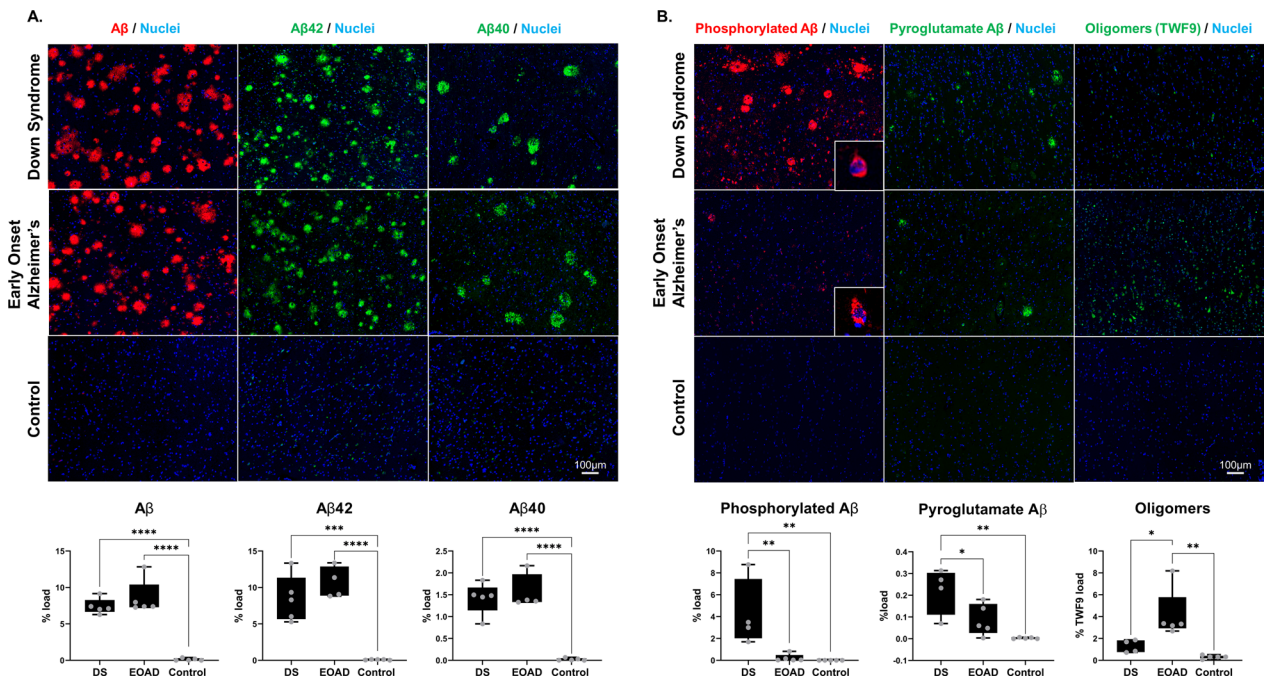

Fig. 2 Comparison of levels of different Aβ species and oligomers in DS, EOAD and cognitively normal controls. Representative fluorescent immunohistochemistry images show the distribution of total Aβ, Aβ42, Aβ40, phosphorylated Aβ, pyroglutamate Aβ and oligomers in the cortex. **A** Similar amounts of plaques containing Aβ, Aβ42 and Aβ40 were observed in DS in comparison to EOAD. **B** Phosphorylated Aβ was observed in plaques and intraneuronally in both DS and EOAD. Intraneuronal phosphorylated Aβ was observed in both DS and EOAD (higher magnification image inserts in B). Pyroglutamate Aβ was only observed in plaques in DS and EOAD. Immunostaining for the conformational oligomer antibody TWF9 was observed intraneuronally, but not in plaques. Significantly higher amounts of plaque-associated phosphorylated Aβ and pyroglutamate Aβ were observed in DS in comparison to EOAD and controls. In contrast, significantly higher amounts of oligomers were observed in EOAD in comparison to DS and controls. Significant differences were determined by one-way ANOVA followed by Tukey's multiple comparisons test. *$p < 0.05$; **$p < 0.01$

of TWF9 immunoreactivity in comparison to EOAD (Fig. 2B).

Proteomic analysis of EOAD and DS amyloid plaques

Proteomic analysis of plaques and neighboring non-plaque tissue identified 2259 proteins (Additional file 1: Table S1). 85% of proteins (1915 proteins) were identified in both EOAD and DS samples, of which 1355 proteins were identified in all 20 samples, therefore confirming that our proteomic approach is a reliable way to quantify amyloid plaque proteins using microscopic amounts of formalin-fixed paraffin embedded human tissue samples. Proteins present in all 20 samples included major AD-associated proteins such as Aβ, Tau and ApoE, therefore confirming the presence of these proteins both inside plaques and in surrounding non-plaque tissue.

Proteins enriched in plaques in both EOAD and DS

The main aim of this study was to identify proteins that were enriched in amyloid plaques in EOAD and DS in comparison to surrounding non-plaque tissue. 127 proteins were significantly enriched in amyloid plaques in either EOAD or DS (Additional file 1: Table S1). 48 proteins were consistently enriched in both DS and EOAD plaques (Table 2, Fig. 3). Systematic literature searches revealed that 33/48 proteins have been previously confirmed as amyloid plaque proteins in late-onset AD, therefore validating our mass spectrometry approach and providing new evidence that similar proteins are enriched in amyloid plaques in different subtypes of AD (Table 2). In addition, we identified 15 proteins that were enriched in plaques in both EOAD and DS (Table 2) that were not previously known to be plaque associated proteins. Four of these proteins have been previously associated with either Aβ or APP. Here, we provide the first evidence that these proteins are enriched in amyloid plaques. The remaining 11 proteins are amyloid plaque proteins that have not been previously associated with Aβ, APP or amyloid plaques in any subtype of AD (Table 2).

As expected, Aβ was highly enriched in plaques in comparison to the surrounding non-plaque tissue (12 and sevenfold enriched in EOAD and DS plaques respectively; Fig. 3B). In contrast, while tau was abundant in both plaques and neighboring non-plaque tissue in DS and EOAD, there was no evidence of enrichment of tau in amyloid plaques. Examination of the abundance (overall intensity in plaques) of the 48 proteins enriched in both EOAD and DS showed that the most abundant proteins present were well-known plaque proteins (e.g. APP, ApoE, vimentin, clusterin, complement C3 and complement C4a; Fig. 3C). We also observed a very high correlation in the total concentration of these proteins in plaques between EOAD and DS (Fig. 3C). The most abundant novel plaque protein in both DS and EOAD was ezrin (EZR), which was one of the proteins selected for immunohistochemistry validation studies (Fig. 3C).

Examination of the proteins that had the highest enrichment in plaques in both DS and EOAD included many proteins less studied in the AD field (Table 2; Additional file 1: Table S3). For example, COL25A1 was the most highly enriched protein in plaques in both EOAD and DS (104 and 113-fold enriched respectively). Other highly enriched plaque proteins in both EOAD and DS included MDK, NTN1, HTRA1, SMOC1 and OLFML3 (Fig. 4A, B). The 48 proteins consistently enriched in plaques in both EOAD and DS also showed a highly significant degree of protein–protein interaction ($p < 1.0 \times 10^{-16}$; Fig. 3D) and were almost exclusively classified as either vesicle (enrichment FDR: 4.32×10^{-9}) or extracellular proteins (enrichment FDR: 3.34×10^{-8}). The enrichment of vesicle proteins was predominantly driven by endosome or lysosome proteins (Fig. 3D; Additional file 1: Table S3). Synapse proteins were also particularly enriched (enrichment FDR: 1.90×10^{-3}).

Differences in plaque enriched proteins in EOAD and DS

Our results suggest that that major plaque enriched proteins in EOAD and DS were largely the same. The consistency of protein enrichment in plaques was even noted at an individual case level (Fig. 4C, D). However, we were interested to determine whether there was evidence of plaque protein enrichment that was unique to either DS or EOAD beyond these common plaque-enriched proteins. 20 proteins were uniquely enriched in plaques in EOAD (Additional file 1: Table S4) and 59 proteins were uniquely enriched in plaques in DS (Additional file 1: Table S5). Pathway analysis of proteins that were uniquely enriched in plaques in either DS or EOAD showed that these proteins were also enriched in endosomal or lysosomal proteins, similar to the commonly enriched plaque proteins. These protein differences between DS and EOAD did not suggest the presence of unique disease mechanisms driving plaque development in DS or EOAD: pathway analysis showed that these proteins did not cluster to a particular functional pathway and the majority of proteins showed the same trend for enrichment in plaques in the other group. 80% (63/79 proteins) of proteins uniquely enriched in plaques in either EOAD or DS were still increased in plaques in the other subtype of AD, albeit at a level that did not meet our criteria for 'enrichment in plaques'. Therefore, these results suggest that largely the same proteins are enriched in amyloid plaques in EOAD and DS.

We also directly compared plaque protein levels in DS and EOAD. For this analysis, plaque protein levels that were normalized against background protein levels for

Table 2 48 proteins consistently enriched in plaques in EOAD and DS

Uniprot	Gene	Protein	Enrichment in EOAD plaques (fold change)	Enrichment in DS plaques (fold change)	Known plaque protein?	Difference in AD brain tissue	Mediates Aβ pathology?
Previously confirmed plaque proteins—immunohistochemistry							
Q9BXS0	COL25A1	Collagen alpha-1	104.3	113.1	Yes [74]	Increased	Increases pathology [6, 75]
O95631	NTN1	Netrin-1	34.9	58.7	Yes [60]	Increased	Decreases pathology [76]
P21741	MDK	Midkine	31.4	70.4	Yes [77]	Increased	Decreases pathology [78]
Q92743	HTRA1	Serine protease HTRA1	19.0	42.8	Yes [79]	Increased	Decreases pathology [80]
Q9H4F8	SMOC1	SPARC-related modular calcium-binding protein 1	12.9	58.8	Yes [60]	Increased	Unknown
P02649	APOE	Apolipoprotein E	10.4	17.2	Yes [81]	Increased	Increases pathology [82, 83]
Q14956	GPNMB	Transmembrane glycoprotein NMB	7.8	17.8	Yes (in plaque-associated microglia) [84]	Increased	Unknown
P0C0L4	C4A	Complement C4-A	7.5	10.1	Yes [85]	Increased	Unknown
P35052	GPC1	Glypican-1	7.5	8.5	Yes [86]	Decreased	Increases pathology [87]
P02743	APCS	Serum amyloid P-component	4.9	10.8	Yes [88]	Increased	Increases pathology [89]
Q9UIK5	TMEFF2	Tomoregulin-2	4.8	6.9	Yes [90]	N/a	Decreases pathology [91]
P02746	C1QB	Complement C1q subcomponent subunit B	3.3	4.3	Yes [92]	N/a	Increases pathology [93, 94]
P10909	CLU	Clusterin	3.2	4.0	Yes [95]	Increased	Increases pathology [7, 96]
Q00604	NDP	Norrin	2.9	4.6	Yes [79]	Increased	Unknown
P05067	APP	Amyloid-beta precursor protein	2.8	5.9	Yes [97]	Increased	Increases pathology [98]
P02747	C1QC	Complement C1q subcomponent subunit C	2.7	8.4	Yes [92]	Increased	Increases pathology [93, 94]
P01024	C3	Complement C3	2.5	2.9	Yes [92]	Increased	Increases pathology [94, 99, 100]
P41222	PTGDS	Prostaglandin-H2 D-isomerase	2.2	3.0	Yes [101]	Increased	Decreases pathology [101]
P26038	MSN	Moesin	2.1	2.6	Yes, in plaque-associated microglia [102]	Increased	Decreases pathology [103]
P07093	SERPINE2	Glia-derived nexin	2.1	4.3	Yes [104]	Decreased	Increases pathology [105, 106]
Q9UBP4	DKK3	Dickkopf-related protein 3	2.1	1.8	Yes [107]	Increased	Decreases pathology [108]
Q8IV08	PLD3	Phospholipase D3	2.0	2.0	Yes [109]	N/a	Decreases pathology [110, 111]
O00468	AGRN	Agrin	1.9	2.9	Yes [112]	Increased	Decreases pathology [113]
Q07954	LRP1	Prolow-density lipoprotein receptor-related protein 1	1.8	2.1	Yes [114]	Increased	Inconsistent effects on pathology [115]
P08670	VIM	Vimentin	1.7	1.8	Yes, in surrounding astrocytes [116]	Increased	Increases pathology [117]

Table 2 (continued)

Uniprot	Gene	Protein	Enrichment in EOAD plaques (fold change)	Enrichment in DS plaques (fold change)	Known plaque protein?	Difference in AD brain tissue	Mediates Aβ pathology?
P16870	CPE	Carboxypeptidase E	1.6	2.1	Yes [118]	Increased	Unknown
Q15818	NPTX1	Neuronal pentraxin-1	1.6	1.7	Yes [119]	Increased	Increases pathology [120]
Previously confirmed plaque protein—proteomics							
Q9NRN5	OLFML3	Olfactomedin-like protein 3	19.2	18.9	Yes [44]	Increased	Unknown
Q9HCB6	SPON1	Spondin-1	6.9	16.5	Yes [44]	N/a	Decreases pathology [121, 122]
O94985	CLSTN1	Calsyntenin-1	5.4	8.1	Yes [44]	Decreased	Increases pathology [123]
Q9ULB1	NRXN1	Neurexin-1	2.9	2.8	Yes [44]	Increased	Unknown
P51797	CLCN6	Chloride transport protein 6	2.8	9.7	Yes [44]	Increased	Unknown
Q9NVJ2	ARL8B	ADP-ribosylation factor-like protein 8B	2.2	2.9	Yes [44]	Increased	Decreases pathology [124]
Novel plaque proteins—mechanistic link with Aβ or APP							
O75110	ATP9A	Probable phospholipid-transporting ATPase IIA	1.8	2.3	No, but associated with Aß [125]	Increased	Increases pathology [125]
P15311	EZR	Ezrin	1.7	2.6	No, but associated with APP [103]	Increased	Decreases pathology [103]
O00299	CLIC1	Chloride intracellular channel protein 1	1.6	1.7	No, but associated with Aß [126]	Increased	Increases pathology [126]
O14773	TPP1	Tripeptidyl-peptidase 1	1.6	2.1	No, but associated with Aß [127]	Increased	Decreases pathology [127]
Novel plaque proteins—no previous association with Aβ or APP							
P51809	VAMP7	Vesicle-associated membrane protein 7	3.0	4.0	No	N/a	Unknown
Q9UNK0	STX8	Syntaxin-8	3.2	2.4	No	Increased	Unknown
Q5TH69	ARFGEF3	Brefeldin A-inhibited guanine nucleotide-exchange protein 3	3.2	5.2	No	Increased	Unknown
Q6IAA8	LAMTOR1	Ragulator complex protein LAMTOR1	2.6	2.9	No	N/a	Unknown
Q59EK9	RUNDC3A	RUN domain-containing protein 3A	2.3	5.6	No	N/a	Unknown
P40121	CAPG	Macrophage-capping protein	2.2	1.9	No	Increased	Unknown
Q9NQ79	CRTAC1	Cartilage acidic protein 1	2.1	2.2	No	N/a	Unknown
Q9P2S2	NRXN2	Neurexin-2	1.9	2.5	No	N/a	Unknown
Q99435	NELL2	Protein kinase C-binding protein NELL2	1.8	3.9	No	N/a	Unknown
Q9HB90	RRAGC	Ras-related GTP-binding protein C	1.9	2.2	No	N/a	Unknown
Q86Y82	STX12	Syntaxin-12	1.5	2.0	No	N/a	Unknown

Proteins listed in order of fold change enrichment in EOAD; separated into previously confirmed plaque proteins, associated with Aβ or APP, and novel. "Previously confirmed plaque proteins" were determined by published immunohistochemistry evidence of protein presence in plaque or by > 1.5 fold enrichment in plaque in comparison to neighboring non-plaque tissue in late onset AD or preclinical AD [44]. Difference in AD tissue was determined by comparison with 33 previous proteomic studies of human AD brain tissue. "Mediates Aβ pathology?" determined by literature searches for "Alzheimer's disease and gene ID or protein name". Protein was designated as mediating Aβ pathology if altering protein expression in transgenic animal models or cell culture affected amyloid pathology

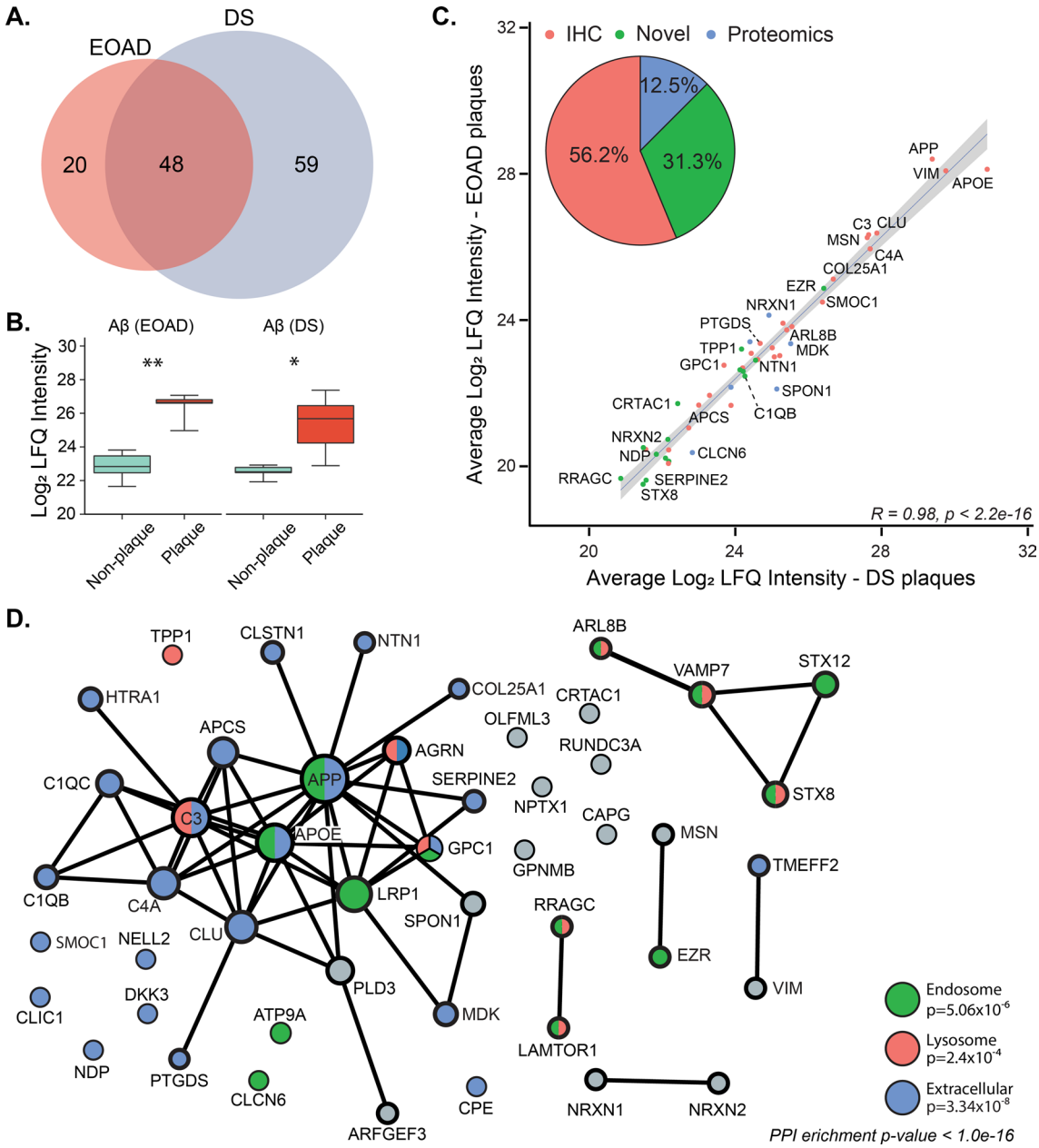

Fig. 3 48 proteins were significantly enriched in plaques in both DS and EOAD. **A** 107 proteins were enriched in DS plaques and 68 proteins were enriched in EOAD plaques. Of these, 48 proteins were enriched in both DS and EOAD. **B** Aβ was significantly enriched in plaques in comparison to neighboring non-plaque tissue in both DS (11.92 fold enriched) and EOAD (6.96 fold enriched; paired *t*-test). **C** There was a highly significant correlation in the abundance (determined by intensity values from LC–MS) of common plaque enriched proteins in DS and EOAD. Apolipoprotein E (APOE), APP and vimentin (VIM) were the three most abundant proteins in plaques in both DS and EOAD. Proteins are coloured to show if each is a previously validated plaque protein (red: 56.2% proteins previously validated as a plaque protein in a targeted immunohistochemistry [IHC] study; blue: 12.5% proteins previously validated as a plaque protein in a proteomics study only) or a novel identified plaque protein (green; 31.3% proteins). **D** Pathway analysis of the 48 proteins commonly enriched in plaques in both DS and EOAD showed a highly significant degree of protein–protein interactions ($p < 1.0 \times 10^{-16}$). Pathway analysis showed that these proteins were highly enriched extracellular proteins (blue), endosome proteins (green) or lysosome proteins (red). *$p < 0.05$; **$p < 0.01$

each individual case were used. 38 proteins were significantly different between DS and EOAD plaques after correction for background protein differences. 25 proteins were significantly higher and 13 proteins were significantly lower in DS plaques in comparison to EOAD plaques (Additional file 1: Table S7). Pathway analysis did not highlight enrichment of any cellular compartments or pathways for significantly different proteins in DS and EOAD plaques. Again, suggesting that plaque protein composition was largely the same in DS and EOAD.

We also examined if the triplication of chromosome 21 in DS resulted in any major differences in plaque associated proteins. Our proteomic analysis identified 22 proteins with genes on chromosome 21 (Additional file 1: Table S6). Of these, only three proteins were enriched in plaques in DS: APP, ITGB2 and COL18A1. APP was commonly enriched in plaques in both EOAD and DS. While ITGB2 and COL18A1 both had higher levels in plaques in comparison to non-plaques in EOAD, their level did not meet our criteria for designation as "enriched". Therefore, our results suggest that the triplication of chromosome 21 is not necessarily associated with enrichment of those gene products in plaques, but rather may enhance the enrichment of selected proteins in plaques.

Validation: comparison with previous proteomic studies

Only one prior study has examined the proteome of amyloid plaques in comparison to surrounding non-plaque tissue [44]. This study identified proteins that were enriched in amyloid plaques in late-onset AD and preclinical AD. Despite the power of their dataset being limited by a small sample size (n = 3 cases/group, pooled prior to mass spectrometry) and the different subtypes of AD analyzed in their study in comparison to ours, we were pleased to see that many of our plaque enriched proteins were validated in this previous study. 43 proteins were identified in both our study and enriched in late-onset AD plaques in Xiong et al. 26/43 commonly identified proteins were significantly enriched in either DS or EOAD plaques (Additional file 1: Table S1). The majority of the remaining proteins were also increased in plaques in our study, however they did not reach the criteria for significance in our study. All of the top 10 most highly enriched proteins in plaques in DS and EOAD in our study were also enriched in plaques in late onset AD (Fig. 5).

Xiong et al. also identified 78 proteins that were enriched in plaques in preclinical AD. 53 of these proteins were also identified in our study, of which, 30 were enriched in DS or EOAD plaques (Additional file 1: Table S1). The most notable protein that was not enriched in preclinical AD plaques was COL25A1, which was the most highly enriched protein in both DS and EOAD plaques in our study and was enriched in late-onset AD plaques in Xiong et al. [44]. This suggests that COL25A1 may only become enriched in plaques at a later stage of disease development. In contrast, the remaining top 10 most enriched proteins for both DS and EOAD were also enriched in plaques in preclinical AD (Fig. 5), suggesting that plaques in preclinical AD largely contain the same proteins present in plaques at advanced stages of AD.

We also compared our data to Bai et al. [60] who identified 28 proteins that correlated with Aβ abundance in human brain tissue throughout the progression of AD. 20 of these proteins were also identified in our study, of which 13 were significantly enriched in DS and/or EOAD plaques (Additional file 1: Table S1). The remaining 7 proteins were also increased in DS and/or EOAD plaques, however these did not reach our statistical stringency level to be considered a plaque-enriched protein.

The combined analysis of our data with these two previous studies identified 30 proteins that were consistently enriched in plaques or correlated with Aβ in at least 3 analyses (Fig. 5). This group of proteins represent a consistent amyloid plaque signature highlighting proteins that likely have an important role in amyloid plaque pathology in addition to Aβ. While the some of these proteins are well known plaque proteins (e.g. APP, ApoE, clusterin), the role of many of these proteins in AD is comparatively much less studied including 8 proteins that have only been discovered as an amyloid plaque protein in proteomic studies (OLFML3, SPON1, CLSTN1, NRXN1, CLCN6, ARL8B, SYT11, SCIN). Combined, these comparisons with previous studies validates our findings and provides additional evidence that amyloid plaques are enriched in many proteins in addition to Aβ, many of which are likely to be of pathological importance in AD and merit further investigation.

(See figure on next page.)

Fig. 4 Significantly altered proteins in plaques in comparison to neighboring non-plaque tissue. **A**, **B** Volcano plots highlight proteins in red that were significantly altered in plaques in comparison to non-plaque tissue. Significance was determined by a combination of $p < 0.05$ and a fold change difference of greater than 1.5 fold. Proteins that have a fold change difference of greater than 1.5 fold only are shown in green and proteins that had a difference of $p < 0.05$ only are shown in blue. The total number of proteins included in the analysis was 2059 proteins for DS and 2115 proteins for EOAD. Proteins are identified by gene IDs. **C**, **D** Unsupervised clustering heatmaps for proteins that were significantly altered in DS or EOAD. Plaque and non-plaque samples independently clustered, highlighting the significantly different protein expression between plaque and non-plaque samples for DS and EOAD. All gene IDs are indicated for EOAD in each row whilst only genes from cluster 1 and 4 are marked for DS, constituting a divergent cluster and highly enriched cluster of genes respectively for DS plaques

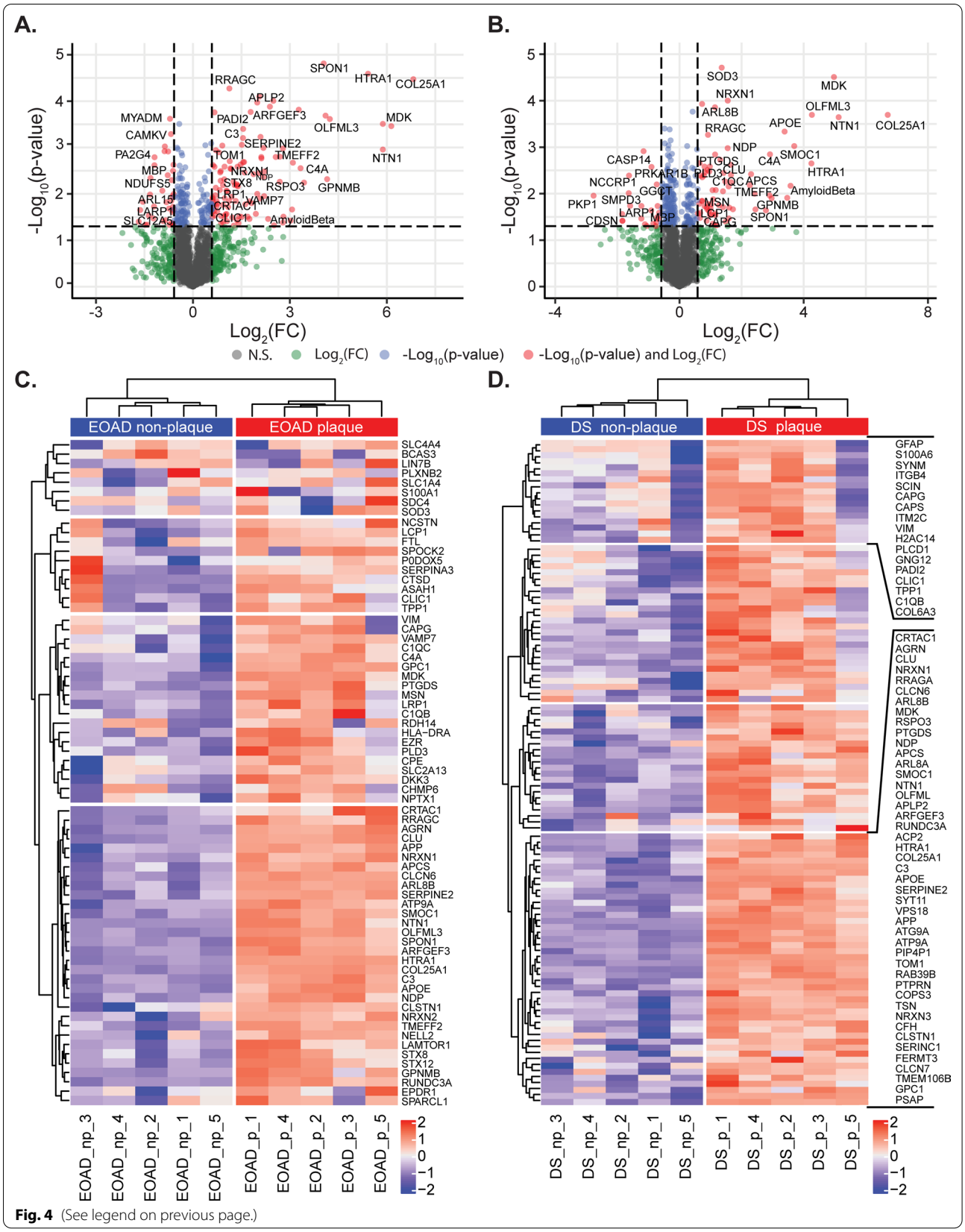

Fig. 4 (See legend on previous page.)

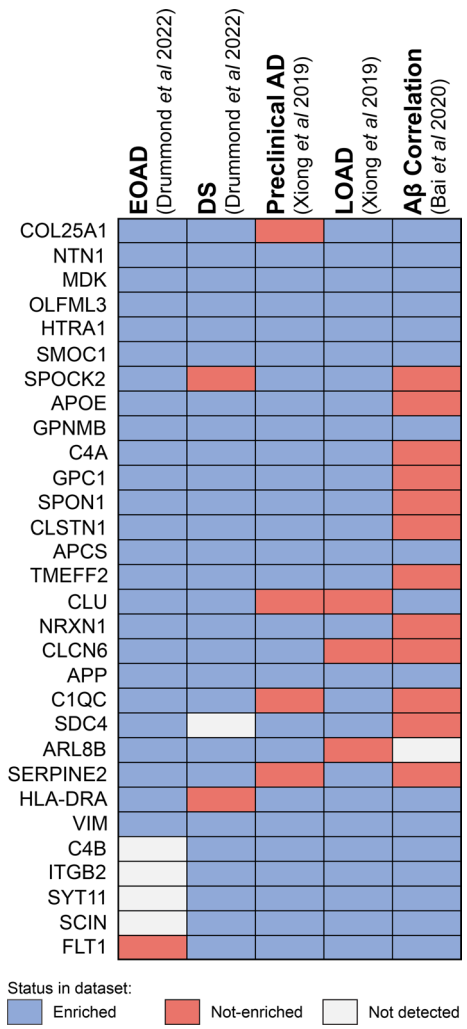

Fig. 5 Comparison of common plaque enriched proteins in DS and EOAD with previous proteomic studies. Plot shows the 30 plaque proteins that were either identified in plaques or correlated with Aβ in at least 3 previous proteomic studies. Proteomic data was obtained from [44] for enrichment in preclinical AD or LOAD plaques and [60] for correlation with Aβ. Blue boxes indicate protein significantly enriched in plaques in comparison to surrounding non-plaque tissue or significantly correlated with Aβ. Red boxes indicate detection in the study but no enrichment in plaques or correlation with Aβ. White boxes indicate instances when a protein was not detected. Proteins are listed in order of fold change enrichment in plaques in EOAD followed by fold change enrichment in DS plaques if not enriched in EOAD

Validation: immunohistochemistry

Fluorescent immunohistochemistry was used to validate the enrichment of four proteins in amyloid plaques. Ezrin (EZR) was selected as it was the most abundant novel plaque protein identified in our study. ARL8B was selected as a representative plaque-enriched lysosomal protein that had no prior immunohistochemistry evidence of presence in amyloid plaques. Moesin (MSN) and SMOC1 were selected as both have only one prior publication confirming their presence in plaques using immunohistochemistry, but no immunohistochemistry evidence of enrichment in plaques in EOAD or DS. Fluorescent immunohistochemistry confirmed that ezrin, moesin, ARL8B and SMOC1 were enriched in amyloid plaques in comparison to surrounding non-plaque tissue in DS, EOAD and late-onset sporadic AD. Moesin (Fig. 6), Ezrin (Fig. 7), and SMOC1 (Fig. 8) strongly co-localized with Aβ in amyloid plaques. Particularly intense immunoreactivity was observed in the aggregated core of dense-cored plaques for these proteins. Moesin was also observed in cells with a microglial morphology in both AD and control cases, consistent with a previous study that confirmed that moesin is a microglial protein [102].

SMOC1 strongly co-localized with amyloid fibrils only in a subset of amyloid plaques (Fig. 8). The proportion of SMOC1 immunoreactive plaques in the hippocampus varied between subtypes of AD; SMOC1 was present in 58% amyloid plaques in DS in comparison to 47% of plaques in EOAD and 32% of plaques in late-onset AD (Fig. 8A, B). This was consistent with our proteomic results that found a greater enrichment of SMOC1 in DS plaques in comparison to EOAD plaques. Both neuritic and diffuse plaques showed SMOC1 immunoreactivity (Fig. 8C). Qualitatively, the proportion of SMOC1 immunoreactive plaques was higher in the hippocampus than in the neighboring cortex in all subtypes of AD. Interestingly, there was a large amount of colocalization of SMOC1 with plaques that also contained post-translationally modified Aβ species (white arrows, Fig. 8D). Minimal basal SMOC1 staining was observed in age-matched control cases, with the most consistent basal SMOC1 expression present in localized pockets of the choroid plexus.

ARL8B was also abundant in amyloid plaques in all subgroups (Fig. 9). In contrast to SMOC1, the proportion of ARL8B immunoreactive plaques in the hippocampus was similar in DS and EOAD (77% and 79%, respectively; Fig. 9A, B). However, a significantly lower proportion of plaques contained ARL8B in late-onset AD in comparison to EOAD (Fig. 9A, B). Two distinct patterns of plaque-associated ARL8B staining were observed. In one subset of amyloid plaques, bright puncta of ARL8B were diffusely present throughout plaques (Fig. 9C). In these plaques, ARL8B did not strongly colocalize with Aβ. Instead, ARL8B was often observed in the regions of amyloid plaques that were not brightly stained for Aβ (Fig. 9C). Qualitatively, ARL8B colocalization in amyloid plaques was more commonly observed in the hippocampus than the cortex. Basal ARL8B staining in control hippocampal sections was observed in neuron

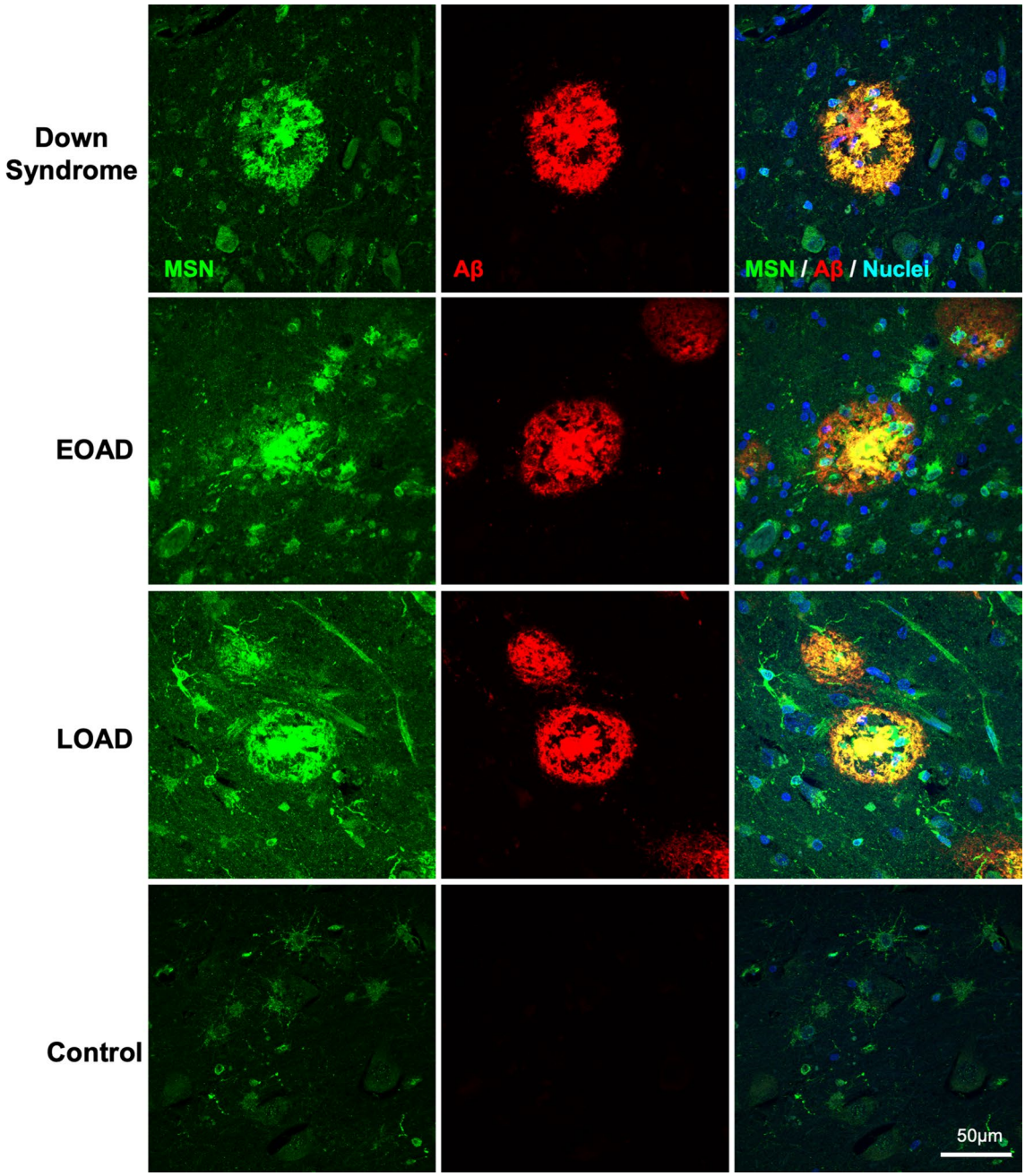

Fig. 6 Validation of moesin as a plaque enriched protein in human brain tissue by immunohistochemistry. Enrichment of moesin (MSN) in amyloid plaques was observed in DS, EOAD and LOAD cases. Moesin was also observed outside of plaques in all tissue examined (including cognitively normal control tissue) in cells consistent with a microglial morphology

soma throughout the cytoplasm and occasionally in primary processes (Fig. 9C). Staining was particularly bright in hippocampal pyramidal neurons. Abundant ARL8B was also observed in granule cells in the dentate gyrus, in the choroid plexus, and in the nucleus of some cells in white matter. The same pattern of basal staining was observed in controls and all subtypes of AD. In the second subset of amyloid plaques, intense ARL8B immunoreactivity was observed in specific plaque-associated cells (Fig. 9D). These cells were located at the periphery of plaques and had bright, punctate ARL8B throughout the cell cytoplasm and primary processes (Fig. 9D) and

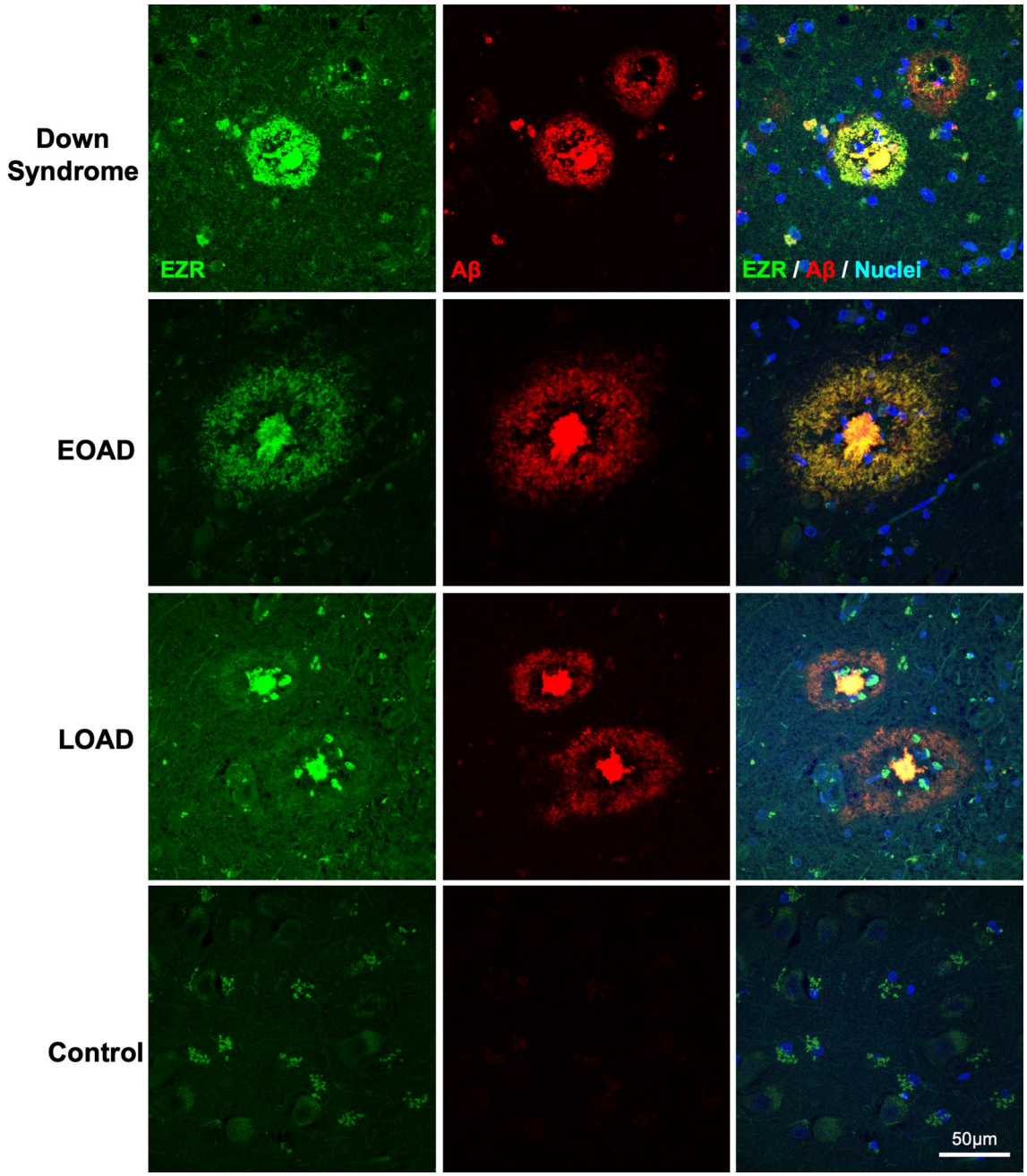

Fig. 7 Validation of ezrin as a plaque enriched protein in human brain tissue by immunohistochemistry. Enrichment of ezrin (EZR) was observed in amyloid plaques in DS, EOAD and LOAD cases

had morphology consistent with reactive glia. Double fluorescent immunohistochemistry against ARL8B and MAP2, IBA1, or GFAP showed that these ARL8B positive plaque-associated cells were a subset of reactive plaque associated astrocytes.

We also validated the presence or absence of these four plaque proteins in vascular amyloid pathology. MSN, EZR and SMOC1 immunoreactivity occasionally co-localized with CAA or in plaques which were in direct contact with blood vessels. However, ARL8B immunoreactivity was absent in vascular amyloid pathology, which is consistent with its weak direct colocalization with Aβ in amyloid plaques (Fig. 10).

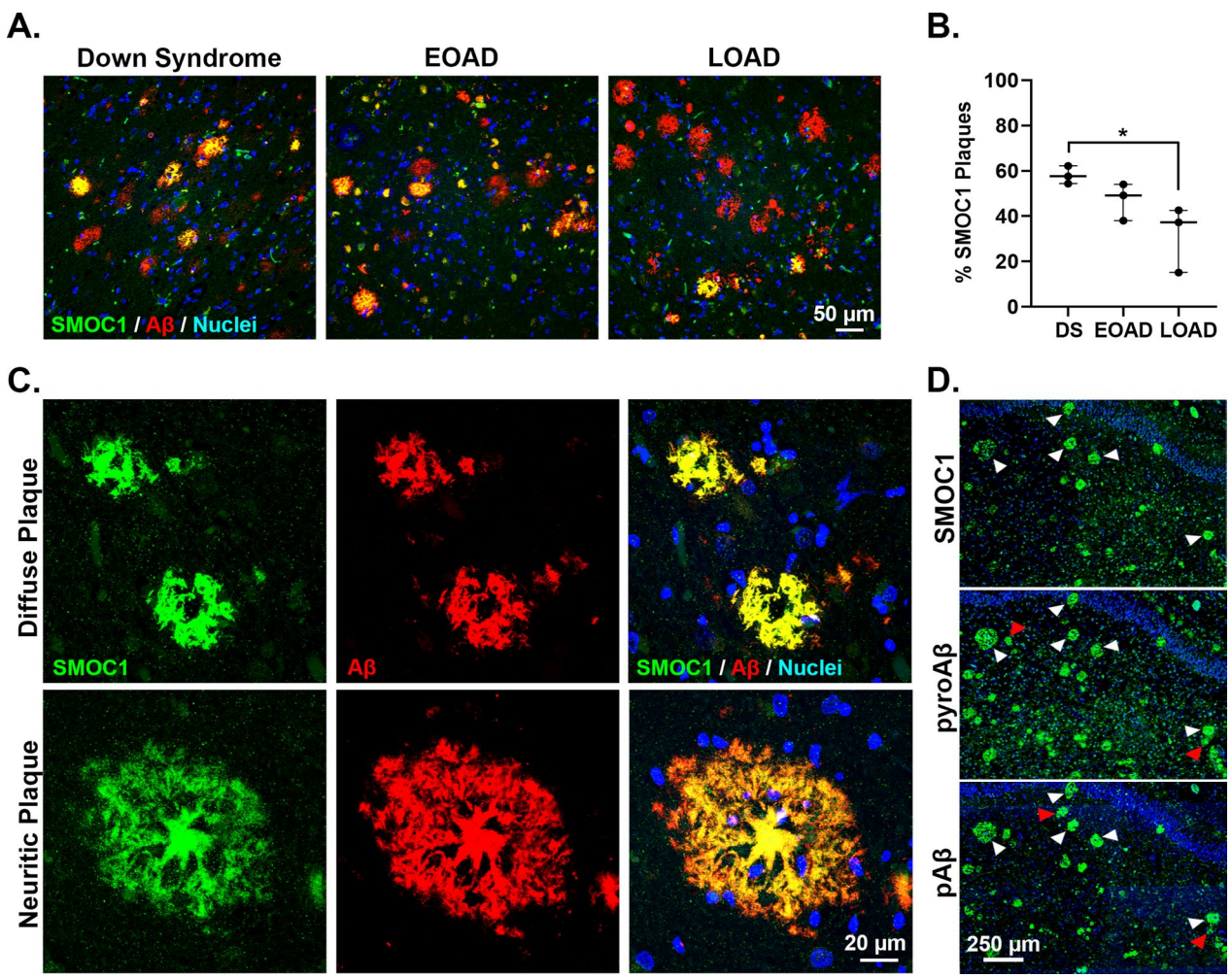

Fig. 8 Validation of SMOC1 as a plaque enriched protein in human brain tissue by immunohistochemistry. **A** Enrichment of SMOC1 was observed in a sub-population of amyloid plaques in DS, EOAD and LOAD cases. **B** Plot shows percentage of SMOC1 immunoreactive plaques in the hippocampus of DS, EOAD and LOAD cases (n = 3/group). Results generated by an analysis of 321 ± 47 hippocampal plaques (average ± SEM) in each case. The ratio of SMOC1 positive plaques (immunoreactive for both Aβ and SMOC1) over the total number of amyloid plaques was calculated for each case in DS, EOAD and LOAD. **C** Representative images of diffuse and neuritic plaques immunolabeled with SMOC1. **D** Representative images of SMOC1, pyroglutamate Aβ and phosphorylated Aβ immunolabelled plaques in the hippocampus of a representative Down syndrome case. Fluorescent immunohistochemistry was used to identify SMOC1, pyroglutamate Aβ or phosphorylated Aβ immunoreactive plaques on three sequential hippocampal sections from the same case. White arrowheads show SMOC1 immunoreactive amyloid plaques that were also immunoreactive for pyroglutamate Aβ and phosphorylated Aβ species. Red arrowheads show pyroglutamate Aβ and/or phosphorylated Aβ immunoreactive plaques negative for SMOC1. *$p < 0.05$

Discussion

Our results show that amyloid plaques in DS and EOAD are highly enriched in many proteins in addition to Aβ. Here, we have identified a core group of 48 proteins that are consistently enriched in plaques in comparison to neighboring non-plaque tissue in DS and EOAD. Many of these enriched plaque proteins have been validated in previous studies to colocalize with plaques or correlate with Aβ pathology in typical late onset AD, suggesting that this core group of enriched plaque proteins is consistent in both early and late onset AD subtypes. We also identified 15 novel proteins that were consistently enriched in plaques in both DS and EOAD. Our immunohistochemistry studies showed that while similar proteins are present in plaques in DS and EOAD the relative abundance of some of these proteins (e.g. pyroglutamate Aβ, phosphorylated Aβ, SMOC1) is distinct in plaques in DS and EOAD.

Our unbiased proteomics approach highlighted the striking enrichment of many proteins in amyloid plaques that have not been extensively studied in the context of AD such as COL25A1, SMOC1, NTN1,

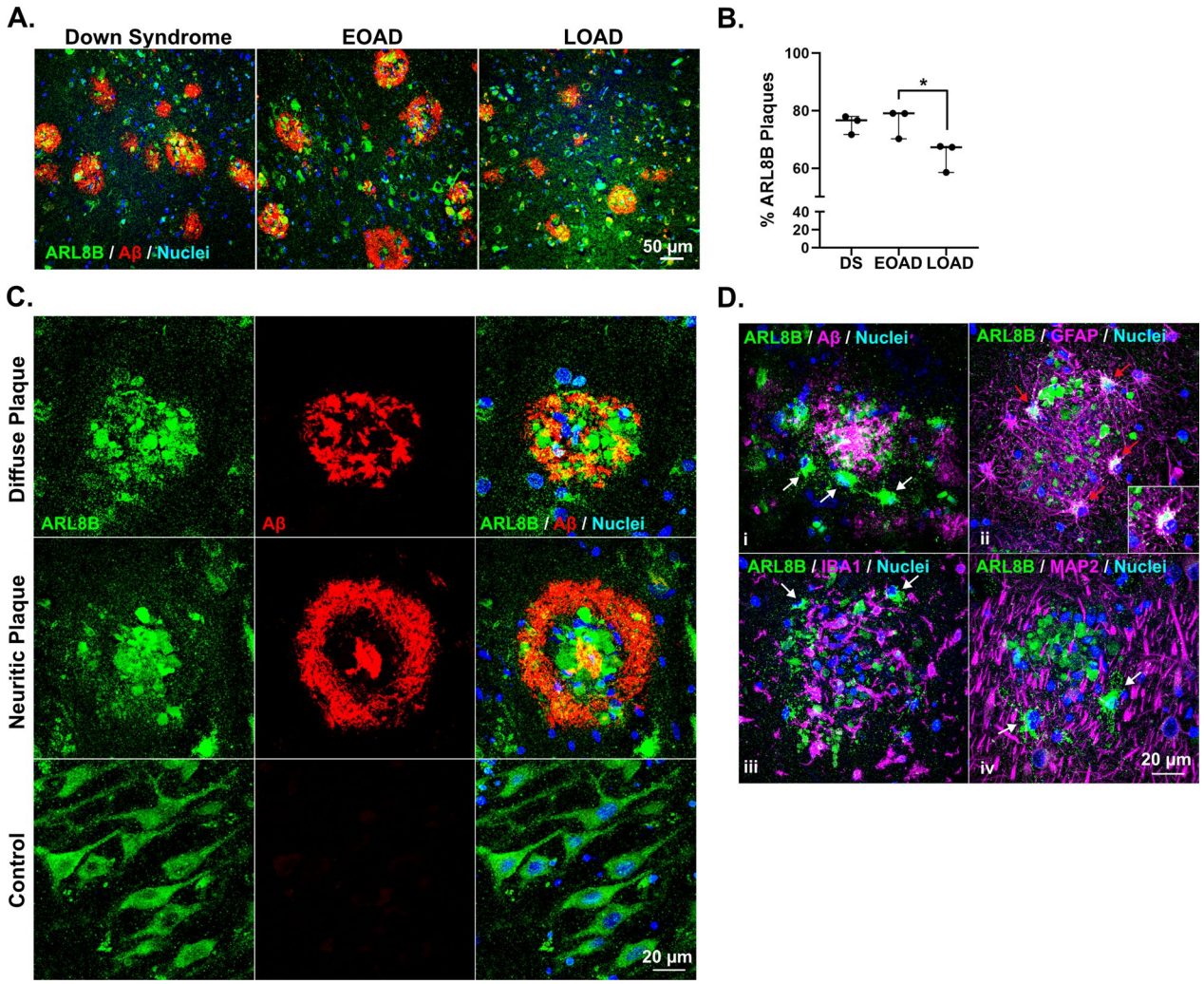

Fig. 9 Validation of ARL8B as a plaque enriched protein in human brain tissue by immunohistochemistry. **A** Enrichment of ARL8B in amyloid plaques was observed in DS, EOAD and LOAD cases. **B** Plot shows percentage of ARL8B immunoreactive plaques in the hippocampus of DS, EOAD and LOAD cases (n = 3/group). Results generated by an analysis of 309 ± 41 hippocampal plaques (average ± SEM) in each case. The ratio of ARL8B positive plaques (immunoreactive for both Aβ and ARL8B) over the total number of amyloid plaques was calculated for each case in DS, EOAD and LOAD. **C** Representative images showing ARL8B distribution in amyloid plaques. Bright puncta of ARL8B were diffusely present throughout both diffuse and neuritic plaques. Basal ARL8B staining was observed in controls in neuron soma. **D** Intense ARL8B immunoreactivity was observed in plaque-associated cells (i; arrows). Double-fluorescent immunohistochemistry showed that these plaque-associated cells with intense ARL8B immunoreactivity were a subset of plaque-associated reactive astrocytes (ii; GFAP, red arrows), and not plaque associated reactive microglia (iii; IBA1, white arrows) or neurons (iv; MAP2, white arrows). Insert in ii shows a higher magnification image of the colocalization of ARL8B and GFAP in plaque associated astrocytes

MDK, OLFML3 and HTRA1. The small number of previous studies examining the role of these proteins in AD suggest that these proteins likely have an important role in AD pathology. All of these highly enriched plaque proteins were also enriched in amyloid plaques in typical late onset AD [44] and 5/6 of these proteins were enriched in plaques in preclinical stages of AD [44], suggesting a possible role in the development of early AD pathology. Proteomic studies of human AD brain bulk tissue homogenate showed that all 6 highly enriched plaque proteins were increased in AD brain tissue in multiple brain regions in comparison to age-matched cognitively normal control brain tissue [53–55, 57, 62, 128]. Prior studies have shown that COL25A1 expression increases Aβ pathology, while NTN1, MDK and HTRA1 decreases Aβ pathology in either mouse models or cell models of AD [75, 76, 80, 129], therefore showing that these proteins have an

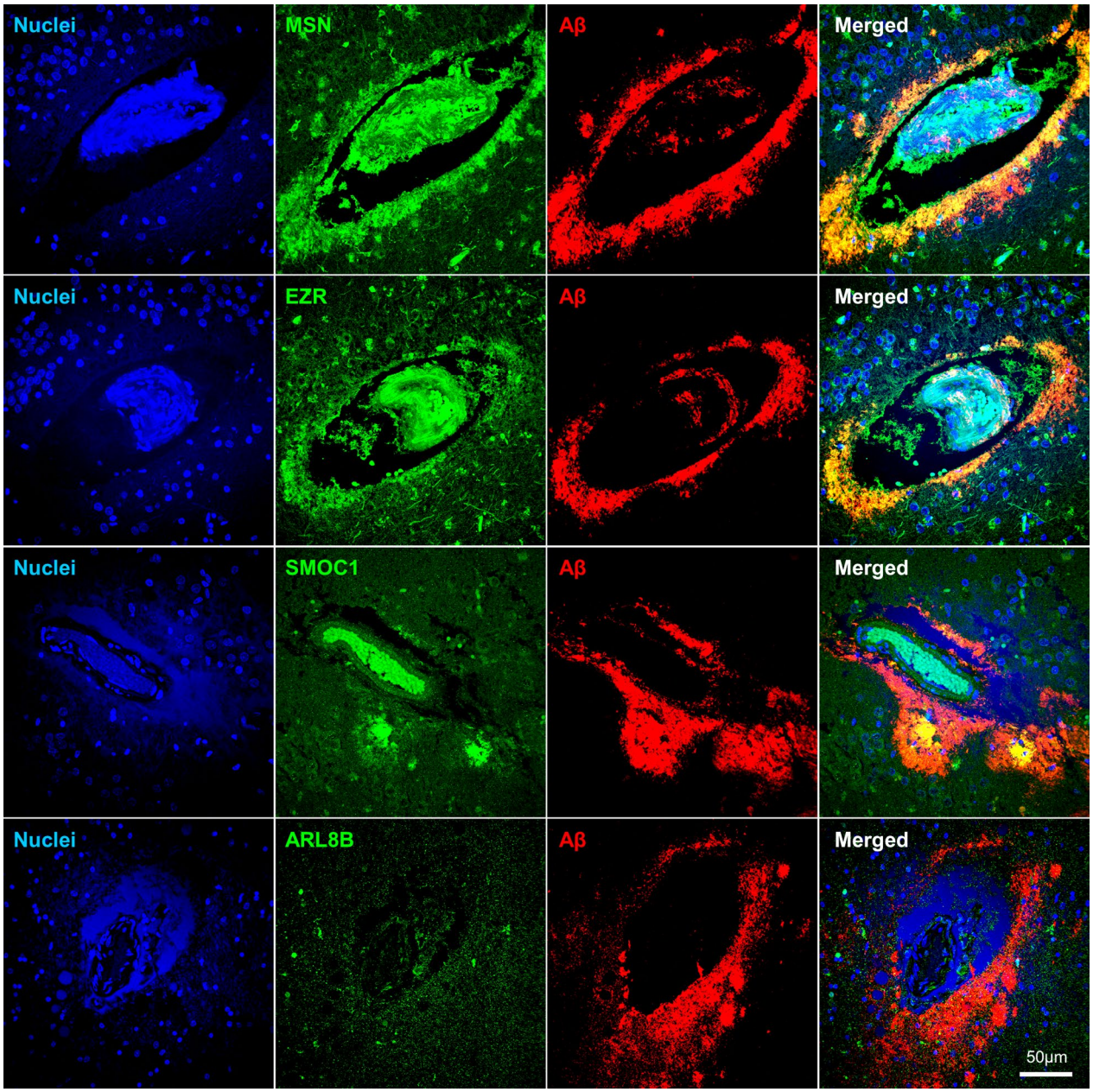

Fig. 10 Co-localization of plaque enriched proteins with vascular amyloid deposition. Representative images of vascular amyloid pathology immunolabeled with moesin (MSN), ezrin (EZR), SMOC1, ARL8B (green) and Aβ (4G8/6E10, red). Moesin, ezrin and SMOC1 co-localized with vascular amyloid pathology while ARL8B did not

important mechanistic role in AD. All of these major enriched plaque proteins tightly correlate with Aβ levels in the brain [60] and SMOC1, OLFML3, NTN1 were recently identified as novel CSF biomarkers for AD [62, 128]. Together, these results show that these major enriched amyloid plaque proteins have excellent potential as novel drug targets and/or biomarkers for AD, and should be the focus of future studies.

One of these highly enriched plaque proteins—SMOC1—was the focus of our immunohistochemistry validation studies. The role of SMOC1 in AD and its function in the brain is currently unknown. Single cell RNAseq studies suggest that SMOC1 is enriched in oligodendrocyte precursor cells in the brain [130] and previous studies have highlighted its role in glucose homeostasis [131], angiogenesis [132] and ocular and

limb development [133]. Here we show for the first time that it is highly enriched in a subpopulation of amyloid plaques. It is not yet known why SMOC1 co-localizes only with some plaques, but this could be due to SMOC1 interacting with a particular Aβ species such as pyroglutamate or phosphorylated Aβ. Indeed, our findings suggest that a large amount of SMOC1 immunoreactive amyloid plaques present in the hippocampus also contained post-translationally modified Aβ species. A hierarchical occurrence of Aβ1–40/42, pyroglutamate and pAβ throughout the course of AD has been proposed, suggesting that detection of pyroglutamate Aβ in amyloid plaques starts in preclinical AD, while phosphorylated Aβ preferentially starts aggregating in symptomatic AD [134]. Combined with our results, this might suggest that SMOC1 aggregation starts early in plaque development. A more comprehensive study looking at SMOC1 immunoreactivity in these plaque subtypes at different disease stages would provide a more definite answer. Together, our results provide further support for the important role of SMOC1 in AD and highlights the need for future studies to examine its mechanistic role in AD, particularly given the elevation of SMOC1 in the brain in preclinical AD [54]. Importantly, the finding that SMOC1 is not enriched in all plaques highlights the fact that not all amyloid plaques contain the same protein composition, which is consistent with our previous finding that plaques in rapidly progressive AD have a significantly different plaque protein expression than typical late onset AD [11].

We hypothesize that the proteins that are highly enriched in amyloid plaques have an important mechanistic role in AD pathology. A common criticism regarding the pathological importance of proteins that accumulate in plaques is that they may not have a mechanistic role in driving pathology and are simply present in plaques by chance. However, a comprehensive review of the literature does not support this criticism. 60% of the 48 proteins commonly enriched in plaques in EOAD and DS have already been confirmed to have a mechanistic role in driving AD pathology in transgenic mouse models or in vitro (Table 2). Previous studies show that 15 plaque enriched proteins pathologically promote Aβ aggregation/plaque formation or enhance Aβ associated toxicity. Notable examples include apolipoprotein E [82, 83], clusterin [7] and complement proteins (C1QB, C1QC, C3) [94, 99]. Conversely, previous studies show that 13 proteins are protective against AD pathology and can inhibit Aβ aggregation/plaque formation or protect against Aβ associated toxicity. For many of these proteins, previous research examining their mechanistic role in AD is limited to only a small number of studies. This suggests that plaque enriched proteins are not simply "tombstone markers" of disease, but instead can provide important insight into the factors that either drive or modulate the development of pathology in AD. Additionally, this also shows that proteins enriched in amyloid plaques are a mix of pathological and protective proteins and that enrichment in plaques does not automatically suggest a detrimental role in AD.

The core group of 48 proteins enriched in plaques in both DS and EOAD were highly enriched in extracellular proteins and endosomal-lysosomal system proteins. The enrichment of extracellular proteins is expected given the extracellular location of amyloid plaques. However, the significant enrichment of endosomal-lysosomal system proteins in plaques was intriguing. A growing body of evidence convincingly shows that Aβ accumulates intraneuronally within endolysosomal vesicles at early stages of AD [135, 136]. Endolysosomal vesicles provide an ideal environment for Aβ production and aggregation: it is the location where many of the key AD associated proteins colocalize (e.g. APP, presenilin-1), the acidic environment promotes Aβ aggregation and, the enclosed space promotes increased interaction and aggregation [137]. These observations have prompted the inside-out amyloid hypothesis, which proposes that the gradual accumulation of intraneuronal Aβ42 aggregates result in eventual synaptic/neuronal degeneration and the release of Aβ42 into the extracellular space which forms the nidus of amyloid plaques [135, 137–141]. Our finding of the enrichment of endolysomal proteins and other selected synaptic proteins in amyloid plaques in DS and EOAD supports this hypothesis.

Arl8b (encoded by the gene ARL8B) is an example novel lysosomal protein that we identified as enriched in amyloid plaques in both DS and EOAD. Arl8 is a small GTPase located on lysosomes that facilitates lysosomal trafficking along axons by acting as the linking molecule between lysosomes and kinesin-1 [142, 143]. Disruption of Arl8 function contributes to impaired lysosomal transport in axons, autophagic stress and neuron death in the neurodegenerative lysosomal storage disorder Niemann-Pick disease type C [144], confirming that it can contribute to neurodegenerative disease. The role of Arl8 in AD has not yet been studied and it has only been linked to AD in bulk-tissue 'omics studies [54, 59]. Arl8a, the other paralog of arl8 in vertebrates, was also enriched in amyloid plaques in DS and showed a strong trend for enrichment in plaques in EOAD. Our finding that arl8b, as well as other endosomal-lysosomal proteins, were enriched in amyloid plaques provides additional support for the potential importance of lysosomes in the formation of amyloid plaques.

Our immunohistochemistry and literature validation studies showed that amyloid plaque enriched proteins had

different colocalization patterns in amyloid plaques. For example, endolysosomal proteins typically have punctate/granular localization in plaques. This staining pattern was observed for ARL8B in our study, which was identical to the staining pattern seen for other lysosomal proteins in past studies such as cathepsin D [145], cathepsin B [146], LAMP1 [147], and lipofuscin [145], which is an accumulation of highly oxidized cross-linked molecules that accumulate in lysosomes during aging. The lack of colocalization of these lysosomal proteins with Aβ in plaques suggests that these lysosomal proteins may not be directly interacting with Aβ, but may instead be located in small pockets in amyloid plaques where Aβ is either not present or in the process of being degraded. In contrast, SMOC1, moesin and ezrin showed high colocalization with Aβ fibrils in plaques, particularly in the plaque core, suggesting that these proteins likely interact directly with Aβ. A similar staining pattern was also observed in past studies for other major plaque proteins such as apolipoprotein E [81] and COL25A1 [148]. These results also highlight an important limitation of our study; designation as a "plaque-enriched protein" does not imply direct interaction with Aβ, instead this identifies a group of proteins that are significantly enriched in plaques in comparison to non-plaque tissue. While our immunohistochemistry validation results strongly suggest that some of these novel plaque-associated proteins interact with Aβ, future studies are required to confirm this.

Direct comparison of the amyloid plaque proteome in EOAD and DS showed that amyloid plaques in the two subtypes of younger onset AD had a very similar plaque protein composition. This shows that despite the different disease initiating factors, the resulting amyloid plaques still largely contain the same proteins. While some proteins were enriched to a much greater extent in amyloid plaques in either DS or EOAD (e.g. SMOC1), the trend for enrichment in both subtypes was highly similar. It is still unclear how these relative plaque protein differences influence AD pathogenesis. Future mechanistic studies examining how each of these proteins influence Aβ aggregation or clearance are needed. Future proteomic studies examining whether these major plaque enriched proteins are also enriched in other subtypes of AD (such as late onset AD, rapidly progressive AD or familial EOAD) would also potentially provide insight into differences into the rate, topography or type of plaque pathology between these subtypes.

In conclusion, we provide a new resource for the AD field that comprehensively characterizes proteins that are enriched in amyloid plaques in multiple subtypes of AD. We propose that these consistently enriched amyloid plaque proteins provide insight into the mechanisms driving amyloid plaque development in AD and are potentially novel drug targets and/or biomarkers for AD.

Supplementary Information

The online version contains supplementary material available at https://doi.org/10.1186/s40478-022-01356-1.

Additional file 1: Table S1. Total imputed dataset. **Table S2**. Unimputed data. **Table S3**. Proteins enriched in plaques in both EOAD and DS (used to generate Figs. 2 and 4). **Table S4**. Proteins uniquely enriched in plaques in EOAD. **Table S5**. Proteins uniquely enriched in DS plaques. **Table S6**. Chromosome 21 proteins identified in our proteomic analysis. **Table S7**. DS vs EOAD plaque protein differences.

Additional file 2: Figure S1. *APOE* genotyping. (A) Schematic diagram of the *APOE* genotyping methodology. Six scrolls of 8 µm were sectioned from FFPE blocks and DNA was isolated with the automated QIAsymphony SP. An endpoint PCR was performed, samples were resolved in a 2% agarose gel and amplified DNA was purified from the gel. A second PCR with the purified DNA was performed and un-purified PCR products were sequenced to determine the *APOE* genotype. (B) Representative gel of EOAD and DS samples used for sequencing. *APOE* band is located at 348 bp. (C) Sanger sequencing chromatogram showing the nucleotides located in the single-nucleotide polymorphisms (SNPs) rs429358 and rs7412, which determine the *APOE* variant ε3.

Acknowledgements

This study was supported by funding from the Bluesand Foundation and the Dementia Australia Research Foundation (ED), NIH/NIA (AG056850, AG066512 and AG060882 to TW), and funding to ForeFront, a collaborative research group dedicated to the study of frontotemporal dementia and motor neuron disease, from the National Health and Medical Research Council of Australia (NHMRC) program Grant (#1132524) to ED and TK. This study was also supported by funding from the Chatrier Fondation (GP). The mass spectrometric experiments were supported with a shared instrumentation Grant from the NIH, 1S10OD010582-01A1, for the purchase of an Orbitrap Fusion Lumos. We thank Jenny Diaz for her expert advice regarding the APOE genotyping of FFPE tissue samples.

Author's contributions

ED and TW wrote and edited the manuscript. ED, BU and TW designed the experiments and supervised the study. ED, GP, MMA, SN, AF, VB performed the experiments. TK performed the bioinformatics. EK performed the proteomic data analysis. All authors have read and approved the final manuscript.

Declarations

Conflict of interests

The authors declare that they have no competing interests.

Author details

[1]Brain and Mind Centre and School of Medical Sciences, Faculty of Medicine and Health, University of Sydney, 94 Mallett Street, Camperdown, NSW, Australia. [2]Centre for Cognitive Neurology, Department of Neurology, New York University Grossman School of Medicine, Science Building, Rm 1017, 435 East 30th Street, New York, NY 10016, USA. [3]Proteomics Laboratory, Division of Advanced Research Technologies, New York University Grossman School of Medicine, New York, NY, USA. [4]Present Address: Merck & Co., Inc, Computational & Structural Chemistry, Kenilworth, NJ, USA. [5]Department of Biochemistry and Molecular Pharmacology, NYU Grossman School of Medicine, New York, NY, USA. [6]Departments of Pathology and Psychiatry, Neuroscience Institute, New York University Grossman School of Medicine, New York, NY, USA.

Received: 31 January 2022 Accepted: 28 March 2022
Published online: 13 April 2022

References

1. Wisniewski T, Frangione B (1992) Apolipoprotein E: a pathological chaperone protein in patients with cerebral and systemic amyloid. Neurosci Lett 135(2):235–238
2. Grundke-Iqbal I et al (1986) Microtubule-associated protein tau. A component of Alzheimer paired helical filaments. J Biol Chem 261(13):6084–9
3. Cras P et al (1991) Senile plaque neurites in Alzheimer disease accumulate amyloid precursor protein. Proc Natl Acad Sci U S A 88(17):7552–7556
4. Pires G et al (2019) Secernin-1 is a novel phosphorylated tau binding protein that accumulates in Alzheimer's disease and not in other tauopathies. Acta Neuropathol Commun 7(1):195
5. Wisniewski T, Drummond E (2020) APOE-amyloid interaction: therapeutic targets. Neurobiol Dis 138:104784
6. Hashimoto T et al (2020) Collagenous Alzheimer amyloid plaque component impacts on the compaction of amyloid-beta plaques. Acta Neuropathol Commun 8(1):212
7. DeMattos RB et al (2002) Clusterin promotes amyloid plaque formation and is critical for neuritic toxicity in a mouse model of Alzheimer's disease. Proc Natl Acad Sci U S A 99(16):10843–10848
8. Keren-Shaul H et al (2017) A unique microglia type associated with restricting development of Alzheimer's disease. Cell 169(7):1276–1290
9. Perez-Nievas BG, Serrano-Pozo A (2018) Deciphering the astrocyte reaction in Alzheimer's disease. Front Aging Neurosci 10:114
10. Serrano-Pozo A et al (2011) Neuropathological alterations in Alzheimer disease. Cold Spring Harb Perspect Med 1(1):a006189
11. Drummond E et al (2017) Proteomic differences in amyloid plaques in rapidly progressive and sporadic Alzheimer's disease. Acta Neuropathol 133(6):933–954
12. Drummond E et al (2020) Phosphorylated tau interactome in the human Alzheimer's disease brain. Brain 143(9):2803–2817
13. Drummond ES et al (2015) Proteomic analysis of neurons microdissected from formalin-fixed, paraffin-embedded Alzheimer's disease brain tissue. Sci Rep 5:15456
14. Cohen ML et al (2015) Rapidly progressive Alzheimer's disease features distinct structures of amyloid-beta. Brain 138(Pt 4):1009–1022
15. Murray ME et al (2011) Neuropathologically defined subtypes of Alzheimer's disease with distinct clinical characteristics: a retrospective study. Lancet Neurol 10(9):785–796
16. Emrani S et al (2020) APOE4 is associated with cognitive and pathological heterogeneity in patients with Alzheimer's disease: a systematic review. Alzheimers Res Ther 12(1):141
17. Neff RA et al (2021) Molecular subtyping of Alzheimer's disease using RNA sequencing data reveals novel mechanisms and targets. Sci Adv 7(2):eabb5398
18. Reitz C, Rogaeva E, Beecham GW (2020) Late-onset vs nonmendelian early-onset Alzheimer disease: a distinction without a difference? Neurol Genet 6(5):e512
19. Ballard C et al (2016) Dementia in Down's syndrome. Lancet Neurol 15(6):622–636
20. Teller JK et al (1996) Presence of soluble amyloid beta-peptide precedes amyloid plaque formation in Down's syndrome. Nat Med 2(1):93–95
21. Gyure KA et al (2001) Intraneuronal abeta-amyloid precedes development of amyloid plaques in Down syndrome. Arch Pathol Lab Med 125(4):489–492
22. Mori C et al (2002) Intraneuronal Abeta42 accumulation in Down syndrome brain. Amyloid 9(2):88–102
23. Lemere CA et al (1996) Sequence of deposition of heterogeneous amyloid beta-peptides and APO E in Down syndrome: implications for initial events in amyloid plaque formation. Neurobiol Dis 3(1):16–32
24. Wisniewski KE, Wisniewski HM, Wen GY (1985) Occurrence of neuropathological changes and dementia of Alzheimer's disease in Down's syndrome. Ann Neurol 17(3):278–282
25. Davidson YS et al (2018) The age of onset and evolution of Braak tangle stage and Thal amyloid pathology of Alzheimer's disease in individuals with Down syndrome. Acta Neuropathol Commun 6(1):56
26. Cohen AD et al (2018) Early striatal amyloid deposition distinguishes Down syndrome and autosomal dominant Alzheimer's disease from late-onset amyloid deposition. Alzheimers Dement 14(6):743–750
27. Mann DMA et al (2018) Patterns and severity of vascular amyloid in Alzheimer's disease associated with duplications and missense mutations in APP gene, Down syndrome and sporadic Alzheimer's disease. Acta Neuropathol 136(4):569–587
28. Kumar S, Lemere CA, Walter J (2020) Phosphorylated Abeta peptides in human Down syndrome brain and different Alzheimer's-like mouse models. Acta Neuropathol Commun 8(1):118
29. Frost JL et al (2013) Pyroglutamate-3 amyloid-beta deposition in the brains of humans, non-human primates, canines, and Alzheimer disease-like transgenic mouse models. Am J Pathol 183(2):369–381
30. Saido TC et al (1995) Dominant and differential deposition of distinct beta-amyloid peptide species, A beta N3(pE), in senile plaques. Neuron 14(2):457–466
31. Iwatsubo T et al (1996) Full-length amyloid-beta (1–42(43)) and amino-terminally modified and truncated amyloid-beta 42(43) deposit in diffuse plaques. Am J Pathol 149(6):1823–1830
32. Montine TJ et al (2012) National Institute on Aging-Alzheimer's Association guidelines for the neuropathologic assessment of Alzheimer's disease: a practical approach. Acta Neuropathol 123(1):1–11
33. Miller DL et al (2011) High-affinity rabbit monoclonal antibodies specific for amyloid peptides amyloid-beta40 and amyloid-beta42. J Alzheimers Dis 23(2):293–305
34. Mehta PD et al (2018) Generation and partial characterization of rabbit monoclonal antibody to pyroglutamate amyloid-beta3-42 (pE3-Abeta). J Alzheimers Dis 62(4):1635–1649
35. Herline K et al (2018) Immunotherapy to improve cognition and reduce pathological species in an Alzheimer's disease mouse model. Alzheimers Res Ther 10(1):54
36. Drummond E et al (2018) Isolation of amyloid plaques and neurofibrillary tangles from archived Alzheimer's disease tissue using laser-capture microdissection for downstream proteomics. Methods Mol Biol 1723:319–334
37. Drummond E et al (2017) Isolation of amyloid plaques and neurofibrillary tangles from archived Alzheimer's disease tissue using laser capture microdissection for downstream proteomics. Methods Mol Biol 1723:319–334
38. Cox J et al (2014) Accurate proteome-wide label-free quantification by delayed normalization and maximal peptide ratio extraction, termed MaxLFQ. Mol Cell Proteomics 13(9):2513–2526
39. Cox J et al (2011) Andromeda: a peptide search engine integrated into the MaxQuant environment. J Proteome Res 10(4):1794–1805
40. Tyanova S et al (2016) The Perseus computational platform for comprehensive analysis of (prote)omics data. Nat Methods 13(9):731–740
41. Seyfried NT et al (2017) A multi-network approach identifies protein-specific co-expression in asymptomatic and symptomatic Alzheimer's disease. Cell Syst 4(1):60–72
42. R Core Team (2020) R: a language and environment for statistical computing. R Foundation for Statistical Computing, Vienna
43. Szklarczyk D et al (2020) The STRING database in 2021: customizable protein–protein networks, and functional characterization of user-uploaded gene/measurement sets. Nucl Acids Res 49(D1):D605–D612
44. Xiong F, Ge W, Ma C (2019) Quantitative proteomics reveals distinct composition of amyloid plaques in Alzheimer's disease. Alzheimers Dement 15:429–440
45. Liao L et al (2004) Proteomic characterization of postmortem amyloid plaques isolated by laser capture microdissection. J Biol Chem 279(35):37061–37068
46. Musunuri S et al (2014) Quantification of the brain proteome in Alzheimer's disease using multiplexed mass spectrometry. J Proteome Res 13(4):2056–2068
47. Andreev VP et al (2012) Label-free quantitative LC-MS proteomics of Alzheimer's disease and normally aged human brains. J Proteome Res 11(6):3053–3067
48. Donovan LE et al (2012) Analysis of a membrane-enriched proteome from postmortem human brain tissue in Alzheimer's disease. Proteomics Clin Appl 6(3–4):201–211
49. Manavalan A et al (2013) Brain site-specific proteome changes in aging-related dementia. Exp Mol Med 45:e39
50. Hondius DC et al (2016) Profiling the human hippocampal proteome at all pathologic stages of Alzheimer's disease. Alzheimers Dement 12(6):654–668

51. Ho Kim J et al (2015) Proteome-wide characterization of signalling interactions in the hippocampal CA4/DG subfield of patients with Alzheimer's disease. Sci Rep 5:11138
52. Sweet RA et al (2016) Apolipoprotein E*4 (APOE*4) genotype is associated with altered levels of glutamate signaling proteins and synaptic coexpression networks in the prefrontal cortex in mild to moderate Alzheimer disease. Mol Cell Proteomics 15(7):2252–2262
53. Hales CM et al (2016) Changes in the detergent-insoluble brain proteome linked to amyloid and tau in Alzheimer's disease progression. Proteomics 16(23):3042–3053
54. Johnson ECB et al (2018) Deep proteomic network analysis of Alzheimer's disease brain reveals alterations in RNA binding proteins and RNA splicing associated with disease. Mol Neurodegener 13(1):52
55. Zhang Q et al (2018) Integrated proteomics and network analysis identifies protein hubs and network alterations in Alzheimer's disease. Acta Neuropathol Commun 6(1):19
56. Mendonca CF et al (2019) Proteomic signatures of brain regions affected by tau pathology in early and late stages of Alzheimer's disease. Neurobiol Dis 130:104509
57. Xu J et al (2019) Regional protein expression in human Alzheimer's brain correlates with disease severity. Commun Biol 2:43
58. Muraoka S et al (2020) Proteomic and biological profiling of extracellular vesicles from Alzheimer's disease human brain tissues. Alzheimers Dement 16:896–907
59. Johnson ECB et al (2020) Large-scale proteomic analysis of Alzheimer's disease brain and cerebrospinal fluid reveals early changes in energy metabolism associated with microglia and astrocyte activation. Nat Med 26(5):769–780
60. Bai B et al (2020) Deep multilayer brain proteomics identifies molecular networks in Alzheimer's disease progression. Neuron 105:975–991
61. Haytural H et al (2020) The proteome of the dentate terminal zone of the perforant path indicates presynaptic impairment in Alzheimer disease. Mol Cell Proteomics 19(1):128–141
62. Higginbotham L et al (2020) Integrated proteomics reveals brain-based cerebrospinal fluid biomarkers in asymptomatic and symptomatic Alzheimer's disease. Sci Adv 6(43):eaaz9360
63. Stepler KE et al (2020) Inclusion of African American/Black adults in a pilot brain proteomics study of Alzheimer's disease. Neurobiol Dis 146:105129
64. Ping L et al (2020) Global quantitative analysis of the human brain proteome and phosphoproteome in Alzheimer's disease. Sci Data 7(1):315
65. Sathe G et al (2020) Quantitative proteomic analysis of the frontal cortex in Alzheimer's disease. J Neurochem 156:988
66. Wang Z et al (2020) 27-plex tandem mass tag mass spectrometry for profiling brain proteome in Alzheimer's disease. Anal Chem 92(10):7162–7170
67. Li X et al (2021) Sequence of proteome profiles in preclinical and symptomatic Alzheimer's disease. Alzheimers Dement 17:946–958
68. Hondius DC et al (2021) The proteome of granulovacuolar degeneration and neurofibrillary tangles in Alzheimer's disease. Acta Neuropathol 141:341–358
69. Wingo AP et al (2020) Shared proteomic effects of cerebral atherosclerosis and Alzheimer's disease on the human brain. Nat Neurosci 23(6):696–700
70. McKetney J et al (2019) Proteomic atlas of the human brain in Alzheimer's disease. J Proteome Res 18(3):1380–1391
71. Pearson A et al (2020) Molecular abnormalities in autopsied brain tissue from the inferior horn of the lateral ventricles of nonagenarians and Alzheimer disease patients. BMC Neurol 20(1):317
72. Dai J et al (2018) Effects of APOE genotype on brain proteomic network and cell type changes in Alzheimer's disease. Front Mol Neurosci 11:454
73. Carlyle BC et al (2021) Synaptic proteins associated with cognitive performance and neuropathology in older humans revealed by multiplexed fractionated proteomics. Neurobiol Aging 105:99–114
74. Hashimoto T et al (2002) CLAC: a novel Alzheimer amyloid plaque component derived from a transmembrane precursor. CLAC-P/collagen type XXV EMBO J 21(7):1524–1534
75. Tong Y et al (2010) COL25A1 triggers and promotes Alzheimer's disease-like pathology in vivo. Neurogenetics 11(1):41–52
76. Spilman PR et al (2016) Netrin-1 interrupts amyloid-beta amplification, increases sAbetaPPalpha in vitro and in vivo, and improves cognition in a mouse model of Alzheimer's disease. J Alzheimers Dis 52(1):223–242
77. Yasuhara O et al (1993) Midkine, a novel neurotrophic factor, is present in senile plaques of Alzheimer disease. Biochem Biophys Res Commun 192(1):246–251
78. Muramatsu H et al (2011) Midkine as a factor to counteract the deposition of amyloid beta-peptide plaques: in vitro analysis and examination in knockout mice. Int Arch Med 4(1):1
79. Hondius DC et al (2018) Proteomics analysis identifies new markers associated with capillary cerebral amyloid angiopathy in Alzheimer's disease. Acta Neuropathol Commun 6(1):46
80. Grau S et al (2005) Implications of the serine protease HtrA1 in amyloid precursor protein processing. Proc Natl Acad Sci U S A 102(17):6021–6026
81. Namba Y et al (1991) Apolipoprotein E immunoreactivity in cerebral amyloid deposits and neurofibrillary tangles in Alzheimer's disease and kuru plaque amyloid in Creutzfeldt-Jakob disease. Brain Res 541(1):163–166
82. Bales KR et al (1997) Lack of apolipoprotein E dramatically reduces amyloid beta-peptide deposition. Nat Genet 17(3):263–264
83. Holtzman DM et al (2000) Apolipoprotein E isoform-dependent amyloid deposition and neuritic degeneration in a mouse model of Alzheimer's disease. Proc Natl Acad Sci U S A 97(6):2892–2897
84. Huttenrauch M et al (2018) Glycoprotein NMB: a novel Alzheimer's disease associated marker expressed in a subset of activated microglia. Acta Neuropathol Commun 6(1):108
85. Eikelenboom P, Stam FC (1984) An immunohistochemical study on cerebral vascular and senile plaque amyloid in Alzheimer's dementia. Virchows Arch B Cell Pathol Incl Mol Pathol 47(1):17–25
86. van Horssen J et al (2001) Heparan sulfate proteoglycan expression in cerebrovascular amyloid beta deposits in Alzheimer's disease and hereditary cerebral hemorrhage with amyloidosis (Dutch) brains. Acta Neuropathol 102(6):604–614
87. Watanabe N et al (2004) Glypican-1 as an Abeta binding HSPG in the human brain: its localization in DIG domains and possible roles in the pathogenesis of Alzheimer's disease. FASEB J 18(9):1013–1015
88. McGeer EG et al (2001) The pentraxins: possible role in Alzheimer's disease and other innate inflammatory diseases. Neurobiol Aging 22(6):843–848
89. Tennent GA, Lovat LB, Pepys MB (1995) Serum amyloid P component prevents proteolysis of the amyloid fibrils of Alzheimer disease and systemic amyloidosis. Proc Natl Acad Sci U S A 92(10):4299–4303
90. Siegel DA et al (2006) Tomoregulin-2 is found extensively in plaques in Alzheimer's disease brain. J Neurochem 98(1):34–44
91. Hong HS et al (2015) Tomoregulin (TMEFF2) binds Alzheimer's disease amyloid-beta (Abeta) oligomer and AbetaPP and protects neurons from abeta-induced toxicity. J Alzheimers Dis 48(3):731–743
92. Eikelenboom P, Stam FC (1982) Immunoglobulins and complement factors in senile plaques: an immunoperoxidase study. Acta Neuropathol 57(2–3):239–242
93. Fonseca MI et al (2004) Absence of C1q leads to less neuropathology in transgenic mouse models of Alzheimer's disease. J Neurosci 24(29):6457–6465
94. Hong S et al (2016) Complement and microglia mediate early synapse loss in Alzheimer mouse models. Science 352(6286):712–716
95. Choi-Miura NH et al (1992) SP-40,40 is a constituent of Alzheimer's amyloid. Acta Neuropathol 83(3):260–264
96. Oh SB et al (2019) Clusterin contributes to early stage of Alzheimer's disease pathogenesis. Brain Pathol 29(2):217–231
97. Glenner GG, Wong CW (1984) Alzheimer's disease: initial report of the purification and characterization of a novel cerebrovascular amyloid protein. Biochem Biophys Res Commun 120(3):885–890
98. Drummond E, Wisniewski T (2017) Alzheimer's disease: experimental models and reality. Acta Neuropathol 133(2):155–175
99. Shi Q et al (2017) Complement C3 deficiency protects against neurodegeneration in aged plaque-rich APP/PS1 mice. Sci Transl Med 9(392)
100. Wu T et al (2019) Complement C3 is activated in human AD brain and is required for neurodegeneration in mouse models of amyloidosis and tauopathy. Cell Rep 28(8):2111–2123
101. Kanekiyo T et al (2007) Lipocalin-type prostaglandin D synthase/beta-trace is a major amyloid beta-chaperone in human cerebrospinal fluid. Proc Natl Acad Sci U S A 104(15):6412–6417
102. Rayaprolu S et al (2020) Flow-cytometric microglial sorting coupled with quantitative proteomics identifies moesin as a highly-abundant microglial protein with relevance to Alzheimer's disease. Mol Neurodegener 15(1):28

103. Darmellah A et al (2012) Ezrin/radixin/moesin are required for the purinergic P2X7 receptor (P2X7R)-dependent processing of the amyloid precursor protein. J Biol Chem 287(41):34583–34595
104. Rosenblatt DE, Geula C, Mesulam MM (1989) Protease nexin I immunostaining in Alzheimer's disease. Ann Neurol 26(5):628–634
105. Jacobsen JS et al (2008) Enhanced clearance of Abeta in brain by sustaining the plasmin proteolysis cascade. Proc Natl Acad Sci U S A 105(25):8754–8759
106. Liu RM et al (2011) Knockout of plasminogen activator inhibitor 1 gene reduces amyloid beta peptide burden in a mouse model of Alzheimer's disease. Neurobiol Aging 32(6):1079–1089
107. Bruggink KA et al (2015) Dickkopf-related protein 3 is a potential Abeta-associated protein in Alzheimer's disease. J Neurochem 134(6):1152–1162
108. Zhang L et al (2017) Dickkopf 3 (Dkk3) Improves amyloid-beta pathology, cognitive dysfunction, and cerebral glucose metabolism in a transgenic mouse model of Alzheimer's disease. J Alzheimers Dis 60(2):733–746
109. Satoh J et al (2014) PLD3 is accumulated on neuritic plaques in Alzheimer's disease brains. Alzheimers Res Ther 6(9):70
110. Mukadam AS, Breusegem SY, Seaman MNJ (2018) Analysis of novel endosome-to-Golgi retrieval genes reveals a role for PLD3 in regulating endosomal protein sorting and amyloid precursor protein processing. Cell Mol Life Sci 75(14):2613–2625
111. Demirev AV et al (2019) V232M substitution restricts a distinct O-glycosylation of PLD3 and its neuroprotective function. Neurobiol Dis 129:182–194
112. Donahue JE et al (1999) Agrin in Alzheimer's disease: altered solubility and abnormal distribution within microvasculature and brain parenchyma. Proc Natl Acad Sci U S A 96(11):6468–6472
113. Rauch SM et al (2011) Changes in brain beta-amyloid deposition and aquaporin 4 levels in response to altered agrin expression in mice. J Neuropathol Exp Neurol 70(12):1124–1137
114. Rebeck GW et al (1995) Multiple, diverse senile plaque-associated proteins are ligands of an apolipoprotein E receptor, the alpha 2-macroglobulin receptor/low-density-lipoprotein receptor-related protein. Ann Neurol 37(2):211–217
115. Shinohara M et al (2017) Role of LRP1 in the pathogenesis of Alzheimer's disease: evidence from clinical and preclinical studies. J Lipid Res 58(7):1267–1281
116. Yamada T et al (1992) Vimentin immunoreactivity in normal and pathological human brain tissue. Acta Neuropathol 84(2):157–162
117. Kamphuis W et al (2015) GFAP and vimentin deficiency alters gene expression in astrocytes and microglia in wild-type mice and changes the transcriptional response of reactive glia in mouse model for Alzheimer's disease. Glia 63(6):1036–1056
118. Pla V et al (2013) Secretory sorting receptors carboxypeptidase E and secretogranin III in amyloid beta-associated neural degeneration in Alzheimer's disease. Brain Pathol 23(3):274–284
119. Cummings DM et al (2017) Neuronal and peripheral pentraxins modify glutamate release and may interact in blood-brain barrier failure. Cereb Cortex 27(6):3437–3448
120. Abad MA et al (2006) Neuronal pentraxin 1 contributes to the neuronal damage evoked by amyloid-beta and is overexpressed in dystrophic neurites in Alzheimer's brain. J Neurosci 26(49):12735–12747
121. Hafez DM et al (2012) F-spondin gene transfer improves memory performance and reduces amyloid-beta levels in mice. Neuroscience 223:465–472
122. Park SY et al (2020) SPON1 can reduce amyloid beta and reverse cognitive impairment and memory dysfunction in Alzheimer's disease mouse model. Cells 9(5):1275
123. Gotoh N et al (2020) Amyloidogenic processing of amyloid beta protein precursor (APP) is enhanced in the brains of alcadein alpha-deficient mice. J Biol Chem 295(28):9650–9662
124. Griffin EF et al (2018) Distinct functional roles of Vps41-mediated neuroprotection in Alzheimer's and Parkinson's disease models of neurodegeneration. Hum Mol Genet 27(24):4176–4193
125. Teranishi Y et al (2015) Proton myo-inositol cotransporter is a novel gamma-secretase associated protein that regulates Abeta production without affecting Notch cleavage. FEBS J 282(17):3438–3451
126. Novarino G et al (2004) Involvement of the intracellular ion channel CLIC1 in microglia-mediated beta-amyloid-induced neurotoxicity. J Neurosci 24(23):5322–5330
127. Sole-Domenech S et al (2018) Lysosomal enzyme tripeptidyl peptidase 1 destabilizes fibrillar Abeta by multiple endoproteolytic cleavages within the beta-sheet domain. Proc Natl Acad Sci U S A 115(7):1493–1498
128. Wang H et al (2020) Integrated analysis of ultra-deep proteomes in cortex, cerebrospinal fluid and serum reveals a mitochondrial signature in Alzheimer's disease. Mol Neurodegener 15(1):43
129. Chen G et al (2021) Netrin-1 receptor UNC5C cleavage by active delta-secretase enhances neurodegeneration, promoting Alzheimer's disease pathologies. Sci Adv 7(16)
130. Allen Institute for Brain Science (2019) Allen cell types database-multiple cortical areas smart-seq. https://celltypes.brain-map.org/rnaseq/human_ctx_smart-seq
131. Montgomery MK et al (2020) SMOC1 is a glucose-responsive hepatokine and therapeutic target for glycemic control. Sci Transl Med 12(559):eaaz8048
132. Awwad K et al (2015) Role of secreted modular calcium-binding protein 1 (SMOC1) in transforming growth factor beta signalling and angiogenesis. Cardiovasc Res 106(2):284–294
133. Okada I et al (2011) SMOC1 is essential for ocular and limb development in humans and mice. Am J Hum Genet 88(1):30–41
134. Rijal Upadhaya A et al (2014) Biochemical stages of amyloid-beta peptide aggregation and accumulation in the human brain and their association with symptomatic and pathologically preclinical Alzheimer's disease. Brain 137(Pt 3):887–903
135. Gouras GK et al (2000) Intraneuronal Abeta42 accumulation in human brain. Am J Pathol 156(1):15–20
136. Takahashi RH et al (2002) Intraneuronal Alzheimer abeta42 accumulates in multivesicular bodies and is associated with synaptic pathology. Am J Pathol 161(5):1869–1879
137. Gouras GK et al (2010) Intraneuronal beta-amyloid accumulation and synapse pathology in Alzheimer's disease. Acta Neuropathol 119(5):523–541
138. Gouras GK, Willen K, Faideau M (2014) The inside-out amyloid hypothesis and synapse pathology in Alzheimer's disease. Neurodegener Dis 13(2–3):142–146
139. D'Andrea MR et al (2001) Evidence that neurones accumulating amyloid can undergo lysis to form amyloid plaques in Alzheimer's disease. Histopathology 38(2):120–134
140. Pensalfini A et al (2014) Intracellular amyloid and the neuronal origin of Alzheimer neuritic plaques. Neurobiol Dis 71:53–61
141. Knopman DS et al (2021) Alzheimer disease. Nat Rev Dis Primers 7(1):33
142. Rosa-Ferreira C, Munro S (2011) Arl8 and SKIP act together to link lysosomes to kinesin-1. Dev Cell 21(6):1171–1178
143. Farias GG et al (2017) BORC/kinesin-1 ensemble drives polarized transport of lysosomes into the axon. Proc Natl Acad Sci U S A 114(14):E2955–E2964
144. Roney JC et al (2021) Lipid-mediated motor-adaptor sequestration impairs axonal lysosome delivery leading to autophagic stress and dystrophy in Niemann-Pick type C. Dev Cell 56(10):1452–1468
145. Cataldo AM, Hamilton DJ, Nixon RA (1994) Lysosomal abnormalities in degenerating neurons link neuronal compromise to senile plaque development in Alzheimer disease. Brain Res 640(1–2):68–80
146. Cataldo AM et al (1990) Lysosomal proteinase antigens are prominently localized within senile plaques of Alzheimer's disease: evidence for a neuronal origin. Brain Res 513(2):181–192
147. Hassiotis S et al (2018) Lysosomal LAMP1 immunoreactivity exists in both diffuse and neuritic amyloid plaques in the human hippocampus. Eur J Neurosci 47(9):1043–1053
148. Kowa H et al (2004) Mostly separate distributions of CLAC- versus Abeta40- or thioflavin S-reactivities in senile plaques reveal two distinct subpopulations of beta-amyloid deposits. Am J Pathol 165(1):273–281

Publisher's Note

6.2. Comparative CSF proteomics in DS and AD.

Article 3: Proteomic analysis of Down syndrome cerebrospinal fluid compared to late-onset and autosomal dominant Alzheimer´s disease.

nature communications

Article

https://doi.org/10.1038/s41467-025-61054-z

Proteomic analysis of Down syndrome cerebrospinal fluid compared to late-onset and autosomal dominant Alzheimer´s disease

Received: 12 May 2025

Accepted: 11 June 2025

Published online: 01 July 2025

Check for updates

A list of authors and their affiliations appears at the end of the paper

Almost all individuals with Down Syndrome (DS) develop Alzheimer's disease (AD) by mid to late life. However, the degree to which AD in DS shares pathological changes with sporadic late-onset AD (LOAD) and autosomal dominant AD (ADAD) beyond core AD biomarkers such as amyloid-β (Aβ) and tau is unknown. Here, we used proteomics of cerebrospinal fluid from individuals with DS ($n = 229$) in the Down Alzheimer Barcelona Neuroimaging Initiative (DABNI) cohort to assess the evolution of AD pathophysiology from asymptomatic to dementia stages and compared the proteomic biomarker changes in DS to those observed in LOAD and ADAD. Although many proteomic alterations were shared across DS, LOAD, and ADAD, DS demonstrated more severe changes in immune-related proteins, extracellular matrix pathways, and plasma proteins likely related to blood-brain barrier dysfunction compared to LOAD. These changes were present in young adults with DS prior to the onset of Aβ or tau pathology, suggesting they are associated with trisomy 21 and may serve as risk factors for DSAD. DSAD showed an earlier increase in markers of axonal and white matter pathology and earlier changes in markers potentially associated with cerebral amyloid angiopathy compared to ADAD. The unique features of DSAD may have important implications for treatment strategies in this population.

Down syndrome (DS), caused by triplication of chromosome 21, is the most common genetic form of intellectual disability, affecting approximately 1 in 1000 live births[1]. Advances in health care for individuals with DS have significantly extended life expectancy in this population. However, the increase in life expectancy up to the seventh decade is now limited by Alzheimer's disease (AD) dementia, which affects more than 90% of individuals with DS by this age, and has become the leading cause of mortality in this population[2–4]. Trisomy 21 leads to triplication of the APP gene, resulting in overproduction of the amyloid-β (Aβ) peptide and the development of Aβ plaques. By age 40, all individuals with DS develop extensive AD neuropathology[5,6].

Early research on DS neuropathology was pivotal in the development of the AD amyloid hypothesis. Glenner and Wong first purified the Aβ peptide from DS cerebrovasculature and found it homologous to the Aβ protein from late-onset AD (LOAD) brains, linking chromosome 21 to AD neuropathology[7]. Later, mutations in *APP* on chromosome 21, which increase $Aβ_{42}$ peptide production, were identified as a cause of ADAD[8,9], establishing a shared pathophysiology of Aβ dyshomeostasis among LOAD, ADAD, and DSAD. Mutations in the APP, PSEN1, and PSEN2 genes in ADAD also lead to early β-amyloidosis and subsequent dementia[5,6]. Existing fluid and imaging biomarkers for AD show strikingly similar changes between ADAD and DSAD[5,10]. However,

e-mail: jfortea@santpau.cat; erik.johnson@emory.edu

despite these similarities in core AD biomarkers between DSAD and ADAD, DS is associated with neurodevelopmental abnormalities and other conditions, resulting in differences compared to the general population in brain structure[5,6], immune function[11,12], and even in standard biochemical and hematological parameters[13]. Therefore, it remains unclear whether, and to what extent, the biological pathways associated with dementia in DSAD are similar to LOAD and ADAD beyond those reflected by the core AD biomarkers Aβ and tau. With the advent of effective anti-Aβ therapies for LOAD and considering the significant drug development efforts targeting other pathways, understanding the pathophysiology and natural history of DSAD and its relationship to other forms of AD has become an urgent priority to advance therapeutic opportunities for this important clinical population.

One way to advance understanding of the pathological changes associated with neurodegenerative disease is through proteomics. Proteomics analyzes disease-related changes at the level of proteins, which are the effectors of most biological functions and the source of most molecular disease biomarkers. Proteomic analysis of LOAD brain tissue and cerebrospinal fluid (CSF) over the past decade has illustrated the complex molecular pathology related to Aβ plaques, tau neurofibrillary tangles (NFTs), and cognitive decline in LOAD[14–20], the most common form of AD. More recently, targeted proteomic analysis of ADAD CSF in the dominantly inherited Alzheimer network (DIAN) has shown how multiple biological pathways are altered after the onset of cerebral Aβ deposition[21]. A powerful characteristic of ADAD is the ability to place any measurement within a longitudinal framework due to the predictability of symptom onset—often operationalized as the estimated year of onset (EYO) metric—which enables study of the natural history of the disease using cross-sectional data. DSAD has similar predictability of symptom onset compared to ADAD[4–6], and this predictability has been leveraged to study the evolution of imaging measures and standard AD CSF and plasma biomarkers in DSAD over the course of decades[5,6].

To better understand the constitutive or neurodevelopmental features in DS and those features related to DSAD, here we report proteomic changes in DS CSF and how they compare to changes in established AD CSF biomarkers. We used tandem mass tag mass spectrometry (TMT-MS) to measure hundreds of proteins and analyzed the data using a systems biology approach to identify biological pathways influenced by trisomy 21 and DSAD. We compared the proteomic findings in DS to LOAD and to those reported in a previous study on ADAD. We found similarities in several biological processes between DSAD, LOAD, and ADAD, but also unique constitutive features in DS that occur prior to AD biomarker abnormalities, and differences in the temporal progression of many proteins compared to ADAD. These differences might have important implications for therapeutic development and clinical trial design in DSAD.

Results

Most proteomic changes in DS CSF occur prior to the onset of AD symptoms

In this study, we analyzed CSF samples from a total of 365 participants using mass spectrometry-based proteomics. Cohort characteristics are provided in Table 1. The cohort included euploid controls ($n = 72$), euploid individuals with late-onset sporadic preclinical, prodromal, or AD dementia (LOAD; $n = 64$), asymptomatic DS (asymDS; $n = 96$), individuals with DS and cognitive decline not due to AD (oDS = 14), individuals with DS and prodromal AD (proDS; $n = 47$), and individuals with DS and AD dementia (demDS; $n = 72$). Detailed demographic and clinical characteristics are provided in Supplementary Data 1. Proteomic TMT-MS-based analysis yielded a total of 1122 protein measurements across 365 cross-sectional cases. After correction for batch effects and filtering for proteins with abundance measurements in at least 80% of samples balanced across case groups, we identified 838 proteins for individual protein analyses. To determine whether a given protein was significantly altered in DS compared to controls, we employed a modeling framework previously used in ADAD to estimate protein levels in DS and control cases across estimated year of onset (EYO) using a Bayesian statistical approach[21,22]. We used age 50.2 for symptom onset (EYO = 0) in DS based on previous estimates[5]. Both DS and control cases were placed within this EYO framework to estimate the difference between protein levels in DS and controls from EYO −32 to 24 in 0.5 EYO intervals. The model allowed for non-linear protein level changes (Supplementary Fig. 1A). Examples of two altered proteins, amyloid precursor protein (APP) and neuronal pentraxin-2 (NPTX2), are shown in Fig. 1. Given the distribution of DS and control cases across EYO, the confidence of our estimates was greatest between EYO −20 and 10. Out of the 838 proteins analyzed, we observed 556 that were either increased or decreased in DS compared to controls at any EYO (Fig. 2, Supplementary Figs. 2, 3, Supplementary Data 2, and Supplementary Information). A large majority (87%) of these proteins were altered prior to AD symptom onset and mapped to multiple biological pathways affected in the AD brain previously identified through AD brain protein co-expression analysis (Supplementary Fig. 2 and Supplementary Data 2)[17]. Although proteins increased and decreased in DS showed a similar pattern of change across EYO, there was a slight bias towards earlier changes in proteins that were increased in DS compared to those that were decreased in DS (Supplementary Fig. 3A). Five proteins had mixed direction of change (Supplementary Fig. 3B). We next assessed for effects of *APOE* and sex on the DS CSF proteome by first filtering for proteins significantly altered in DS and then separately for sex and *APOE* ε4 and ε2 effects on these filtered proteins (Supplementary Fig. 1B, C). We observed 18 proteins that were both significantly altered in DS and influenced by *APOE* ε4 across EYO (Supplementary Fig. 4 and Supplementary Data 3), and six proteins that were influenced by *APOE* ε2 (Supplementary Fig. 5 and Supplementary Data 3), although the *APOE* ε2 analysis was less powered. There was no overlap between proteins significantly altered in DS and influenced by *APOE* ε4 and ε2. We observed a greater number of proteins (79) significantly different in DS that were also significantly influenced by sex (Supplementary Fig. 6 and Supplementary Data 4). In summary, we observed 556 proteins that were significantly altered in DS across the EYO continuum, the vast majority of which were altered prior to AD symptom onset, illustrating early changes across multiple CSF protein measures in DS.

Identification of systems pathological changes in DS using protein co-expression

To more clearly identify the biological processes altered in DS, we used protein co-expression network analysis to reduce the dimensionality of the CSF proteomic data. Protein co-expression analysis is a powerful technique to identify groups of proteins related by their common changes in abundance across individuals. Protein groups, or "modules," can then be interrogated for the biological pathways they represent through ontology analysis. We constructed a protein co-expression network from the CSF of individuals with DS, identifying 29 distinct modules reflecting multiple different biological processes or pathways (Fig. 3, Supplementary Data 5, and Supplementary Information). Each module eigenprotein, or the first principal component of module protein expression, was assessed for correlation with established CSF AD biomarkers as well as cognitive function, age, sex, and *APOE* ε4. Module levels were also assessed across case groups, and for overlap with brain cell-type specific markers (Supplementary Data 6 and Supplementary Information). We observed a group of related modules strongly positively correlated with CSF total-tau (tTau), pTau181, pTau217, and pTau231, neurofilament light polypeptide (NFL, referred to subsequently as NEFL for consistency in nomenclature across proteins), and chitinase-3-like protein 1 (CHI3L1, also known as YKL-40) levels, and negatively correlated with Aβ42/40

https://doi.org/10.1038/s41467-025-61054-z

Table 1 | Study participants

Characteristic	*N*	CN, *N* = 72[a]	*preAD*, *N* = 8[a]	AD, *N* = 56[a]	oDS, *N* = 14[a]	asymDS, *N* = 96[a]	proDS, *N* = 47[a]	demDS, *N* = 72[a]
Sex	365							
Female		47 (65.3%)	4 (50.0%)	34 (60.7%)	5 (35.7%)	42 (43.8%)	21 (44.7%)	34 (47.2%)
Male		25 (34.7%)	4 (50.0%)	22 (39.3%)	9 (64.3%)	54 (56.2%)	26 (55.3%)	38 (52.8%)
Age at visit	365	57.2 (9.8)	69.7 (7.4)	72.2 (6.7)	42.4 (7.7)	38.3 (9.8)	51.3 (4.1)	52.4 (5.4)
CSF AD biomarkers								
Aβ1–40	329	11,973.0 (3,716.9)	14,764.4 (2,826.8)	11,795.7 (3,175.1)	10,653.4 (3692.9)	12,655.4 (4,830.4)	11,796.3 (4,489.0)	10,460.6 (4,595.6)
Aβ1–42	329	1,229.0 (394.7)	757.4 (241.1)	519.6 (137.5)	839.0 (400.0)	990.7 (469.2)	515.3 (179.6)	475.6 (192.7)
NFL (NEFL)	349	459.4 (245.5)	719.3 (217.6)	1,137.2 (506.4)	521.5 (277.8)	449.7 (367.5)	978.6 (593.1)	1,350.1 (835.7)
YKL-40 (CHI3L1)	321	194.5 (70.9)	245.6 (72.4)	256.1 (60.0)	135.0 (48.2)	134.8 (66.4)	229.9 (83.9)	245.4 (101.4)
pTau181	329	40.0 (39.1)	76.8 (26.9)	129.7 (72.1)	35.8 (17.6)	42.9 (43.5)	148.5 (120.2)	152.8 (92.4)
pTau217	344	2.80 (6.32)	7.65 (3.73)	17.6 (10.3)	2.62 (2.95)	4.40 (5.17)	16.2 (12.8)	17.0 (10.9)
pTau231	362	147.6 (252.8)	381.2 (207.8)	585.7 (400.5)	128.3 (64.8)	144.9 (149.6)	480.2 (339.7)	522.8 (409.3)
tTau	329	270.4 (187.0)	462.6 (162.6)	758.3 (372.6)	314.5 (136.4)	349.4 (254.1)	855.7 (574.7)	942.9 (557.6)
APOE genotype	363							
ε2/ε2		0 (0.0%)	0 (0.0%)	0 (0.0%)	0 (0.0%)	0 (0.0%)	1 (2.2%)	1 (1.4%)
ε2/ε3		5 (6.9%)	1 (12.5%)	1 (1.8%)	2 (14.3%)	9 (9.4%)	9 (19.6%)	3 (4.2%)
ε2/ε4		0 (0.0%)	0 (0.0%)	0 (0.0%)	0 (0.0%)	1 (1.0%)	1 (2.2%)	2 (2.8%)
ε3/ε3		49 (68.1%)	3 (37.5%)	26 (46.4%)	12 (85.7%)	69 (71.9%)	26 (56.5%)	51 (70.8%)
ε3/ε4		17 (23.6%)	4 (50.0%)	21 (37.5%)	0 (0.0%)	15 (15.6%)	8 (17.4%)	14 (19.4%)
ε4/ε4		1 (1.4%)	0 (0.0%)	7 (12.5%)	0 (0.0%)	1 (1.0%)	1 (2.2%)	1 (1.4%)

CN cognitively normal controls, *preAD* preclinical AD, *oDS* other DS such as psychiatric disease, *asymDS* asymptomatic DSAD, *proDS* prodromal DSAD, *demDS* dementia DSAD.
[a]*n* (%); Mean (SD).

https://doi.org/10.1038/s41467-025-61054-z

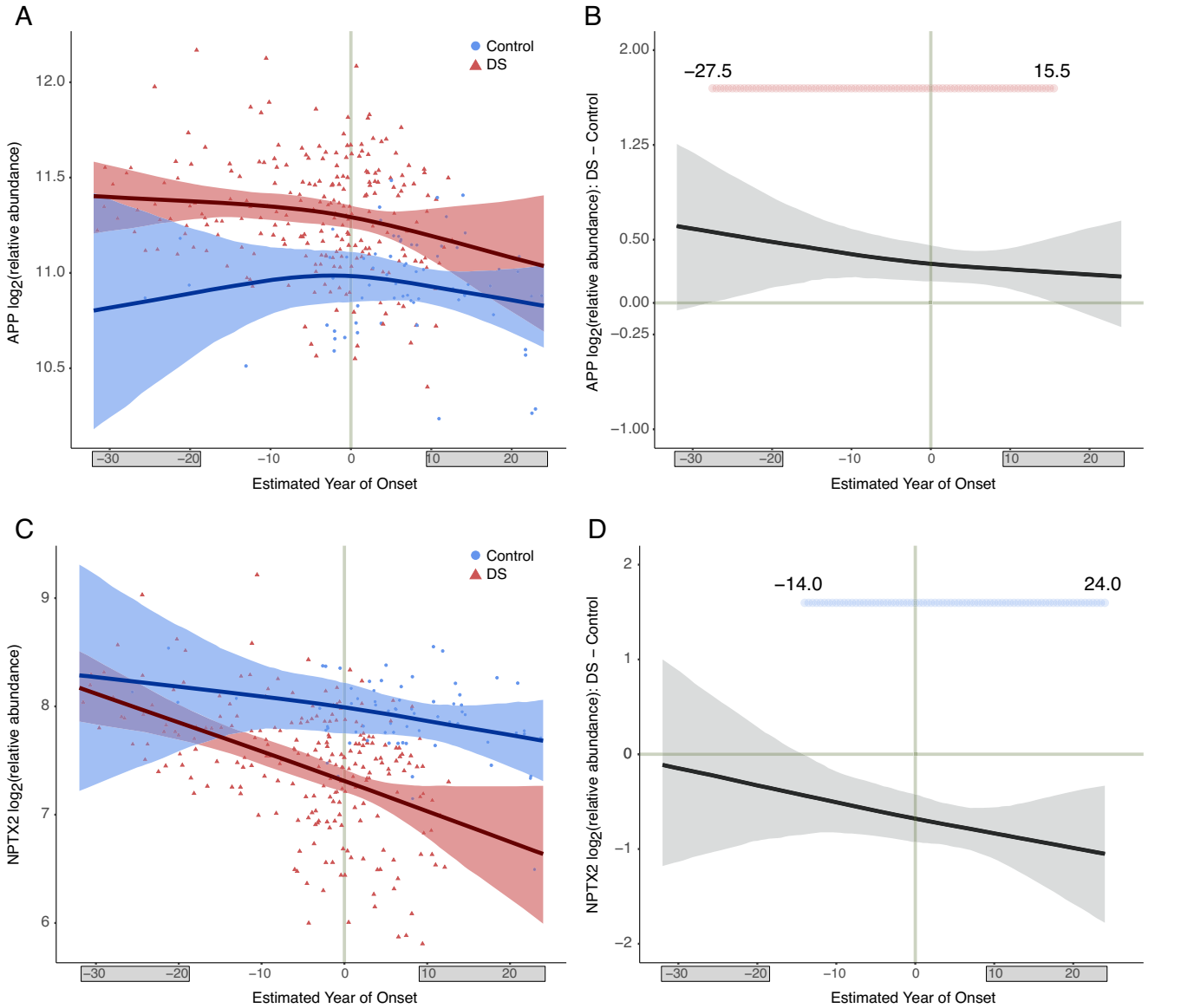

Fig. 1 | Modeling of APP and NPTX2 protein levels in DS CSF by estimated year of symptom onset. A, **B** Levels of the amyloid precursor protein (APP), located on chromosome 21, in DS (red) and control (blue) cerebrospinal fluid (CSF) (**A**), and the difference in APP levels between DS and controls (**B**), by estimated year of symptom onset (EYO). One outlier was removed from **A** for visualization purposes. **C**, **D** CSF levels of neuronal pentraxin-2 (NPTX2), a synaptic protein, in DS and controls (**C**), and the difference between NPTX2 levels in DS and controls (**D**). Two outliers were removed from **C** for visualization purposes. Solid lines indicate the mean protein level; shaded areas indicate the 99% credible interval. Periods of significant difference between DS and controls are highlighted in (**B**, **D**) (red indicates significantly increased levels in DS, blue indicates significantly decreased levels in DS). Shaded EYO values on the x-axis indicate periods of lower confidence estimates due to the smaller number of participants over the indicated EYO range. Plots for other proteins are provided in the Supplementary Information.

ratio and cognitive function. These modules included 14-3-3 proteins and microtubule-associated protein tau (MAPT), glucose/energy metabolism, immune response, and actin cytoskeleton pathways. Notably, the M8 14-3-3/MAPT/Mixed module (Fig. 3B) was most strongly correlated with AD traits and AD-related cognitive impairment and was strongly elevated in DS with symptomatic AD (Fig. 3C). Modules that showed opposite relationships with these measures included M22 glycoprotein biosynthesis/endoplasmic reticulum (ER), M10 neuron migration/organization, and M6 cell migration. In addition, we identified a module, M23 Chr21/APP/SOD1/leukocyte migration, that was strongly elevated in DS and contained approximately half (8 out of 15) of the chromosome 21 proteins measured in our dataset, including superoxide dismutase (SOD1) and leukocyte migration markers (Supplementary Fig. 7). This module was not elevated in LOAD. Other modules that were strongly elevated in DS and not LOAD but were less strongly correlated to pTau included M18 extracellular matrix, M5 collagen, M25 complement, and M3 immunoglobulins. M2 plasma proteins was also elevated in DS, although to a lesser degree. In summary, we identified groups of proteins related by their co-abundance patterns that were both elevated and decreased in DS, some of which were highly correlated with LOAD biomarkers such as M8 14-3-3/MAPT/mixed and M4 glucose/energy metabolism, and some of which were unique to DS such as M23 Chr21/APP/SOD1/leukocyte migration and M3 immunoglobulins.

Many protein co-expression modules in DS are altered prior to decreases in CSF Aβ42/40

To assess the temporal progression of protein module changes in DS, we modeled module eigenprotein levels in DS and controls across EYO in a similar fashion to individual protein levels (Fig. 4 and

https://doi.org/10.1038/s41467-025-61054-z

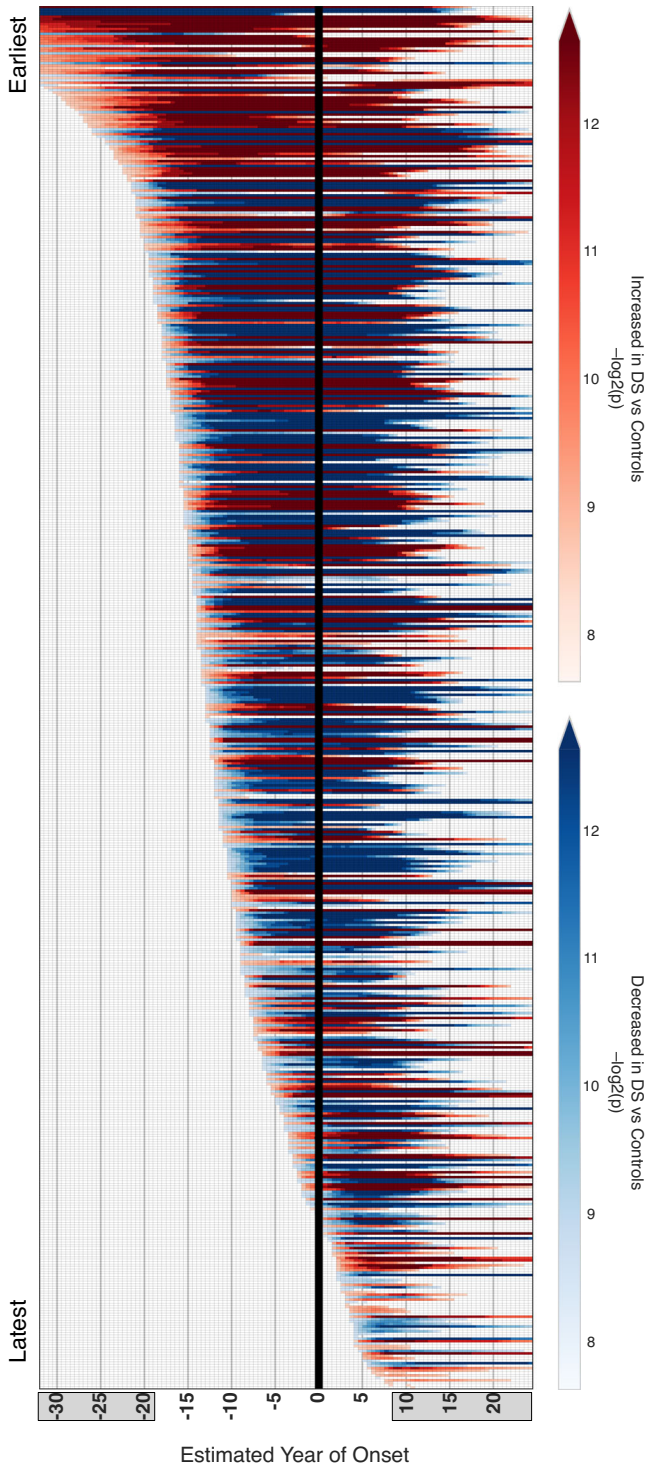

Fig. 2 | Individual protein changes in DS by EYO. 556 out of 838 CSF proteins analyzed had different levels in DS at any EYO. Differences were assessed in 0.5 EYO intervals. Red indicates increased levels in DS and blue indicates decreased levels in DS. Heat indicates the significance of the difference between DS and controls, with scale provided in the arrows on the right. The vertical black line highlights EYO = 0 (age 50.2). Shaded EYO values on the x-axis indicate periods of lower confidence estimates, including after EYO = 10, where DS data were sparse and therefore only proteins with strong differences are considered significant. Periods of significant change and direction of change for all 556 significant proteins and other CSF ELISA measurements are provided in Supplementary Fig. 2 and Supplementary Data 2. About 266 proteins were increased and 294 proteins were decreased across EYO, with five proteins showing mixed direction of change. Visualization of proteins separated by direction of change in DS is provided in Supplementary Fig. 3. Empirical *p* values were computed within a Bayesian analysis framework. All tests were two-sided with a pre-specified significance level of 0.01, corresponding to tail probabilities of 0.005 and 0.995. No multiple testing correction was applied.

Supplementary Data 7). Out of the 29 modules, 22 showed significant differences in DS at any EYO. Of these 22 modules, 11 were significantly altered in DS prior to changes in the Aβ42/40 or Aβ42/tTau ratio—commonly used to assess Aβ plaque deposition—and included M5 collagen, M18 extracellular matrix, and M25 complement. Modules demonstrating the earliest change in DS were M23 Chr21/APP/SOD1/leukocyte migration, as expected, and M13 Golgi/glycosylation. Modules that were strongly correlated to LOAD biomarkers—M8 14-3-3/MAPT/mixed and M9 actin cytoskeleton—were elevated approximately 10 years prior to symptom onset, whereas modules altered closer to symptom onset included M24 immune response and M11 neurogenesis/synapse. Interestingly, NEFL was elevated in DS CSF prior to elevations in tTau and pTau, suggesting early white matter pathology and axonal degeneration prior to Aβ-related elevations in pTau[23–25]. CHI3L1, a proposed biomarker of astrocytosis[26], was elevated about 5 years prior to symptom onset at approximately the same time as M24 immune response, demonstrating consistent change in measures of inflammation preceding cognitive decline. Lastly, modules M20 semaphorins/lysosome, M26 endosome/lysosome and M4 glucose/energy metabolism were altered after symptom onset, with M4 glucose/energy metabolism demonstrating the largest progressive change among these modules affected late in the disease continuum. In summary, we identified multiple modules in DS CSF that were elevated prior to changes in Aβ and tau, with immune and synaptic modules temporally associated with the onset of cognitive symptoms.

Comparison of individual protein measures in DS to ADAD highlights common alterations but unique temporal patterns

We have previously illustrated the temporal progression of key AD biomarkers in ADAD CSF over the course of approximately 60 years[21]. To assess how and when these biomarkers are altered in DS, we applied the same modeling approach used in ADAD (Fig. 5). Measurements in the ADAD cohort were performed using a targeted mass spectrometry approach, whereas measurements in the DS cohort were performed using an untargeted mass spectrometry approach. We selected synaptic markers to validate measurements between the two mass spectrometry-based techniques, and observed good agreement (Supplementary Fig. 8). Because of the differences in power between the ADAD and DS cohorts, absolute EYO changes between measures in ADAD and DS are not directly comparable; however, relative temporal changes among markers can be compared. Taking this consideration into account, we observed very similar changes in Aβ42 and Aβ42/40 levels in ADAD and DS, with significant differences occurring approximately 15 years prior to symptom onset. In DS, similar to ADAD, multiple protein changes occurred prior to alterations in pTau181 and pTau217 (Supplementary Fig. 9). However, the relative temporal progression of these changes and direction of change was unique in DS for several proteins. SMOC1 and SPON1—members of the brain M42 matrisome module that show early elevation in ADAD—were elevated closer to the EYO in DS and around the time of changes in pTau levels, with stronger elevation of SPON1 in DS than observed in ADAD. NEFL demonstrated the earliest increase in DS, prior to increases in the 14-3-3 proteins YWHAZ and YWHAG (Supplementary Fig. 9). Proteins with notably earlier relative decreases in DS compared to ADAD included secretogranin-2 (SCG2), neurosecretory protein VGF (VGF), neuronal pentraxin-2 (NPTX2), and lactadherin (MFGE8). MFGE8 is the precursor to the protein fragment medin, which has previously been shown to be a significant protein component within the cerebrovasculature in cerebral amyloid angiopathy (CAA)[27]. Of the overlapping protein measurements with ADAD, MFGE8 demonstrated the

https://doi.org/10.1038/s41467-025-61054-z

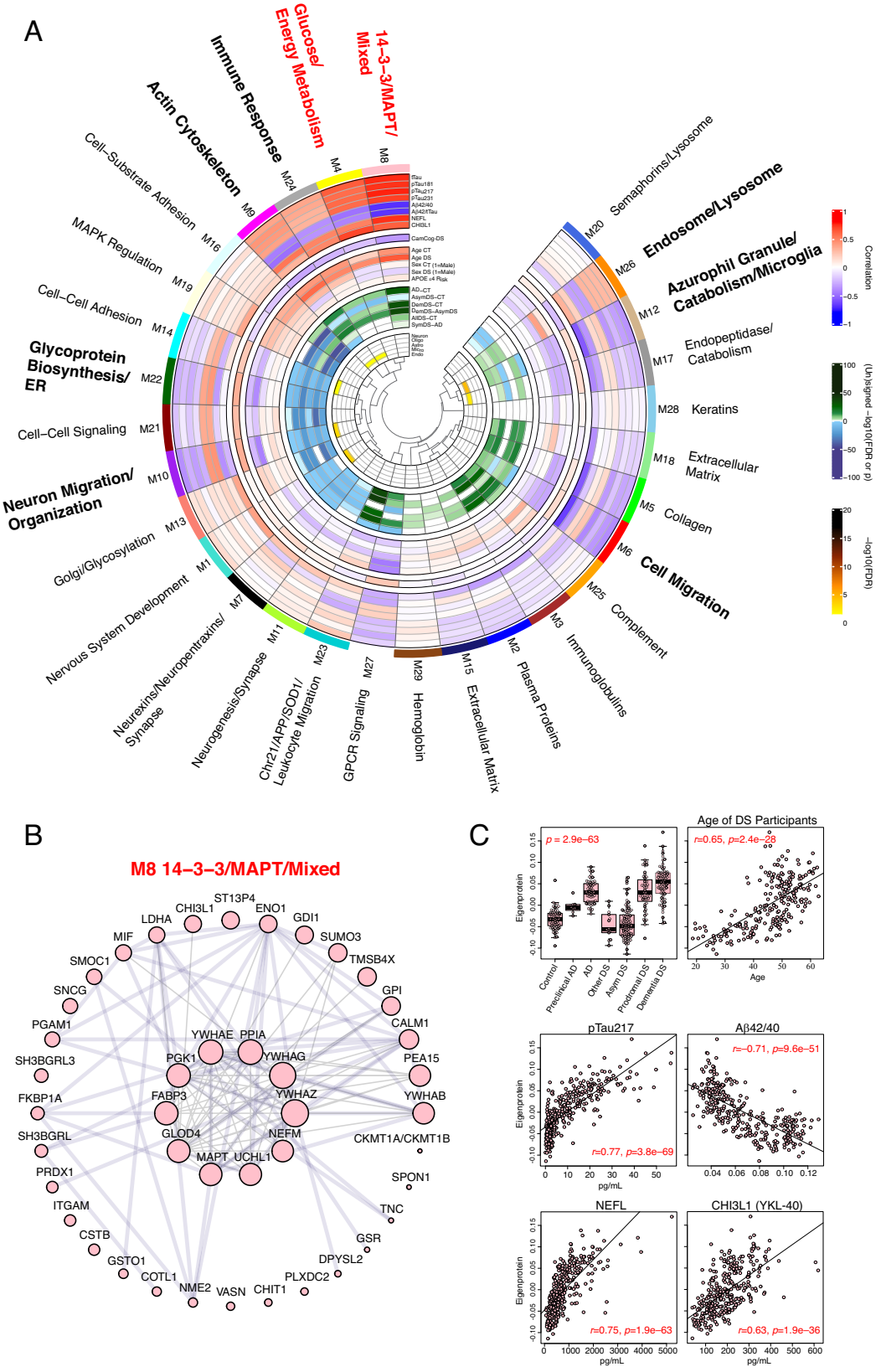

earliest decrease in protein levels that remained decreased throughout the EYO timeframe (Supplementary Fig. 9). Interestingly, a select number of proteins mapping to brain metabolic modules were noted to change in the opposite direction to that observed in ADAD, including L-lactate dehydrogenase B chain (LDHB), alpha-enolase (ENO1), Parkinson disease protein 7 (PARK7), phosphatidylethanolamine-binding protein 1 (PEBP1), and glyceraldehyde-3-phosphate dehydrogenase (GAPDH). Some of these proteins such as LDHB, ENO1, PARK7, and MFGE8 were altered prior to changes in CSF Aβ42/40 levels. In summary, we observed many common protein changes between ADAD and DS, but unique temporal ordering of certain proteins related to Aβ plaques (SMOC1 and SPON1),

Fig. 3 | DSAD CSF protein co-expression network. A–C About 1116 proteins measured across control, DS, and AD cases were used to construct a CSF protein co-expression network (**A**). Modules were annotated with their primary ontologies. Module eigenproteins were correlated to CSF total tau (tTau), pTau181, pTau217, pTau231, Aβ42/40, Aβ42/tTau, neurofilament light polypeptide (NEFL), chitinase-3-like protein 1 (CHI3L1), CamCog score (higher scores reflect better cognitive function in DS), age of controls (CT), age of DS cases, sex in CT (1 = male), sex in DS (1 = male), and *APOE ε4* risk (ε2/2 = −2, ε4/4 = +2). Red indicates positive correlation; blue indicates negative correlation. Differences in module eigenprotein levels were assessed between AD and control (AD-CT), asymptomatic DS and control (AsymDS-CT), demented DS and control (DemDS-CT), demented DS and asymptomatic DS (DemDS-AsymDS), all DS and control (allDS-CT), and symptomatic DS (prodromal and demented) and AD (SymDS-AD) using a two-sided *t*-test without correction for multiple comparisons. Green indicates increased levels; blue indicates decreased levels. Brain cell type enrichment in each module was performed for neurons, oligodendrocytes (oligo), astrocytes (astro), microglia (micro), and endothelia (endo) using one-tailed Fisher's exact test with Benjamini–Hochberg correction. Only cell type overlaps that reached statistical significance are colored. Module ontologies highlighted in bold demonstrated strong associations with AD traits, with modules highlighted in red showing the strongest associations. Module protein memberships are provided in Supplementary Data 5. Heatmap values are provided in Supplementary Data 6. **B** Protein members of the M8 14-3-3/MAPT/Mixed module, which was the module most strongly correlated to CSF AD biomarkers. Circle size indicates the strength of correlation to the module eigenprotein. Transparent blue lines represent human protein-protein interactions as provided in the BioGRID database. Gray lines represent top-ranked co-expression network edges. **C** Differences in M8 eigenprotein levels among groups (boxplot; control $n = 72$, preclinical AD $n = 8$, AD $n = 56$, other DS $n = 14$, Asym DS $n = 96$, prodromal DS $n = 47$, dementia DS $n = 72$), and correlation of the M8 eigenprotein to age in DS cases, CSF tau phosphorylated at residue 217 (pTau217), CSF amyloid-β 42/40 ratio (Aβ42/40), CSF neurofilament light polypeptide (NEFL) levels, and CSF chitinase-3-like protein 1 (CHI3L1, also known as YKL-40) levels. The difference between groups was assessed by one-way ANOVA and adjusted for age and sex. Correlations were performed using midweight bicorrelation. Boxplots represent the median, 25th, and 75th percentile extremes; thus, hinges of a box represent the interquartile range of the two middle quartiles of data within a group. The farthest data points up to 1.5 times the interquartile range away from box hinges define the extent of whiskers (error bars). Plots for other modules are provided in the Supplementary Information.

synaptic changes (SCG2, VGF, and NPTX2), axonal and white matter changes (tTau and NEFL), and cerebral amyloid angiopathy (MFGE8) in DS, and differences in some metabolic proteins that may be related to trisomy 21.

Comparison of DS CSF and brain proteomes reveals concordant and discordant alterations between compartments

To better understand the relationship between protein alterations in DS CSF and DS brain tissue, we compared CSF proteomic changes in our study to those recently reported from a localized proteomics study in DS brain on both plaque and non-plaque tissue using laser-capture microdissection[28]. A total of 376 matching gene symbols were present between the two proteomic datasets. In DS brain tissue without plaque, we observed significant increases in extracellular matrix (ECM) proteins including collagens and fibrinogens (such as COL6A3, COL6A1, COL1A1, and FGA), blood proteins such as hemoglobin (HBB and HBA1) and haptoglobin (HP), and Chr21 proteins (such as APP and NCAM2), concordant with alterations in these proteins observed in CSF (Fig. 6A). The prominent increase in immunoglobulins such as IGHG3 and IGHA1 in DS CSF was less notable in brain. Markers of myelination and white matter such as myelin-oligodendrocyte glycoprotein (MOG) and myelin-associated glycoprotein (MAG) were concordantly decreased in DS brain and CSF, as well as some neuronal markers such as VGF and parvalbumin (PVALB). As we have observed previously when comparing brain and CSF proteomic changes[14,16], not all neuronal protein alterations were concordant between compartments. For instance, neuronal proteins such as YWHAG, neuromodulin (GAP43), and brain acid soluble protein 1 (BASP1) were increased in CSF but decreased in brain, whereas proteins such as NPTX1, chromogranin-A (CHGA), and pro-neuropeptide Y (NPY) were decreased in CSF but increased in DS brain. When the analysis was restricted to plaques, plaque-associated proteins such as serine protease HTRA1 (HTRA1), midkine (MDK), and SMOC1 were more significantly altered in DS brain compared to control, as expected[17].

We also examined differences between DSAD and LOAD brain and CSF (Fig. 6B). Compared to LOAD, DSAD had higher levels of ECM and Chr21 proteins, and lower levels of white matter proteins and PVALB in brain and CSF compartments. Immunoglobulins were prominently increased in DSAD CSF compared to LOAD CSF, but this difference was not observed in brain tissue. Except for immunoglobulins, these alterations were noted in both non-plaque and plaque tissue. Some plaque-associated proteins, such as SPON1, were significantly increased in DSAD compared to LOAD, consistent with the more prominent elevation in SPON1 in DSAD CSF compared to ADAD CSF. In a separate analysis, we tested for differences in DS CSF protein network module eigenproteins in brain tissue for 19 modules that had sufficient brain protein coverage (Fig. 6C and Supplementary Information). Consistent with individual protein changes, we observed concordant changes in a number of module,s such as M23 Chr21/APP/SOD1/leukocyte migration, M5 collagen, M9 actin cytoskeleton, and M14 cell-cell adhesion. We also observed discordant changes in the 14-3-3/MAPT/mixed module heavily influenced by 14-3-3 proteins such as YWHAG, and in the M7 neurexins/neuropentraxins/synapse module, consistent with the discordant changes in module driver proteins noted above.

Given the concordant and prominent decrease in PVALB levels in DS brain and CSF, as well as the importance of this protein as a marker of PV+ inhibitory interneurons that are critical for proper excitation/inhibition balance in the brain[29], we performed IHC for PVALB in control, LOAD, and DS brain tissue (Supplementary Fig. 10). PVALB was lower in both DSAD and LOAD brain compared to controls. Although we had few cases of young DS brain, PVALB levels in DS individuals in their twenties and thirties were the same levels as controls, whereas PVALB levels in DS individuals in their fifties and sixties were lower than those in controls or LOAD. The observed age dependence in PVALB levels in DS brain was consistent with the decline in PVALB levels in DS CSF with increasing EYO (Supplementary Fig. 10C).

In summary, we identified concordant changes in ECM, plasma, Chr21, myelin, and some neuronal proteins between DS brain and CSF compartments, whereas other neuronal proteins demonstrated discordant levels between brain and CSF as previously observed. PVALB, a marker of inhibitory interneurons, was prominently decreased in both brain and CSF compared to both control and LOAD, suggesting that potential disruption of excitatory/inhibitory balance may be a key feature of DS.

Discussion

In this study, we used proteomics in the CSF of individuals with DS to understand the pathological changes that are associated with trisomy 21 and how they evolve over the course of the syndrome prior to, during, and after the onset of AD-related cognitive symptoms. We compared these pathological changes to those observed in LOAD and ADAD and observed both common and unique features. DS exhibits constitutive marked elevations in CSF levels of immunoglobulins, complement, collagen and ECM proteins before changes in markers of Aβ plaque formation, suggesting that they could be linked to the triplication of genes encoded in chromosome 21. Moreover, the marked elevations of

https://doi.org/10.1038/s41467-025-61054-z

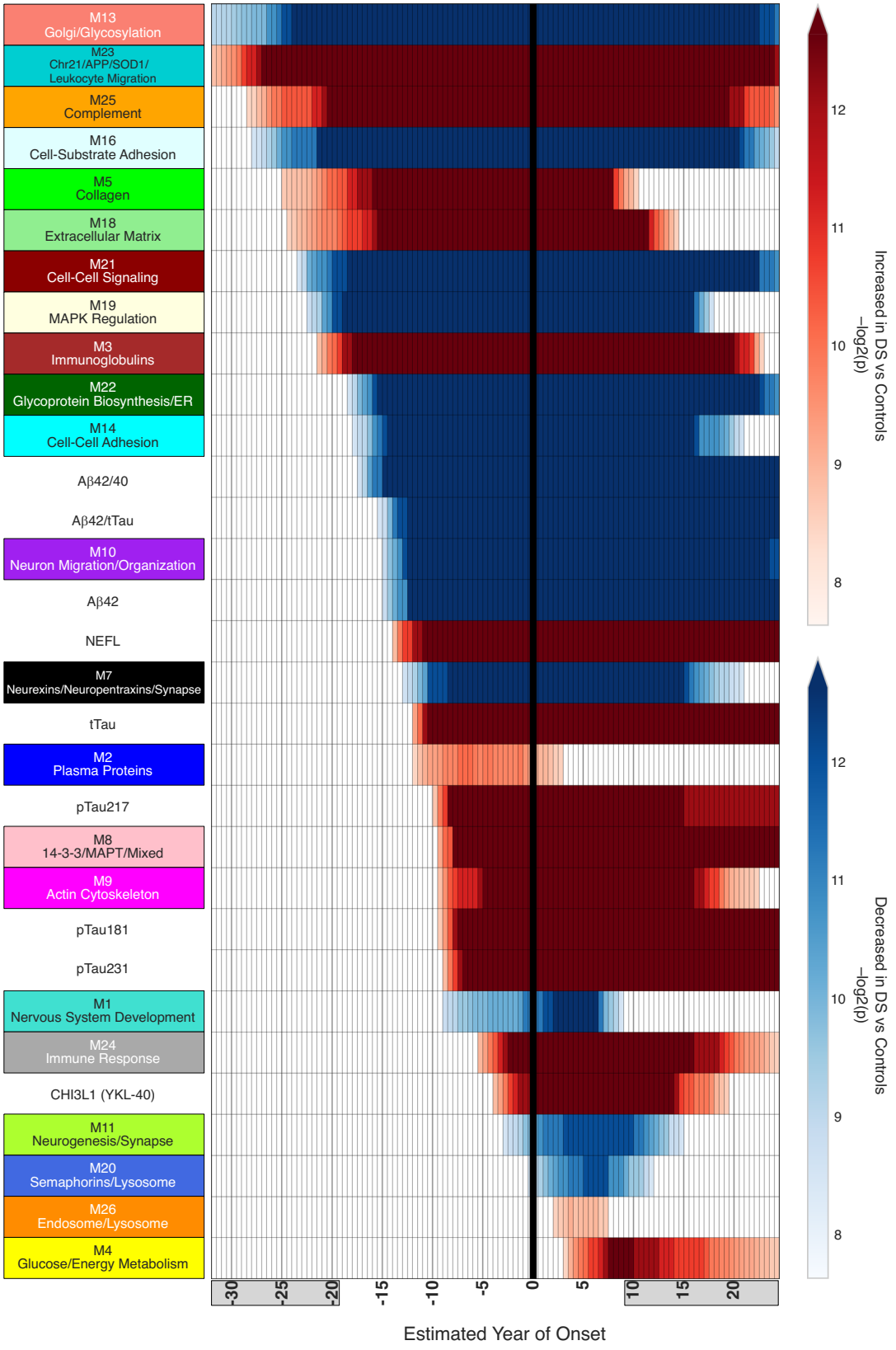

Fig. 4 | DSAD protein network module changes by EYO. Module eigenproteins, representing the first principal component of module protein abundance, were assessed for changes in DS by EYO. Differences were assessed in 0.5 EYO intervals. 22 out of 29 modules were significantly different in DS at any EYO. Module changes were compared to standard amyloid, tau, and neurodegeneration (AT(N)) CSF AD biomarkers. Red indicates increased levels in DS and blue indicates decreased levels in DS. The vertical black line highlights EYO = 0 (age 50.2). Shaded EYO values on the x-axis indicate periods of lower confidence estimates. Periods of significant change and direction of change for each module and CSF ELISA measurement are provided in Supplementary Data 7. Empirical *p* values were computed within a Bayesian analysis framework. All tests were two-sided with a prespecified significance level of 0.01, corresponding to tail probabilities of 0.005 and 0.995. No multiple testing correction was applied.

https://doi.org/10.1038/s41467-025-61054-z

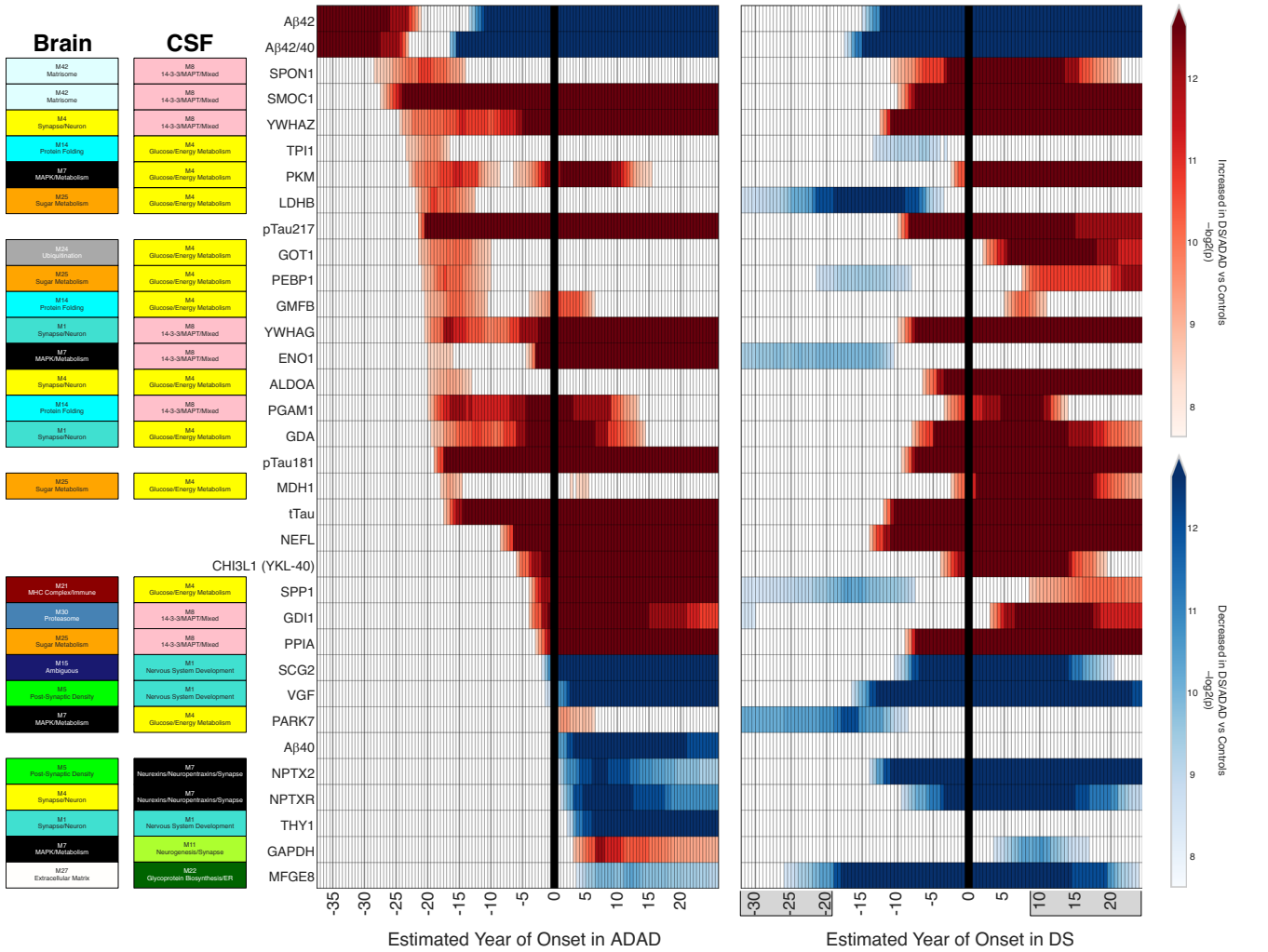

Fig. 5 | Comparison of individual protein measures between DS and ADAD. Protein level differences between ADAD mutation carriers and non-carriers as described in ref. 21 (left) and DS and euploid individuals (right) were modeled in the same fashion across EYO. Red indicates increased levels in ADAD and DS and blue indicates decreased levels in ADAD and DS. The vertical black line highlights EYO = 0. Shaded EYO values on the x-axis in DS indicate periods of lower confidence estimates. Each protein was mapped to its corresponding brain co-expression network module as described in ref. 17 and DSAD CSF co-expression network module as shown in Fig. 3A. Colors for each module correspond to module numbers in each network (for example, M4 is yellow). Biomarker measurements that do not map to a module were measured using immunoassays. The progression of protein changes in DS were not the same as in ADAD. Empirical *p* values were computed within a Bayesian analysis framework. All tests were two-sided with a prespecified significance level of 0.01, corresponding to tail probabilities of 0.005 and 0.995. No multiple testing correction was applied. ALDOA fructose-bisphosphate aldolase A, CHI3L1 chitinase-3-like protein 1, ENO1 alpha-enolase, GAPDH glyceraldehyde-3-phosphate dehydrogenase, GDA guanine deaminase, GDI1 rab GDP dissociation inhibitor alpha, GMFB glia maturation factor beta, GOT1 aspartate aminotransferase, cytoplasmic, LDHB L-lactate dehydrogenase B chain, MDH1 malate dehydrogenase, cytoplasmic, MFGE8 lactadherin, NEFL neurofilament light polypeptide, NPTX2 neuronal pentraxin-2, NPTXR neuronal pentraxin receptor, PARK7 Parkinson disease protein 7, PEBP1 phosphatidylethanoamine-binding protein 1, PGAM1 phosphoglycerate mutase 1, PKM pyruvate kinase PKM, PPIA peptidyl-prolyl cis-trans isomerase A, SCG2 secretogranin-2, SMOC1 SPARC-related modular calcium-binding protein 1, SPON1 spondin-1, SPP1 osteopontin, THY1 thy-1 membrane glycoprotein, TPI1 triosephosphate isomerase, VGF neurosecretory protein VGF, YWHAG 14-3-3 protein gamma, YWHAZ 14-3-3 protein zeta/delta.

plasma proteins in DS CSF, perhaps suggesting loss of blood–brain barrier (BBB) integrity, and early evidence of CAA suggest that cerebrovascular dysfunction is an important early pathological change in DS. Moreover, DSAD was associated with earlier decreases in synaptic proteins, neurofilament light, and MFGE8—a proposed protein marker of CAA—than ADAD, and more prominent changes in ECM, plaque-associated, myelin-associated, and PV+ inhibitory neuron-associated proteins than LOAD. These findings indicate that although many pathway alterations are shared between DSAD, ADAD, and LOAD, DSAD has unique features compared to other forms of AD.

One of the key findings from our study is the clear elevation of individual proteins and protein modules related to the ECM in the CSF of individuals with DS. The M5 Collagen and M18 Extracellular Matrix modules showed increased levels prior to decreases in Aβ. These ECM changes may be related to trisomy 21 but could also be risk factors for DSAD or DSAD-associated complications. These closely related modules contained the two matrix metalloproteinases measured in our dataset—MMP2 and MMP14. MMP activity has been implicated in loss of arteriole integrity and consequent cerebral microhemorrhage[30–32]. Interestingly, metalloproteinase inhibitors 1 and 2 (TIMP1 and TIMP2) were also present in these modules. Elevated levels of TIMPs have been found to be increased in the leptomeningeal arteries in CAA[32]. Although atherosclerotic and arteriosclerotic vascular pathologies are uncommon in individuals with DS, CAA is more frequent in DS than in sporadic LOAD, likely due in part to APP overexpression and

https://doi.org/10.1038/s41467-025-61054-z

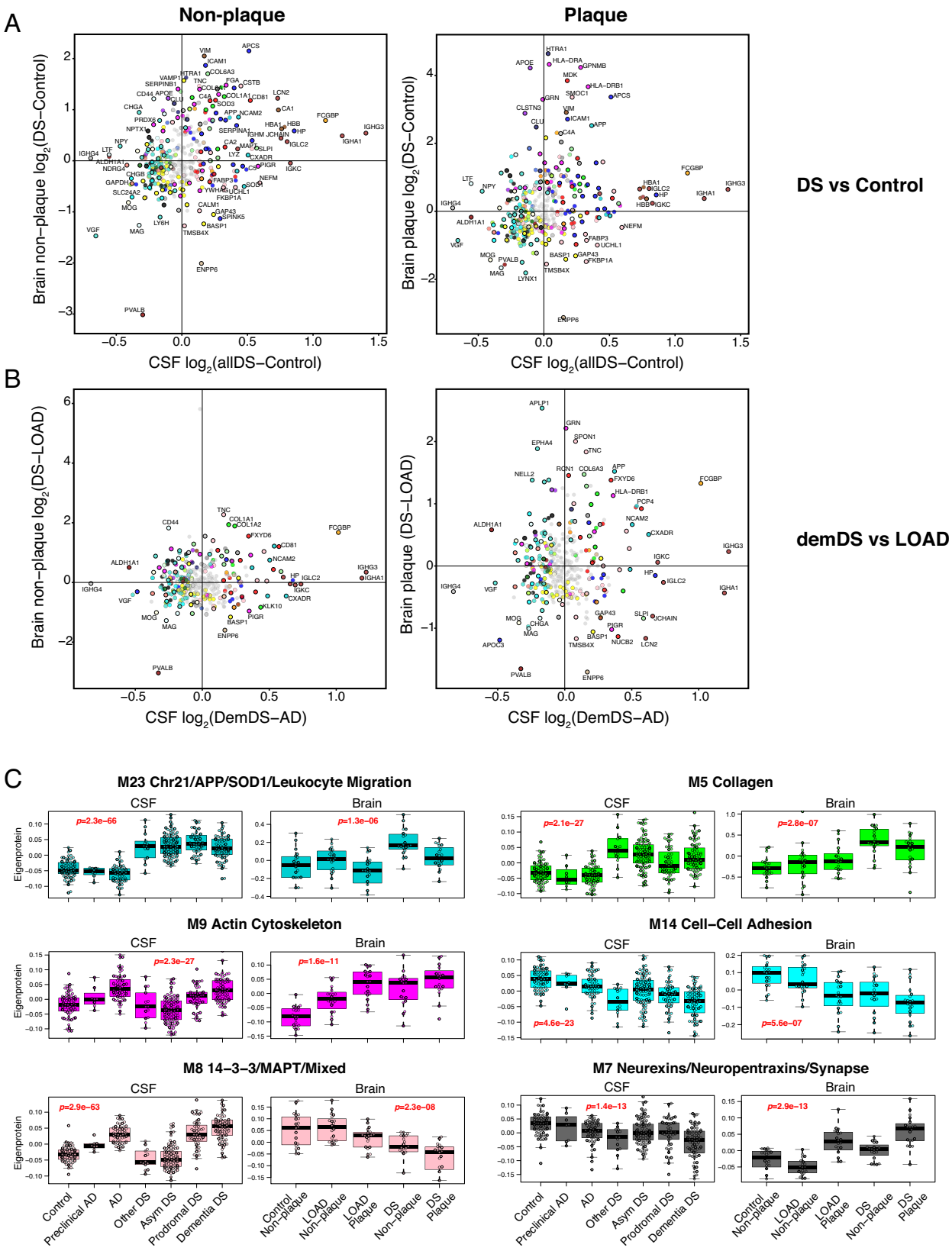

associated Aβ accumulation in blood vessels[33]. Neuropathological studies have identified CAA in individuals with DS as early as age 42, with severity increasing with age[34,35]. Furthermore, we observed a striking decrease in levels of MFGE8 in DS CSF, more prominently than observed in ADAD. One of the protein cleavage products of MFGE8—the medin fragment—accumulates in the smooth muscle of arterioles and catalyzes the aggregation of Aβ and subsequent development of CAA. Whether medin deposition is a principal driver of CAA in DS is currently unclear, as APP duplication itself can cause ADAD with prominent CAA[36].

In addition to increased levels of APP and Aβ production caused by trisomy 21, other proteins on chromosome 21 may also be involved

Fig. 6 | Comparison of CSF and Brain Proteomic Changes in DS and LOAD. CSF proteomic data were compared to localized brain proteomic data from Aβ plaque and non-plaque tissue in DS and LOAD[28]. **A** CSF proteomic changes in all participants with DS (allDS) compared to control versus DS non-plaque tissue (left) and DS plaques (right) compared to control. **B** CSF proteomic changes in participants with dementia due to DSAD compared to LOAD versus DS non-plaque tissue (left) and DS plaques (right) compared to LOAD. Proteins that were significantly different in either CSF or brain at FDR <0.05 in each contrast are colored by the CSF network module in which they reside. (**C**) CSF network module eigenproteins were tested for differences in DS and LOAD brain tissue in both plaque and non-plaque regions (control $n = 72$, preclinical AD $n = 8$, AD $n = 56$, other DS $n = 14$, Asym DS $n = 96$, prodromal DS $n = 47$, dementia DS $n = 72$; $n = 20$ for each brain group). Differences in module eigenprotein by case status were assessed by Kruskal-Wallis one-way ANOVA. Boxplots represent the median, 25th, and 75th percentile extremes; thus, hinges of a box represent the interquartile range of the two middle quartiles of data within a group. The farthest data points up to 1.5 times the interquartile range away from box hinges define the extent of whiskers (error bars). Plots for other CSF network modules are provided in the Supplementary Information.

in causing cerebrovascular dysfunction. The collagens COL6A1, COL6A2, and COL18A1 located on chromosome 21, were found to be elevated in the CSF of individuals with DS, and other collagens such as COL6A1 and COL1A1 were also noted to be elevated in DS brain tissue compared to controls and LOAD[28]. Increased levels of COL6A2 have been observed in vessels affected by CAA[37]. Other proteins that can form amyloids, such as serum amyloid P-component (APCS), which has also been observed in vessels affected by CAA[37], were found to be elevated early in DS, well before changes in Aβ levels. APCS mapped to the M2 Plasma Protein module that was elevated in DS, suggesting the abnormal presence of plasma proteins in DS CSF. Other classes of proteins elevated in the CSF of individuals with DS that may indicate leakage across the BBB included complement and immunoglobulins. As mentioned, alterations in proteins and protein modules related to the ECM reflect the importance of considering trisomy-related (constitutive of the syndrome) and DSAD-related (associated with the AD process) changes. While the two might be differentiated, the two can also interact to converge in a specific phenotype, in this case CAA, that might have relevant implications for anti-Aβ immunotherapy administration, such as potential increased risk of amyloid-related imaging abnormality (ARIA) side effects[38].

Interestingly, M16 cell-substrate adhesion and M14 cell-cell adhesion modules were decreased early in DS, perhaps in part reflecting vascular endothelial dysfunction. Loss of BBB integrity may lead to leakage of plasma proteins such as fibrinogen into the brain parenchyma in DS[28,39]. Brain deposition of fibrinogen and its cleavage product fibrin is a pathological feature of loss of BBB integrity in multiple sclerosis and has been shown to promote neuroinflammation, loss of myelin integrity, and neurodegeneration[40,41]. Other plasma proteins, such as hemoglobin, that are released into the brain parenchyma in DS may also lead to progressive neurodegeneration. Notably, some of the trisomy-related modules were not strongly correlated to AD phenotypes but could function as risk factors for the development of AD-related cognitive impairment or for specific phenotypes such as CAA. Additional mechanistic studies and potential therapeutic trials targeting ECM proteins in DS are required to further test this hypothesis and determine their relevance for disease onset and effect on therapeutic strategies.

When examining the standard amyloid, tau, and neurodegeneration (AT(N)) CSF biomarkers for AD, NEFL emerged as the first marker to exhibit alterations following reductions in Aβ levels among individuals with DS. Elevations in NEFL and tTau occurred before elevation in pTau181 and pTau217, in contrast to what is observed in LOAD, but consistent with previous results in DSAD[5]. Increases in NEFL and tTau occurred relatively earlier in DS compared to ADAD in the DIAN cohort. In the large Colombian kindred of *PSEN1* mutation carriers, plasma NEFL levels were found to be different from those of non-carriers 22 years before symptom onset[42] with a similar relative temporal change to other core AD biomarkers compared to DS. The matrix (plasma *versus* CSF), cohort size, and specific ADAD mutations may affect direct comparisons for a given protein between DSAD and ADAD. NEFL has been shown to be associated with axonal and myelin integrity in both DSAD and ADAD[23–25], and although it is not an AD-specific marker for neurodegeneration, both CSF and plasma concentrations of NEFL have shown outstanding diagnostic and prognostic performance for symptomatic DSAD with yearly augmented rates of change evident along the AD continuum[43]. White matter pathology is a key feature of DS[25,44–46] and may be a predisposing factor for the development of DSAD. We observed decreased levels of the myelin markers MAG and MOG in DS brain and CSF compared to LOAD brain and CSF, and both markers were decreased in DS CSF compared to controls at least 20 years before estimated symptom onset. Individuals with DS may have increased susceptibility to myelin pathology, given that abnormalities and delays in myelination can be observed from birth[47]. Changes in MAG and MOG occurred after the earliest changes reflected in DS Chr21, ECM, complement, and immunoglobulin modules, but before changes in NEFL, pTau, and tau levels. It is therefore possible that the earlier elevations in NEFL levels in DSAD may be attributed to pronounced ECM and other early pathologies leading to dysfunction in myelination and subsequent axonal loss.

Previous studies have indicated no disparities in NEFL, tTau, or pTau levels among DS individuals when stratified by *APOE* genotype[48,49] or sex[50,51], two common risk factors for LOAD[52,53]. In our study, we also did not observe differences in these biomarkers by *APOE* genotype or sex; however, we identified other proteins different in DS and influenced by *APOE* ε4 (18), ε2 (6), and sex (79). The effects of *APOE* on the proteins assessed in this study were weak and transient within the EYO window of highest confidence, suggesting that *APOE* does not have a strong effect in DSAD. More proteins were affected by sex. The strongest differences in males were observed in proteins such as complement C1s subcomponent (C1S), versican core protein (VCAN) and the M16 Cell-Substrate Adhesion module involved in ECM interaction, APCS, and fibronectin (FN1), suggesting that males with DS may have more problems with the BBB than females. Conversely, females had higher levels of peptidyl-prolyl cis-trans isomerase A (PPIA, a marker of brain metabolism), phosphoglycerate kinase 1 (PGK1), ENO1, and GAPDH, similar to what is observed in LOAD CSF, suggesting females with DS may share more of a classical AD metabolic phenotype than males with DS. Because our DS cohort had slightly more males than females, in contrast to the DIAN cohort, which had slightly more females than males, this may be one reason why we observed a slight decrease in some metabolic markers compared to ADAD. Further study of sex differences surrounding the AD metabolic phenotype in DS and ADAD is needed.

Synaptic markers SCG2, VGF, and NPTX2 demonstrated markedly earlier relative changes in DS compared to ADAD. These markers have also been shown to change closer to the time of symptom onset in LOAD[15,54]. This observation suggests that pathologic processes leading to synaptic changes as reflected by these markers in ADAD and LOAD are occurring earlier in DSAD, yet are not proximately associated with AD-related cognitive decline. We observed changes in NPTX2 14 years prior to symptom onset in DSAD, consistent with a previous observation that NPTX2 levels in DS are not strongly associated with AD-related cognitive changes[55]. Other synaptic changes, as reflected in the M1 nervous system development and M11 neurogenesis and synapse modules, were more closely associated with AD-related cognitive decline, illustrating the complex evolution of neuronal and synaptic

changes in DSAD. Elevations in the M24 Immune Response module also occurred proximate to the onset of cognitive decline. Inflammation is widely recognized as a pivotal factor in AD pathogenesis; interestingly, individuals with DS have been shown to have abnormal immune systems compared to euploid individuals from birth, as well as unique neuroinflammatory responses compared to individuals with LOAD[56,57]. Individuals with DS have elevations in pro-inflammatory markers including tumor necrosis factor α (TNFα), vascular endothelial growth factor A (VEGF-A), monocyte chemoattractant protein 1 (MCP-1), interleukin-1 beta (IL-1β), interstitial collagenase (MMP1), stromelysin-1 (MMP3), interleukin-22 (IL-22), and c-reactive protein (CRP)[11,57,58]. An important finding in our study was the early elevation in CSF complement levels. Complement has been shown to be involved in synaptic pruning processes by microglia, a process that can go awry in models of AD prior to Aβ plaque formation[59,60]. Complement activation in the brain is also associated with Aβ and tau NFT deposition[61]. Given the genetic evidence for the complement pathway as a risk factor for LOAD[62,63], the combination of altered immune function, elevated CSF complement levels, and overproduction of Aβ may be a particularly important feature in the pathophysiology of DSAD.

Processes that were observed to change the latest in the disease course in DSAD were M20 Semaphorins/Lysosome, M26 Endosome/Lysosome, and M4 Glucose/Energy Metabolism. Multiple studies have identified various morphological and molecular abnormalities in the endo-lysosomal pathway in DS due to the causative role of APP triplication in endo-lysosomal dysfunction. Overproduction of the APP beta c-terminal fragment (β-CTF, also known as C99) causes dysfunctional endosomal recycling resulting in aberrant endosome accumulation in synapses[64], and potentially catalyzes the formation of Aβ plaques[65–67]. Although we observed late changes in endosomal proteins in CSF, enlargement of endosomes in DS brains is observed very early, preceding Aβ deposition[65,68]. Interestingly, while conventional confocal microscopy has revealed larger EEA1-positive endosomes, super-resolution and electron microscopy has indicated these endosomes are normal in size but clustered[69]. We did not measure most vacuolar protein sorting (VPS) and RAS-related protein Rab (rab) proteins involved in the endosome recycling pathway, and further proteomic characterization of these proteins in DS CSF is needed. We did observe a decrease in the M13 Golgi/glycosylation module in DS, which, along with the M23 chromosome 21 module, were the earliest changes noted in the DS network. Because endosomes can be trafficked through the trans-Golgi network[70], this early change may represent pathological changes in endosome recycling.

We noted a decrease in CSF PVALB levels 15 years before symptom onset—approximately the time of increases in NEFL—and PVALB was also the most decreased protein measured in non-plaque DS brain tissue compared to control and LOAD. IHC for PVALB showed decreased levels in older individuals with DS, consistent with previous findings[71]. PVALB is a marker of a class of fast-spiking inhibitory interneurons critical to the generation of gamma frequencies in the brain[29], and loss of PV+ interneuron function has been associated with cognitive impairment and abnormal excitatory network activity[72,73]. Studies in animal models and clinical trials of the anti-epileptic medication levetiracetam have shown promise in LOAD[74–76], and this medication may be particularly helpful in DSAD given the prevalence of epileptiform activity in DS. Other therapeutic strategies to target PV+ interneuron function, such as gamma entrainment, that are being tested in LOAD may also be a promising therapeutic strategy in DSAD, given our findings[77,78]. CSF PVALB could serve as a biomarker of target engagement and efficacy in DSAD clinical trials targeting this pathophysiology.

Our study has some limitations. There were few controls at younger ages in our cohort, leading to large uncertainty in the protein level estimates between DS and controls at younger ages. For instance, we did not observe expected elevated levels of Aβ42 in younger DS CSF as we have previously observed in ADAD CSF[21], and as others have observed in DS CSF[79], likely due to lack of power at earlier EYO. Future studies that include a larger number of young control and DS CSF samples will help to reduce this uncertainty. No other cohorts with sufficient CSF samples across the age range were available for longitudinal analysis, but analysis of such cohorts once they become available will be important for validation of our findings. Our proteomic depth was partly limited by the exclusion of proteins with higher levels of missing values. Future studies that incorporate multiple proteomic platforms and methods of measurement can help to increase the depth of coverage while minimizing missing values, as well as provide additional validation beyond the TMT to SRM MS validation performed in this study. Finally, analysis of even larger DS cohorts could provide more statistical power to develop a fourth model to incorporate the main and interaction effects of both sex and *APOE* genotype in relation to EYO.

In summary, the results from this study illustrate the multiple pathological alterations in DS that evolve over many years prior to AD onset and related cognitive decline. The early pathological alterations in immune function, blood–brain barrier, myelin, and inhibitory interneurons associated with trisomy 21 may contribute to the onset of AD pathology in DS. While many pathological alterations are shared among DSAD, ADAD, and LOAD, the temporal ordering of these changes in DS exhibits several unique features that may have important implications for therapeutic strategies in this population.

Methods

Study design and participants

We conducted a study at Hospital de Sant Pau in Barcelona, Spain, on adults with Down syndrome (DS) across the AD continuum. Our participants were enrolled through a population-based healthcare program that involves annual neurological and neuropsychological evaluations. Those who expressed interest in research were included in the Down Alzheimer Barcelona Neuroimaging Initiative (DABNI) cohort. We administered a semi-structured adapted health questionnaire, the Cambridge Examination for Mental Disorders of Older People with Down syndrome and other Intellectual Disabilities (CAMDEX-DS), to caregivers. This assessment tool was originally developed in Cambridge and has been adapted for use in Spanish. Information was gathered through family interviews and the review of medical or educational records containing past assessment results. To classify participants with DS along the AD continuum, we conducted consensus meetings involving neurologists/psychiatrists and neuropsychologists, who assessed participants blindly to biomarker data, as described previously, to classify individuals in asymptomatic (asymDS), those with prodromal AD (proDS) and AD dementia (demDS)[5]. We also had a subset of DS participants with cognitive impairment not due to AD (oDS) but rather from other non-degenerative causes such as psychiatric disease. Euploid participants underwent a structured neurological assessment along with a comprehensive neuropsychological battery. Genetic screening for trisomy 21 was conducted in adults with Down syndrome, and *APOE* ε4 carrier status was determined following previously published protocols[80]. Additionally, we recruited control participants without Down syndrome and individuals with sporadic preclinical AD or AD dementia from the Sant Pau Initiative on Neurodegeneration (SPIN) cohort[80]. SPIN participants underwent a structured neurological assessment and a comprehensive neuropsychological battery, brain imaging, and lumbar puncture for AD biomarkers. Controls had normal neuropsychological results for their age and education, a clinical dementia rating scale score of 0 and normal levels of core AD biomarkers in CSF[81]. Those with preclinical AD were cognitively unimpaired but had positive CSF AD biomarkers, and those with AD were cognitively impaired with positive CSF AD biomarkers. Recruitment took place between November 2008 and May 2022. For brain proteomic analyses,

postmortem formalin-fixed and paraffin-embedded (FFPE) brain tissues from DS, LOAD, and cognitively normal age-matched controls were obtained from the National Institutes of Health NeuroBioBank (Maryland and Mt. Sinai brain banks), UK Brain Bank Network (South West Dementia brain bank), IDIBAPS Biobank from Barcelona, University of Pennsylvania, and NYU Grossman School of Medicine, including autopsy tissues from NYU Alzheimer's Disease Research Center (ADRC), Center for Biospecimen Research and Development (CBRD)/Department of Pathology, and the North American SUDEP Registry (NASR) at NYU Comprehensive Epilepsy Center (CEC). Control cases ($n = 20$) were age 66 ± 13 (SD) at time of death, sex-balanced, and ≤A1, B1, and C1 on ABC AD neuropathology staging. LOAD and DS cases were matched by pathology. LOAD cases ($n = 20$) were age 82 ± 6, sex-balanced, and A3, B3, and C3 or Braak VI. DS cases were age 60 ± 5, 7 F/13 M, and equivalent to A3, B3, and C3 score or Braak V-VI. FFPE tissue blocks containing hippocampus and surrounding entorhinal and temporal cortex from $n = 20$ cases per group were used for laser-capture microdissection (LCM) and proteomic analysis. Detailed information on the LCM proteomics cohort is provided in ref. 28. For IHC, a subset of FFPE brain tissues containing the superior frontal gyrus (Brodmann area 8) from control, DS, and LOAD ($n = 6$ per group) was used for parvalbumin staining. IHC tissue samples were sourced from the same brain banks as the proteomics cohort, except IDIBAPS and the University of Pennsylvania. Data on ADAD were taken from a prior study in the Dominantly Inherited Alzheimer Network (DIAN) as described in Johnson et al[21]. Briefly, individuals at 50% risk of carrying an autosomal-dominant Alzheimer's disease mutation in one of three genes (*APP, PSEN1, PSEN2*) were enrolled in the DIAN observational study (i.e., mutation carriers and non-carriers from the same family). DIAN participants are assessed at baseline and at subsequent follow-up visits that occur every one to three years. Assessments include collection of body fluids (CSF, blood), clinical testing (CDR), neuropsychological testing, and imaging modalities (MRI, PET with Pittsburgh Compound B (PiB-PET), and 18F-FDG) as previously described[82–86]. Data on ADAD included a total of 230 controls (mutation non-carriers) and 355 mutation carriers across preclinical and clinical disease stages.

Ethics

All procedures in this study were approved by the Sant Pau Ethics Committee (IIBSP-NGF-2018-36 and IIBSP-DOW-2014-30), following the standards for medical research in humans recommended by the Declaration of Helsinki. All participants or their legally authorized representative gave written informed consent before enrollment. We included all adults with Down syndrome that had CSF samples available. The DIAN study is supervised by the Institutional Review Board at Washington University in St. Louis, USA, and all study procedures were approved by the Human Research Protection Office and the Institutional Review Board at Washington University or the respective participating sites.

Sample collection and measurement of CSF Alzheimer´s disease biomarkers

Briefly, CSF samples were collected in 10 mL polypropylene tubes (Sarstedt, #62.610.018), centrifuged, aliquoted and stored at −80 °C within 2 h[81]. CSF measures of Aβ1-40, Aβ1–42, pTau181, and tTau were obtained on the automated Lumipulse G600II platform (Fujirebio) as previously described[87]. NfL was measured using the ultrasensitive equipment Simoa SR-X (Quanterix, Billerica, MA, USA) using commercially available kits (NF-light, Quanterix)[43]. CSF pTau181[88] and pTau231 were measured by in-house Simoa assays at the University of Gothenburg[89]. CSF pTau217 levels were analyzed with the commercial ALZpath pTau217 assay for Simoa HD-X, as previously described[90]. CSF YLK-40 levels were measured by YKL-40 human chitinase-3-like 1 immunoassay, DC3L10, R&D Systems, USA (ELISA) using a dilution of 1:100 and by YKL-40 MicroVue, Quidel, San Diego (USA).

CSF digestion and tandem mass Tag (TMT) peptide labeling

Samples of 50 μl CSF were reduced and alkylated. Thirteen μl of 24.2 mM TCEP in 5% sodium deoxycholate (DOC), 0.5 M triethylammonium bicarbonate (TEAB) was added to each sample, followed by incubation for 1 h at 55 °C. Next, 3.2 μl of fresh 400 mM iodoacetamide solution was added to the samples and incubated for 30 min at room temperature in the dark. Samples were digested by adding 2.6 μg of trypsin (Promega Sequencing grade modified trypsin Ref V5115) and incubated overnight at 37 °C in an oven. The next day, samples were labeled using TMT 16-plex Label Reagent (Thermo Fisher, Ref#: A44520; Lot#: XB341490)/TMT pro-134C, TMT pro-135N (Thermo Fisher, Ref: #A52046; Lot: #XA338615). The TMT reagents were equilibrated to room temperature before 10 μl was added to each sample, and then incubated for 1 h at room temperature while shaking. The labeling process was quenched by adding 6 μl 5% v/v hydroxylamine solution (50% hydroxylamine is diluted 1:10 with H2O) and incubating for 30 min. All samples were mixed in a 15-ml Falcon tube and acidified by adding 168.5 μl (10% of the vol.) of 0.5 M HCl, and subsequently, 4.15 mL 0.1% TFA was added to reduce the ACN to <3%. Samples were then further acidified to precipitate DOC, which was then removed by centrifugation at 4000×*g* for 15 min at 4 °C. The supernatant was desalted by solid-phase extraction (Waters Sep-Pak C18, WAT023501). The column was washed twice with 1 ml 0.1% TFA in 80% acetonitrile and equilibrated with 2 ml 0.1% TFA. The sample was then applied to the column, washed twice with 1 ml 0.1% TFA, and eluted with 1 ml 0.1% TFA in 80% acetonitrile. The collected eluate was split into four aliquots, lyophilized via vacuum centrifugation, before being stored at −80 °C until further use.

Off-line fractionation

The TMT-sets were fractionated by basic reversed-phase chromatography using a Dionex Ultimate 3000 UPLC system (Thermo Fischer Scientific) equipped with a reversed-phase XBridge BEH C18 column (3.5 μm, 3.0 × 150 mm, Waters Corporation). Peptides were eluted with a stepped gradient from 3 to 55% solvent B over 35 min, followed by an increase to 100% B at a flow of 400 μL/min. Solvent A was 10 mM ammonium formate at pH 10, and solvent B was 90% acetonitrile (ACN), 10% solvent A. The 36 primary fractions were combined to 12 final fractions which were evaporated and reconstituted in 3% ACN, 0.1% trifluoroacetic acid for LC-MS analysis.

LC-MS analysis

The fractions were analyzed on an Orbitrap Fusion Lumos Tribrid mass spectrometer equipped with a FAIMS-Pro ion mobility system and interfaced with an Easy-nLC1200 liquid chromatography system (all Thermo Fisher Scientific). Peptides were trapped on an Acclaim Pepmap 100 C18 trap column (100 μm × 2 cm, particle size 5 μm, Thermo Fisher Scientific) and separated on an in-house packed analytical column (38 cm × 75 μm, particle size 3 μm, Reprosil-Pur C18, Dr. Maisch) using a stepped gradient from 6 to 35% acetonitrile in 0.2% formic acid over 77 min at a flow of 300 nL/min. FAIMS-Pro was alternating between compensation voltages (CVs) of −50 and −70, with the same data-dependent settings for both CVs. The precursor ion mass spectra were acquired at a resolution of 120,000 and an m/z range of 375–1375. Using a cycle time of 1.5 s, the most abundant precursors with charges 2–7 were isolated with an m/z window of 0.7 and fragmented by collision-induced dissociation (CID) at 35%. Fragment spectra were recorded in the ion trap at a Rapid scan rate. The ten most abundant MS2 fragment ions were isolated using multi-notch isolation for further MS3 fractionation. MS3 fractionation was performed using higher-energy collision dissociation (HCD) at 55%, and the MS3 spectra were

recorded in the Orbitrap at 50,000 resolution and an m/z range of 100–500.

Proteomic data analysis

Data analysis was performed using Proteome Discoverer (Version 2.4, Thermo Fisher Scientific) and Mascot (Version 2.5.1) as a search engine. The data were matched against the swissprot *Homo sapiens* database (May 2022, 20,377 entries) allowing one missed cleavage. Precursor mass tolerance was set to 5 ppm, and fragment mass tolerance was set to 0.6 Da. Cysteine carbamidomethylation and TMTpro were set as fixed modifications, while methionine oxidation was set as a variable modification. Percolator was used for PSM validation at an FDR of 1%. TMTpro reporter ions peak integration was set to 3 mmu and only unique peptides were considered for protein quantification.

Protein abundance data processing

The Proteome Discoverer v2.4 results were exported as tab-separated values (TSV) using Proteome Discoverer v2.5. The raw TMT reporter ion counts from this file were loaded in Microsoft R Open v4.0.2, and human protein isoforms identified with medium confidence or better were kept. We used TAMPOR—a median polish batch correction method—to remove batch effects[91]. Only the global internal standard (GIS) sample in each batch was used for TAMPOR batch correction. The open-source TAMPOR R function is available from https://www.github.com/edammer/TAMPOR/. There were 1122 proteins output with less than 50% missing values across the 512 samples, including GIS. Samples were reduced to 365 first-draw CSF samples for 365 unique individuals analyzed by TMT-MS (Table 1). Sample connectivity outliers at least three standard deviations (SD) below the mean connectivity were checked using the WGCNA R package v1.69, both before and after reduction of sample count. Ten outliers were found before sample set reduction, and nine entirely different outliers were found after reduction to 365 first-measure samples. Therefore, no consistent outliers were identified or removed in the dataset. Quality control (QC) of batch correction using the variancePartition package in R identified a number of proteins that retained batch covariance, which may have been due to internal standard variations across batches, as the last batch GIS channel contained only ~50% of the GIS peptides of other batches' GIS TMT channel. Therefore, bootstrap regression for covariance specific to any of the 29 TMT batches was performed on $\log_2$(abundance) output of TAMPOR in R, protecting the diagnosis group in the regression model. After regression of batch effects, variancePartition demonstrated that nearly all proteins had variance explained by batch of less than 5 percent. Additional QC was performed using limma package-based MDS plotting to segregate samples using only blood marker protein quantification (blood markers used were HBA1/HBA2, HBB, HBG1, and HP); no separation of samples into high- or low-blood clusters was found, confirming consistent lumbar punctures had resulted in CSF free of variable blood contamination. After controlling for missingness less than 50% in the first 365 measure samples, 1116 protein isoforms across 365 samples with $\log_2$(abundance) in the QC-passed matrix were used for subsequent analyses. SRM data for selected proteins in the DS cohort were generated as previously described in the ADAD DIAN cohort, using the same peptides, transitions, and analysis software for measurement[21].

Bayesian modeling

Our analytical approach utilized a Bayesian generalized linear model (GLM) with an identity link function to assess the association between a particular measure and diagnoses over the estimated years to onset (EYO). In this phase of our analysis, we concentrated on 877 measures with less than 20% missing values across the cohort. These measures included ELISA assays for existing CSF biomarkers, proteins measured by TMT-MS, and CSF network module eigenproteins. We examined two diagnostic categories: individuals with DS and controls. The methodology used was similar to the one employed in our previous study on ADAD[21]. The Bayesian framework's core advantage is its capability in generating posterior distribution samples that replicate the population distribution of the measure at EYO. This enabled us to quantify the variation of the observed measure compared to the population distribution in both diagnostic groups. For the implementation of the Bayesian GLM, we employed the R package rstanarm, which leverages the Hamiltonian Monte Carlo (HMC) algorithm. HMC is an advanced and dependable Markov Chain Monte Carlo (MCMC) method that enhanced the robustness of our analysis[92].

Before delving into the details of our model, it's important to outline the technique utilized for capturing the non-linear relationships between the measures and EYO. We applied a restricted cubic spline transformation to EYO, setting knots at the 10th, 50th, and 90th percentiles, as depicted in **Formula 1**. This method breaks down EYO into its linear and cubic components, which guarantees a seamless and consistent model fit at each designated percentile. These components were then used to replace the original EYO for the Bayesian GLM fitting. The use of restricted cubic splines is not only substantiated by prior research validating its capability to model data non-linearities, but also through visual assessments that confirm its concordance with the actual observed data in this study[21,22].

The primary goal of our analysis was to examine the patterns of measures in individuals with DS compared to a control group, specifically looking at how the differences between these two diagnostic groups evolved over time. Model 1, which is detailed in **Formula 2**, was developed for this purpose. Within this model, we included several independent covariates with fixed effects: the diagnosis, a linear term for EYO, a cubic term for EYO, and interaction terms between the diagnosis and both the linear and cubic EYO terms. For the regression coefficients, we used the default weak informative normal priors with a mean of 0 and a variance parameter set to $2.5 \times \frac{S_y}{S_x}$, where S_y represents the standard deviation of the outcome measure and S_x represents the standard deviation of the independent covariate. Similarly, the intercept's prior was also the default prior that is a weak informative normal distribution with a mean of 0 and a variance parameter of $2.5 \times S_y$, promoting an approach that is more objective and data-driven[93]. The MCMC simulations were conducted by initializing eight chains across four cores. Each chain ran for 10,000 iterations, discarding the first 5000 as a warmup. To reduce the data, every tenth iteration post-warmup was selected. We ensured the reliability of the remaining 4000 post-warmup samples by rigorously monitoring the convergence of the parameters. Bayesian two-sided credible intervals for continuous outcomes were estimated for both the DS group and the control group, as well as for the differences between these groups, at increments of 0.5 EYO units ranging from −32 to 24. Additionally, we computed the empirical p value to evaluate the likelihood of an observed difference under the null hypothesis, $H_{M1,0}$, where M1 stands for Model 1.

A secondary objective of our study was to assess whether *APOE* genotype and sex—both important risk factors for AD—influenced these measures. For coding purposes in this study, individuals having one or two copies of the *APOE* ε4 allele were considered *APOE* ε4 carriers, individuals having one or two copies of the *APOE* ε2 allele were considered *APOE* ε2 carriers, and those without any *APOE* ε4 or ε2 alleles were defined as non-carriers for the respective ε4 or ε2 analysis.

In Model 2, which builds upon Model 1, we introduced the main effect of *APOE* ε4 or ε2 status along with its interaction with both the linear and cubic EYO terms. These additional terms are detailed in **Formula 3**. Three hypotheses were tested under this model. The first null hypothesis, $H_{M2.1,0}$, examined whether there was a significant amount of evidence to support that significant differences exist between DS individuals and controls by EYO, accounting for the main and interaction effects of *APOE* ε4 or ε2 status over time. The second null hypothesis, $H_{M2.2,0}$, evaluated whether there was significant

evidence of differences between *APOE* ε4 carriers and non-carriers or between *APOE* ε2 carriers and non-carriers across EYO. The analyses for ε4 and ε2 status were conducted separately, each accounting for the main and interaction effects of diagnosis over time. The final hypothesis, $H_{M2.3,0}$, assessed whether there was a significant amount evidence to support the difference between the control group—who are also *APOE* ε4 or ε2 non-carriers—and the DS individuals who are also *APOE* ε4 or ε2 carriers.

The methodology for Model 3 was the same as that of Model 2, which was also built upon Model 1 but with sex replacing *APOE* status (**Formula 4**). In Model 3, females were set as the reference group, analogous to *APOE* ε4 or ε2 non-carriers in Model 2. The interpretation of Model 3 and its hypothesis also mirrors that of Model 2.

Formula 1:

$$\text{splinefit} = \text{rcspline.eval(EYO, nk = 3, norm = 2, pc = FALSE, inclx = TRUE)} \quad (1)$$

Formula 2:

$$\begin{aligned}\text{Model1}: \text{Measure} = {} & \alpha + \beta_1 \times EYO_{\text{Linear}} + \beta_2 \times EYO_{\text{Cubic}} + \gamma \times \text{Diagnose} \\ & + \delta_1 \times \text{Diagnose} \times EYO_{\text{Linear}} + \delta_2 \times \text{Diagnose} \times EYO_{\text{Cubic}}\end{aligned} \quad (2)$$

Nul hypothesis, H_0, in Model 1 (M1):

$$H_{M1,0}: \delta_1 = \delta_2 = \gamma \quad (3)$$

Formula 3:

$$\begin{aligned}\text{Model2}: \text{Measure} = {} & \alpha + \beta_1 \times EYO_{\text{Linear}} + \beta_2 \times EYO_{\text{Cubic}} + \gamma \times \text{Diagnose} \\ & + \phi \times \text{ApoE} + \delta_1 \times \text{Diagnose} \times EYO_{\text{Linear}} + \delta_2 \\ & \times \text{Diagnose} \times EYO_{\text{Cubic}} + \delta_3 \times \text{ApoE} \times EYO_{\text{Linear}} + \delta_4 \\ & \times \text{ApoE} \times EYO_{\text{Cubic}}\end{aligned} \quad (4)$$

Null hypothesis, H_0, in Model 2 (M2):

$$H_{M2.1,0}: \delta_1 = \delta_2 = \gamma \quad (5)$$

$$H_{M2.2,0}: \delta_3 = \delta_4 = \phi \quad (6)$$

$$H_{M2.3,0}: \delta_1 = \delta_2 = \gamma = \delta_3 = \delta_4 = \phi \quad (7)$$

Formula 4:

$$\begin{aligned}\text{Model3}: \text{Measure} = {} & \alpha + \beta_1 \times EYO_{\text{Linear}} + \beta_2 \times EYO_{\text{Cubic}} + \gamma \times \text{Diagnose} \\ & + \phi \times \text{Sex} + \delta_1 \times \text{Diagnose} \times \text{EYO}_{\text{Linear}} + \delta_2 \\ & \times \text{Diagnose} \times \text{EYO}_{\text{Cubic}} + \delta_3 \times \text{Sex} \times \text{EYO}_{\text{Linear}} + \delta_4 \\ & \times \text{Sex} \times \text{EYO}_{\text{Cubic}}\end{aligned} \quad (8)$$

Null hypothesis, H_0, in Model 3 (M3):

$$H_{M3.1,0}: \delta_1 = \delta_2 = \gamma \quad (9)$$

$$H_{M3.2,0}: \delta_3 = \delta_4 = \phi \quad (10)$$

$$H_{M3.3,0}: \delta_1 = \delta_2 = \gamma = \delta_3 = \delta_4 = \phi \quad (11)$$

Differential expression analysis

Differential expression and plotting of results were performed using an in-house open-source set of R functions available via https://www.github.com/edammer/parANOVA/. For every protein in a pairwise comparison, a one-way ANOVA F statistic is calculated, and the probability that a larger *F* statistic would occur by chance is reported as *p*, which for a two-group comparison is equivalent to an unpaired two-tailed equal variance *t*-test *p* value. These *p* values were further corrected to FDR within each set of 1116 *p* values using p.adjust R function with the Benjamini–Hochberg method. Log_2 fold change, as the difference of $\log_2$(abundance) group means, is also provided with the statistics in Supplementary Data 5 for each of ten pairwise group comparisons. Volcano plots were generated using the parANOVA source function plotVolc().

Protein co-expression network analysis

The 1116 protein × 365 participant $\log_2$(abundance) matrix was tested for scale-free topology as evidenced by output of the pickSoftThreshold function in the WGCNA v1.69 package, which determined a power series over which a maximum R^2 is approached with diminishing slope or rate of increase in R^2 (y) versus power (x). The power occurring in the range of diminished slope has lowered sample connectivity and represents an adjacency matrix where spurious correlations (e.g., due to noise) are minimized. Based on the output of this function, a scale-free power of 9 was chosen, at which median connectivity was 13.5 and R^2 equaled 0.89. The blockwiseModules function was employed with this power to cluster modules according to a dissimilarity metric derived from the square adjacency matrix of 1116 × 1116 pairwise correlations calculated using midweight bicorrelation. Parameters used were deepSplit = 4; minModuleSize = 4; mergeCutHeight = 0.07; TOMDenom = "mean"; networkType = "signed"; pamStage = TRUE; pamRespectsDendro = TRUE; reassignThreshold = 0.05, and a maxBlockSize greater than 1116, ensuring a single dendrogram calculation in one block.

Following initial module assignment of the 1116 proteins, resulting in 29 modules, a kME table was calculated, assigning every protein in the network a bicor correlation to each of the module eigenproteins, which were in turn calculated as the first principal component of variance of all proteins assigned to that module. An iterative post hoc kME table cleanup algorithm was employed whereby proteins with module assignments inconsistent with a minimum intramodular kME (>0.30), or having a higher kME to a module eigenprotein for a module to which they are not assigned, respectively, result in demotion to gray (proteins not in a module) or conditional reassignment to the module with which the protein is best correlated (highest kME), as previously described[17]. The condition for reassignment required that the difference in kME_{max} and $\text{kME}_{\text{intramodule}}$ as assigned in any iteration of the algorithm be greater than 0.10. The module reassignment proceeds iteratively until no more exceptions to the above rules are found, or a thirtieth iteration is reached. The final kME table after the *post hoc* cleanup procedure is provided in Supplementary Data 5.

Ontology enrichment

We used our open-source R function GOparallel (https://www.github.com/edammer/GOparallel/) to find ontologies (among those in the following six categories: [1] biological processes, [2] molecular functions, [3] cellular components, [4] wiki pathways, [5] reactome, or [6] the Broad M2 molecular signatures database) which were significantly enriched in co-expression module gene product lists. Briefly, this function leverages the R piano package to perform a one-tailed Fisher's exact test, which we modified to output signed *z* score for either enrichment or depletion, as well as *p* value and Benjamini–Hochberg FDR for the enrichment significance. Human protein ontology annotations were obtained from the Bader lab[94].

Cell type marker enrichment analyses

We used a previously published list of five brain cell type specific protein markers[17] to determine significant overlap of gene products in each module using an in-house open-source R function (available from https://github.com/edammer/CellTypeFET). The function geneListFET

calculates Fisher's exact p value for overlap with each established list, given the background of all gene products in the input (here, $N = 1122$ total proteins).

Synthetic eigenprotein analysis

We performed calculations of first principal components of template CSF network module hubs with minimum kME of 0.70 and minimum two hubs in brain laser-capture microdissection proteomics data as described in ref. 28, using $\log_2$(abundances). Using these parameters, the calculations were otherwise performed as previously reported[17] using the WGCNA moduleEigengenes function.

Immunohistochemistry

Formalin-fixed, paraffin-embedded tissue sections (8 μm) from the frontal cortex were collected on glass slides. Sections from each cohort were deparaffinized and rehydrated through a series of xylene and ethanol washes. Antigen retrieval was performed using a 7-min treatment with 88% formic acid, followed by heat-induced citrate buffer treatment (10 mM sodium citrate, 0.05% Tween-20, pH 6). Primary antibodies against parvalbumin (1:150, Thermo Scientific, cat. PA5-47693), MAP2 (1:200, BD Biosciences, cat. 556320), and Aβ (D54D2, 1:1000, Cell Signaling, cat. 8243S) were incubated overnight at 4 °C. Alexa Fluor 488, 568, and 647 (Thermo Scientific) secondary antibodies were used for detection. Whole slide scans were acquired at 10× magnification using a Leica Aperio Versa 8 microscope. Ten regions of interest from each case were analyzed in ImageJ 1.54 f. Images for the parvalbumin and MAP2 channels were converted to 8-bit, and a Median filter with a radius of 1 was applied. The "Enhance Contrast" function was applied with a pixel saturation of 0.1% and the "Normalize" option enabled. Thresholding for both channels was performed using the "Otsu" method. The MAP2 and parvalbumin areas were calculated using the "Analyze Particles" function, with a minimum particle size threshold of 50. Parvalbumin area was normalized to the MAP2 area, and the parvalbumin percentage area was used for statistical analysis.

Other statistics and graphic visualization

iGraph layouts of module member proteins organized by their intramodular kME (bicor, correlation to the first principal component of a module) were generated using the netOps buildIgraphs function (https://www.github.com/edammer/netOps/). Nodes are connected by the strongest correlation-based edges as calculated by topology overlap, which is a derived matrix after calculation of the bicor adjacency matrix in the WGCNA framework. The circular network module-trait correlation and enrichment significance heatmap was generated using statistics calculated by the WGCNA bicor function, one-way ANOVA for two groups, or a Fisher's exact test for enrichment of brain cell type markers in the gene product lists for each network module as described above. Visualization of the heatmap was performed using the R circlize package v0.4.10[95]. Scatterplots were plotted using the WGCNA verboseScatterplot function. Midweight bicorrelation rho and associated Student's p values were calculated using the WGCNA bicorAndPvalue function. The investigators were blinded during data acquisition but not outcome assessment.

Reporting summary

Further information on research design is available in the Nature Portfolio Reporting Summary linked to this article.

Data availability

The mass spectrometry proteomics data have been deposited in the ProteomeXchange Consortium with the dataset identifier PXD064699. Data output after batch correction and regression are available at https://www.synapse.org/DownSynAD. Extended Data, including plots of DS versus control for all significant proteins, proteins influenced by *APOE* ε4, *APOE* ε2, and sex, co-expression network plots, network module ontologies, and brain synthetic eigenproteins, are available at https://doi.org/10.6084/m9.figshare.29265053.

Code availability

Custom code is available at https://www.github.com/edammer.

References

1. Chen, L. et al. Global, regional, and national burden and trends of Down syndrome from 1990 to 2019. *Front. Genet.* **13**, 908482 (2022).
2. Hithersay, R. et al. Association of dementia with mortality among adults with Down syndrome older than 35 years. *JAMA Neurol.* **76**, 152–160 (2019).
3. McCarron, M. et al. A prospective 20-year longitudinal follow-up of dementia in persons with Down syndrome. *J. Intellect. Disabil. Res.* **61**, 843–852 (2017).
4. Iulita, M. F. et al. Association of Alzheimer disease with life expectancy in people with Down syndrome. *JAMA Netw. Open* **5**, e2212910 (2022).
5. Fortea, J. et al. Clinical and biomarker changes of Alzheimer's disease in adults with Down syndrome: a cross-sectional study. *Lancet* **395**, 1988–1997 (2020).
6. Fortea, J. et al. Alzheimer's disease associated with Down syndrome: a genetic form of dementia. *Lancet Neurol.* **20**, 930–942 (2021).
7. Glenner, G. G. & Wong, C. W. Alzheimer's disease and Down's syndrome: sharing of a unique cerebrovascular amyloid fibril protein. *Biochem. Biophys. Res. Commun.* **122**, 1131–1135 (1984).
8. Chartier-Harlin, M. C. et al. Early-onset Alzheimer's disease caused by mutations at codon 717 of the beta-amyloid precursor protein gene. *Nature* **353**, 844–846 (1991).
9. Goate, A. et al. Segregation of a missense mutation in the amyloid precursor protein gene with familial Alzheimer's disease. *Nature* **349**, 704–706 (1991).
10. Fagan, A. M. et al. Comparison of CSF biomarkers in Down syndrome and autosomal dominant Alzheimer's disease: a cross-sectional study. *Lancet Neurol.* **20**, 615–626 (2021).
11. Iulita, M. F. et al. An inflammatory and trophic disconnect biomarker profile revealed in Down syndrome plasma: relation to cognitive decline and longitudinal evaluation. *Alzheimers Dement.* **12**, 1132–1148 (2016).
12. Montoliu-Gaya, L., Strydom, A., Blennow, K., Zetterberg, H. & Ashton, N. J. Blood biomarkers for Alzheimer's disease in Down syndrome. *J. Clin. Med.* **10**, 3639 (2021).
13. de Gonzalo-Calvo, D. et al. Evaluation of biochemical and hematological parameters in adults with Down syndrome. *Sci. Rep.* **10**, 13755 (2020).
14. Dammer, E. B. et al. Multi-platform proteomic analysis of Alzheimer's disease cerebrospinal fluid and plasma reveals network biomarkers associated with proteostasis and the matrisome. *Alzheimers Res. Ther.* **14**, 174 (2022).
15. Haque, R. et al. A protein panel in cerebrospinal fluid for diagnostic and predictive assessment of Alzheimer's disease. *Sci. Transl. Med.* **15**, eadg4122 (2023).
16. Higginbotham, L. et al. Integrated proteomics reveals brain-based cerebrospinal fluid biomarkers in asymptomatic and symptomatic Alzheimer's disease. *Sci. Adv.* **6**, eaaz9360 (2020).
17. Johnson, E. C. B. et al. Large-scale deep multi-layer analysis of Alzheimer's disease brain reveals strong proteomic disease-related changes not observed at the RNA level. *Nat. Neurosci.* **25**, 213–225 (2022).
18. Johnson, E. C. B. et al. Large-scale proteomic analysis of Alzheimer's disease brain and cerebrospinal fluid reveals early changes in energy metabolism associated with microglia and astrocyte activation. *Nat. Med.* **26**, 769–780 (2020).

19. Zhou, M. et al. Targeted mass spectrometry to quantify brain-derived cerebrospinal fluid biomarkers in Alzheimer's disease. *Clin. Proteom.* **17**, 19 (2020).
20. Johnson, E. C. B. et al. Deep proteomic network analysis of Alzheimer's disease brain reveals alterations in RNA binding proteins and RNA splicing associated with disease. *Mol. Neurodegener.* **13**, 52 (2018).
21. Johnson, E. C. B. et al. Cerebrospinal fluid proteomics define the natural history of autosomal dominant Alzheimer's disease. *Nat. Med.* **29**, 1979–1988 (2023).
22. Preische, O. et al. Serum neurofilament dynamics predicts neurodegeneration and clinical progression in presymptomatic Alzheimer's disease. *Nat. Med.* **25**, 277–283 (2019).
23. Schultz, S. A. et al. Serum neurofilament light chain levels are associated with white matter integrity in autosomal dominant Alzheimer's disease. *Neurobiol. Dis.* **142**, 104960 (2020).
24. Rosas, H. D. et al. Association of plasma neurofilament light chain with microstructural white matter changes in Down syndrome. *Alzheimers Dement.* **16**, e70023 (2024).
25. Morcillo-Nieto, A. O. et al. Characterization of white matter hyperintensities in Down syndrome. *Alzheimers Dement.* **20**, 6527–6541 (2024).
26. Connolly, K. et al. Potential role of chitinase-3-like protein 1 (CHI3L1/YKL-40) in neurodegeneration and Alzheimer's disease. *Alzheimers Dement.* **19**, 9–24 (2023).
27. Marazuela, P. et al. MFG-E8 (LACTADHERIN): a novel marker associated with cerebral amyloid angiopathy. *Acta Neuropathol. Commun.* **9**, 154 (2021).
28. Marta-Ariza, M. et al. Comparison of the amyloid plaque proteome in Down syndrome, early-onset Alzheimer's disease, and late-onset Alzheimer's disease. *Acta Neuropathol.* **149**, 9 (2025).
29. Sohal, V. S., Zhang, F., Yizhar, O. & Deisseroth, K. Parvalbumin neurons and gamma rhythms enhance cortical circuit performance. *Nature* **459**, 698–702 (2009).
30. Duits, F. H. et al. Matrix metalloproteinases in Alzheimer's disease and concurrent cerebral microbleeds. *J. Alzheimer's. Dis.* **48**, 711–720 (2015).
31. Jakel, L. et al. Disturbed balance in the expression of MMP9 and TIMP3 in cerebral amyloid angiopathy-related intracerebral haemorrhage. *Acta Neuropathol. Commun.* **8**, 99 (2020).
32. Manousopoulou, A. et al. Systems proteomic analysis reveals that clusterin and tissue inhibitor of metalloproteinases 3 increase in leptomeningeal arteries affected by cerebral amyloid angiopathy. *Neuropathol. Appl. Neurobiol.* **43**, 492–504 (2017).
33. Carmona-Iragui, M., Videla, L., Lleo, A. & Fortea, J. Down syndrome, Alzheimer disease, and cerebral amyloid angiopathy: the complex triangle of brain amyloidosis. *Dev. Neurobiol.* **79**, 716–737 (2019).
34. Davidson, Y. S., Robinson, A., Prasher, V. P. & Mann, D. M. A. The age of onset and evolution of Braak tangle stage and Thal amyloid pathology of Alzheimer's disease in individuals with Down syndrome. *Acta Neuropathol. Commun.* **6**, 56 (2018).
35. Head, E. et al. Cerebrovascular pathology in Down syndrome and Alzheimer disease. *Acta Neuropathol. Commun.* **5**, 93 (2017).
36. Rovelet-Lecrux, A. et al. APP locus duplication causes autosomal dominant early-onset Alzheimer disease with cerebral amyloid angiopathy. *Nat. Genet.* **38**, 24–26 (2006).
37. Hondius, D. C. et al. Proteomics analysis identifies new markers associated with capillary cerebral amyloid angiopathy in Alzheimer's disease. *Acta Neuropathol. Commun.* **6**, 46 (2018).
38. Rafii, M. S. & Fortea, J. Down Syndrome in a new era for Alzheimer disease. *JAMA* **330**, 2157–2158 (2023).
39. Aguilar, L. F. & Head, E. 2. Cerebrovascular neuropathology in the brains of people with Down syndrome. *Alzheimer's. Dement.* **19**, e075657 (2023).
40. Alruwaili, M. et al. Pathogenic role of fibrinogen in the neuropathology of multiple sclerosis: a tale of sorrows and fears. *Neurochem. Res.* **48**, 3255–3269 (2023).
41. Davalos, D. et al. Fibrinogen-induced perivascular microglial clustering is required for the development of axonal damage in neuroinflammation. *Nat. Commun.* **3**, 1227 (2012).
42. Quiroz, Y. T. et al. Plasma neurofilament light chain in the presenilin 1 E280A autosomal dominant Alzheimer's disease kindred: a cross-sectional and longitudinal cohort study. *Lancet Neurol.* **19**, 513–521 (2020).
43. Carmona-Iragui, M. et al. Diagnostic and prognostic performance and longitudinal changes in plasma neurofilament light chain concentrations in adults with Down syndrome: a cohort study. *Lancet Neurol.* **20**, 605–614 (2021).
44. Powell, D. et al. Frontal white matter integrity in adults with Down syndrome with and without dementia. *Neurobiol. Aging* **35**, 1562–1569 (2014).
45. Bazydlo, A. et al. White matter microstructure associations with episodic memory in adults with Down syndrome: a tract-based spatial statistics study. *J. Neurodev. Disord.* **13**, 17 (2021).
46. Miyoshi, E. et al. Spatial and single-nucleus transcriptomic analysis of genetic and sporadic forms of Alzheimer's disease. *Nat. Genet.* **56**, 2704–2717 (2024).
47. Azrak, O. et al. Early white matter microstructure alterations in infants with Down syndrome. Preprint at *medRxiv* 2025.2002.2026.25322913 (2025).
48. Bejanin, A. et al. Association of apolipoprotein E varepsilon4 allele with clinical and multimodal biomarker changes of Alzheimer disease in adults with Down syndrome. *JAMA Neurol.* **78**, 937–947 (2021).
49. Boerwinkle, A. H. et al. Comparison of amyloid burden in individuals with Down syndrome versus autosomal dominant Alzheimer's disease: a cross-sectional study. *Lancet Neurol.* **22**, 55–65 (2023).
50. Lai, F. et al. Sex differences in risk of Alzheimer's disease in adults with Down syndrome. *Alzheimers Dement.* **12**, e12084 (2020).
51. Iulita, M. F. et al. Association of biological sex with clinical outcomes and biomarkers of Alzheimer's disease in adults with Down syndrome. *Brain Commun.* **5**, fcad074 (2023).
52. Beam, C. R. et al. Differences between women and men in incidence rates of dementia and Alzheimer's disease. *J. Alzheimer's. Dis.* **64**, 1077–1083 (2018).
53. Fortea, J. et al. APOE4 homozygosity represents a distinct genetic form of Alzheimer's disease. *Nat. Med.* **30**, 2093 (2024).
54. Nilsson, J. et al. Cerebrospinal fluid biomarker panel for synaptic dysfunction in a broad spectrum of neurodegenerative diseases. *Brain* **147**, 2414–2427 (2024).
55. Belbin, O. et al. Cerebrospinal fluid profile of NPTX2 supports role of Alzheimer's disease-related inhibitory circuit dysfunction in adults with Down syndrome. *Mol. Neurodegener.* **15**, 46 (2020).
56. Gansa, W. et al. Dysregulation of the immune system in a natural history study of 1299 individuals with Down syndrome. *J. Clin. Immunol.* **44**, 130 (2024).
57. Wilcock, D. M. et al. Down syndrome individuals with Alzheimer's disease have a distinct neuroinflammatory phenotype compared to sporadic Alzheimer's disease. *Neurobiol. Aging* **36**, 2468–2474 (2015).
58. Zhang, Y. et al. Aberrations in circulating inflammatory cytokine levels in patients with Down syndrome: a meta-analysis. *Oncotarget* **8**, 84489–84496 (2017).
59. Hong, S. et al. Complement and microglia mediate early synapse loss in Alzheimer mouse models. *Science* **352**, 712–716 (2016).
60. Shi, Q. et al. Complement C3 deficiency protects against neurodegeneration in aged plaque-rich APP/PS1 mice. *Sci. Transl. Med.* **9**, eaaf6295 (2017).

61. Batista, A. F., Khan, K. A., Papavergi, M. T. & Lemere, C. A. The importance of complement-mediated immune signaling in Alzheimer's disease pathogenesis. *Int. J. Mol. Sci.* **25**, 817 (2024).
62. Bellenguez, C. et al. New insights into the genetic etiology of Alzheimer's disease and related dementias. *Nat. Genet.* **54**, 412–436 (2022).
63. Karch, C. M. & Goate, A. M. Alzheimer's disease risk genes and mechanisms of disease pathogenesis. *Biol. Psychiatry* **77**, 43–51 (2015).
64. Ferrer-Raventós, P. et al. Amyloid precursor protein βCTF accumulates in synapses in sporadic and genetic forms of Alzheimer's disease. *Neuropathol. Appl. Neurobiol.* **49**, e12879 (2023).
65. Jiang, Y. et al. Alzheimer's-related endosome dysfunction in Down syndrome is Abeta-independent but requires APP and is reversed by BACE-1 inhibition. *Proc. Natl Acad. Sci. USA* **107**, 1630–1635 (2010).
66. Jiang, Y. et al. Partial BACE1 reduction in a Down syndrome mouse model blocks Alzheimer-related endosomal anomalies and cholinergic neurodegeneration: role of APP-CTF. *Neurobiol. Aging* **39**, 90–98 (2016).
67. Lee, J. H. et al. Faulty autolysosome acidification in Alzheimer's disease mouse models induces autophagic build-up of Abeta in neurons, yielding senile plaques. *Nat. Neurosci.* **25**, 688–701 (2022).
68. Cataldo, A. M. et al. Endocytic pathway abnormalities precede amyloid beta deposition in sporadic Alzheimer's disease and Down syndrome: differential effects of APOE genotype and presenilin mutations. *Am. J. Pathol.* **157**, 277–286 (2000).
69. Botte, A. et al. Ultrastructural and dynamic studies of the endosomal compartment in Down syndrome. *Acta Neuropathol. Commun.* **8**, 89 (2020).
70. Buser, D. P. & Spang, A. Protein sorting from endosomes to the TGN. *Front. Cell Dev. Biol.* **11**, 1140605 (2023).
71. Kobayashi, K. et al. Cerebral cortical calbindin D28K and parvalbumin neurones in Down's syndrome. *Neurosci. Lett.* **113**, 17–22 (1990).
72. Vossel, K. A. et al. Incidence and impact of subclinical epileptiform activity in Alzheimer's disease. *Ann. Neurol.* **80**, 858–870 (2016).
73. Verret, L. et al. Inhibitory interneuron deficit links altered network activity and cognitive dysfunction in Alzheimer model. *Cell* **149**, 708–721 (2012).
74. Sanchez, P. E. et al. Levetiracetam suppresses neuronal network dysfunction and reverses synaptic and cognitive deficits in an Alzheimer's disease model. *Proc. Natl Acad. Sci. USA* **109**, E2895–E2903 (2012).
75. Mohs, R. et al. The HOPE4MCI study: a randomized double-blind assessment of AGB101 for the treatment of MCI due to AD. *Alzheimers Dement.* **10**, e12446 (2024).
76. Bakker, A., Rani, N., Mohs, R. & Gallagher, M. The HOPE4MCI study: AGB101 treatment slows progression of entorhinal cortex atrophy in APOE epsilon4 non-carriers with mild cognitive impairment due to Alzheimer's disease. *Alzheimers Dement.* **10**, e70004 (2024).
77. Martorell, A. J. et al. Multi-sensory gamma stimulation ameliorates Alzheimer's-associated pathology and improves cognition. *Cell* **177**, 256–271 e222 (2019).
78. He, Q. et al. A feasibility trial of gamma sensory flicker for patients with prodromal Alzheimer's disease. *Alzheimers Dement.* **7**, e12178 (2021).
79. Englund, H. et al. Increase in beta-amyloid levels in cerebrospinal fluid of children with Down syndrome. *Dement. Geriatr. Cogn. Disord.* **24**, 369–374 (2007).
80. Alcolea, D. et al. The Sant Pau Initiative on Neurodegeneration (SPIN) cohort: a data set for biomarker discovery and validation in neurodegenerative disorders. *Alzheimers Dement.* **5**, 597–609 (2019).
81. Lleo, A. et al. Phosphorylated tau181 in plasma as a potential biomarker for Alzheimer's disease in adults with Down syndrome. *Nat. Commun.* **12**, 4304 (2021).
82. Bateman, R. J. et al. Clinical and biomarker changes in dominantly inherited Alzheimer's disease. *N. Engl. J. Med.* **367**, 795–804 (2012).
83. Gordon, B. A. et al. Spatial patterns of neuroimaging biomarker change in individuals from families with autosomal dominant Alzheimer's disease: a longitudinal study. *Lancet Neurol.* **17**, 241–250 (2018).
84. McKay, N. S. et al. Positron emission tomography and magnetic resonance imaging methods and datasets within the Dominantly Inherited Alzheimer Network (DIAN). *Nat. neurosci.* **26**, 1449–1460 (2023).
85. Morris, J. C. The clinical dementia rating (CDR): current version and scoring rules. *Neurology* **43**, 2412–2414 (1993).
86. Folstein, M. F., Folstein, S. E. & McHugh, P. R. Mini-mental state". A practical method for grading the cognitive state of patients for the clinician. *J. Psychiatr. Res.* **12**, 189–198 (1975).
87. Fortea, J. et al. Plasma and CSF biomarkers for the diagnosis of Alzheimer's disease in adults with Down syndrome: a cross-sectional study. *Lancet Neurol.* **17**, 860–869 (2018).
88. Karikari, T. K. et al. Blood phosphorylated tau 181 as a biomarker for Alzheimer's disease: a diagnostic performance and prediction modelling study using data from four prospective cohorts. *Lancet Neurol.* **19**, 422–433 (2020).
89. Ashton, N. J. et al. Plasma p-tau231: a new biomarker for incipient Alzheimer's disease pathology. *Acta Neuropathol.* **141**, 709–724 (2021).
90. Ashton, N. J. et al. Diagnostic accuracy of a plasma phosphorylated tau 217 immunoassay for Alzheimer disease pathology. *JAMA Neurol.* **81**, 255–263 (2024).
91. Dammer, E. B., Seyfried, N. T. & Johnson, E. C. B. Batch correction and harmonization of -omics datasets with a tunable median polish of ratio. *Front. Syst. Biol.* **3**, 1092341 (2023).
92. Muth, C., Oravecz, Z. & Gabry, J. User-friendly Bayesian regression modeling: a tutorial with rstanarm and shinystan. *Quant. Methods Psychol.* **14**, 99–119 (2018).
93. Gabry, J. & Goodrich, B. Prior distributions for rstanarm models. (2020).
94. Reimand, J. et al. Pathway enrichment analysis and visualization of omics data using g:profiler, GSEA, Cytoscape and EnrichmentMap. *Nat. Protoc.* **14**, 482–517 (2019).
95. Gu, Z., Gu, L., Eils, R., Schlesner, M. & Brors, B. circlize Implements and enhances circular visualization in R. *Bioinformatics* **30**, 2811–2812 (2014).

Acknowledgements

We thank all the participants and investigators involved in these consortia for their tireless efforts and invaluable contributions to the field. This study was supported by K08AG068604 and R01AG089497 (E.C.B.J.); the Goizueta Alzheimer's Disease Research Center (P30AG066511); the Jerome Lejeune Foundation (GRT-2023B – 2303), Åhlen-Stiftelsen (2021-203061) and Alzheimerfonden (AF-968621) (L.M.G.); the Fondo de Investigaciones Sanitario, Carlos III Health Institute INT21/00073, PI20/01473, and PI23/01786 (J.F.) and the Centro de Investigación Biomédica en Red sobre Enfermedades Neurodegenerativas Program 1, partly jointly funded by Fondo Europeo de Desarrollo Regional, Unión Europea, Una Manera de Hacer Europa; R01 AG056850, R21 AG056974, R01 AG061566, R01 AG081394, and R61AG066543 (J.F.), P30 AG066512 (T.W.), R01 AG087280 (T.W.), the Department de Salut de la Generalitat de Catalunya, Pla Estratègic de Recerca i Innovació en Salut (SLT006/17/00119) (J.F.), Fundación Tatiana Pérez de Guzmán el Bueno (IIBSP-DOW-2020-151) (J.F.), and Horizon 2020–Research and Innovation Framework Program from the European

Union (H2020-SC1-BHC-2018-2020) (J.F.). Proteomic analysis was performed at the Proteomics Core Facility, Sahlgrenska Academy, Gothenburg University, with financial support from SciLifeLab and BioMS.

Author contributions

L.M.-G., D.A., M.M.-A., T.W., H.Z., J.F., N.T.S., A.I.L., and E.C.B.J. designed the experiments; L.M.-G., M.S., J.L.-R., J.Fuchs, M.M.-A., T.W., C.M.W., L.P., and D.M.D. carried out experiments; S.B., E.B.D., M.M.-A., T.W., and E.C.B.J. analyzed data; N.J.A., O.B., J.N., I.B., L.V., K.B., B.B., B.R.R., M.C.-I., J.G., and A.L. provided advice on the interpretation of data and manuscript review; E.C.B.J., L.M.-G., M.M.-A., J.F., E.B.D., and S.B. wrote the manuscript with input from coauthors.

Competing interests

E.C.B.J. has served on an advisory board for Eli Lilly and has received royalties from EmTheraPro (outside submitted work). J.F. reported receiving personal fees for service on the advisory boards, adjudication committees or speaker honoraria from AC Immune, Adamed, Alzheon, Biogen, Eisai, Esteve, Fujirebio, Ionis, Laboratorios Carnot, Life Molecular Imaging, Lilly, Lundbeck, Perha, Roche and outside the submitted work. O.B., D.A., A.L., and J.F. report holding a patent for markers of synaptopathy in neurodegenerative disease (WO2019175379, applicant Fundació Institut de Recerca de L'hospital de la Santa Creu, Sant Pau, "Markers of synaptopathy in neurodegenerative diseases", EP19709749.6, priority date 16/3/2018, patent pending, inventors O Belbin, A Lleó, A Bayés, J Fortea, and D Alcolea, licensed to ADX NeuroSciences, N.V. EPI8382175.0 to develop antibodies and immunoassays for Calsyntenin-1, GluR2, GluR4, Neuroligin-2, neurexin-2a, neurexin-3a, syntaxin-1b, thy-1, tenascin-r, and vamp-2). N.T.S. and A.I.L. are founders of EmTheraPro (outside submitted work). H.Z. has served at scientific advisory boards and/or as a consultant for Abbvie, Acumen, Alector, Alzinova, ALZPath, Annexon, Apellis, Artery Therapeutics, AZTherapies, Cognito Therapeutics, CogRx, Denali, Eisai, Nervgen, Novo Nordisk, Optoceutics, Passage Bio, Pinteon Therapeutics, Prothena, Red Abbey Labs, reMYND, Roche, Samumed, Siemens Healthineers, Triplet Therapeutics, and Wave, has given lectures in symposia sponsored by Cellectricon, Fujirebio, Alzecure, Biogen, and Roche, and is a co-founder of Brain Biomarker Solutions in Gothenburg AB (BBS), which is a part of the GU Ventures Incubator Program (outside submitted work). K.B. has served as a consultant, on advisory boards, or at data monitoring committees for Abcam, Axon, BioArctic, Biogen, and JOMDD/Shimadzu. Julius Clinical, Lilly, MagQu, Novartis, Ono Pharma, Pharmatrophix, Prothena, Roche Diagnostics, and Siemens Healthineers, and is a co-founder of Brain Biomarker Solutions in Gothenburg AB (BBS), which is a part of the GU Ventures Incubator Program, outside the work presented in this paper. T.W. has served as a consultant or on data monitoring committees for Acumen, Biogen, Grifols, Lilly and ProMIS Neurosciences. The remaining authors declare no competing interests.

Additional information

Supplementary information The online version contains supplementary material available at https://doi.org/10.1038/s41467-025-61054-z.

Correspondence and requests for materials should be addressed to Juan Fortea or Erik C. B. Johnson.

Peer review information *Nature Communications* thanks the anonymous reviewers for their contribution to the peer review of this work. A peer review file is available.

Reprints and permissions information is available at http://www.nature.com/reprints

Publisher's note Springer Nature remains neutral with regard to jurisdictional claims in published maps and institutional affiliations.

Laia Montoliu-Gaya[1,18], Shijia Bian[2,18], Eric B. Dammer[3,4,18], Daniel Alcolea[5], Mathias Sauer[1], Mitchell Martá-Ariza[6,7,8], Nicholas J. Ashton[1], Olivia Belbin[5], Johannes Fuchs[9], Caroline M. Watson[4,10], Lingyan Ping[3,4,10], Duc M. Duong[3,4], Johanna Nilsson[1], Isabel Barroeta[5], Juan Lantero-Rodriguez[1], Laura Videla[5], Bessy Benejam[5], Blaine R. Roberts[3,4], Kaj Blennow[1,11], Nicholas T. Seyfried[3,4,10], Allan I. Levey[4,10], María Carmona-Iragui[5], Johan Gobom[1], Alberto Lleó[5], Thomas Wisniewski[6,7,12,13], Henrik Zetterberg[1,11,14,15,16,17], Juan Fortea[5,19] ✉ & Erik C. B. Johnson[4,10,19] ✉

[1]Department of Psychiatry and Neurochemistry, Institute of Neuroscience & Physiology, The Sahlgrenska Academy at the University of Gothenburg, Mölndal, Sweden. [2]Department of Biostatistics and Bioinformatics, Rollins School of Public Health, Emory University, Atlanta, GA, USA. [3]Department of Biochemistry, Emory University School of Medicine, Atlanta, GA, USA. [4]Goizueta Alzheimer's Disease Research Center, Emory University School of Medicine, Atlanta, GA, USA. [5]Sant Pau Memory Unit, Department of Neurology, Hospital de la Santa Creu i Sant Pau, Biomedical Research Institute Sant Pau (IIB Sant Pau), Universitat Autònoma de Barcelona, Barcelona, Spain. [6]Department of Neurology, NYU Grossman School of Medicine, New York, NY, USA. [7]Center for Cognitive Neurology, NYU Grossman School of Medicine, New York, NY, USA. [8]Institut de Neurociències, Universitat Autònoma de Barcelona, Barcelona, Spain. [9]Proteomics Core Facility at Sahlgrenska Academy, University of Gothenburg, Gothenburg, Sweden. [10]Department of Neurology, Emory University School of Medicine, Atlanta, GA, USA. [11]Clinical Neurochemistry Laboratory, Sahlgrenska University Hospital, Mölndal, Sweden. [12]Department of Pathology, NYU Grossman School of Medicine, New York, NY, USA. [13]Department of Psychiatry, NYU Grossman School of Medicine, New York, NY, USA. [14]Department of Neurodegenerative Disease, Institute of Neurology, UCL, London, UK. [15]UK Dementia Research Institute, UCL, London, UK. [16]Hong Kong

Center for Neurodegenerative Diseases, Clear Water Bay, Hong Kong, China. [17]Wisconsin Alzheimer's Disease Research Center, University of Wisconsin School of Medicine and Public Health, Madison, WI, USA. [18]These authors contributed equally: Laia Montoliu-Gaya, Shijia Bian, Eric B. Dammer. [19]These authors jointly supervised this work: Juan Fortea, Erik C.B. Johnson. ✉e-mail: jfortea@santpau.cat; erik.johnson@emory.edu

6.3. Future directions - Evaluation of pTau and Aβ interactomes.

Article 4: The influence of APOE ε4 on the pTau interactome in sporadic Alzheimer's disease.

Acta Neuropathologica (2024) 147:91
https://doi.org/10.1007/s00401-024-02744-8

ORIGINAL PAPER

The influence of *APOE*$^{\varepsilon 4}$ on the pTau interactome in sporadic Alzheimer's disease

Manon Thierry[1] · Jackeline Ponce[2] · Mitchell Martà-Ariza[1,3] · Manor Askenazi[4] · Arline Faustin[1] · Dominique Leitner[1,5] · Geoffrey Pires[1] · Evgeny Kanshin[2] · Eleanor Drummond[6] · Beatrix Ueberheide[2] · Thomas Wisniewski[1,7]

Received: 11 March 2024 / Revised: 12 April 2024 / Accepted: 12 May 2024

Abstract

APOE$^{\varepsilon 4}$ is the major genetic risk factor for sporadic Alzheimer's disease (AD). Although *APOE*$^{\varepsilon 4}$ is known to promote Aβ pathology, recent data also support an effect of *APOE* polymorphism on phosphorylated Tau (pTau) pathology. To elucidate these potential effects, the pTau interactome was analyzed across *APOE* genotypes in the frontal cortex of 10 advanced AD cases ($n=5$ *APOE*$^{\varepsilon 3/\varepsilon 3}$ and $n=5$ *APOE*$^{\varepsilon 4/\varepsilon 4}$), using a combination of anti-pTau pS396/pS404 (PHF1) immunoprecipitation (IP) and mass spectrometry (MS). This proteomic approach was complemented by an analysis of anti-pTau PHF1 and anti-Aβ 4G8 immunohistochemistry, performed in the frontal cortex of 21 advanced AD cases ($n=11$ *APOE*$^{\varepsilon 3/\varepsilon 3}$ and $n=10$ *APOE*$^{\varepsilon 4/\varepsilon 4}$). Our dataset includes 1130 and 1330 proteins enriched in IP_{PHF1} samples from *APOE*$^{\varepsilon 3/\varepsilon 3}$ and *APOE*$^{\varepsilon 4/\varepsilon 4}$ groups (fold change ≥ 1.50, IP_{PHF1} *vs* $IP_{IgG\ ctrl}$). We identified 80 and 68 proteins as probable pTau interactors in *APOE*$^{\varepsilon 3/\varepsilon 3}$ and *APOE*$^{\varepsilon 4/\varepsilon 4}$ groups, respectively (SAINT score ≥ 0.80; false discovery rate (FDR) ≤ 5%). A total of 47/80 proteins were identified as more likely to interact with pTau in *APOE*$^{\varepsilon 3/\varepsilon 3}$ *vs APOE*$^{\varepsilon 4/\varepsilon 4}$ cases. Functional enrichment analyses showed that they were significantly associated with the nucleoplasm compartment and involved in RNA processing. In contrast, 35/68 proteins were identified as more likely to interact with pTau in *APOE*$^{\varepsilon 4/\varepsilon 4}$ *vs APOE*$^{\varepsilon 3/\varepsilon 3}$ cases. They were significantly associated with the synaptic compartment and involved in cellular transport. A characterization of Tau pathology in the frontal cortex showed a higher density of plaque-associated neuritic crowns, made of dystrophic axons and synapses, in *APOE*$^{\varepsilon 4}$ carriers. Cerebral amyloid angiopathy was more frequent and severe in *APOE*$^{\varepsilon 4/\varepsilon 4}$ cases. Our study supports an influence of *APOE* genotype on pTau-subcellular location in AD. These results suggest a facilitation of pTau progression to Aβ-affected brain regions in *APOE*$^{\varepsilon 4}$ carriers, paving the way to the identification of new therapeutic targets.

Keywords Alzheimer · Tau · ApoE · Interactome · Proteomics · Neuropathology

✉ Manon Thierry
manon.thierry@nyulangone.org

✉ Thomas Wisniewski
thomas.wisniewski@nyulangone.org

[1] Department of Neurology, Center for Cognitive Neurology, Grossman School of Medicine, New York University, Science Building, Rm 1023J, 435 East 30th Street, New York, NY, USA

[2] Department of Biochemistry and Molecular Pharmacology, Proteomics Laboratory, Grossman School of Medicine, New York University, New York, NY, USA

[3] Institut de Neurociències, Universitat Autònoma de Barcelona, Barcelona, Spain

[4] Biomedical Hosting LLC, Arlington, MA, USA

[5] Department of Neurology, Comprehensive Epilepsy Center, Grossman School of Medicine, New York University, New York, NY, USA

[6] Brain and Mind Centre, School of Medical Science, University of Sydney, Sydney, Australia

[7] Departments of Pathology and Psychiatry, Grossman School of Medicine, New York University, Science Building, Rm 1017, 435 East 30 Street, New York, NY 10016, USA

Published online: 21 May 2024

Introduction

Alzheimer's disease (AD) is characterized by the extracellular deposition and self-aggregation of β-amyloid peptides (Aβ) into various types of Aβ deposits [22, 34], along with the intraneuronal accumulation and self-assembly of abnormally phosphorylated Tau proteins (pTau) into neurofibrillary tangles [14, 36, 37]. These neuropathological lesions affect successively different regions of the brain, following distinct stereotypical sequences described by the five Thal phases (0–5 for Aβ pathology [82]) and the six Braak stages (0-VI for Tau pathology [12]). A polymorphism of the *apolipoprotein E* gene (*APOE*) is the major genetic risk factor associated with sporadic AD. In comparison with the common $APOE^{\varepsilon 3}$ allele, the $APOE^{\varepsilon 4}$ allele is associated with an increased risk and an earlier onset for AD, in a dose-dependent manner (Odds Ratio $APOE^{\varepsilon 4/\varepsilon 4} = 14.2$; www.alzgene.org; [19, 77]). In contrast, the rare $APOE^{\varepsilon 2}$ allele confers a protection against the development of AD (Odds Ratio $APOE^{\varepsilon 2/\varepsilon 2} = 0.7$; www.alzgene.org; [18]). In the brain, Apolipoprotein E (ApoE) is a glycoprotein predominantly secreted by astrocytes under physiologic conditions [11] and is involved in phospholipid and cholesterol transport: the C-terminus domain of ApoE binds with phospholipid packed into HDL-like particles conveying cholesterol [30, 68], while the N-terminus domain interacts with receptors of the LDLR family [41, 66].

ApoE is colocalized with parenchymal Aβ deposits in AD, as well as with vascular Aβ accumulation in a context of cerebral amyloid angiopathy (CAA) [57, 91]. The presence of the $APOE^{\varepsilon 4}$ allele is strongly associated with an exacerbation of Aβ pathology [70]. Experimental data confirm the influence of *APOE* expression on Aβ accumulation [6, 31], unravelling a differential effect of ApoE isoforms on Aβ clearance impairment, aggregation and fibrillation (ApoE2 < ApoE3 < ApoE4) [15, 23, 39, 89]. In addition to these established effects of ApoE on Aβ pathology, emerging evidence suggests that ApoE also plays an important role in Tau pathology. The neuroanatomical progression of Tau pathology follows the expression gradients of *APOE* [54]. Furthermore, an exceptional resistance to an autosomal dominant familial AD mutation, associated with a massive parenchymal Aβ deposition but a surprisingly discrete Tau pathology, was recently attributed to the co-occurrence of a protective mutation in the $APOE^{\varepsilon 3}$ sequence [1, 73]. Although ApoE is known to be colocalized with pTau within neurofibrillary tangles, their relationship remains elusive [57, 76]. In vivo experiments support an Aβ-independent effect of $APOE^{\varepsilon 4}$ on pTau accumulation [44, 74], which may involve a promotion of Tau phosphorylation [13, 69] or a disruption of cholesterol metabolism and lysosomal functions [48]. Further investigations are needed in the AD brain to understand how *APOE* impacts Tau pathology, which correlates better than Aβ deposition with the cognitive status of AD cases [58].

The development of localized proteomics on *post-mortem* human brains, by our group, identified de novo proteins associated with Tau pathology [25, 26, 63, 64]. More particularly, the combination of anti-pTau pS396/pS404 immunoprecipitation with downstream proteomic analysis allowed the identification of proteins that specifically interact with pathologic pTau species involved in AD pathology [26]. In contrast, similar approaches focused on proteins interacting with total Tau, without discriminating its physiologic and pathologic forms [4, 9, 40, 49, 51, 53, 85, 87]. In this study, we took advantage of our unbiased strategy to fully uncover the effects of the AD risk factor $APOE^{\varepsilon 4}$ on pTau metabolism: we combined anti-pTau immunoprecipitation with MS to map out, for the very first time, the pTau interactome in the AD brain of $APOE^{\varepsilon 3}$ *vs* $APOE^{\varepsilon 4}$ carriers.

Materials and methods

Cases

All procedures were performed under protocols approved by Institutional Review Boards at New York University Alzheimer's Disease Research Center (NYU ADRC, NY, USA) and Columbia University Alzheimer's Disease Research Center (CU ADRC, NY, USA). In all cases, written informed consent for research was obtained from the patient or legal guardian, and the material used had appropriate ethical approval for use in this project. All patients' data and samples were coded and handled according to NIH guidelines to protect patients' identities. A total of 25 cases of sporadic AD were included in this study. Cases were selected from donated brain tissue collected at the NYU ADRC and CU ADRC, based on their ABC score (A3, B3, C3; [55]), severity of Tau pathology in the frontal cortex and *APOE* genotype. The $APOE^{\varepsilon 3/\varepsilon 3}$ and $APOE^{\varepsilon 4/\varepsilon 4}$ groups were matched to the best of our ability in terms of age, sex and co-morbidities, as shown in Table 1. Our inclusion criteria involved indeed the absence of any additional primary tauopathy and of any major co-proteinopathy. For the neuropathological analysis, the presence of a concomitant Lewy Body disease of the amygdala-predominant type was tolerated for $n = 2$ cases per group to increase our number of cases, as this co-pathology is common in the elderly population and because its even distribution among our groups did not impact our comparative study design. Individual case information is detailed in Table 1 (age, sex, *APOE* genotype, *post-mortem*

Table 1 Cohort description

Case	Age	Sex	APOE	PMI	Source	ABC score	Braak	Neuropathological findings (other than AD-related changes)	Study
A/1	77	F	ε3/ε3	66	NYU ADRC	A3, B3, C3	VI	Hippocampal sclerosis	P, H
B/2	90	F	ε3/ε3	21	NYU ADRC	A3, B3, C3	VI	CAA and Binswanger's disease	P, H
C/3	67	M	ε3/ε3	< 48	NYU ADRC	A3, B3, C3	VI	CAA	P, H
D/4	83	M	ε3/ε3	142	NYU ADRC	A3, B3, C3	VI	CAA, Binswanger's disease and hemorrhages	P
E/5	85	F	ε3/ε3	< 24	NYU ADRC	A3, B3, C3	VI	CAA and Binswanger's disease	P
F	91	F	ε3/ε3	< 48	NYU ADRC	A3, B3, C3	VI	Hippocampal sclerosis and Binswanger's disease	H
G	87	F	ε3/ε3	26	NYU ADRC	A3, B3, C3	VI	Binswanger's disease and chronic ischemia (insula)	H
H	73	M	ε3/ε3	< 24	NYU ADRC	A3, B3, C3	VI	CAA and Binswanger's disease	H
I	87	F	ε3/ε3	10	CU ADRC	A3, B3, C3	VI	Subdural hematoma (parieto-occipital, left), meningioma psammomatous clival (left) and athero-arteriolosclerosis	H
J	83	F	ε3/ε3	18	CU ADRC	A3, B3, C3	VI	Infarct (putamen—posterior limb of internal capsule—body of the caudate), status cribrosus (lenticular nucleus, thalamus), athero-arteriolosclerosis and intracortical telangiectasia (superior parietal lobule, left)	H
K	77	F	ε3/ε3	11	CU ADRC	A3, B3, C3	VI	Vascular brain injury, athero-arteriolosclerosis, CAA and synechia (hippocampo-ventricular, left)	H
L	72	M	ε3/ε3	12	CU ADRC	A3, B3, C3	VI	Lewy body disease (amygdala predominant), vascular brain injury, athero-arteriolosclerosis and CAA	H
M	70	F	ε3/ε3	21	CU ADRC	A3, B3, C3	VI	Lewy body disease (amygdala predominant), vascular brain injury, athero-arteriolosclerosis, CAA, ferro-calcic vasculopathy (pallidum), hypoxic-ischemic encephalopathy and atrophy of the optic nerve (left > right) and of the lateral geniculate body	H
N/6	91	F	ε4/ε4	21	NYU ADRC	A3, B3, C3	VI	CAA and Binswanger's disease	P
O/7	81	F	ε4/ε4	< 48	NYU ADRC	A3, B3, C3	VI	CAA, Binswanger's disease and hippocampal sclerosis (with TDP43 inclusions)	P, H
P/8	79	F	ε4/ε4	< 72	NYU ADRC	A3, B3, C3	VI	CAA and arachnoid cyst	P
Q/9	73	F	ε4/ε4	< 48	NYU ADRC	A3, B3, C3	VI	CAA and Binswanger's disease	P, H
R/10	69	M	ε4/ε4	< 24	NYU ADRC	A3, B3, C3	VI	CAA	P, H
S	68	F	ε4/ε4	29	NYU ADRC	A3, B3, C3	VI	CAA, Binswanger's disease and atrophy of the grey and white matter	H
T	63	M	ε4/ε4	64	NYU ADRC	A3, B3, C3	VI	N/A	H
U	90	F	ε4/ε4	39	CU ADRC	A3, B3, C3	VI	Infarcts (putamen — external capsule, right; cortico-subcortical, angular parietal gyrus, left), hemorrhage (frontal cortex, right), status cribrosus (striatum), athero-arteriolosclerosis and CAA	H
V	81	F	ε4/ε4	14	CU ADRC	A3, B3, C3	VI	Lewy body disease (amygdala predominant), metastatic carcinoma, hemorrhage, athero-arteriolosclerosis, CAA and synechia (hippocampo-ventricular, bilateral)	H
W	75	F	ε4/ε4	14	CU ADRC	A3, B3, C3	VI	Status cribrosus (striatum), synechia (hippocampo-ventricular, bilateral), athero-arteriolosclerosis and CAA	H
X	77	F	ε4/ε4	22	CU ADRC	A3, B3, C3	VI	Lewy body disease (amygdala predominant), vascular brain injury, athero-arteriolosclerosis, occlusive clot in small leptomeninges artery (superior parietal lobule, right), CAA with dyshoric changes (calcarine cortex), ferro-calcic vasculopathy (globus pallidus), small aneurysms (Willis circle)	H
Y	81	M	ε4/ε4	17	CU ADRC	A3, B3, C3	VI	Arteriolosclerosis and CAA	H

The 25 cases of neuropathologically confirmed sporadic AD included in our study are listed in this table. The latter discloses their age at death, sex, APOE genotype (APOE), PMI in hours, source, ABC score of AD-related pathologic changes [55], Braak stage [12] and summary of any other neuropathological findings. A letter was attributed to all 25 disidentified cases (A-Y), associated with an additional number for the 10 cases included in the proteomic study to match the proteomic dataset annotations (1–10). The last column detailed the study in which the case was included ("P" for proteomics when frozen tissue was available; "H" for histology when formalin-fixed paraffin-embedded tissue was available). *AD* Alzheimer's disease, *CAA* Cerebral Amyloid Angiopathy, *CU ADRC* Columbia University Alzheimer's Disease Research Center, *NYU ADRC* New York University Alzheimer's Disease Research Center

interval (PMI), ABC score, Braak stage, neuropathological findings, technical application).

Genotyping

APOE genotypes were provided by the NYU ADRC and CUMC brain banks for 15 out of 25 cases. For cases 1, 2, 4, 6, 7, 8, 14, 15, 16 and 18, *APOE* genotyping was performed as previously described [24]. A fragment of frozen frontal cortex was dissected (~25 mg), then collected into a 1.5 mL tube using single-use consumables in DNA-free experimental conditions. DNA was isolated using the DNeasy Blood & Tissue kit following the manufacturer's instructions (#69,504, Qiagen). A single endpoint PCR was performed in a total volume of 25 µl containing 0.2 µM of each custom primer (Forward primer 5′ AGCCCTTCTCCCCGCCTC CCACTGT 3′; reverse primer 5′ CTCCGCCACCTGCTC CTTCACCTCG 3′; Millipore Sigma), 10 µl of DreamTaq Green PCR Master Mix 2X (#K1081, Thermo Scientific) and 4.2 µl of Betaine (#B0300, Millipore Sigma). Cycling conditions were set as follows: 98 °C for 4 min, 35 cycles at 98 °C/10 s, 63 °C/45 s and 72 °C/1 min 10 s, followed by 72 °C for 10 min. Unpurified PCR products were submitted to Genewiz for Sanger sequencing and the sequences were analyzed using the SnapGene 5.3.1 software.

Homogenization

Ten cases of sporadic AD were used for proteomic analysis (Table 1). The grey matter was dissected from the frontal cortex of archived fresh frozen human tissue samples stored at −80 °C (~0.25 g per sample). Cortical tissue was homogenized as previously described [26]. Frozen tissue was enveloped into aluminum foil and pulverized on dry ice using a hammer. The powder was collected into a Dounce homogenizer, then homogenized on ice with ~25 strokes in a low salt homogenization buffer (50 mM HEPES pH 7.0, 250 mM sucrose, 1 mM EDTA) with inhibitors of proteases (cOmplete ULTRA Tablets, Mini, EDTA-free; #5,892,791,001, Millipore Sigma) and phosphatases (PhosphoSTOP EASYpack; #4,906,845,001, Millipore Sigma). The total protein concentration of homogenates was assessed with the Micro BCA Protein Assay Kit, following the supplier's guidelines (#23,235, Thermo Scientific). Samples were stored at −80 °C until use.

Immunoprecipitation

For each case, two immunoprecipitation products were obtained: the first using the mouse antibody anti-pTau pS396/pS404 (PHF1, provided by Dr. Peter Davies, Albert Einstein University, NY, USA [35]) to enrich pTau and its binding partners, the second using a mouse isotype antibody to control non-specific binding (#400,202, BioLegend). As a result, 20 separate IP products were individually analyzed for proteomics. Each IP product required a total of six-reaction mixes to collect enough material for downstream biochemistry and proteomics analyses, using the Dynabeads Protein G Immunoprecipitation Kit and following the supplier's guidelines with minor adjustments (#10007D, Thermo Scientific). For each reaction mix, brain homogenate (300 µg total proteins/mix) and antibodies (4 µg antibodies/mix) were incubated overnight at 4 °C with over-end rotation to allow antigen–antibody interaction. The next day, the samples containing antigen–antibody complexes were mixed with Dynabeads (1.5 mg/mix), then incubated overnight at 4 °C with over-end rotation. The antigen–antibody-Dynabeads complexes were recovered and washed using a DynaMag-2 magnet (#12321D, Thermo Scientific), then resuspended in 100 µl of phosphate buffered saline at pH 7.4. The six-reaction mixes were pooled into a new tube (600 µL total), to avoid the co-elution of proteins bound to the tube wall. A total of 500 µL of the IP product was kept at 4 °C until proteomics analysis. The remaining 100 µL were eluted by capturing the antigen–antibody-Dynabeads complexes with the magnet, before incubating the beads in 20 µL of a denaturing buffer (141 mM Tris base, 106 mM Tris HCl, 2% SDS, 0.51 mM EDTA, pH 8.5; 15 min at 70 °C and 1000 rpm). The eluted fractions were recovered on the magnet and stored at −20 °C until analysis.

Biochemistry analysis

Western blotting was performed to confirm the enrichment of pTau in the IP products. The equivalent of 10% of the IP product submitted to proteomic analyses was mixed with DTT 100 mM and 4X Bolt LDS Sample Buffer (#B0007, Thermo Scientific), then boiled at 98 °C for 5 min. Proteins were resolved on 4–12% Bis–Tris gels (#NP0322BOX, Thermo Scientific), then transferred onto a 0.2 µm nitrocellulose membrane (#1,620,112, BioRad). Membranes were blocked with 5% milk in Tris-buffered saline with 0.1% Tween-20 for 1 h, then probed with an anti-pTau S199/S202 antibody (1:1500; #44-768G, Thermo Scientific) at room temperature for 1 h, before being incubated with an anti-rabbit horseradish peroxidase antibody (1:3000; #NA934, Cytiva). The signal was revealed using the Pierce ECL Western Blotting Substrate (#32,106, Thermo Scientific) and membranes were imaged with the ChemiDoc MP Imaging System (BioRad). Silver staining was conducted to confirm the presence of a sufficient amount of proteins in our samples for proteomics downstream analysis. The equivalent of 5% of the IP product used in proteomics was mixed with DTT 100 mM and 4X Bolt LDS Sample Buffer (#B0007, Thermo Scientific), then boiled at 98 °C for 5 min. Proteins were resolved on 4–12% Bis–Tris gels (#NP0322BOX, Thermo

Scientific). The gels were extracted and the proteins were stained using the SilverQuest Silver Staining Kit following the supplier's guidelines (#LC6070, Thermo Scientific), to confirm the presence of a sufficient amount of proteins for proteomic downstream analyses. Gels were imaged with the ChemiDoc MP Imaging System (BioRad).

Proteomic analysis

IP products were analyzed by liquid-chromatography and mass spectrometry (LC–MS/MS), as previously detailed with some adjustments [26].

On-bead digestion and protein extraction

The antigen–antibody-bead complexes were recovered on a magnet then washed twice with ammonium bicarbonate 100 mM. Samples were reduced with DTT 0.2 M at 57 °C for 1 h, then alkylated with iodoacetamide 0.5 M at RT in the dark for 45 min. Sequencing-grade modified trypsin (Promega) was added to the sample for overnight digestion on a shaker at room temperature (300 ng). The next day, samples were acidified to pH 2 using 10% trifluoroacetic acid, then loaded onto equilibrated Ultra-Micro SpinColumns (Harvard Apparatus) using a microcentrifuge, before being rinsed three times with 0.1% TFA. The extracted samples were further washed with 0.5% acetic acid. The peptides were eluted with 40% acetonitrile in 0.5% acetic acid, followed by the addition of 80% acetonitrile in 0.5% acetic acid. Organic solvent was removed using a SpeedVac concentrator, before reconstituting samples in 0.5% acetic acid.

LC–MS/MS analysis

A total of 1 µg of protein was analyzed for each sample. A liquid chromatography (LC) separation was performed online with MS using the autosampler of an EASY-nLC 1000 (Thermo Scientific). Peptides were gradient-eluted from the column into the Orbitrap Eclipse using an 85 min gradient (Thermo Scientific). Solvent A consisted of 2% acetonitrile in 0.5% acetic acid and solvent B of 80% acetonitrile in 0.5% acetic acid. The gradient was held at 5% solvent B for 5 min, ramped to 35% solvent B in 60 min, to 45% solvent B in 10 min and to 100% solvent B in another 10 min. High-resolution full MS spectra were acquired with a resolution of 120,000, an AGC target of 4e5, a maximum ion time of 50 ms and a scan range of 400 to 1,500 m/z. All MS/MS spectra were recorded in the orbitrap analyzer using the following instrument parameters: resolution of 30,000, AGC target of 2e5, maximum ion time of 200 ms, one microscan, 2 m/z isolation window and NCE of 27.

Data processing

The MS/MS spectra were searched against the UniProt human database using Sequest within Proteome Discoverer 1.4. The data were filtered to better than 1% peptide and protein FDR searched against a decoy database. Only proteins with at least two different peptides were considered for downstream analysis. To asses if there are any differences in phosphorylation between the *APOE* groups, we analyzed Tau-protein phosphorylation using Byos (ProteinMetrics). The phosphorylation assignment and area integration were manually verified using the Byos interface. The area under the curve for the same peptide, with and without phosphorylation, was integrated and the amount of phosphorylation reported as a percentage. Note: not all phospho-sites have been observed in all samples and their frequency of observation has been highlighted in Fig. 4.

Data analysis

Data were analyzed using the Significance Analysis of INTeractome express algorithm (SAINT), as previously detailed [26, 78]. All non-human proteins, introduced during sample preparation, were removed from the results. The proteins were ranked by SAINT score and proteins with a SAINT score ≥ 0.80, equivalent to a FDR of $\leq 5\%$, were considered as pTau interactors and further studied. Three lists of pTau interactors of interest were submitted to and analyzed with STRING 11.5 and Cytoscape 3.9.1, to investigate network functional enrichments based on the Gene Ontology (GO) terms "cellular component" and "biological process", using the total genome as background and a redundancy cut-off of 0.7: (1) proteins identified as pTau interactors in both *APOE* groups (SAINT score ≥ 0.80 in $APOE^{\varepsilon 3/\varepsilon 3}$ and $APOE^{\varepsilon 4/\varepsilon 4}$ groups, $n = 33$ proteins), (2) proteins identified as pTau interactors associated with an $APOE^{\varepsilon 3/\varepsilon 3}$ genotype (SAINT score ≥ 0.80 in $APOE^{\varepsilon 3/\varepsilon 3}$ cases, SAINT score < 0.80 in $APOE^{\varepsilon 4/\varepsilon 4}$ cases, $n = 47$ proteins) and 3) proteins identified as pTau interactors associated with an $APOE^{\varepsilon 4/\varepsilon 4}$ genotype (SAINT score ≥ 0.80 in $APOE^{\varepsilon 4/\varepsilon 4}$ cases, SAINT score < 0.80 in $APOE^{\varepsilon 3/\varepsilon 3}$ cases, $n = 35$ proteins). Network images were extracted and enrichment tables were exported then analyzed using Excel and GraphPad Prism 9. 4. 1. In addition, proteins considered as pTau interactors associated with one *APOE* genotype or the other were further compared among *APOE* groups based on their fold change (FC), calculated as follows: FC = [mean #peptide spectral matches

(group of interest) + 1]/[mean #peptide spectral matches (group of reference) + 1].

Data comparison with previous MS-based studies

Our data were systematically compared to previous AD-related proteomic studies, using two complementary approaches. First, the pTau interactors identified here were compared to our previous study using the same anti-pTau pS396/pS404 (PHF1) antibody and a similar experimental strategy, but different AD tissues and a less stringent SAINT score cut-off (SAINT score ≥ 0.65, FDR ≤ 10% [26]). Second, we interrogated our probable pTau interactors using the NeuroPro searchable database v1.12 [3]. NeuroPro is a website that compiled 38 experimental MS-based proteomic datasets designed to assess protein changes occurring specifically in the AD brain. The following filters were applied: conditions "AD" (proteins associated with the AD brain) and "AD/C" (proteins altered in AD *vs* control brains). The resulting tables were exported and analyzed using Excel.

Immunohistochemistry

Immunohistochemistry was performed on formalin-fixed paraffin-embedded 8 µm-thick sections of frontal cortex. Sections were deparaffinized and rehydrated through a series of xylene and ethanol washes. Antigen retrieval was performed by treatment with 88% formic acid for 7 min, followed by boiling in citrate buffer (10 mM sodium citrate, 0.05% Tween-20; pH 6). Sections were blocked with 10% normal goat serum, then incubated overnight at 4 °C with a primary antibody anti-pTau pS396/pS404 (1:200; mouse antibody PHF1; provided by Dr. Peter Davies, Albert Einstein University, NY, USA) or anti-Aβ 4G8 (1:1000; mouse antibody; #800,711, BioLegend), diluted in 4% normal goat serum. Sections were incubated for 1 h at room temperature with an anti-mouse secondary antibody (1:1000, #BA-2000, Vector Laboratories), revealed with an avidin–biotin complex HRP detection kit (#PK-6100, Vector Laboratories) in combination with a DAB substrate kit (#34,065, Thermo Scientific), counterstained with Mayer's hematoxylin (#MHS16, Millipore Sigma) and coverslipped (#P36970, Thermo Scientific). This technique was applied on 21 cases ($n = 11$ $APOE^{\varepsilon 3/\varepsilon 3}$ cases, $n = 10$ $APOE^{\varepsilon 4/\varepsilon 4}$ cases; Table 1).

Immunohistochemistry quantification

Tau pathology was quantified in the frontal cortex on anti-pTau pS396/pS404 PHF1 immunohistochemistry. Slides were scanned at a 40 × magnification with the Aperio VERSA 8 scanner and analyzed with Aperio ImageScope 12.4.3.5008 (Leica Biosystems). For each case, Tau pathology was quantified in the grey matter from three ROIs of 5.0×10^6 µm^2 ($\pm 0.5 \times 10^6$ µm^2), encompassing all cortical layers and evenly spread over the cortical section. The total burden of PHF1 immunoreactive material was obtained by running the open source "Positive Pixel Count 2004-08-11" algorithm on each ROI, with the color saturation threshold set at 0.2. Raw data were exported on Excel to calculate the averaged percentage of immunopositive pixels out of the total number of pixels per case. Each neuropathological lesion composing Tau pathology was analyzed on their respective ROI: the first ROI was used to count the number of PHF1 positive neuronal profiles (pre-tangles, tangles and ghost tangles) per µm^2; the second ROI was used to count the number of PHF1 positive neuritic crowns per µm^2; in the third ROI, the burden of PHF1 positive neuropil threads was evaluated by assessing the averaged percentage of immunopositive pixels out of the total number of pixels from ten sub-ROIs of 1.0×10^4 µm^2, covering neuropil areas evenly spread within the ROI and devoid of any neuronal profiles or neuritic crowns. Tau pathology was also quantified in the white matter from ten ROIs of 1.0×10^5 µm^2 to assess the averaged percentage of immunopositive pixels out of the total number of pixels reflecting the burden of axonal threads. Unpaired non-parametric Mann–Whitney tests were performed on GraphPad Prism 9. 4. 1. to compare each of these ratios among *APOE* groups at a risk level of $\alpha = 0.05$. Aβ pathology was quantified in the frontal cortex on anti-Aβ 4G8 immunohistochemistry. Slides were scanned at a 20 × magnification with the Aperio VERSA 8 scanner and analyzed with Aperio ImageScope 12.4.3.5008 (Leica Biosystems). For each case, Aβ pathology was quantified in the grey matter from three ROIs of 5.0×10^6 µm^2 ($\pm 0.5 \times 10^6$ µm^2), encompassing all cortical layers and evenly spread over the cortical section. The total burden of 4G8 immunoreactive material was obtained by running the open source "Positive Pixel Count 2004-08-11" algorithm on each ROI, with the color saturation threshold set at 0.1. Raw data were exported on Excel to calculate the averaged percentage of immunopositive pixels out of the total number of pixels per case. CAA was analyzed in the parenchyma of the frontal cortex on anti-Aβ 4G8 immunohistochemistry, by attributing a semi-quantitative score to each case using the following criteria: 0 if none (no Aβ-positive vessel detected), 1 if sparse (< 25% of Aβ-positive vessels), 2 if moderate (about 50% of Aβ-positive vessels), 3 if severe (about 100% of Aβ-positive vessels). The type of CAA was evaluated by attributing a "Type 1" to cases presenting with capillary CAA along with CAA in larger vessels or a "Type 2" to cases presenting with CAA without capillary involvement [80].

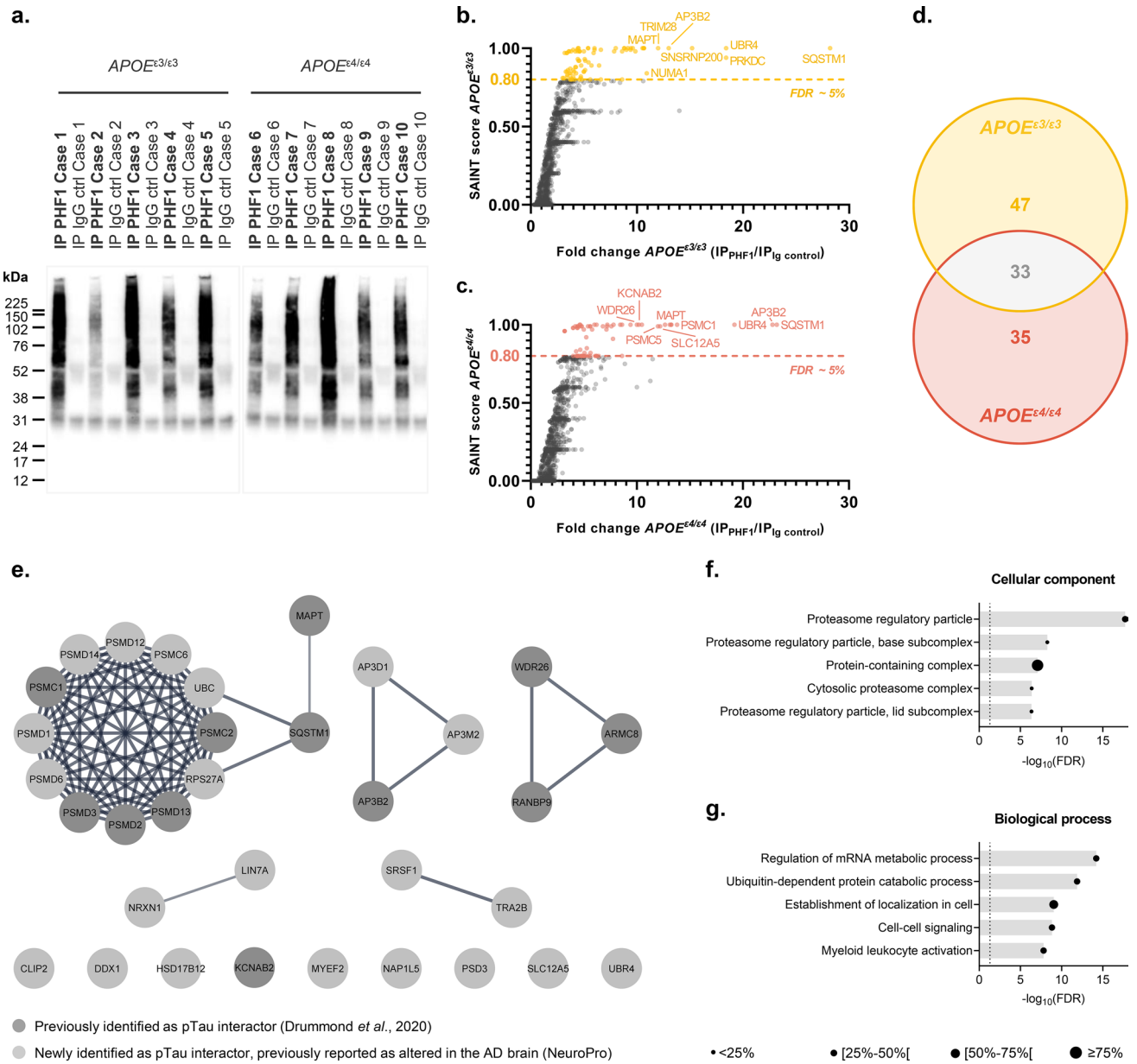

Fig. 1 Proteomic overview of the pTau interactome in sporadic AD cases of various *APOE* genotypes. **a** Western blot of the equivalent of 10% of the IP_{PHF1} or $IP_{IgG\ ctrl}$ products obtained from homogenates of frozen frontal cortex from 10 neuropathologically confirmed AD cases (cases 1–5 of $APOE^{\varepsilon3/\varepsilon3}$ genotype, cases 6–10 of $APOE^{\varepsilon4/\varepsilon4}$ genotype). **b**–**c**. One-sided volcano plots representing, for all proteins identified by LC–MS/MS, their SAINT score as a function of their fold change $IP_{PHF1}/IP_{IgG\ ctrl}$ for the $APOE^{\varepsilon3/\varepsilon3}$ group (**b**) or for the $APOE^{\varepsilon4/\varepsilon4}$ group (**c**). d. Venn diagram representing the 80 and 68 proteins identified as probable pTau interactors in the $APOE^{\varepsilon3/\varepsilon3}$ and $APOE^{\varepsilon4/\varepsilon4}$ groups, respectively; 33 of these pTau interactors were common to both groups (SAINT score ≥ 0.80, FDR ≤ 5%). **e** Network representation of the 33 common pTau interactors. Each protein is represented by its gene ID as a node. The interacting nodes are connected by edges and their thickness indicates the strength of data support with a high confidence interaction score set at 0.7 (STRING). The node color reflects the protein status regarding previous AD-related proteomic studies, as detailed in the legend. **f**–**g**. Description of the functional enrichments associated with the 33 common pTau interactors as a function of $-\log_{10}$(FDR), using "genome" as background and a redundancy cut-off of 0.7. The incorporated bubble plots reflect the number of corresponding proteins in the network as a percentage, as detailed in the legend (PPI enrichment p value $= 1.0 \times 10^{-16}$; STRING and Cytoscape). The top panel details the top 5 GO terms "cellular component" (**f**) while the bottom panel shows the top 5 GO terms "biological process" (**g**). *AD: Alzheimer's disease*; *IP: Immunoprecipitation; FDR: false discovery rate*

Results

Proteomic overview

Immunoprecipitated fractions were obtained from frontal cortex homogenates of 10 advanced sporadic AD cases ($n=5$ $APOE^{\varepsilon3/\varepsilon3}$ and $n=5$ $APOE^{\varepsilon4/\varepsilon4}$ cases), using anti-pTau PHF1 (IP_{PHF1}) or control IgG ($IP_{IgG\ ctrl}$) antibodies. The enrichment of pTau in the IP_{PHF1} products was confirmed by western blot (Fig. 1a). A total of 1130 and 1330 proteins were detected in the IP_{PHF1} samples of the $APOE^{\varepsilon3/\varepsilon3}$ and $APOE^{\varepsilon4/\varepsilon4}$ groups (fold change ≥ 1.50, IP_{PHF1} *vs* $IP_{IgG\ ctrl}$, Online Resource 1). Our dataset was filtered using the probabilistic SAINT score to identify the most likely pTau interactors, leading to the identification of 80 proteins of interest in the $APOE^{\varepsilon3/\varepsilon3}$ group and 68 in the $APOE^{\varepsilon4/\varepsilon4}$ group (SAINT scores ≥ 0.80, FDR $\leq 5\%$). Among these, 33 proteins were common to both *APOE* groups (Fig. 1b–d). They included 12/33 proteins previously identified as pTau interactors by our laboratory: AP3B2, ARMC8, KCNAB2, MAPT, PSMC1, PSMC2, PSMD13, PSMD2, PSMD3, RANBP9, SQSTM1 and WDR26 [26]. The remaining 21/33 proteins were identified as pTau interactors for the first time here, although they have been previously reported to have significantly altered protein levels in AD brain tissue (Fig. 1e and Online Resource 2; [3]). A significant network functional enrichment was associated with the 33 most probable pTau interactors common to $APOE^{\varepsilon3/\varepsilon3}$ and $APOE^{\varepsilon4/\varepsilon4}$ cases (PPI enrichment p value $=1.0\times10^{-16}$; Online Resource 3a): they were predominantly associated with the proteasome system (GO terms "cellular component", Fig. 1f) and involved in the regulation of mRNA metabolism, ubiquitin-dependent catabolic process or establishment of localization in cell (GO terms "biological process", Fig. 1g).

The pTau interactome in sporadic AD cases with an $APOE^{\varepsilon3/\varepsilon3}$ genotype

A total of 47 proteins were identified as most likely pTau interactors only for $APOE^{\varepsilon3/\varepsilon3}$ cases (SAINT score ($APOE^{\varepsilon3/\varepsilon3}$) ≥ 0.80, average SAINT score ($APOE^{\varepsilon3/\varepsilon3}$) $\pm$ SEM $= 0.91 \pm 0.01$ *vs* SAINT score ($APOE^{\varepsilon4/\varepsilon4}$) < 0.80, average SAINT score ($APOE^{\varepsilon4/\varepsilon4}$) $\pm$ SEM $= 0.52 \pm 0.04$). A significant network functional enrichment was attributed to these 47 proteins (PPI enrichment p value $=7.1\times10^{-3}$; Online Resource 3b). In this network, 7/47 proteins were previously reported as probable pTau interactors by our group: KIF5C, LANCL2, PIN1, PIP4K2B, PSMC3, PSMD8 and PSMD11 [26]. The remaining 40/47 proteins were identified as pTau interactors for the first time here, although they included 38 proteins previously reported to have significantly altered protein levels in AD brain tissue (Fig. 2a and Online Resource 2; [3]). We detected four proteins particularly enriched in $APOE^{\varepsilon3/\varepsilon3}$ cases, in comparison to the $APOE^{\varepsilon4/\varepsilon4}$ group: NOP56, NOP58, PNN, TXNDC5 (fold change ≥ 1.50, $IP_{PHF1}(APOE^{\varepsilon3/\varepsilon3})$ *vs* $IP_{PHF1}(APOE^{\varepsilon4/\varepsilon4})$, ranked by relative abundance). The 47 proteins were predominantly enriched in proteins associated with the nucleoplasm (29/47 proteins; #1 GO term "cellular component") and involved in RNA metabolic processes (19/47 proteins; #1 GO term "biological process"; Fig. 2a). A detailed analysis of the top significant functional enrichments associated with this network, ranked as per their FDR, emphasized a large predominance of functions associated with RNA binding and processing (Fig. 2b, top 5 GO terms "Cellular component"; Fig. 2c, top 5 GO terms "biological process").

The pTau interactome in sporadic AD cases with an $APOE^{\varepsilon4/\varepsilon4}$ genotype

By analogy, 35 proteins were identified as most likely pTau interactors only for $APOE^{\varepsilon4/\varepsilon4}$ cases (SAINT score ($APOE^{\varepsilon4/\varepsilon4}$) ≥ 0.80, average SAINT score ($APOE^{\varepsilon4/\varepsilon4}$) $\pm$ SEM $= 0.88 \pm 0.02$ *vs* SAINT score ($APOE^{\varepsilon3/\varepsilon3}$) < 0.80, average SAINT score ($APOE^{\varepsilon3/\varepsilon3}$) $\pm$ SEM $= 0.60 \pm 0.02$). A significant network functional enrichment was associated with these 35 proteins (PPI enrichment p value $=2.4\times10^{-3}$; Online Resource 3c). In this network, 4/35 proteins were previously reported as probable pTau interactors by our laboratory: GLS, PSMC4, PSMC5 and SSBP1 [26]. The remaining 31/35 proteins corresponded to pTau interactors identified for the first time here, although they included 30 proteins previously reported to have significantly altered protein levels in AD brain tissue (Fig. 3a and Online Resource 2; [3]). We identified eight proteins particularly enriched in $APOE^{\varepsilon4/\varepsilon4}$ cases, in comparison to the $APOE^{\varepsilon3/\varepsilon3}$ group: ARRB1, SFXN5, GNL1, GRIA2, PP2R2A, SH3GL3, GLS, AP3B1 (fold change ≥ 1.50, IP_{PHF1} ($APOE^{\varepsilon4/\varepsilon4}$) *vs* IP_{PHF1} ($APOE^{\varepsilon3/\varepsilon3}$), ranked by relative abundance). This network of 35 proteins was predominantly associated with the synaptic compartment (14/35; #1 GO term "cellular component") and involved in intracellular transport (21/35; #1 GO term "biological process"; Fig. 3a). A detailed analysis of the top significant functional enrichments associated with this network, ranked by FDR, depicted a majority of functions associated with synaptic transmission and cellular trafficking (Fig. 3b, top 5 GO terms "cellular component"; Fig. 3c, top 5 GO terms "biological process").

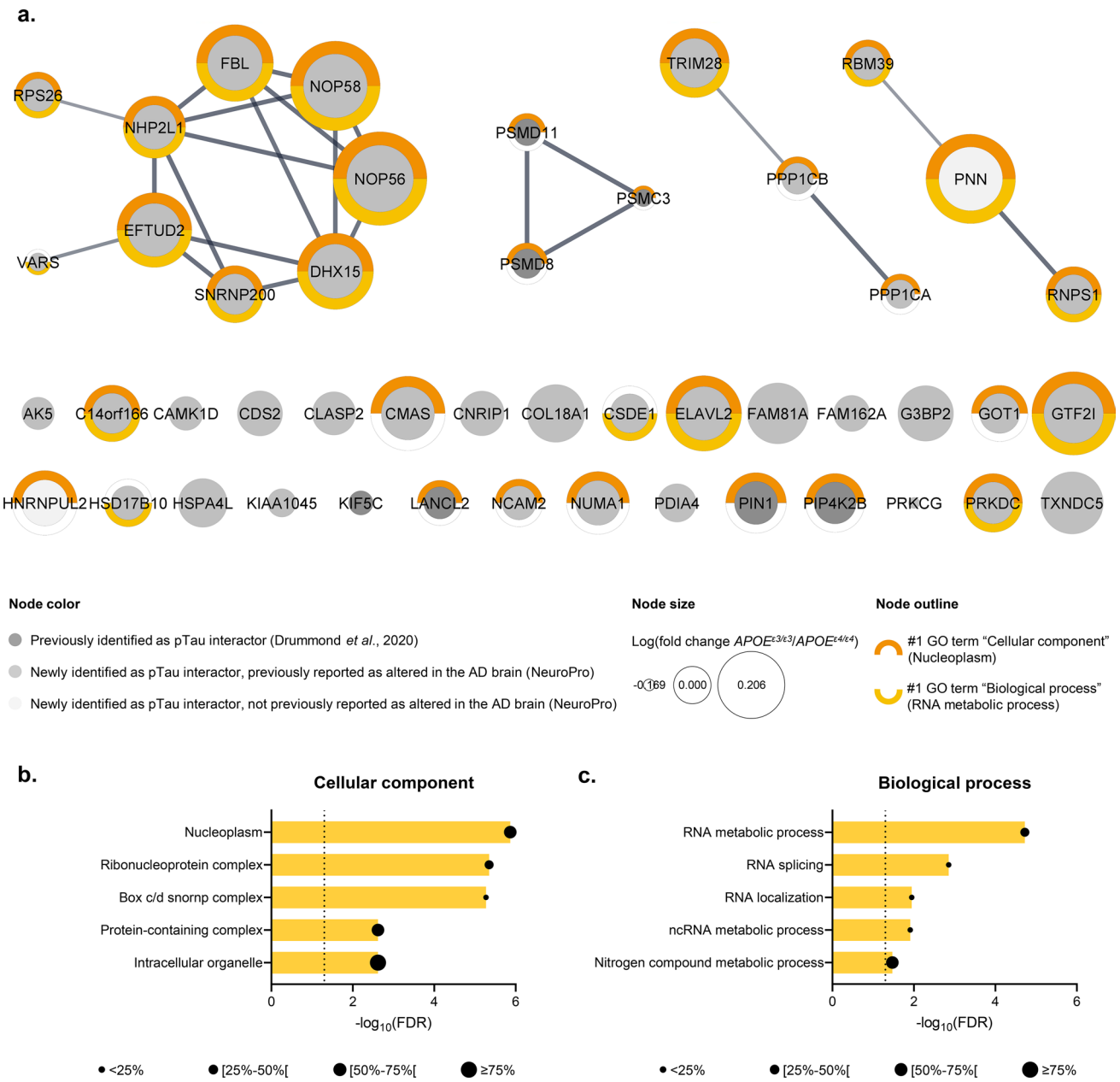

Fig. 2 The pTau interactome associated with sporadic AD cases of $APOE^{\varepsilon3/\varepsilon3}$ genotype. **a** Network representation of the 47 proteins identified as probable pTau interactors associated with the $APOE^{\varepsilon3/\varepsilon3}$ group (SAINT score ($APOE^{\varepsilon3/\varepsilon3}$) ≥ 0.80 *vs* SAINT score ($APOE^{\varepsilon4/\varepsilon4}$) < 0.80). Each protein is represented by its gene ID as a node, which size reflects its relative abundance in comparison to the $APOE^{\varepsilon4/\varepsilon4}$ group ($\log_{10}$(fold change $APOE^{\varepsilon3/\varepsilon3}/APOE^{\varepsilon4/\varepsilon4}$)). The interacting nodes are connected by edges and their thickness indicates the strength of data support with a high confidence interaction score set at 0.7 (STRING). The node color reflects the protein status regarding previous AD-related proteomic studies, as detailed in the legend. These 47 proteins were mainly associated with the nucleoplasm (29/47; #1 GO term "cellular component", *orange outline*) and involved in RNA metabolic processes (19/47; #1 GO term "biological process", *yellow outline*). **b–c** Description of the functional enrichments associated with these 47 pTau interactors specific to the $APOE^{\varepsilon3/\varepsilon3}$ group as a function of $-\log_{10}$(FDR), using "genome" as background and a redundancy cut-off of 0.7. The incorporated bubble plots reflect the number of corresponding proteins in the network as a percentage, as detailed in the legend (PPI enrichment p value = 7.1×10^{-3}; STRING and Cytoscape). The left panel details the top 5 GO terms "cellular component" (**b**), the right panel shows the top 5 GO terms "biological process" (**c**). All terms were ranked according to their FDR, the dashed lines materializing a significance threshold of FDR = 5%. *FDR* false discovery rate

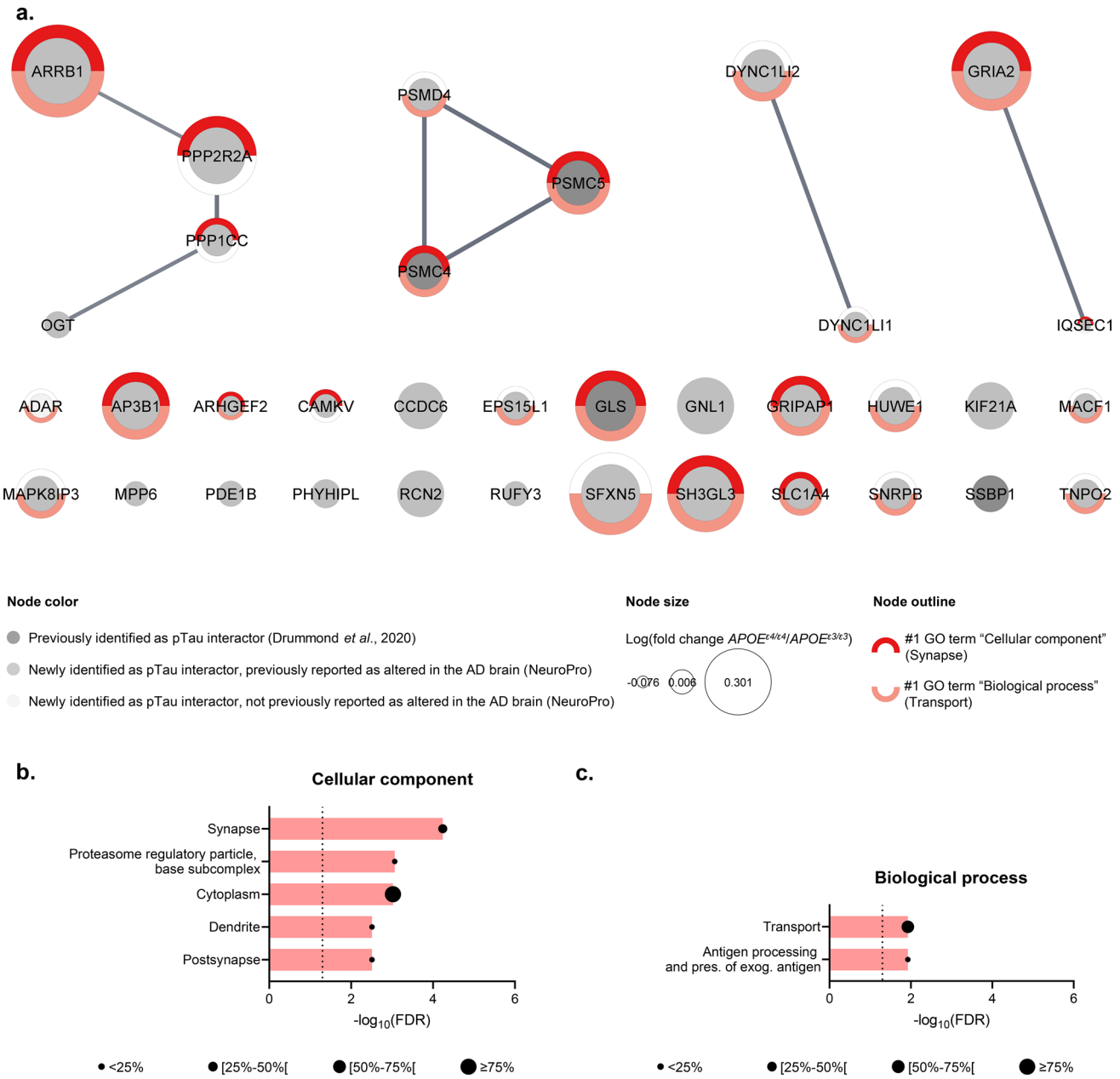

Fig. 3 The pTau interactome associated with sporadic AD cases of $APOE^{\varepsilon4/\varepsilon4}$ genotype. **a** Network representation of the 35 proteins identified as probable pTau interactors associated with the $APOE^{\varepsilon4/\varepsilon4}$ group ($APOE^{\varepsilon4/\varepsilon4}$) ≥ 0.80 *vs* SAINT score ($APOE^{\varepsilon3/\varepsilon3}$) < 0.80). Each protein is represented by its gene ID as a node, which size reflects its relative abundance in comparison to the $APOE^{\varepsilon3/\varepsilon3}$ group ($\log_{10}$(fold change $APOE^{\varepsilon4/\varepsilon4}/APOE^{\varepsilon3/\varepsilon3}$)). The interacting nodes are connected by edges and their thickness indicates the strength of data support with a high confidence interaction score set at 0.7 (STRING). The node color reflects the protein status regarding previous AD-related proteomic studies, as detailed in the legend. These 35 proteins were mainly associated with the synapse (14/35; #1 GO term "cellular component", *red outline*) and involved in transport pathways (21/35; #1 GO term "biological process", *pink outline*). **b**–**c**. Description of the functional enrichments associated with these 35 pTau interactors specific to $APOE^{\varepsilon4/\varepsilon4}$ cases as a function of $-\log_{10}$(FDR), using the total genome as background and a redundancy cut-off of 0.7. The incorporated bubble plots reflect the number of corresponding proteins in the network as a percentage, as detailed in the legend (PPI enrichment *p* value = 2.4×10^{-2}; STRING and Cytoscape). The left panel details the top 5 GO terms "cellular component" (**b**), the right panel shows the top five GO terms "biological process" (**c**). All terms were ranked according to their FDR, the dashed lines materializing a significance threshold of FDR = 5%. *FDR* false discovery rate

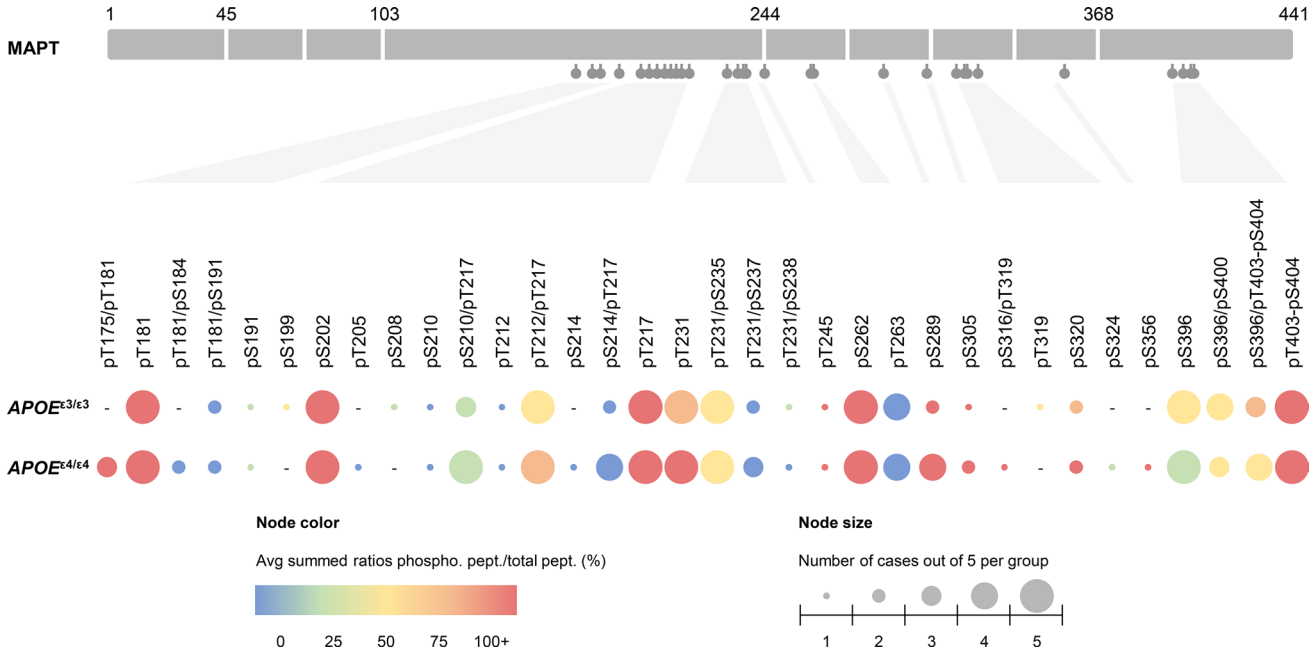

Fig. 4 The phosphorylation landscape of Tau protein across *APOE* genotypes. Tau-phosphorylation sites were identified by mass spectrometry in anti-pTau PHF1 immunoprecipitated fractions ($n=5$ $APOE^{\varepsilon3/\varepsilon3}$ cases, $n=5$ $APOE^{\varepsilon4/\varepsilon4}$ cases). All detected sites were mapped along the Tau-protein sequence, based on the 2N4R Tau isoform of 441 amino acids. The relative abundance of each phosphorylation site was represented by the node color, as detailed in the legend. The node color-code reflects the average percentage of phosphorylated peptide normalized to all observed versions of the respective peptide, for each *APOE* group. Note that some phosphorylation sites were detected across multiple Trypsin cleavage products, hence the use of summed percentages for all peptides containing the same site(s). The frequency of observation of each phosphorylated modification within a group is represented separately by the node size, as shown in the legend. The node size reflects the number of cases out of 5 total presenting with the corresponding phosphorylation site(s), for each *APOE* group. The absence of any phosphorylation site is represented by a "- "

Tau-phosphorylation landscape across APOE genotypes

The MS analysis of IP_{PHF1} products identified 30 phosphorylation sites associated with Tau proteins. Each site was mapped along Tau sequence based on the 2N4R Tau isoform of 441 amino acids, associated with its relative abundance and frequency of observation within each *APOE* group. MS analysis could not always identify the exact position of a phosphate group between T403 and S404 as the peptide backbone cleavage between these two amino acids was sometimes missing and because of an identical retention time under the LC conditions used. We therefore combined the information associated with the pT403 and pS404 sites in this analysis, referred to as pT403-pS404. The most abundant and frequently detected phosphorylation sites, alone or in combination on the same peptide, were the following: pT175 with pT181, pT181, pS202, pT212 with pT217, pT217, pT231, pT231 with pS235, pS262, pS289, pS396, pS396 with pS400, pS396 with pT403-pS404, pT403-pS404. Of note, the phosphorylation sites recognized by the anti-pTau PHF1 antibody, pS396 and pS404, were observed for all cases in both *APOE* groups, validating our success in enriching the targeted pTau proteins. As shown in Fig. 4 and Online Resource 4, the phosphorylation landscapes of Tau protein analyzed in our samples were similar between $APOE^{\varepsilon3/\varepsilon3}$ and $APOE^{\varepsilon4/\varepsilon4}$ groups, except for one observation: the combination of both pT175 and pT181 sites was only seen in the $APOE^{\varepsilon4/\varepsilon4}$ group, in which it was observed in three out of five cases on a unique peptide (IPAKpTPPAPKpTPPSSGEPPK). The unphosphorylated version of this peptide was not identified, which confirms this modification further as Trypsin can only cleave peptide bonds at the C-terminal side of lysine (K) and arginine (R) residues and will not cleave at the N-terminal side of a phosphorylated residue (Fig. 4 and Online Resource 4).

Characterization of Tau lesions among APOE groups

Our proteomic observations suggest that the expression of the AD risk factor $APOE^{\varepsilon4}$ mostly impacts pTau-subcellular location. To validate this hypothesis, a comparative quantification of Tau pathology across *APOE* genotypes was performed in the frontal cortex of 21 advanced sporadic AD cases, after an anti-pTau PHF1 immunohistochemistry ($n=11$ $APOE^{\varepsilon3/\varepsilon3}$ and $n=10$ $APOE^{\varepsilon4/\varepsilon4}$ cases).

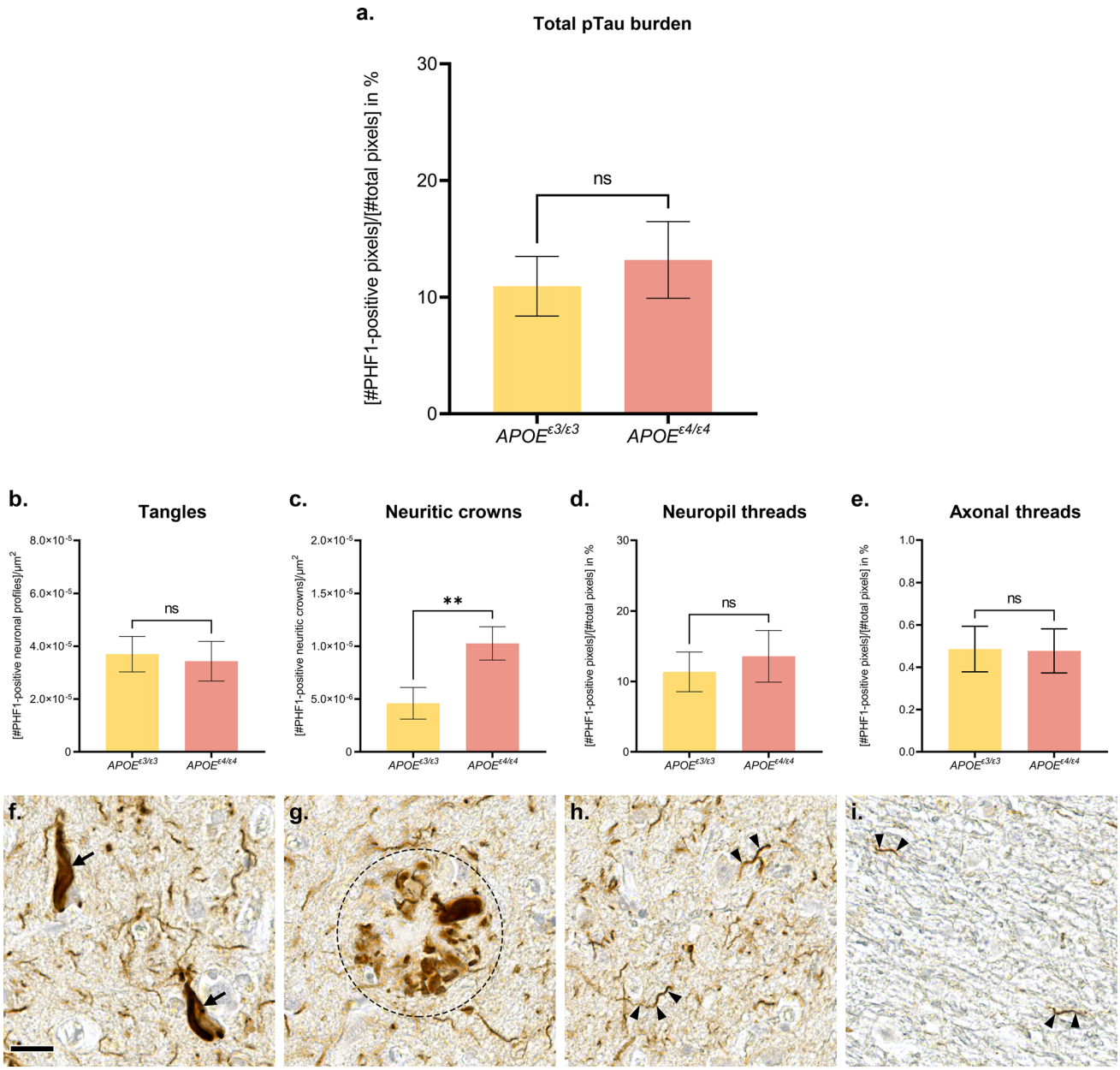

Fig. 5 Influence of *APOE*$^{\varepsilon 4}$ on Tau pathology in the frontal cortex of advanced AD cases. **a**–**i**. Histologic analysis of Tau pathology conducted on a total of $n=11$ *APOE*$^{\varepsilon 3/\varepsilon 3}$ cases and $n=10$ *APOE*$^{\varepsilon 4/\varepsilon 4}$ cases, presenting with advanced AD. Anti-pTau PHF1 immunohistochemistry with DAB revelation. Human brain, formalin-fixed paraffin-embedded frontal cortex, ×40 magnification. **a** Quantification of the total pTau burden in the frontal cortex as an averaged percentage of PHF1 positive pixels in $n=3$ ROIs/case of 5.0×10^6 µm^2 ($\pm0.5\times10^6$ µm^2) each, encompassing all cortical layers and evenly spread over the cortical section. **b** Quantification of the density of tangles in the frontal cortex as a number of PHF1 positive neuronal profiles (pre-tangles, tangles, ghost tangles) per µm^2. Analysis performed on $n=1$ ROI/case of 5.0×10^6 µm^2 ($\pm0.5\times10^6$ µm^2) covering all the cortical layers of the grey matter. **c** Quantification of the density of neuritic crowns in the frontal cortex as a number of PHF1 positive neuritic crowns per µm^2. Analysis performed on $n=1$ ROI/case of 5.0×10^6 µm^2 ($\pm0.5\times10^6$ µm^2) covering all the cortical layers of the grey matter. **d** Quantification of the burden of PHF1 positive neuropil threads as an averaged percentage of PHF1 positive pixels from $n=10$ sub-ROIs/case of 1.0×10^4 µm^2, covering neuropil areas evenly spread over all cortical layers of the grey matter and devoid of any neuronal profiles or neuritic crowns, within $n=1$ ROI/case of 5.0×10^6 µm^2 ($\pm0.5\times10^6$ µm^2). e. Quantification of the burden of PHF1 positive axonal threads as an averaged percentage of PHF1 positive pixels from $n=10$ ROIs/case of 1.0×10^5 µm^2 covering the white matter. **f**–**h**. Illustration of a tangle (f, arrows), neuritic crown (**g**, circle) and neuropil thread (**h**, arrowheads) observed in the grey matter. **i** Illustration of thin and fragmented axonal threads seen in the white matter (arrowheads). Scale bar: 20 µm. Unpaired non-parametric Mann–Whitney tests, ns $p>0.05$, $^{**}p<0.01$. *AD* Alzheimer's disease, *ROI* region of interest

As expected, the pTau burden detected in the grey matter of the frontal cortex was similar between the $APOE^{\varepsilon3/\varepsilon3}$ and $APOE^{\varepsilon4/\varepsilon4}$ groups, composed of advanced AD cases (unpaired non-parametric Mann–Whitney test, $p > 0.05$; Fig. 5a). To assess the influence of $APOE^{\varepsilon4}$ on pTau-subcellular location, the distribution of pTau aggregates among the various neuronal compartment were further analyzed. All of the well-characterized subtypes of pTau pathologic lesions linked to AD were observed in both $APOE^{\varepsilon3/\varepsilon3}$ and $APOE^{\varepsilon4/\varepsilon4}$ groups, including: neurofibrillary tangles consisting of pTau aggregates in the neuronal soma ("tangles", Fig. 5b and f), pTau-positive neuritic crowns consisting of degenerated axonal terminals and enlarged synapses which compose the neuritic amyloid plaques ("neuritic crowns", Fig. 5c and g), neuropil threads consisting of the accumulation of pTau

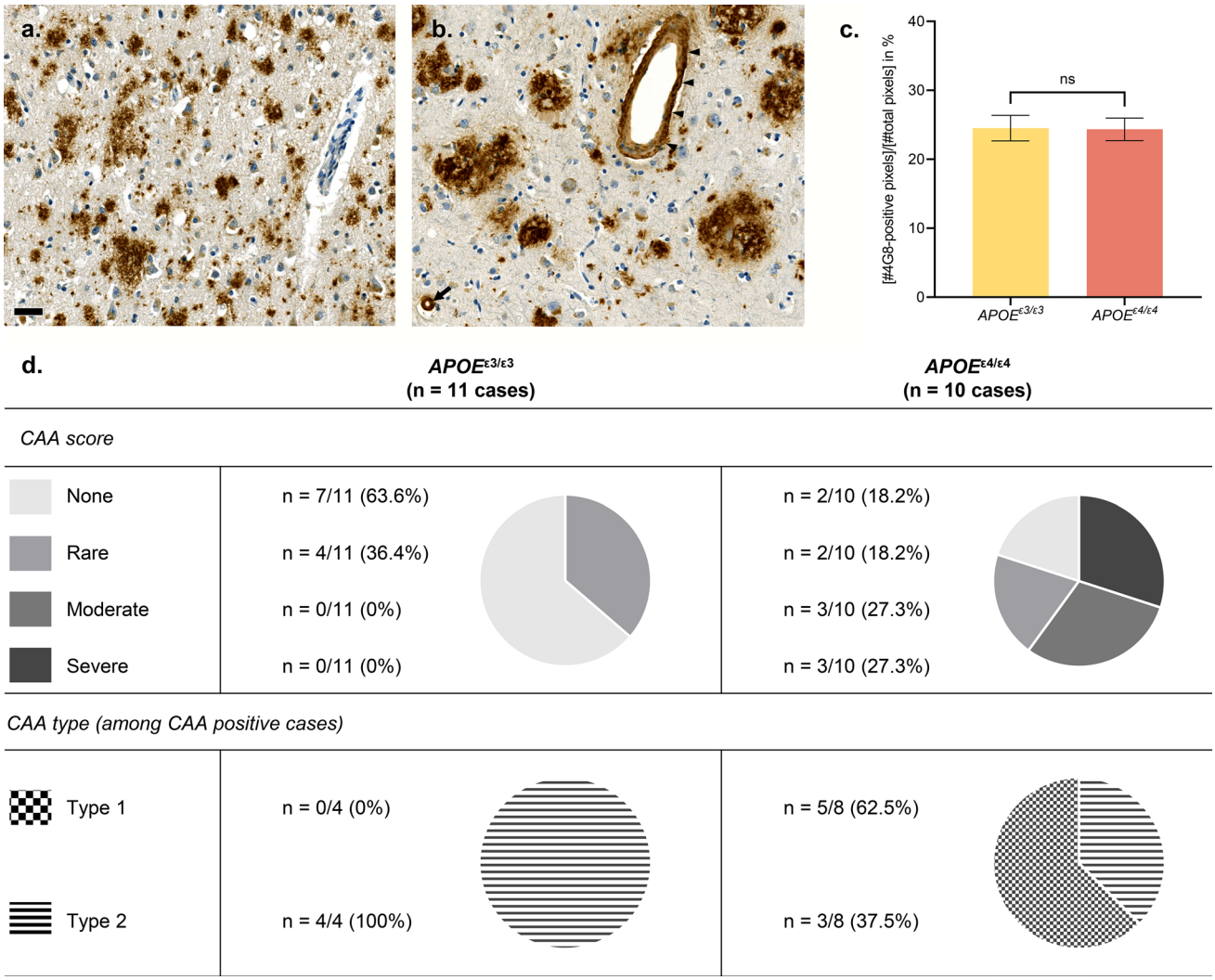

Fig. 6 Influence of $APOE^{\varepsilon4}$ on CAA frequency, severity and type in the frontal cortex of advanced AD cases. **a**–**d**. Histologic analysis of Aβ pathology conducted on a total of $n = 11$ $APOE^{\varepsilon3/\varepsilon3}$ cases and $n = 10$ $APOE^{\varepsilon4/\varepsilon4}$ cases, presenting with advanced AD. Anti-Aβ 4G8 immunohistochemistry with DAB revelation. Human brain, formalin-fixed paraffin-embedded frontal cortex, ×20 magnification. **a**–**b** Representative illustration of Aβ deposits seen in the frontal cortex of an $APOE^{\varepsilon3/\varepsilon3}$ case (**a**) and $APOE^{\varepsilon4/\varepsilon4}$ case (**b**). Note the presence of CAA in the parenchyma of the $APOE^{\varepsilon4/\varepsilon4}$ case, involving a capillary (arrow) and a larger vessel (arrowheads). Scale bar: 20 µm. **c** Quantification of the total Aβ burden in the frontal cortex as an averaged percentage of 4G8 positive pixels in $n = 3$ ROIs/case of 5.0×10^6 µm^2 ($\pm 0.5 \times 10^6$ µm^2) each, encompassing all cortical layers and evenly spread over the cortical section. Unpaired non-parametric Mann–Whitney tests, ns $p > 0.05$. **d** Descriptive table and circle diagrams showing the frequency, severity and type of CAA among a total of $n = 11$ $APOE^{\varepsilon3/\varepsilon3}$ cases and $n = 10$ $APOE^{\varepsilon4/\varepsilon4}$ cases. A semi-quantitative CAA score was attributed to each case as follows: none (no Aβ-positive vessel detected), rare (scattered Aβ-positive vessels), moderate (about 50% of Aβ-positive vessels), severe (about 100% of Aβ-positive vessels). The CAA type was evaluated among CAA positive cases as follows: type 1 (capillary CAA associated with CAA in larger vessels) or type 2 (CAA without capillary involvement). *AD* Alzheimer's disease, *CAA* Cerebral Amyloid Angiopathy, *ROI* region of interest

mostly in dendrites ("neuropil threads", Fig. 5d and h), and axonal threads consisting of thin and fragmented threads observed in the white matter ("axonal threads", Fig. 5e and i). The quantifications of tangles, neuropil threads and axonal threads did not show any differences between the $APOE^{\varepsilon3/\varepsilon3}$ and $APOE^{\varepsilon4/\varepsilon4}$ groups (unpaired non-parametric Mann–Whitney tests, $p > 0.05$, Fig. 5b, d–e). The density of pTau-positive neuritic crowns was, however, significantly higher in the $APOE^{\varepsilon4/\varepsilon4}$ cases, in comparison with the $APOE^{\varepsilon3/\varepsilon3}$ cases (unpaired non-parametric Mann–Whitney test, $p = 0.0062$, Fig. 5c); results were similar after data normalization with the pTau burden of each respective ROI (unpaired non-parametric Mann–Whitney test, $p = 0.0159$; not shown).

CAA profile among APOE groups

A comparative analysis of Aβ pathology across *APOE* genotypes was performed in the frontal cortex of 21 advanced sporadic AD cases, after an anti-Aβ 4G8 immunohistochemistry ($n = 11$ $APOE^{\varepsilon3/\varepsilon3}$ and $n = 10$ $APOE^{\varepsilon4/\varepsilon4}$ cases, Fig. 6a–b). The Aβ burden detected in the grey matter of the frontal cortex was similar between the $APOE^{\varepsilon3/\varepsilon3}$ and $APOE^{\varepsilon4/\varepsilon4}$ groups, composed of advanced AD cases (unpaired non-parametric Mann–Whitney test, $p > 0.05$; Fig. 6c). It has been recently suggested that CAA interacts with neuritic plaques to enhance Tau pathology [65]. As the expression of ApoE4 is known to exacerbate CAA [71], in addition of being strongly associated with the presence of capillary CAA [80, 81], the CAA profile was analyzed in the parenchyma of the frontal cortex in our cohort (Fig. 6d). A semi-quantitative score was attributed to each case as follows: "none" when no Aβ-positive vessel was detected in the cortical parenchyma, "rare" when only a few scattered Aβ-positive vessels were seen, "moderate" if about 50% of vessels were Aβ-positive, "severe" if about 100% of vessels were Aβ-positive. The presence of CAA was detected in 36.4% of cases in the $APOE^{\varepsilon3/\varepsilon3}$ group, while this proportion reached 72.8% of cases in the $APOE^{\varepsilon4/\varepsilon4}$ group. When present, CAA was scored as "rare" in 100% of the CAA positive cases in the $APOE^{\varepsilon3/\varepsilon3}$ group. In contrast, the CAA scores observed in the $APOE^{\varepsilon4/\varepsilon4}$ group were either "rare" (25% of the CAA positive cases), "moderate" (37.5% of the CAA positive cases) or "severe" (37.5% of the CAA positive cases; Fig. 6). The distribution of CAA types was different among *APOE* groups: whereas no capillary CAA was observed among the CAA positive cases of the $APOE^{\varepsilon3/\varepsilon3}$ group (0% of CAA type 1, 100% of CAA type 2), the presence of capillary CAA was predominant among the CAA positive cases of the $APOE^{\varepsilon4/\varepsilon4}$ group (62.5% of CAA type 1, 37.5% of CAA type 2).

Discussion

By profiling the pTau interactome selectively in $APOE^{\varepsilon3/\varepsilon3}$ and $APOE^{\varepsilon4/\varepsilon4}$ carriers for the first time, we discovered that the *APOE* genotype significantly influences the pTau pS396/pS404 interactome. We determined that the pTau interactome reflects a different subcellular localization of pTau aggregates in $APOE^{\varepsilon3/\varepsilon3}$ and $APOE^{\varepsilon4/\varepsilon4}$ cases. We confirmed this result through our follow-up immunohistochemistry studies and propose that the AD risk factor $APOE^{\varepsilon4}$ facilitates Tau-pathology progression by enhancing the accumulation of pTau in axonal endings and synapses, particularly in Aβ-affected brain regions.

A total of 80 and 68 proteins were identified as probable pTau interactors in the $APOE^{\varepsilon3/\varepsilon3}$ and $APOE^{\varepsilon4/\varepsilon4}$ groups, including 33 proteins that interacted with pTau irrespective of *APOE* genotype. These 33 common pTau interactors showed a preserved interaction of pTau with proteins involved in the ubiquitin–proteasome system among $APOE^{\varepsilon3/\varepsilon3}$ and $APOE^{\varepsilon4/\varepsilon4}$ cases. This observation confirms the importance of the ubiquitin–proteasome system in a context of defective protein clearance and protein accumulation [56, 61], while highlighting some of its key members consistently observed among pTau interactors in the AD brain, such as: SQSTM1 (also known as p62), which is involved in the shuttle of polyubiquitinated Tau for proteasomal degradation; ubiquitin/polyubiquitin precursors such as RPS27A and UBC; ubiquitin protein ligases such as ARMC8 and UBR4; several members of the PSMC and PSMD families constituting the proteasome [5, 10, 26, 60]. The detected PSMC and PSMD members constitute only the lid and base of the 26S proteasome regulatory subunit involved in substrate recognition, deubiquitylation and unfolding, underlining the specificity of our approach [7]. Proteins involved in the regulation of RNA processing were also detected among the common pTau interactors, supporting an important role of RNA metabolism and translational stress response in Tau pathology as suggested by other studies [43]. These new results extend our previous analysis by bringing to light additional RNA-associated proteins of interest, which were previously detected as present in the neurofibrillary tangle proteome, although they were below the threshold to be considered as pTau interactors so far [26]: the splicing factors SRSF1 (also known as SF2/ASF) and TRA2B, involved in the regulation of the alternative splicing of Tau exon 10 impacting the ratio of Tau isoforms with three or four microtubule binding repeats domains (3R or 4R, with a 4R:3R ratio shifted from approximately 1:1 to 2:1 in AD) [17, 20, 33]. Interestingly, a large proportion of the proteins identified as probable pTau interactors in the $APOE^{\varepsilon3/\varepsilon3}$ and $APOE^{\varepsilon4/\varepsilon4}$ groups did not overlap. This observation

cannot be explained by the inclusion of differing stages of AD pathology among *APOE* groups, as this study was conducted on an homogenous selection of sporadic cases diagnosed with an advanced AD pathology at autopsy (A3, B3, C3 scores [55]). This key result supports an influence of *APOE* expression on pTau metabolism in the AD brain.

A total of 47 proteins were identified as probable pTau interactors only for $APOE^{\varepsilon3/\varepsilon3}$ cases, while 35 proteins were detected as probable pTau interactors only for $APOE^{\varepsilon4/\varepsilon4}$ cases. A robust segregation of their associated functions and cell compartments was observed. The pTau interactome specific to $APOE^{\varepsilon3/\varepsilon3}$ cases contained a majority of nucleoplasmic proteins, involved in RNA binding and processing. PNN, a newly identified pTau interactor, was particularly enriched in $APOE^{\varepsilon3/\varepsilon3}$ cases and recently characterized in vitro as involved in the formation of RNA condensates defining subcellular sites of Tau aggregation [45, 46]. In vitro, Tau coacervates with polyanions, such as RNA, into liquid droplets [38, 47, 95]. The colocalization of Tau with RNA and RNA binding proteins in the cell can result in the formation of stress granules involved in protein-level regulation [2, 62], although experimental observations suggest that such complexes drive Tau aggregation [2, 38, 42, 52]. In AD neurons, pTau is accumulated at the nuclear envelope in a discrete manner, which correlates with nuclear component mis-localization [29, 38]. Our results support a predominance of these biologic events in $APOE^{\varepsilon3/\varepsilon3}$ cases. They can be protective in the early stages of the pathology, slowing down Tau pathology by sequestering pTau species at the nucleus while triggering the translational stress response. Over time, deleterious outcomes may take over including a promotion of pTau self-aggregation [2, 38, 42, 52] or a nucleocytoplasmic transport disruption [29, 94]. In contrast, the pTau interactome specific to $APOE^{\varepsilon4/\varepsilon4}$ cases contained a majority of synaptic proteins, involved in cell transport. ARRB1, a newly identified pTau interactor particularly enriched in the $APOE^{\varepsilon4/\varepsilon4}$ group, is a representative synaptic protein recently described as a promoter of Tau pathology [92]. Tau pathology in $APOE^{\varepsilon4/\varepsilon4}$ cases may be characterized by a predominant pool of dynamic pTau species, more prone to be transported to the synapse, which can facilitate the trans-synaptic progression of Tau pathology [88, 93] and Tau-mediated synaptic disruption [86]. We did not observe any major effect of $APOE^{\varepsilon4}$ on Tau-phosphorylation sites, as suggested by recent experimental observations [69]. Only the pT175/pT181 modification was specific to the $APOE^{\varepsilon4/\varepsilon4}$ group, although this result requires further investigations since this study is based on a selected fraction of pTau that is phosphorylated on pS396/pS404 and obtained from *post-mortem* material [32]. We suggest that the expression of the AD risk factor $APOE^{\varepsilon4}$ mostly impacts pTau-subcellular location.

A comprehensive analysis of the various subcellular lesions composing Tau pathology in $APOE^{\varepsilon3/\varepsilon3}$ and $APOE^{\varepsilon4/\varepsilon4}$ cases confirmed our hypothesis. The density of pTau-positive neuritic crowns was higher in $APOE^{\varepsilon4/\varepsilon4}$ vs $APOE^{\varepsilon3/\varepsilon3}$ cases, despite the confirmation of an even burden of Tau pathology among cases. Neuritic crowns are made of pTau-positive degenerated neurites wrapping the most mature type of Aβ deposits, constituting the neuritic amyloid plaque – or senile plaque [27]. The immunohistochemical signature of these pTau-positive neuritic crowns [72, 84], along with the observation of presynaptic vesicles [79], demonstrate their axonal nature. This observation aligns with our proteomics findings and further support an effect of $APOE^{\varepsilon4}$ on pTau cellular transport and relocation toward axonal endings and synapses. Tau pathology progresses from neuron to neuron through synaptic connections [16, 28, 83, 88, 93]; we hypothesize that the spreading of pathological pTau species is accelerated in $APOE^{\varepsilon4/\varepsilon4}$ carriers, in accordance with recent clinical observations [8, 75]. In vivo experiments support an Aβ-independent influence of $APOE^{\varepsilon4}$ on Tau-pathology spreading, by demonstrating an exacerbation of Tau pathology in PS19 mice expressing human $APOE^{\varepsilon4/\varepsilon4}$ [74], but a recent study questions this scenario [21]. These results suggest a direct consequence of *APOE* genotype itself on Tau pathology (*e.g.,* the proteins identified in the present study as pTau interactors more associated with one *APOE* genotype or another could have different expression levels in control brains). This possibility is illustrated by the recent identification of 25 unique proteins defining the incipient AD proteomic signature, including 24 increased in young heterogenous $APOE^{\varepsilon4}$ carriers, while 1 protein was reduced in comparison to aged-matched *APOEε4* non-carriers [67]. Although we could not identify any of our 47 $APOE^{\varepsilon3}$-associated and 35 $APOE^{\varepsilon4}$-associated pTau interactors in this list of 25 candidates, future studies are needed to address this possibility by better understanding how the AD risk factor $APOE^{\varepsilon4}$ shapes the basal metabolism of the brain. While they are not mutually exclusive, an alternative scenario involves an Aβ-mediated effect of *APOE* on Tau pathology. The expression of the $APOE^{\varepsilon4}$ allele is indeed strongly associated with an exacerbation of Aβ pathology, by promoting particularly the development of neuritic amyloid plaques and of CAA with a capillary involvement [70, 81, 90], as confirmed in our cohort. Recent neuropathological and clinical studies show that CAA interacts with neuritic amyloid plaques to enhance tau pathology and white-matter rarefaction [50, 59, 65]. We propose that the AD risk factor $APOE^{\varepsilon4}$ promotes neuritic degeneration, resulting in the accumulation of pTau in axonal endings and synapses which may facilitate Tau-pathology progression, particularly toward Aβ-affected brain regions.

Limitations

While there were many consistencies with our previous pTau interactome study [26], our results did not completely replicate our previous findings. The inter-individual variability associated with *post-mortem* human brain studies, combined with a modified MS method used here, could explain these differences. In our current study, our MS protocol was adjusted to simplify our workflow. To prevent the excess of antibodies co-eluted in the immunoprecipitated product from hindering the detection of proteins with similar mass weight and elution times, immunoprecipitated products were previously run on a gel from which bands containing antibodies were excised and analyzed separately on the mass spectrometer [26]. Here, we opted for a different strategy to minimize sample processing prior to MS analysis: a proteolytic digestion was performed straight on the antigen–antibody-bead complexes without removing antibodies prior to downstream proteomic analysis, increasing the power of our study by allowing a better technical consistency. Furthermore, our designation of "pTau interactors" relied on the binarization of a continuum of probabilistic scores, based on the use of a stringent threshold corresponding to a FDR of 5%. Although this strategy allows for the reduction of false positives and a focus on the most probable pTau interactors for a more stringent analysis, it increases the risk of false negatives among the proteins that did not pass the threshold. Altogether, these limitations explain why some important pTau interactors may be missing in the present study and emphasize the need to generate more AD-related proteomic datasets, to counterbalance inter-experimental differences. Although pathologically relevant, these proteomic findings may reflect advanced biologic responses in AD, as they are associated with the late epitope pTau pS396/pS404 extracted from advanced AD cases. It is still unclear if a different subset of pTau species interacts with different proteins. These aspects need to be further addressed in future investigations by exploring the interactome of alternative pTau epitopes, especially early ones extracted from early and intermediate stage AD cases.

Conclusion and perspectives

This study provides evidence for an influence of *APOE* expression on pTau-subcellular location, suggesting a greater variation of Tau pathology across AD cases. Indeed, these new results emphasize the complexity of Tau studies, as factors such as genotype can modify the subcellular localization of pTau and therefore its interactome. Our results pave the way to the potential identification of new therapeutic targets specific for $APOE^{\varepsilon 4}$ carriers.

Supplementary Information The online version contains supplementary material available at https://doi.org/10.1007/s00401-024-02744-8.

Acknowledgements This manuscript was supported by NIH grants P01AG060882 and P30AG066512 (to T.W.), and funding from the Bluesand Foundation (to E.D.). We thank the Columbia University Alzheimer's Disease Research Center, funded by NIH grant P30AG066462 to S.A. Small (P.I.), and A. Teich for providing biological samples and associated information. We also thank A. Cardiel and J. Xie for their technical assistance with this project.

Data availability The mass spectrometric raw files are accessible at https://massive.ucsd.edu under accession MassIVE MSV000094757 and at www.proteomexchange.org under accession PXD052263.

References

1. Arboleda-Velasquez J, Lopera F, O'Hare M, Delgado-Tirado S, Marino C, Chmielewska N et al (2019) Resistance to autosomal dominant Alzheimer's disease in an APOE3 Christchurch homozygote: a case report. Nat Med 25:1680–1683. https://doi.org/10.1038/S41591-019-0611-3
2. Ash PEA, Lei S, Shattuck J, Boudeau S, Carlomagno Y, Medalla M et al (2021) TIA1 potentiates tau phase separation and promotes generation of toxic oligomeric tau. Proc Natl Acad Sci USA. https://doi.org/10.1073/PNAS.2014188118/-/DCSUPPLEMENTAL
3. Askenazi M, Kavanagh T, Pires G, Ueberheide B, Wisniewski T, Drummond E (2023) Compilation of reported protein changes in the brain in Alzheimer's disease. Nat Commun 141(14):1–15. https://doi.org/10.1038/s41467-023-40208-x
4. Ayyadevara S, Balasubramaniam M, Parcon PA, Barger SW, Griffin WST, Alla R et al (2016) Proteins that mediate protein aggregation and cytotoxicity distinguish Alzheimer's hippocampus from normal controls. Aging Cell 15:924–939. https://doi.org/10.1111/ACEL.12501
5. Babu JR, Geetha T, Wooten MW (2005) Sequestosome 1/p62 shuttles polyubiquitinated tau for proteasomal degradation. J Neurochem 94:192–203. https://doi.org/10.1111/J.1471-4159.2005.03181.X
6. Bales KR, Verina T, Dodel RC, Du Y, Altstiel L, Bender M et al (1997) Lack of apolipoprotein E dramatically reduces amyloid β-peptide deposition. Nat Genet 173(17):263–264. https://doi.org/10.1038/ng1197-263
7. Bard JAM, Goodall EA, Greene ER, Jonsson E, Dong KC, Martin A (2018) Structure and function of the 26S proteasome. Annu Rev

Biochem 87:697. https://doi.org/10.1146/ANNUREV-BIOCHEM-062917-011931
8. Benson GS, Bauer C, Hausner L, Couturier S, Lewczuk P, Peters O et al (2022) Don't forget about tau: the effects of ApoE4 genotype on Alzheimer's disease cerebrospinal fluid biomarkers in subjects with mild cognitive impairment-data from the Dementia competence network. J Neural Transm 129:477–486. https://doi.org/10.1007/S00702-022-02461-0
9. Betters RK, Luhmann E, Gottschalk AC, Xu Z, Shin MR, Ptak CP et al (2023) Characterization of the Tau interactome in human brain reveals isoform-dependent interaction with 14–3–3 family proteins. Neuro 10:1–11. https://doi.org/10.1523/ENEURO.0503-22.2023
10. Blaudin de Thé FX, Lassus B, Schaler AW, Fowler SL, Goulbourne CN, Jeggo R et al (2021) P62 accumulates through neuroanatomical circuits in response to tauopathy propagation. Acta Neuropathol Commun. https://doi.org/10.1186/S40478-021-01280-W
11. Boyles JK, Pitas RE, Wilson E, Mahley RW, Taylor JM (1985) Apolipoprotein E associated with astrocytic glia of the central nervous system and with nonmyelinating glia of the peripheral nervous system. J Clin Invest 76:1501–1513. https://doi.org/10.1172/JCI112130
12. Braak H, Braak E (1991) Neuropathological stageing of Alzheimer-related changes. Acta Neuropathol 82:239–259
13. Brecht WJ, Harris FM, Chang S, Tesseur I, Yu GQ, Xu Q et al (2004) Neuron-specific apolipoprotein e4 proteolysis is associated with increased tau phosphorylation in brains of transgenic mice. J Neurosci 24:2527–2534. https://doi.org/10.1523/JNEUROSCI.4315-03.2004
14. Brion JP, Passareiro H, Nunez J, Flament-Durand J (1985) Mise en évidence immunologique de la protéine Tau au niveau des lésions de dégénérescence neurofibrillaire de la maladie d'Alzheimer. Arch Biol (Bruxelles) 95:229–235
15. Castellano JM, Kim J, Stewart FR, Jiang H, DeMattos RB, Patterson BW et al (2011) Human apoE isoforms differentially regulate brain amyloid-β peptide clearance. Sci Transl Med. https://doi.org/10.1126/SCITRANSLMED.3002156/SUPPL_FILE/3-89RA57_SM.PDF
16. Clavaguera F, Bolmont T, Crowther RAA, Abramowski D, Frank S, Probst A et al (2009) Transmission and spreading of tauopathy in transgenic mouse brain. Nat Cell Biol 11:909–913. https://doi.org/10.1038/ncb1901
17. Conrad C, Zhu J, Conrad C, Schoenfeld D, Fang Z, Ingelsson M et al (2007) Single molecule profiling of tau gene expression in Alzheimer's disease. J Neurochem 103:1228–1236. https://doi.org/10.1111/J.1471-4159.2007.04857.X
18. Corder E, Saunders A, Risch N, Strittmatter W, Schmechep D, Gaskell P et al (1994) Protective effect of apolipoprotein E type 2 allele for late onset Alzheimer disease. Nat Gen 7:180–184
19. Corder E, Saunders A, Strittmatter W, Schmechel D, Gaskell P, Small G et al (1993) Gene dose of apolipoprotein E type 4 allele and the risk of Alzheimer's disease in late onset families. Science (80-) 261:921–923
20. D'Souza I, Schellenberg GD (2006) Arginine/serine-rich protein interaction domain-dependent modulation of a tau exon 10 splicing enhancer: altered interactions and mechanisms for functionally antagonistic FTDP-17 mutations Delta280K AND N279K. J Biol Chem 281:2460–2469. https://doi.org/10.1074/JBC.M505809200
21. Davies C, Tulloch J, Yip E, Currie L, Colom-Cadena M, Wegmann S et al (2023) Apolipoprotein E isoform does not influence trans-synaptic spread of tau pathology in a mouse model. Brain Neurosci Adv. https://doi.org/10.1177/23982128231191046
22. Delaère P, Duyckaerts C, He Y, Piette F, Hauw JJ (1991) Subtypes and differential laminar distributions of beta A4 deposits in Alzheimer's disease: relationship with the intellectual status of 26 cases. Acta Neuropathol 81:328–335. https://doi.org/10.1007/bf00305876
23. Dodart JC, Marr RA, Koistinaho M, Gregersen BM, Malkani S, Verma IM et al (2005) Gene delivery of human apolipoprotein E alters brain Aβ burden in a mouse model of Alzheimer's disease. Proc Natl Acad Sci USA 102:1211. https://doi.org/10.1073/PNAS.0409072102
24. Drummond E, Kavanagh T, Pires G, Marta-Ariza M, Kanshin E, Nayak S et al (2022) The amyloid plaque proteome in early onset Alzheimer's disease and Down syndrome. Acta Neuropathol Commun 101(10):1–24. https://doi.org/10.1186/S40478-022-01356-1
25. Drummond E, Nayak S, Pires G, Ueberheide B, Wisniewski T (2018) Isolation of amyloid plaques and neurofibrillary tangles from archived alzheimer's disease tissue using laser-capture microdissection for downstream proteomics. Methods Mol Biol 1723:319–334. https://doi.org/10.1007/978-1-4939-7558-7_18
26. Drummond E, Pires G, MacMurray C, Askenazi M, Nayak S, Bourdon M et al (2020) Phosphorylated tau interactome in the human Alzheimer's disease brain. Brain 143:2803–2817. https://doi.org/10.1093/BRAIN/AWAA223
27. Duyckaerts C, Delatour B, Potier M-C (2009) Classification and basic pathology of Alzheimer disease. Acta Neuropathol 118:5–36. https://doi.org/10.1007/s00401-009-0532-1
28. Duyckaerts C, Uchihara T, Seilhean D, He Y, Hauw J-J (1997) Dissociation of Alzheimer type pathology in a disconnected piece of cortex. Acta Neuropathol 93:501–507
29. Eftekharzadeh B, Daigle JG, Kapinos LE, Coyne A, Schiantarelli J, Carlomagno Y et al (2018) Tau protein disrupts nucleocytoplasmic transport in alzheimer's disease. Neuron 99:925-940.e7. https://doi.org/10.1016/J.NEURON.2018.07.039
30. Fagan AM, Holtzman DM, Munson G, Mathur T, Schneider D, Chang LK et al (1999) Unique lipoproteins secreted by primary astrocytes from wild type, apoE (-/-), and human apoE transgenic mice. J Biol Chem 274:30001–30007. https://doi.org/10.1074/JBC.274.42.30001
31. Fryer JD, Taylor JW, DeMattos RB, Bales KR, Paul SM, Parsadanian M et al (2003) Apolipoprotein E markedly facilitates age-dependent cerebral amyloid angiopathy and spontaneous hemorrhage in amyloid precursor protein transgenic mice. J Neurosci 23:7889–7896. https://doi.org/10.1523/JNEUROSCI.23-21-07889.2003
32. Gärtner U, Janke C, Holzer M, Vanmechelen E, Arendt T (1998) Postmortem changes in the phosphorylation state of tau-protein in the rat brain. Neurobiol Aging 19:535–543. https://doi.org/10.1016/S0197-4580(98)00094-3
33. Ginsberg SD, Che S, Counts SE, Mufson EJ (2006) Shift in the ratio of three-repeat tau and four-repeat tau mRNAs in individual cholinergic basal forebrain neurons in mild cognitive impairment and Alzheimer's disease. J Neurochem 96:1401–1408. https://doi.org/10.1111/J.1471-4159.2005.03641.X
34. Glenner GG, Wong CW (1984) Alzheimer's disease: initial report of the purification and characterization of a novel cerebrovascular amyloid protein. Biochem Biophys Res Commun 120:885–890. https://doi.org/10.1016/s0006-291x(84)80190-4
35. Greenberg SG, Davies P, Schein JD, Binder LI (1992) Hydrofluoric acid-treated tau PHF proteins display the same biochemical properties as normal tau. J Biol Chem 267:564–569. https://doi.org/10.1016/S0021-9258(18)48531-6
36. Grundke-Iqbal I, Iqbal K, Quinlan M, Tung Y, Zaidi M, Wisniewski H (1986) Microtubule-associated protein tau. A component of Alzheimer paired helical filaments. J Biol Chem 261:6084–6089
37. Grundke-Iqbal I, Iqbal K, Tung YC, Quinlan M, Wisniewski HM, Binder LI (1986) Abnormal phosphorylation of the microtubule-associated protein tau (tau) in Alzheimer cytoskeletal

pathology. 83:4913–4917. https://doi.org/10.1073/pnas.83.13.4913
38. Hochmair J, Exner C, Franck M, Dominguez-Baquero A, Diez L, Brognaro H, Kraushar ML, Mielke T, Radbruch H, Kaniyappan S, Falke S, Mandelkow E, Betzel C, Wegmann S (2022) Molecular crowding and RNA synergize to promote phase separation, microtubule interaction, and seeding of Tau condensates. EMBO J https://doi.org/10.15252/EMBJ.2021108882/SUPPL_FILE/EMBJ2021108882-SUP-0002-MOVIEEV1.ZIP
39. Holtzman DM, Bales KR, Tenkova T, Fagan AM, Parsadanian M, Sartorius LJ et al (2000) Apolipoprotein E isoform-dependent amyloid deposition and neuritic degeneration in a mouse model of Alzheimer's disease. Proc Natl Acad Sci U S A 97:2892–2897. https://doi.org/10.1073/PNAS.050004797/ASSET/63D22B0F-2005-4799-9F0A-55761F108B24/ASSETS/GRAPHIC/PQ0500047005.GIF
40. Hsieh YC, Guo C, Yalamanchili HK, Abreha M, Al-Ouran R, Li Y et al (2019) Tau-mediated disruption of the spliceosome triggers cryptic RNA splicing and neurodegeneration in Alzheimer's disease. Cell Rep 29:301-316.e10. https://doi.org/10.1016/J.CELREP.2019.08.104
41. Innerarity TL, Friedlander EJ, Rall SC, Weisgraber KH, Mahley RW (1983) The receptor-binding domain of human apolipoprotein E. Binding of apolipoprotein E fragments. J Biol Chem 258:12341–12347. https://doi.org/10.1016/S0021-9258(17)44180-9
42. Kanaan NM, Hamel C, Grabinski T (2020) Combs B (2020) Liquid-liquid phase separation induces pathogenic tau conformations in vitro. Nat Commun 111(11):1–16. https://doi.org/10.1038/s41467-020-16580-3
43. Kavanagh T, Halder A, Drummond E (2022) Tau interactome and RNA binding proteins in neurodegenerative diseases. Mol Neurodegener. https://doi.org/10.1186/S13024-022-00572-6
44. Koutsodendris N, Blumenfeld J, Agrawal A, Traglia M, Grone B, Zilberter M, Yip O, Rao A, Nelson MR, Hao Y, Thomas R, Yoon SY, Arriola P, Huang Y (2023) Neuronal APOE4 removal protects against tau-mediated gliosis, neurodegeneration and myelin deficits. https://doi.org/10.1038/s43587-023-00368-3
45. Lester E, Van Alstyne M, McCann KL, Reddy S, Cheng LY, Kuo J et al (2023) Cytosolic condensates rich in polyserine define subcellular sites of tau aggregation. Proc Natl Acad Sci USA. https://doi.org/10.1073/PNAS.2217759120
46. Lester E, Ooi FK, Bakkar N, Ayers J, Woerman AL, Wheeler J et al (2021) Tau aggregates are RNA-protein assemblies that mislocalize multiple nuclear speckle components. Neuron 109:1675-1691.e9. https://doi.org/10.1016/J.NEURON.2021.03.026
47. Lin Y, McCarty J, Rauch JN, Delaney KT, Kosik KS, Fredrickson GH et al (2019) Narrow equilibrium window for complex coacervation of tau and RNA under cellular conditions. Elife. https://doi.org/10.7554/ELIFE.42571
48. Litvinchuk A, Suh JH, Guo JL, Lin K, Davis SS, Bien-Ly N et al (2023) Amelioration of Tau and ApoE4-linked glial lipid accumulation and neurodegeneration with an LXR agonist. Neuron. https://doi.org/10.1016/J.NEURON.2023.10.023
49. Liu C, Song X, Nisbet R, Götz J (2016) Co-immunoprecipitation with Tau Isoform-specific antibodies reveals distinct protein interactions and highlights a putative role for 2N tau in disease. J Biol Chem 291:8173–8188. https://doi.org/10.1074/JBC.M115.641902
50. Malek-Ahmadi M, Perez SE, Chen K, Mufson EJ (2020) Braak stage, cerebral amyloid angiopathy, and cognitive decline in early Alzheimer's disease. J Alzheimers Dis 74:189. https://doi.org/10.3233/JAD-191151
51. Maziuk BF, Apicco DJ, Cruz AL, Jiang L, Ash PEA, da Rocha EL et al (2018) RNA binding proteins co-localize with small tau inclusions in tauopathy. Acta Neuropathol Commun 6:71. https://doi.org/10.1186/S40478-018-0574-5
52. McMillan PJ, Benbow SJ, Uhrich R, Saxton A, Baum M, Strovas T et al (2023) Tau-RNA complexes inhibit microtubule polymerization and drive disease-relevant conformation change. Brain 146:3206–3220. https://doi.org/10.1093/BRAIN/AWAD032
53. Meier S, Bell M, Lyons DN, Ingram A, Chen J, Gensel JC et al (2015) Identification of novel tau interactions with endoplasmic reticulum proteins in Alzheimer's disease brain. J Alzheimers Dis 48:687–702. https://doi.org/10.3233/JAD-150298
54. Montal V, Diez I, Kim CM, Orwig W, Bueichekú E, Gutiérrez-Zúñiga R et al (2022) Network Tau spreading is vulnerable to the expression gradients of APOE and glutamatergic-related genes. Sci Transl Med. https://doi.org/10.1126/SCITRANSLMED.ABN7273
55. Montine TJ, Phelps CH, Beach TG, Bigio EH, Cairns NJ, Dickson DW et al (2012) National institute on aging-Alzheimer's association guidelines for the neuropathologic assessment of Alzheimer's disease: a practical approach. Acta Neuropathol 123:1–11. https://doi.org/10.1007/s00401-011-0910-3
56. Mori H, Kondo J, Ihara Y (1987) Ubiquitin is a component of paired helical filaments in Alzheimer's disease. Science 235:1641–1644. https://doi.org/10.1126/SCIENCE.3029875
57. Namba Y, Tomonaga M, Kawasaki H, Otomo E, Ikeda K (1991) Apolipoprotein E immunoreactivity in cerebral amyloid deposits and neurofibrillary tangles in Alzheimer's disease and kuru plaque amyloid in Creutzfeldt-Jakob disease. Brain Res 541:163–166
58. Nelson PT, Alafuzoff I, Bigio EH, Bouras C, Braak H, Cairns NJ et al (2012) Correlation of Alzheimer disease neuropathologic changes with cognitive status: a review of the literature. J Neuropathol Exp Neurol 71:362–381
59. Nichols JB, Malek-Ahmadi M, Tariot PN, Serrano GE, Sue LI, Beach TG (2021) Vascular lesions, APOE ε4, and tau pathology in Alzheimer disease. J Neuropathol Exp Neurol 80:240. https://doi.org/10.1093/JNEN/NLAA160
60. Ono M, Komatsu M, Ji B, Takado Y, Shimojo M, Minamihisamatsu T et al (2022) Central role for p62/SQSTM1 in the elimination of toxic tau species in a mouse model of tauopathy. Aging Cell. https://doi.org/10.1111/ACEL.13615
61. Perry G, Friedman R, Shaw G, Chau V (1987) Ubiquitin is detected in neurofibrillary tangles and senile plaque neurites of Alzheimer disease brains. Proc Natl Acad Sci USA 84:3033–3036. https://doi.org/10.1073/PNAS.84.9.3033
62. Piatnitskaia S, Takahashi M, Kitaura H, Katsuragi Y, Kakihana T, Zhang L et al (2019) Fujii M (2019) USP10 is a critical factor for Tau-positive stress granule formation in neuronal cells. Sci Rep 91(9):1–15. https://doi.org/10.1038/s41598-019-47033-7
63. Pires G, McElligott S, Drusinsky S, Halliday G, Potier MC, Wisniewski T et al (2019) Secernin-1 is a novel phosphorylated tau binding protein that accumulates in Alzheimer's disease and not in other tauopathies. Acta Neuropathol Commun. https://doi.org/10.1186/S40478-019-0848-6
64. Pires G, Ueberheide B, Wisniewski T, Drummond E (2023) Use of affinity purification-mass spectrometry to identify phosphorylated tau interactors in Alzheimer's disease. Methods Mol Biol 2561:263–277. https://doi.org/10.1007/978-1-0716-2655-9_14
65. Rabin JS, Nichols E, La Joie R, Casaletto KB, Palta P, Dams-O'Connor K et al (2022) Cerebral amyloid angiopathy interacts with neuritic amyloid plaques to promote tau and cognitive decline. Brain 145:2823–2833. https://doi.org/10.1093/BRAIN/AWAC178
66. Rebeck WG, Reiter JS, Strickland DK, Hyman BT (1993) Apolipoprotein E in sporadic Alzheimer's disease: allelic variation and receptor interactions. Neuron 11:575–580. https://doi.org/10.1016/0896-6273(93)90070-8

67. Roberts JA, Varma VR, An Y, Varma S, Candia J, Fantoni G et al (2021) A brain proteomic signature of incipient Alzheimer's disease in young APOE ε4 carriers identifies novel drug targets. Sci Adv 7:8178. https://doi.org/10.1126/SCIADV.ABI8178
68. Saito H, Dhanasekaran P, Baldwin F, Weisgraber KH, Lund-Katz S, Phillips MC (2001) Lipid binding-induced conformational change in human apolipoprotein E. Evid Two Lipid-Bound States Spher Particles. https://doi.org/10.1074/jbc.M106337200
69. Saroja SR, Gorbachev K, Tcw J, Goate AM, Pereira AC (2022) Astrocyte-secreted glypican-4 drives APOE4-dependent tau hyperphosphorylation. Proc Natl Acad Sci USA. https://doi.org/10.1073/PNAS.2108870119
70. Schmechel DE, Saunders AM, Strittmatter WJ, Crain BJ, Hulette CM, Joo SH et al (1993) Increased amyloid beta-peptide deposition in cerebral cortex as a consequence of apolipoprotein E genotype in late-onset Alzheimer disease. Proc Natl Acad Sci 90:9649–9653. https://doi.org/10.1073/PNAS.90.20.9649
71. Schmechel DE, Saunders AM, Strittmatter WJ, Crain BJ, Hulette CM, Joo SH et al (1993) Increased amyloid beta-peptide deposition in cerebral cortex as a consequence of apolipoprotein E genotype in late-onset Alzheimer disease. Proc Natl Acad Sci U S A 90:9649. https://doi.org/10.1073/PNAS.90.20.9649
72. Schmidt ML, Lee VM, Trojanowski JQ (1991) Comparative epitope analysis of neuronal cytoskeletal proteins in Alzheimer's disease senile plaque neurites and neuropil threads. Lab Invest 64:352–357
73. Sepulveda-Falla D, Sanchez JS, Almeida MC, Boassa D, Acosta-Uribe J, Vila-Castelar C et al (2022) Distinct tau neuropathology and cellular profiles of an APOE3 Christchurch homozygote protected against autosomal dominant Alzheimer's dementia. Acta Neuropathol 144:589–601. https://doi.org/10.1007/S00401-022-02467-8
74. Shi Y, Yamada K, Liddelow SA, Smith ST, Zhao L, Luo W et al (2017) ApoE4 markedly exacerbates tau-mediated neurodegeneration in a mouse model of tauopathy. Nature 549:523–527. https://doi.org/10.1038/nature24016
75. Steward A, Biel D, Dewenter A, Roemer S, Wagner F, Dehsarvi A et al (2023) ApoE4 and connectivity-mediated spreading of Tau pathology at lower amyloid levels. JAMA Neurol 80:1295–1306. https://doi.org/10.1001/JAMANEUROL.2023.4038
76. Strittmatter SA, Goedert M, Weisgraber K, Dong L, Jakes R, Huang D et al (1994) Isoform-specific interactions of apolipoprotein E with microtubule-associated protein tau: implications for Alzheimer disease. Proc Natl Acad Sci 91:11183–11186. https://doi.org/10.1073/PNAS.91.23.11183
77. Strittmatter W, Saunders A, Schmechel D, Pericak-vance M, Enghild J, Salvesen G et al (1993) Apolipoprotein E: high-avidity binding to, B-amyloid and increased frequency of type 4 allele in late-onset familial Alzheimer disease. Proc Natl Acad Sci USA. https://doi.org/10.1073/pnas.90.5.1977
78. Teo G, Liu G, Zhang J, Nesvizhskii AI, Gingras AC, Choi H (2014) SAINTexpress: improvements and additional features in Significance Analysis of Interactome software. J Proteom 100:37. https://doi.org/10.1016/J.JPROT.2013.10.023
79. Terry RD, Gonatas NK, Weiss M (1964) Ultrastructural studies in Alzheimer's presenile dementia. Am J Pathol 44:269–297
80. Thal DR, Ghebremedhin E, Rüb U, Yamaguchi H, Del Tredici K, Braak H (2002) Two types of sporadic cerebral amyloid angiopathy. J Neuropathol Exp Neurol 61:282–293. https://doi.org/10.1093/jnen/61.3.282
81. Thal DR, Papassotiropoulos A, Saido TC, Griffin WST, Mrak RE, Kölsch H et al (2010) Capillary cerebral amyloid angiopathy identifies a distinct APOE epsilon4-associated subtype of sporadic Alzheimer's disease. Acta Neuropathol 120:169–183. https://doi.org/10.1007/S00401-010-0707-9
82. Thal DR, Rüb U, Orantes M, Braak H (2002) Phases of Aβ-deposition in the human brain and its relevance for the development of AD. Neurology 58:1791–1800
83. Thierry M, Boluda S, Delatour B, Marty S, Seilhean D, Letournel F et al (2020) Human subiculo-fornico-mamillary system in Alzheimer's disease: Tau seeding by the pillar of the fornix. Acta Neuropathol. https://doi.org/10.1007/s00401-019-02108-7
84. Thierry M, Marty S, Boluda S, Duyckaerts C (2017) Alzheimer's senile plaque as shown by microcryodissection, a new technique for dissociating tissue structures. J Neural Transm 124:685–694. https://doi.org/10.1007/s00702-017-1718-7
85. Tracy TE, Madero-Pérez J, Swaney DL, Chang TS, Moritz M, Konrad C et al (2022) Tau interactome maps synaptic and mitochondrial processes associated with neurodegeneration. Cell 185:712-728.e14. https://doi.org/10.1016/J.CELL.2021.12.041
86. Wang C, Xiong M, Gratuze M, Bao X, Shi Y, Andhey PS et al (2021) Selective removal of astrocytic APOE4 strongly protects against tau-mediated neurodegeneration and decreases synaptic phagocytosis by microglia. Neuron 109:1657-1674.e7. https://doi.org/10.1016/J.NEURON.2021.03.024
87. Wang P, Joberty G, Buist A, Vanoosthuyse A, Stancu IC, Vasconcelos B et al (2017) Tau interactome mapping based identification of Otub1 as Tau deubiquitinase involved in accumulation of pathological Tau forms in vitro and in vivo. Acta Neuropathol 133:731–749. https://doi.org/10.1007/S00401-016-1663-9
88. Wang Y, Balaji V, Kaniyappan S, Krüger L, Irsen S, Tepper K et al (2017) The release and trans-synaptic transmission of Tau via exosomes. Mol Neurodegener 12:5. https://doi.org/10.1186/s13024-016-0143-y
89. Wisniewski T, Castaño EM, Golabek A, Vogel T, Frangione B (1994) Acceleration of Alzheimer's fibril formation by apolipoprotein E in vitro. Am J Pathol 145:1030
90. Wisniewski T, Drummond E (2020) APOE-amyloid interaction: therapeutic targets. Neurobiol Dis. https://doi.org/10.1016/j.nbd.2020.104784
91. Wisniewski T, Frangione B (1992) Apolipoprotein E: a pathological chaperone protein in patients with cerebral and systemic amyloid. Neurosci Lett 135:235–238. https://doi.org/10.1016/0304-3940(92)90444-C
92. Woo JA, Yan Y, Kee TR, Cazzaro S, Percy KCMG, Wang X, Liu T, Liggett SB, Kang DE (2021) β-arrestin1 promotes tauopathy by transducing GPCR signaling, disrupting microtubules and autophagy. Life Sci Alliance https://doi.org/10.26508/LSA.202101183
93. Wu JW, Hussaini SA, Bastille IM, Rodriguez GA, Mrejeru A, Rilett K et al (2016) Neuronal activity enhances tau propagation and tau pathology in vivo. Nat Neurosci 19:1085–1092. https://doi.org/10.1038/nn.4328
94. Zhang K, Daigle JG, Cunningham KM, Coyne AN, Ruan K, Grima JC et al (2018) Stress granule assembly disrupts nucleocytoplasmic transport. Cell 173:958-971.e17. https://doi.org/10.1016/J.CELL.2018.03.025
95. Zhang X, Lin Y, Eschmann NA, Zhou H, Rauch JN, Hernandez I et al (2017) RNA stores tau reversibly in complex coacervates. PLOS Biol 15:e2002183. https://doi.org/10.1371/JOURNAL.PBIO.2002183

7. DISCUSSION

AD, defined by Aβ and Tau pathology, also involves widespread molecular alterations across multiple biological pathways[101,102,431]. Given the nearly universal development of AD neuropathology in DS by midlife[58,59,74,331], a gap remains between this high prevalence of pathology and the much lower prevalence of dementia, estimated at 2 to 5% at age 40 and rising to over 80% by age 65[432,433]. Because the early development of AD neuropathology in DS precedes the clinical onset of dementia by decades, individuals with DS offer a unique opportunity to study the chronopathology of AD, including its spatial distribution, temporal progression, and clinical relevance[434].

Comparative proteomics across DS and other AD subtypes can help identify both shared and subtype-specific mechanisms, given that proteins carry out most biological functions and serve as key molecular indicators of disease. While answering the overarching question of how DSAD compares to other forms of AD, we proposed or confirmed candidate proteins for future functional studies aimed at identifying novel biomarkers or therapeutic targets.

In **section 6.1** we showed that Aβ plaques are enriched in hundreds of proteins beyond Aβ, and many of these proteins have not been extensively studied in the context of AD. We performed a comprehensive comparison of the Aβ plaque and non-plaque proteomes from individuals with DSAD, EOAD, and LOAD, identifying 43 proteins consistently enriched in plaques across all groups. Plaque proteomes were highly correlated among subtypes indicating a shared Aβ plaque protein signature across DS, EOAD, and LOAD, though some proteins varied in abundance. Functional enrichment and interaction analyses linked these proteins to APP metabolism, lysosomal activity, and immune processes. In contrast, non-plaque proteomes showed subtype-specific differences, reflecting distinct functional profiles and physiological variation between DS and other forms of AD[334,423].

In **section 6.2** we showed that individuals with DS display elevated CSF levels of immunoglobulins, complement proteins, collagens, and extracellular matrix components prior to changes in amyloid plaque markers, suggesting a link to Hsa21 triplication. DSAD was also associated with earlier reductions in synaptic proteins,

neurofilament light, and proposed CAA-related markers compared to ADAD. Comparison of DS CSF with Aβ plaque and non-plaque brain proteomes revealed consistent changes in ECM, plasma-derived, Hsa21, myelin, and select neuronal proteins across compartments, while other neuronal proteins showed divergent patterns between brain and CSF. Overall, these findings indicate similar pathway alterations in DSAD, ADAD and LOAD, although DSAD has unique features compared to other forms of AD[435].

In **section 6.3** we examined the influence of *APOE* genotype on the pTau interactome. The analysis revealed haplotype-specific differences in the subcellular localization of pTau aggregates between *APOEε3/ε3* and *APOEε4/ε4* cases, which were confirmed by immunohistochemistry. These findings suggest that *APOE*ε4 promotes the progression of Tau pathology by increasing pTau accumulation in axonal endings and synapses, particularly in Aβ-rich brain regions. This work lays the foundation for future studies of the Aβ interactome and the application of this approach to DSAD.

Our brain proteomics analysis identified a group of proteins highly enriched in amyloid plaques, including well-studied proteins in AD such as Aβ peptide, APP, ApoE, CLU, and HTRA1[334,423]. Among these enriched proteins, COL25A1 (also known as CLAC-P) emerged as the most enriched protein in plaques, exceeding even Aβ abundance[423]. Supporting our proteomics findings, a recent study by Levites and colleagues confirmed COL25A1 presence in amyloid plaques of both human AD brain tissue and mouse models using an in-house antibody[436]. Previous research has also implicated COL25A1 in the transition from diffuse deposits to mature senile plaques[437,438]. Despite these observations, its role in AD neuropathology remains poorly understood. Our proteomics results provide new evidence showing that COL25A1 is more elevated in DSAD plaques compared to EOAD and LOAD[423], suggesting a potential role in aggravating plaque pathology in DS, beyond the effects of *APP* gene triplication. Earlier studies indicated that the interaction of COL25A1 with Aβ is determined by negatively charged residues in the central region of the amyloid peptide[439]. More recently, Fernandez and collaborators described structural features of $A\beta_{40}$ and $A\beta_{42}$ fibrils in two DSAD cases. Type I and II $A\beta_{42}$ fibrils in DS resemble those observed in sporadic and autosomal dominant

AD, although DS shows similar levels of both fibril types, while sAD predominantly exhibits type I $A\beta_{42}$ fibrils and ADAD predominantly type II fibrils[84]. Interestingly, Fernandez *et al.* also observed structural differences in $A\beta_{40}$ fibrils between DSAD and other AD subtypes[84]. Although we did not evaluate physicochemical interactions between COL25A1 and Aβ fibrils, structural differences in Aβ fibrils may lead to unique interactions with COL25A1 in DSAD[84,440]. Further investigation is required to determine the binding affinity of COL25A1 in DS and other forms of AD, as COL25A1 may represent a promising target for disease-modifying therapies aimed at altering neuropathological progression.

Across DSAD, EOAD, and LOAD, our unbiased localized proteomics identified a broad set of Aβ plaque-associated proteins consistent with previous findings. Several of these proteins have been linked to protective functions against Aβ toxicity or to the regulation of amyloid production, including HTRA1, CLU, CLSTN1, GPC1, MDK, NTN1, SMOC1 and VIM[441-444]. These proteins are strongly correlated with Aβ in AD cases[445], and have been repeatedly reported as significantly altered in multiple proteomics studies, indicating that these changes represent some of the most prevalent alterations in AD human brain tissues[167]. Most of the observed differences in protein abundance in both plaque and non-plaque tissue were consistent in direction across DSAD, EOAD, and LOAD, suggesting that similar molecular changes accompany AD neuropathology in different subtypes of the disease. Furthermore, while the spatial and temporal distribution of Aβ and Tau pathology across the brain has been well established (reviewed in **section 4.1.3.3**), our results indicate that a comparable process may extend to many proteins associated with neuropathological lesions, as also observed in previous human AD brain proteomics studies[167].

Our analyses of Aβ plaques, non-plaque tissue, and CSF also revealed differences in protein enrichment, likely reflecting changes in protein abundance and dynamics of interaction with neuropathological lesions. A meta-analysis by Askenazi and colleagues that integrated multiple proteomics datasets from human AD brain tissue supports this interpretation[167]. Amyloid plaques, for instance, are consistently enriched in lysosomal proteins, in line with recent findings suggesting that plaques form following the accumulation of intraneuronal Aβ within autophagic

vacuoles[167,446]. In contrast, NFT proteomics shows enrichment of neuronal and endoplasmic reticulum proteins, pointing to a strong association between Tau and ribosomal proteins[167,447,448]. Similarly, our non-plaque proteome adjacent to plaques was enriched in ribosomal and RNA-associated proteins[423]. Although NFTs were not directly examined in our study, our laser-capture microdissection method captured dystrophic neurites and neuronal processes located next to plaque deposits. In addition, CAA proteomics studies have demonstrated clear differences between the proteomes of amyloid plaques and vascular lesions, underscoring the distinct protein interactions that contribute to AD pathogenesis and Aβ aggregation[70].

We also identified an *Aβ plaque signature* characterized by functional associations with endo-lysosomal processes, immune and inflammatory responses, and APP metabolism[423]. As discussed in this thesis (see **sections 4.1.4.3**, **4.2.2.2.2** and **4.2.2.2.3**), immune dysregulation and endo-lysosomal dysfunction are central features of AD and DSAD. Our proteomic studies identified several endo-lysosomal proteins, including underexplored proteins such as TPP1, ARL8B, and CLCN6, along with newly associated plaque proteins LAMTOR4 and VAMP7[334,423]. TPP1 and CLCN6 have been implicated in the lysosomal storage disease neuronal ceroid lipofuscinosis (NCL)[449-451].

Our plaque proteomics analysis provided new evidence linking CLCN6 to AD and DSAD pathology, supported by immunohistochemistry validation[423]. CLCN6 is mainly expressed in neurons of the central and peripheral nervous systems and localizes to late endosomes in neuronal cell bodies[450]. Previous work has shown that disruption of CLCN6 leads to lysosomal storage disease with behavioral abnormalities resembling NCL[450,451]. Studies of CLCN6 variants propose that this phenotype may be the result of impaired acidification of late endosomes, thereby disrupting protein degradation and autophagy and leading to neurodegeneration[452-454]. Because of the critical role of late endosomes in generating intraluminal vesicles and sorting ubiquitinated proteins for lysosomal degradation, disruption of CLCN6 could hinder the clearance of proteins such as TDP-43 and Tau, promoting their intracellular accumulation[452,453]. In support of these observations, our weighted correlation network analysis of DS plaques identified a co-expression module including CLCN6 and other highly abundant plaque proteins that associated with

Tau neuropathology levels[423]. Together, these findings suggest that CLCN6 could contribute to the aggregation of Aβ and associated proteins, due to its role in the endo-lysosomal pathway.

In addition to CLCN6, TPP1 is a lysosomal matrix protein broadly expressed in the human brain[455]. TPP1 has been suggested to destabilize Aβ through endoproteolytic cleavage[456], indicating a possible protective function in AD. Although TPP1 has appeared in previous proteomics studies[167,334], our work provides the first preliminary characterization of its role in AD plaque pathology. Using label-free mass spectrometry, we detected a subtle but significant enrichment of TPP1 in plaques, despite the absence of clear differences in our histochemical analyses. Instead, TPP1 showed a punctate expression pattern throughout the parenchyma with notable association to plaques. Similar observations have been reported for other lysosomal proteins, including ARL8B, LAMP1, Cathepsin D, lipofuscin and CLCN6[334,457,458]. These proteins are associated with plaques without directly colocalizing with Aβ, suggesting that TPP1 may not interact directly with Aβ but rather it localizes to small plaque regions where Aβ is either absent or undergoing degradation.

CSF proteomics also revealed alterations in endo-lysosomal proteins in DSAD, though these changes were detected after symptom onset[435]. However, previous evidence has shown that endo-lysosomal dysfunction precedes Aβ deposition in DS brains[321,459]. Our plaque proteomics study used end-stage AD cases, and the CSF proteomics did not include direct measurements of proteins involved in the endosomal recycling pathway, which may explain why we observed only late-stage alterations. However, functional analysis of altered proteins in CSF revealed early changes in the Golgi module, suggesting early disruptions in endosome recycling, a process that involves the trans-Golgi network[460].

Neuroinflammation is a central process in AD pathogenesis, and individuals with DS exhibit immune system alterations even before the onset of AD[362,461]. CSF proteomics revealed early elevations in complement proteins in DS, consistent with our Aβ plaque proteomics findings, which identified complement components C1QC, C4A, and C3, along with CLU, MDK, HLA-DRB1, and the novel plaque-associated protein HLA-DRB5[423,435]. Protein network analyses suggest potential

interactions between these proteins and Aβ, indicating a mechanistic link between amyloid pathology and immune activation. Previous studies have shown that complement activation may contribute to synaptic pruning via microglial activity and is associated with Aβ and Tau deposition[462-464]. Our findings therefore extend earlier evidence by showing that complement dysregulation is not only a feature of AD but also appears early in DS, possibly contributing to the accelerated trajectory of AD in this population. The observed enrichment of CLU and MDK underscores their pathogenic roles, with CLU linked to complement-mediated processes and MDK influencing amyloid deposition, although additional evidence is necessary to define their mechanisms[465,466].

The presence of HLA-DRB1 and HLA-DRB5 in Aβ plaques underscores microglial involvement in amyloid pathology, supported by transcriptomic data linking their expression to AD pathology[172,467]. Our findings are consistent with evidence indicating that immune activation and microglial responses escalate neuroinflammation in DS before the emergence of AD pathology becomes apparent[363]. Elevated pro-inflammatory cytokines such as IL-6 and reduced levels of anti-inflammatory markers including IL-10 and IFNγ have been observed in DS, suggesting that baseline immune dysregulation may exacerbate Aβ-driven inflammation. Genetic studies further support this view, identifying markers in DS that predispose to heightened inflammatory responses and increase susceptibility to AD[468].

Together, our data highlights how complement activation, immune dysregulation, and microglial involvement converge in DS to amplify neuroinflammation and shape the course of AD. This integration of proteomic evidence with existing literature suggests that immune-related pathways are not secondary consequences but may represent upstream modulators of disease progression in both AD and DSAD.

Brain proteomics of both Aβ plaques and neighboring non-plaque tissue highlighted a significant reduction in several oligodendrocyte-associated proteins, including PLP1, MBP, MAG, MOG, HAPLN2 and BCAS1[423]. Functional and co-expression network analyses showed a negative correlation between a module of oligodendrocyte proteins and Aβ neuropathology, suggesting that amyloid aggregation may impair oligodendrocyte function and disrupt myelin stability. Prior

studies have reported that degraded MBP can bind $A\beta_{1-42}$, potentially contributing to plaque formation[469]. Alterations in oligodendrocyte and myelin proteins have been observed in AD and other neurodegenerative disorders, and individuals with DS often show earlier myelin abnormalities than euploid individuals[124,470,471].

Although the proteomic analysis of plaques and adjacent tissue captures changes at the end stage of AD[423], the complementary CSF proteomics data provided additional insights into oligodendrocyte and myelin pathology. Neurofilament light (NfL), a marker of axonal and myelin integrity, was elevated in DS CSF before increases in total Tau and pTau, in contrast to findings in the DIAN ADAD cohort, where NfL rises later[472,473]. However, studies in the Colombian PSEN1 kindred show that NfL elevations can occur as early as 20 years before estimated symptom onset, indicating heterogeneity across ADAD cohorts[474]. CSF proteomics also revealed decreased levels of MAG and MOG in DS compared to LOAD. While MAG and MOG changes appeared early, they followed protein alterations related to the ECM, complement, and immunoglobulins, but preceded NfL elevation[435]. Collectively, these findings suggest that early ECM disruption and immune dysregulation in DSAD may precede Aβ-associated increases in pTau, contributing to subsequent NfL elevation and progressive white matter and axonal damage[472,473].

At the estimated time of NfL elevation in individuals with DS, CSF levels of parvalbumin (PVALB) were already decreased, approximately 15 years before the onset of AD symptoms[435]. Our brain proteomics data support these findings, identifying PVALB as the most reduced protein in non-plaque tissue in DSAD compared to age-matched controls, EOAD, and LOAD[423]. Immunohistochemistry further validated the reduction of PVALB in DSAD, consistent with previous reports[475]. PVALB is a marker of a subset of fast-spiking inhibitory neurons pivotal for generating gamma oscillations, and the loss of these neurons has been linked to abnormal excitatory activity and cognitive dysfunction[476,477]. Targeting PVALB neuron function represents a potential therapeutic strategy, with preliminary evidence in LOAD models showing benefits in reducing AD pathology and improving cognitive outcomes[478,479].

Across brain and CSF proteomes, our findings highlight early and robust dysregulation of ECM-related proteins in individuals with DS compared to EOAD

and LOAD, including collagens, laminins, cell adhesion proteins, proteoglycans, and heparin sulfate proteins[423,435]. In the brain, ECM alterations were specific to non-plaque tissue, suggesting a broader disruption of the extracellular environment that occurs before or independently of plaque formation, or may reflect constitutive changes associated with trisomy 21, some of which could contribute to elevated AD risk. Previous proteomic studies of human AD brain tissue have linked cell–ECM interaction pathways and matrisome components with neuropathological and cognitive traits[170], and ECM components have been observed in pre-clinical AD cases, suggesting early ECM alterations in disease.

In the CSF, changes in ECM and collagen modules preceded the decrease in Aβ levels, indicating early systemic involvement[435]. These alterations may reflect the effects of trisomy 21 on matrix composition and remodeling, with downstream consequences for neural development and vascular integrity. The detection of metalloproteinases such as MMP2 and MMP4, their inhibitors TIMP1 and TIMP2, and the reduction of MFGE8 further support a mechanistic link between ECM dysregulation and cerebrovascular pathology in DS[480,481]. Altogether, our data suggests that ECM disruption may represent an early and central feature of AD pathogenesis, particularly in DSAD, with potential implications for vascular pathology. A proteomics study by Leitner and colleagues showed that many matrisome proteins are highly enriched in CAA in human AD brain tissue, supporting the hypothesis that ECM accumulation is a key feature of both CAA and plaque pathology[70].

Our CSF proteomics analysis confirmed early alterations in Down syndrome, particularly in extracellular matrix components, immune-related proteins, and blood–brain barrier markers, which appeared before measurable changes in classical Aβ or Tau biomarkers[435]. These early alterations may reflect molecular shifts driven by soluble Aβ oligomers rather than by plaque deposition. In parallel, proteomic profiling of Aβ plaques revealed overlapping enriched plaque-associated proteins between DS, EOAD and LOAD, including COL25A1, SMOC1, MDK, and NTN1, along with endo-lysosomal and immune-related signatures[423].

Together, these findings suggest that fluid- and tissue-based proteomics provide complementary information for identifying stage-specific biomarkers. In the CSF,

early dysregulation of immune and vascular markers may signal preclinical disease mechanisms. Plaque proteomics, in contrast, highlights proteins closely associated with lesion pathology and potentially involved in downstream neurodegeneration. The convergence of these profiles, particularly for proteins related to immunity, synaptic integrity, and lysosomal function, supports a multi-modal biomarker framework. Early CSF changes could identify individuals suitable for preventive intervention, while plaque-bound proteins may serve as direct therapeutic targets.

This perspective is consistent with emerging strategies aimed at removing soluble Aβ species before symptom onset. Clinical evidence now supports the potential of anti-amyloid therapy to delay the onset of Alzheimer's disease symptoms when administered early. A long-term open-label extension of the DIAN-TU trial demonstrated that sustained treatment with gantenerumab significantly reduced the risk of developing symptomatic AD in individuals carrying fully penetrant autosomal dominant mutations for Alzheimer's disease[482]. The earlier identification of biomarkers through CSF proteomics in DS could allow interventions to be timed more precisely. At the same time, proteins identified in plaques may inform the development of therapies designed to modulate lesion-specific processes, including lysosomal or immune pathways, in addition to amyloid clearance.

Limitations

While our study provides important insights into Aβ plaque pathology in DS and other AD forms, it has several limitations. Bottom-up proteomics offers high sensitivity and unbiased protein detection but cannot always distinguish specific proteoforms or detect all membrane proteins. Particularly, our plaque proteomics analysis focused on dense Aβ plaques from advanced-stage cases, limiting findings to end-stage pathology and specific brain regions vulnerable to AD. Broader studies across plaque types, brain regions, and age ranges are needed to understand disease progression and resilience. Additionally, genetic variability among samples may influence results. Future work should incorporate known genetic factors, including familial AD mutations and APOE genotypes, to better interpret proteomic differences.

Similarly, the CSF proteomics study had a limited number of younger controls, which introduced uncertainty in protein level estimates, particularly for early $A\beta_{1-42}$ changes in the CSF. Larger cohorts with more young samples are needed to clarify early alterations. The lack of available longitudinal CSF cohorts also restricted validation. Proteomic depth was reduced by excluding proteins with high missingness, which future studies could address by using complementary platforms. Additionally, larger DS cohorts would allow for more robust modeling of sex and APOE genotype effects in relation to estimated year of onset.

An additional limitation is the lack of transcriptomic data alongside proteomic analyses. Future studies incorporating transcriptomic approaches, such as spatial transcriptomics, would complement the proteomic findings by providing non-redundant insights into gene expression alterations in DS and AD, thereby offering a more comprehensive understanding of disease mechanisms.

Future directions

Protein interactions are critical regulators of aggregation processes in neurodegenerative diseases, particularly those involving Aβ and Tau proteins[483]. Mutations, posttranslational modifications and conformational changes in aggregation-prone proteins can disrupt key cellular functions such as vesicle trafficking, cytoskeletal integrity, and immune responses[483]. Interactions between Aβ and cellular proteins contribute to its neurotoxicity, while pTau binding to proteins like synaptogyrin-3 has been linked to synaptic dysfunction[183,484]. Drummond and collaborators used affinity purification coupled with mass spectrometry (AP-MS) to identify proteins directly interacting with pTau[424]. Their study revealed that pTau interacts with components of the ubiquitin-proteasome and phagosome-lysosome systems. The proteasome plays a key role in Tau degradation, and pTau has been shown to inhibit proteasome activity[485,486].

Building on this approach, we describe in **section 6.3** the effect of *APOE* haplotype on pTau metabolism using anti-pTau AP-MS to identify pTau interactors in *APOEε3* and *APOEε4* carriers[429]. Proteins from the ubiquitin-proteasome system were identified as pTau interactors regardless of *APOE* genotype[429], reinforcing earlier findings by Drummond *et al*[424]. Notable proteins included SQSTM1 (p62), which

mediates the transport of polyubiquitinated Tau for proteasomal degradation; ubiquitin precursors RPS27A and UBC; and ubiquitin ligases such as ARMC8 and UBR4[429].

In *APOEε3* carriers, most pTau interactors were nucleoplasmic proteins involved in RNA binding and processing. Tau colocalization with RNA-binding proteins has been linked to the formation of stress granules, which regulate protein function[487]. In contrast, pTau interactors in *APOEε4* carriers were predominantly synaptic transport proteins, including ARRB1, a recently identified Tau interactor implicated in promoting Tau pathology[488].

Immunohistochemistry confirmed a higher density of pTau-positive neuritic crowns in *APOEε4* cases, despite comparable overall Tau pathology between haplotypes[429]. These crowns, composed of degenerated axonal neurites encircling mature Aβ deposits, indicate enhanced axonal accumulation of pTau in *APOEε*4 carriers. This observation supports the hypothesis that *APOEε4* facilitates pTau transport to synaptic terminals, promoting its trans-synaptic spread[489,490].

These findings demonstrate that *APOE* haplotype influences both pTau interactions and its subcellular distribution, contributing to variability in Tau pathology across AD cases. Based on this evidence, we propose extending the AP-MS approach to evaluate the Aβ interactome in DS, sporadic, and autosomal dominant forms of AD. This complementary analysis will enhance our brain and CSF proteomics data and help clarify the molecular mechanisms underlying amyloid pathology and its role in disease progression.

8. CONCLUSION

This thesis provides a comprehensive proteomic analysis of human brain and CSF samples across Down syndrome and distinct forms of Alzheimer's disease. By comparing DSAD with EOAD, LOAD, and ADAD, we identified both shared and distinct molecular features that contribute to amyloid pathology and disease progression. The brain proteomics studies (**section 6.1.**) revealed strong similarities in plaque composition across cohorts, particularly in the enrichment of proteins linked to endo-lysosomal pathways, immune responses, and APP metabolism, while also highlighting distinct alterations in the non-plaque proteome, especially in ECM and chromatin-associated proteins. Complementary CSF proteomics (**section 6.2.**) uncovered early and progressive changes in immune, vascular, myelin, and neuronal markers in DS, underscoring the influence of trisomy 21 on baseline pathology and its potential role in accelerating AD onset. Together, these studies offer new insights into the molecular landscape of DSAD, identifying candidate biomarkers and therapeutic targets, and underscore the value of proteomics in uncovering disease-relevant mechanisms that may inform personalized strategies for intervention across AD subtypes.

In addition to the global proteomic analyses presented in this thesis, complementary work about the influence of *APOE* genotype on the pTau interactome (**section 6.3.**) revealed that *APOEε4* alters the subcellular localization of pTau and reshapes its protein interaction landscape. These findings underscore the heterogeneity of Tau pathology and suggest that genotype-specific mechanisms may contribute to disease progression and therapeutic vulnerability. Building on this approach, future studies will apply affinity purification–mass spectrometry to characterize the Aβ interactome across DS and other forms of AD. This targeted analysis will complement the proteomic profiles of brain and CSF described in this thesis and provide deeper insight into the molecular networks that govern amyloid pathology in distinct forms of AD.

9. REFERENCES

1 Alzheimer, A., Stelzmann, R. A., Schnitzlein, H. N. & Murtagh, F. R. An English translation of Alzheimer's 1907 paper, "Uber eine eigenartige Erkankung der Hirnrinde". *Clin Anat* **8**, 429-431 (1995). https://doi.org/10.1002/ca.980080612

2 Bondi, M. W., Edmonds, E. C. & Salmon, D. P. Alzheimer's Disease: Past, Present, and Future. *J Int Neuropsychol Soc* **23**, 818-831 (2017). https://doi.org/10.1017/S135561771700100X

3 Blessed, G., Tomlinson, B. E. & Roth, M. The association between quantitative measures of dementia and of senile change in the cerebral grey matter of elderly subjects. *Br J Psychiatry* **114**, 797-811 (1968). https://doi.org/10.1192/bjp.114.512.797

4 Roth, M., Tomlinson, B. E. & Blessed, G. Correlation between scores for dementia and counts of 'senile plaques' in cerebral grey matter of elderly subjects. *Nature* **209**, 109-110 (1966). https://doi.org/10.1038/209109a0

5 Katzman, R. Editorial: The prevalence and malignancy of Alzheimer disease. A major killer. *Arch Neurol* **33**, 217-218 (1976). https://doi.org/10.1001/archneur.1976.00500040001001

6 Iqbal, K. *et al*. Protein changes in senile dementia. *Brain Res* **77**, 337-343 (1974). https://doi.org/10.1016/0006-8993(74)90798-7

7 Kidd, M. Paired helical filaments in electron microscopy of Alzheimer's disease. *Nature* **197**, 192-193 (1963). https://doi.org/10.1038/197192b0

8 Terry, R. D., Gonatas, N. K. & Weiss, M. Ultrastructural Studies in Alzheimer's Presenile Dementia. *Am J Pathol* **44**, 269-297 (1964).

9 Glenner, G. G. & Wong, C. W. Alzheimer's disease: initial report of the purification and characterization of a novel cerebrovascular amyloid protein. *Biochem Biophys Res Commun* **120**, 885-890 (1984). https://doi.org/10.1016/s0006-291x(84)80190-4

10 Masters, C. L. *et al*. Amyloid plaque core protein in Alzheimer disease and Down syndrome. *Proc Natl Acad Sci U S A* **82**, 4245-4249 (1985). https://doi.org/10.1073/pnas.82.12.4245

11 Maure-Blesa, L. *et al*. The history of Down syndrome-associated Alzheimer's disease; past, present, and future. *Alzheimers Dement* **21**, e70158 (2025). https://doi.org/10.1002/alz.70158

12 Karran, E. & De Strooper, B. The amyloid cascade hypothesis: are we poised for success or failure? *J Neurochem* **139 Suppl 2**, 237-252 (2016). https://doi.org/10.1111/jnc.13632

13 Hardy, J. A. & Higgins, G. A. Alzheimer's disease: the amyloid cascade hypothesis. *Science* **256**, 184-185 (1992). https://doi.org/10.1126/science.1566067

14 Pimplikar, S. W. Reassessing the amyloid cascade hypothesis of Alzheimer's disease. *Int J Biochem Cell Biol* **41**, 1261-1268 (2009). https://doi.org/10.1016/j.biocel.2008.12.015

15 Ricciarelli, R. & Fedele, E. The Amyloid Cascade Hypothesis in Alzheimer's Disease: It's Time to Change Our Mind. *Curr Neuropharmacol* **15**, 926-935 (2017). https://doi.org/10.2174/1570159X15666170116143743

16 van Dyck, C. H. *et al*. Lecanemab in Early Alzheimer's Disease. *N Engl J Med* **388**, 9-21 (2023). https://doi.org/10.1056/NEJMoa2212948

17 Sims, J. R. *et al*. Donanemab in Early Symptomatic Alzheimer Disease: The TRAILBLAZER-ALZ 2 Randomized Clinical Trial. *JAMA* **330**, 512-527 (2023). https://doi.org/10.1001/jama.2023.13239

18 Atri, A. The Alzheimer's Disease Clinical Spectrum: Diagnosis and Management. *Med Clin North Am* **103**, 263-293 (2019). https://doi.org/10.1016/j.mcna.2018.10.009

19 McKhann, G. M. *et al*. The diagnosis of dementia due to Alzheimer's disease: recommendations from the National Institute on Aging-Alzheimer's Association workgroups on diagnostic guidelines for Alzheimer's disease. *Alzheimers Dement* **7**, 263-269 (2011). https://doi.org/10.1016/j.jalz.2011.03.005

20 2025 Alzheimer's disease facts and figures. *Alzheimer's & Dementia* **21**, e70235 (2025). https://doi.org/https://doi.org/10.1002/alz.70235

21 Jack, C. R., Jr. *et al*. Revised criteria for diagnosis and staging of Alzheimer's disease: Alzheimer's Association Workgroup. *Alzheimers Dement* **20**, 5143-5169 (2024). https://doi.org/10.1002/alz.13859

22 Vermunt, L. *et al*. Duration of preclinical, prodromal, and dementia stages of Alzheimer's disease in relation to age, sex, and APOE genotype. *Alzheimers Dement* **15**, 888-898 (2019). https://doi.org/10.1016/j.jalz.2019.04.001

23 Jack, C. R., Jr. *et al*. NIA-AA Research Framework: Toward a biological definition of Alzheimer's disease. *Alzheimers Dement* **14**, 535-562 (2018). https://doi.org/10.1016/j.jalz.2018.02.018

24 Sperling, R. A. *et al*. Toward defining the preclinical stages of Alzheimer's disease: recommendations from the National Institute on Aging-Alzheimer's Association workgroups on diagnostic guidelines for Alzheimer's disease. *Alzheimers Dement* **7**, 280-292 (2011). https://doi.org/10.1016/j.jalz.2011.03.003

25 Albert, M. S. *et al*. The diagnosis of mild cognitive impairment due to Alzheimer's disease: recommendations from the National Institute on Aging-Alzheimer's Association workgroups on diagnostic guidelines for Alzheimer's disease. *Alzheimers Dement* **7**, 270-279 (2011). https://doi.org/10.1016/j.jalz.2011.03.008

26 Gustavsson, A. *et al*. Global estimates on the number of persons across the Alzheimer's disease continuum. *Alzheimers Dement* **19**, 658-670 (2023). https://doi.org/10.1002/alz.12694

27 Idris, M. *et al*. Staging of Alzheimer's disease progression in Down syndrome using mixed clinical and plasma biomarker measures with machine learning. *Alzheimers Dement* **21**, e70446 (2025). https://doi.org/10.1002/alz.70446

28 Sperling, R., Mormino, E. & Johnson, K. The evolution of preclinical Alzheimer's disease: implications for prevention trials. *Neuron* **84**, 608-622 (2014). https://doi.org/10.1016/j.neuron.2014.10.038

29 Edgin, J. O. *et al*. Development and validation of the Arizona Cognitive Test Battery for Down syndrome. *J Neurodev Disord* **2**, 149-164 (2010). https://doi.org/10.1007/s11689-010-9054-3

30 Mormino, E. C. & Papp, K. V. Amyloid Accumulation and Cognitive Decline in Clinically Normal Older Individuals: Implications for Aging and Early Alzheimer's Disease. *J Alzheimers Dis* **64**, S633-S646 (2018). https://doi.org/10.3233/JAD-179928

31 Startin, C. M. *et al*. The LonDownS adult cognitive assessment to study cognitive abilities and decline in Down syndrome. *Wellcome Open Res* **1**, 11 (2016). https://doi.org/10.12688/wellcomeopenres.9961.1

32 Hyman, B. T. *et al*. National Institute on Aging-Alzheimer's Association guidelines for the neuropathologic assessment of Alzheimer's disease. *Alzheimers Dement* **8**, 1-13 (2012). https://doi.org/10.1016/j.jalz.2011.10.007

33 Jelistratova, I., Teipel, S. J. & Grothe, M. J. Longitudinal validity of PET-based staging of regional amyloid deposition. *Hum Brain Mapp* **41**, 4219-4231 (2020). https://doi.org/10.1002/hbm.25121

34 Sun, Y. *et al*. Distinct spatiotemporal subtypes of amyloid deposition are associated with diverging disease profiles in cognitively normal and mild cognitive impairment individuals. *Transl Psychiatry* **13**, 35 (2023). https://doi.org/10.1038/s41398-023-02328-2

35 Perl, D. P. Neuropathology of Alzheimer's disease. *Mt Sinai J Med* **77**, 32-42 (2010). https://doi.org/10.1002/msj.20157

36 Nelson, P. T. *et al*. Correlation of Alzheimer disease neuropathologic changes with cognitive status: a review of the literature. *J Neuropathol Exp Neurol* **71**, 362-381 (2012). https://doi.org/10.1097/NEN.0b013e31825018f7

37 Goldgaber, D., Lerman, M. I., McBride, O. W., Saffiotti, U. & Gajdusek, D. C. Characterization and chromosomal localization of a cDNA encoding brain amyloid of Alzheimer's disease. *Science* **235**, 877-880 (1987). https://doi.org/10.1126/science.3810169

38 Korte, M., Herrmann, U., Zhang, X. & Draguhn, A. The role of APP and APLP for synaptic transmission, plasticity, and network function: lessons from genetic mouse models. *Exp Brain Res* **217**, 435-440 (2012). https://doi.org/10.1007/s00221-011-2894-6

39 Rice, H. C. *et al*. Secreted amyloid-beta precursor protein functions as a GABA(B)R1a ligand to modulate synaptic transmission. *Science* **363** (2019). https://doi.org/10.1126/science.aao4827

40 Weingarten, J., Weingarten, M., Wegner, M. & Volknandt, W. APP-A Novel Player within the Presynaptic Active Zone Proteome. *Front Mol Neurosci* **10**, 43 (2017). https://doi.org/10.3389/fnmol.2017.00043

41 Haass, C., Kaether, C., Thinakaran, G. & Sisodia, S. Trafficking and proteolytic processing of APP. *Cold Spring Harb Perspect Med* **2**, a006270 (2012). https://doi.org/10.1101/cshperspect.a006270

42 Zhang, Y. W., Thompson, R., Zhang, H. & Xu, H. APP processing in Alzheimer's disease. *Mol Brain* **4**, 3 (2011). https://doi.org/10.1186/1756-6606-4-3

43 Willem, M. *et al*. eta-Secretase processing of APP inhibits neuronal activity in the hippocampus. *Nature* **526**, 443-447 (2015). https://doi.org/10.1038/nature14864

44 Azargoonjahromi, A. The duality of amyloid-beta: its role in normal and Alzheimer's disease states. *Mol Brain* **17**, 44 (2024). https://doi.org/10.1186/s13041-024-01118-1

45 Wilkins, H. M. & Swerdlow, R. H. Amyloid precursor protein processing and bioenergetics. *Brain Res Bull* **133**, 71-79 (2017). https://doi.org/10.1016/j.brainresbull.2016.08.009

46 Wisniewski, T. & Goni, F. Immunotherapeutic approaches for Alzheimer's disease. *Neuron* **85**, 1162-1176 (2015). https://doi.org/10.1016/j.neuron.2014.12.064

47 Armstrong, R. A. Beta-amyloid plaques: stages in life history or independent origin? *Dement Geriatr Cogn Disord* **9**, 227-238 (1998). https://doi.org/10.1159/000017051

48 Tsering, W. & Prokop, S. Neuritic Plaques - Gateways to Understanding Alzheimer's Disease. *Mol Neurobiol* **61**, 2808-2821 (2024). https://doi.org/10.1007/s12035-023-03736-7

49 Abner, E. L. *et al*. Diffuse Amyloid-beta Plaques, Neurofibrillary Tangles, and the Impact of APOE in Elderly Persons' Brains Lacking Neuritic Amyloid Plaques. *J Alzheimers Dis* **64**, 1307-1324 (2018). https://doi.org/10.3233/JAD-180514

50 Liu, F. *et al*. Focal-type, but not Diffuse-type, Amyloid Beta Plaques are Correlated with Alzheimer's Neuropathology, Cognitive Dysfunction, and Neuroinflammation in the Human Hippocampus. *Neurosci Bull* **38**, 1125-1138 (2022). https://doi.org/10.1007/s12264-022-00927-5

51 Crook, R. *et al*. A variant of Alzheimer's disease with spastic paraparesis and unusual plaques due to deletion of exon 9 of presenilin 1. *Nat Med* **4**, 452-455 (1998). https://doi.org/10.1038/nm0498-452

52 Wisniewski, H. M., Sadowski, M., Jakubowska-Sadowska, K., Tarnawski, M. & Wegiel, J. Diffuse, lake-like amyloid-beta deposits in the parvopyramidal layer of the presubiculum in Alzheimer disease. *J Neuropathol Exp Neurol* **57**, 674-683 (1998). https://doi.org/10.1097/00005072-199807000-00004

53 Armstrong, R. A. Beta-amyloid deposition in the medial temporal lobe in elderly non-demented brains and in Alzheimer's disease. *Dementia* **6**, 121-125 (1995). https://doi.org/10.1159/000106933

54 Delaere, P., He, Y., Fayet, G., Duyckaerts, C. & Hauw, J. J. Beta A4 deposits are constant in the brain of the oldest old: an immunocytochemical study of 20 French centenarians. *Neurobiol Aging* **14**, 191-194 (1993). https://doi.org/10.1016/0197-4580(93)90096-t

55 Serrano-Pozo, A., Frosch, M. P., Masliah, E. & Hyman, B. T. Neuropathological alterations in Alzheimer disease. *Cold Spring Harb Perspect Med* **1**, a006189 (2011). https://doi.org/10.1101/cshperspect.a006189

56 Thal, D. R., Capetillo-Zarate, E., Del Tredici, K. & Braak, H. The development of amyloid beta protein deposits in the aged brain. *Sci Aging Knowledge Environ* **2006**, re1 (2006). https://doi.org/10.1126/sageke.2006.6.re1

57 Thal, D. R., Rub, U., Orantes, M. & Braak, H. Phases of A beta-deposition in the human brain and its relevance for the development of AD. *Neurology* **58**, 1791-1800 (2002). https://doi.org/10.1212/wnl.58.12.1791

58 Lemere, C. A. *et al*. Sequence of deposition of heterogeneous amyloid beta-peptides and APO E in Down syndrome: implications for initial events in amyloid plaque formation. *Neurobiol Dis* **3**, 16-32 (1996). https://doi.org/10.1006/nbdi.1996.0003

59 Leverenz, J. B. & Raskind, M. A. Early amyloid deposition in the medial temporal lobe of young Down syndrome patients: a regional quantitative analysis. *Exp Neurol* **150**, 296-304 (1998). https://doi.org/10.1006/exnr.1997.6777

60 Dickson, T. C. & Vickers, J. C. The morphological phenotype of beta-amyloid plaques and associated neuritic changes in Alzheimer's disease. *Neuroscience* **105**, 99-107 (2001). https://doi.org/10.1016/s0306-4522(01)00169-5

61 Delaere, P., Duyckaerts, C., He, Y., Piette, F. & Hauw, J. J. Subtypes and differential laminar distributions of beta A4 deposits in Alzheimer's disease: relationship with the intellectual status of 26 cases. *Acta Neuropathol* **81**, 328-335 (1991). https://doi.org/10.1007/BF00305876

62 Duyckaerts, C., Delatour, B. & Potier, M. C. Classification and basic pathology of Alzheimer disease. *Acta Neuropathol* **118**, 5-36 (2009). https://doi.org/10.1007/s00401-009-0532-1

63 Mirra, S. S. *et al*. The Consortium to Establish a Registry for Alzheimer's Disease (CERAD). Part II. Standardization of the neuropathologic assessment of Alzheimer's disease. *Neurology* **41**, 479-486 (1991). https://doi.org/10.1212/wnl.41.4.479

64 Boon, B. D. C. *et al*. The coarse-grained plaque: a divergent Aβ plaque-type in early-onset Alzheimer's disease. *Acta Neuropathologica* **140**, 811-830 (2020). https://doi.org/10.1007/s00401-020-02198-8

65 Boon, B. D. C. *et al*. Neuroinflammation is increased in the parietal cortex of atypical Alzheimer's disease. *J Neuroinflammation* **15**, 170 (2018). https://doi.org/10.1186/s12974-018-1180-y

66 Ichimata, S., Martinez-Valbuena, I., Forrest, S. L. & Kovacs, G. G. Expanding the spectrum of amyloid-β plaque pathology: the Down syndrome associated 'bird-nest plaque'. *Acta Neuropathologica* (2022). https://doi.org/10.1007/s00401-022-02500-w

67 Charidimou, A. *et al*. Emerging concepts in sporadic cerebral amyloid angiopathy. *Brain* **140**, 1829-1850 (2017). https://doi.org/10.1093/brain/awx047

68 Greenberg, S. M. *et al*. Cerebral amyloid angiopathy and Alzheimer disease - one peptide, two pathways. *Nat Rev Neurol* **16**, 30-42 (2020). https://doi.org/10.1038/s41582-019-0281-2

69 Kapasi, A., DeCarli, C. & Schneider, J. A. Impact of multiple pathologies on the threshold for clinically overt dementia. *Acta Neuropathol* **134**, 171-186 (2017). https://doi.org/10.1007/s00401-017-1717-7

70 Leitner, D. *et al*. Differences in the cerebral amyloid angiopathy proteome in Alzheimer's disease and mild cognitive impairment. *Acta Neuropathol* **148**, 9 (2024). https://doi.org/10.1007/s00401-024-02767-1

71 Head, E. *et al*. Cerebrovascular pathology in Down syndrome and Alzheimer disease. *Acta Neuropathol Commun* **5**, 93 (2017). https://doi.org/10.1186/s40478-017-0499-4

72 Thal, D. R. *et al*. Two types of sporadic cerebral amyloid angiopathy. *J Neuropathol Exp Neurol* **61**, 282-293 (2002). https://doi.org/10.1093/jnen/61.3.282

73 Thal, D. R., Ghebremedhin, E., Orantes, M. & Wiestler, O. D. Vascular pathology in Alzheimer disease: correlation of cerebral amyloid angiopathy and arteriosclerosis/lipohyalinosis with cognitive decline. *J Neuropathol Exp Neurol* **62**, 1287-1301 (2003). https://doi.org/10.1093/jnen/62.12.1287

74 Fortea, J. *et al*. Alzheimer's disease associated with Down syndrome: a genetic form of dementia. *Lancet Neurol* **20**, 930-942 (2021). https://doi.org/10.1016/S1474-4422(21)00245-3

75 Szalardy, L., Lee, S., Kim, A. & Kovacs, G. G. Distinct cerebral amyloid angiopathy patterns in adult Down syndrome. *J Neurol Sci* **476**, 123601 (2025). https://doi.org/10.1016/j.jns.2025.123601

76 Goedert, M. & Jakes, R. Expression of separate isoforms of human tau protein: correlation with the tau pattern in brain and effects on tubulin polymerization. *EMBO J* **9**, 4225-4230 (1990). https://doi.org/10.1002/j.1460-2075.1990.tb07870.x

77 Kent, S. A., Spires-Jones, T. L. & Durrant, C. S. The physiological roles of tau and Abeta: implications for Alzheimer's disease pathology and therapeutics. *Acta Neuropathol* **140**, 417-447 (2020). https://doi.org/10.1007/s00401-020-02196-w

78 Avila, J., Lucas, J. J., Perez, M. & Hernandez, F. Role of tau protein in both physiological and pathological conditions. *Physiol Rev* **84**, 361-384 (2004). https://doi.org/10.1152/physrev.00024.2003

79 Sinsky, J., Pichlerova, K. & Hanes, J. Tau Protein Interaction Partners and Their Roles in Alzheimer's Disease and Other Tauopathies. *Int J Mol Sci* **22** (2021). https://doi.org/10.3390/ijms22179207

80 Congdon, E. E. & Sigurdsson, E. M. Tau-targeting therapies for Alzheimer disease. *Nat Rev Neurol* **14**, 399-415 (2018). https://doi.org/10.1038/s41582-018-0013-z

81 Braak, H., Alafuzoff, I., Arzberger, T., Kretzschmar, H. & Del Tredici, K. Staging of Alzheimer disease-associated neurofibrillary pathology using paraffin sections and immunocytochemistry. *Acta Neuropathol* **112**, 389-404 (2006). https://doi.org/10.1007/s00401-006-0127-z

82 Braak, H., Thal, D. R., Ghebremedhin, E. & Del Tredici, K. Stages of the pathologic process in Alzheimer disease: age categories from 1 to 100 years. *J Neuropathol Exp Neurol* **70**, 960-969 (2011). https://doi.org/10.1097/NEN.0b013e318232a379

83 Grundke-Iqbal, I. *et al*. Abnormal phosphorylation of the microtubule-associated protein tau (tau) in Alzheimer cytoskeletal pathology. *Proc Natl Acad Sci U S A* **83**, 4913-4917 (1986). https://doi.org/10.1073/pnas.83.13.4913

84 Fernandez, A. *et al.* Cryo-EM structures of amyloid-beta and tau filaments in Down syndrome. *Nat Struct Mol Biol* (2024). https://doi.org/10.1038/s41594-024-01252-3

85 Ghosh, U. *et al.* Cryo-EM structures reveal tau filaments from Down syndrome adopt Alzheimer's disease fold. *Acta Neuropathol Commun* **12**, 94 (2024). https://doi.org/10.1186/s40478-024-01806-y

86 Braak, H. & Braak, E. Neuropathological stageing of Alzheimer-related changes. *Acta Neuropathol* **82**, 239-259 (1991). https://doi.org/10.1007/BF00308809

87 Montine, T. J. *et al.* National Institute on Aging-Alzheimer's Association guidelines for the neuropathologic assessment of Alzheimer's disease: a practical approach. *Acta Neuropathol* **123**, 1-11 (2012). https://doi.org/10.1007/s00401-011-0910-3

88 Trejo-Lopez, J. A., Yachnis, A. T. & Prokop, S. Neuropathology of Alzheimer's Disease. *Neurotherapeutics* **19**, 173-185 (2022). https://doi.org/10.1007/s13311-021-01146-y

89 Goedert, M., Jakes, R. & Vanmechelen, E. Monoclonal antibody AT8 recognises tau protein phosphorylated at both serine 202 and threonine 205. *Neurosci Lett* **189**, 167-169 (1995). https://doi.org/10.1016/0304-3940(95)11484-e

90 Jucker, M. & Walker, L. C. Pathogenic protein seeding in Alzheimer disease and other neurodegenerative disorders. *Ann Neurol* **70**, 532-540 (2011). https://doi.org/10.1002/ana.22615

91 Henstridge, C. M., Pickett, E. & Spires-Jones, T. L. Synaptic pathology: A shared mechanism in neurological disease. *Ageing Res Rev* **28**, 72-84 (2016). https://doi.org/10.1016/j.arr.2016.04.005

92 Sudhof, T. C. The cell biology of synapse formation. *J Cell Biol* **220** (2021). https://doi.org/10.1083/jcb.202103052

93 Taddei, R. N. & Duff, K. E. Synapse vulnerability and resilience across the clinical spectrum of dementias. *Nat Rev Neurol* (2025). https://doi.org/10.1038/s41582-025-01094-7

94 DeKosky, S. T. & Scheff, S. W. Synapse loss in frontal cortex biopsies in Alzheimer's disease: correlation with cognitive severity. *Ann Neurol* **27**, 457-464 (1990). https://doi.org/10.1002/ana.410270502

95 Terry, R. D. *et al.* Physical basis of cognitive alterations in Alzheimer's disease: synapse loss is the major correlate of cognitive impairment. *Ann Neurol* **30**, 572-580 (1991). https://doi.org/10.1002/ana.410300410

96 Jackson, R. J. *et al.* Clusterin accumulates in synapses in Alzheimer's disease and is increased in apolipoprotein E4 carriers. *Brain Commun* **1**, fcz003 (2019). https://doi.org/10.1093/braincomms/fcz003

97 Koffie, R. M. *et al.* Apolipoprotein E4 effects in Alzheimer's disease are mediated by synaptotoxic oligomeric amyloid-beta. *Brain* **135**, 2155-2168 (2012). https://doi.org/10.1093/brain/aws127

98 Koffie, R. M. *et al.* Oligomeric amyloid beta associates with postsynaptic densities and correlates with excitatory synapse loss near senile plaques. *Proc Natl Acad Sci U S A* **106**, 4012-4017 (2009). https://doi.org/10.1073/pnas.0811698106

99 Tzioras, M., McGeachan, R. I., Durrant, C. S. & Spires-Jones, T. L. Synaptic degeneration in Alzheimer disease. *Nat Rev Neurol* **19**, 19-38 (2023). https://doi.org/10.1038/s41582-022-00749-z

100 Colom-Cadena, M. *et al*. Synaptic oligomeric tau in Alzheimer's disease - A potential culprit in the spread of tau pathology through the brain. *Neuron* **111**, 2170-2183 e2176 (2023). https://doi.org/10.1016/j.neuron.2023.04.020

101 Korczyn, A. D. & Grinberg, L. T. Is Alzheimer disease a disease? *Nat Rev Neurol* **20**, 245-251 (2024). https://doi.org/10.1038/s41582-024-00940-4

102 Zhang, J. *et al*. Recent advances in Alzheimer's disease: Mechanisms, clinical trials and new drug development strategies. *Signal Transduct Target Ther* **9**, 211 (2024). https://doi.org/10.1038/s41392-024-01911-3

103 Selkoe, D. J. & Hardy, J. The amyloid hypothesis of Alzheimer's disease at 25 years. *EMBO Mol Med* **8**, 595-608 (2016). https://doi.org/10.15252/emmm.201606210

104 De Strooper, B. & Karran, E. The Cellular Phase of Alzheimer's Disease. *Cell* **164**, 603-615 (2016). https://doi.org/10.1016/j.cell.2015.12.056

105 Jonsson, T. *et al*. A mutation in APP protects against Alzheimer's disease and age-related cognitive decline. *Nature* **488**, 96-99 (2012). https://doi.org/10.1038/nature11283

106 Shimohama, S. *et al*. The Icelandic Mutation (APP-A673T) Is Protective against Amyloid Pathology In Vivo. *J Neurosci* **44** (2024). https://doi.org/10.1523/JNEUROSCI.0223-24.2024

107 Herrup, K. The case for rejecting the amyloid cascade hypothesis. *Nat Neurosci* **18**, 794-799 (2015). https://doi.org/10.1038/nn.4017

108 Sha, S. *et al*. Recent advances in immunotherapy targeting amyloid-beta and tauopathies in Alzheimer's disease. *Neural Regen Res* **21**, 577-587 (2026). https://doi.org/10.4103/NRR.NRR-D-24-00846

109 Ganguly, P. *et al*. Tau assembly: the dominant role of PHF6 (VQIVYK) in microtubule binding region repeat R3. *J Phys Chem B* **119**, 4582-4593 (2015). https://doi.org/10.1021/acs.jpcb.5b00175

110 Guo, T. *et al*. Molecular and cellular mechanisms underlying the pathogenesis of Alzheimer's disease. *Mol Neurodegener* **15**, 40 (2020). https://doi.org/10.1186/s13024-020-00391-7

111 Guo, T., Noble, W. & Hanger, D. P. Roles of tau protein in health and disease. *Acta Neuropathol* **133**, 665-704 (2017). https://doi.org/10.1007/s00401-017-1707-9

112 Kamatham, P. T., Shukla, R., Khatri, D. K. & Vora, L. K. Pathogenesis, diagnostics, and therapeutics for Alzheimer's disease: Breaking the memory barrier. *Ageing Res Rev* **101**, 102481 (2024). https://doi.org/10.1016/j.arr.2024.102481

113 Eftekharzadeh, B. *et al*. Tau Protein Disrupts Nucleocytoplasmic Transport in Alzheimer's Disease. *Neuron* **99**, 925-940 e927 (2018). https://doi.org/10.1016/j.neuron.2018.07.039

114 Kosik, K. S. *et al*. Epitopes that span the tau molecule are shared with paired helical filaments. *Neuron* **1**, 817-825 (1988). https://doi.org/10.1016/0896-6273(88)90129-8

115 Braak, H. & Braak, E. Staging of Alzheimer's disease-related neurofibrillary changes. *Neurobiol Aging* **16**, 271-278; discussion 278-284 (1995). https://doi.org/10.1016/0197-4580(95)00021-6

116 Otero-Garcia, M. *et al*. Molecular signatures underlying neurofibrillary tangle susceptibility in Alzheimer's disease. *Neuron* **110**, 2929-2948 e2928 (2022). https://doi.org/10.1016/j.neuron.2022.06.021

117 Bartus, R. T., Dean, R. L., 3rd, Beer, B. & Lippa, A. S. The cholinergic hypothesis of geriatric memory dysfunction. *Science* **217**, 408-414 (1982). https://doi.org/10.1126/science.7046051

118 Terry, A. V., Jr. & Buccafusco, J. J. The cholinergic hypothesis of age and Alzheimer's disease-related cognitive deficits: recent challenges and their implications for novel drug development. *J Pharmacol Exp Ther* **306**, 821-827 (2003). https://doi.org/10.1124/jpet.102.041616

119 Chen, Z. R., Huang, J. B., Yang, S. L. & Hong, F. F. Role of Cholinergic Signaling in Alzheimer's Disease. *Molecules* **27** (2022). https://doi.org/10.3390/molecules27061816

120 Heneka, M. T. *et al*. Neuroinflammation in Alzheimer disease. *Nat Rev Immunol* **25**, 321-352 (2025). https://doi.org/10.1038/s41577-024-01104-7

121 Thakur, S., Dhapola, R., Sarma, P., Medhi, B. & Reddy, D. H. Neuroinflammation in Alzheimer's Disease: Current Progress in Molecular Signaling and Therapeutics. *Inflammation* **46**, 1-17 (2023). https://doi.org/10.1007/s10753-022-01721-1

122 Merighi, S., Nigro, M., Travagli, A. & Gessi, S. Microglia and Alzheimer's Disease. *Int J Mol Sci* **23** (2022). https://doi.org/10.3390/ijms232112990

123 Eikelenboom, P. & Stam, F. C. Immunoglobulins and complement factors in senile plaques. An immunoperoxidase study. *Acta Neuropathol* **57**, 239-242 (1982). https://doi.org/10.1007/BF00685397

124 Sadick, J. S. *et al*. Astrocytes and oligodendrocytes undergo subtype-specific transcriptional changes in Alzheimer's disease. *Neuron* **110**, 1788-1805 e1710 (2022). https://doi.org/10.1016/j.neuron.2022.03.008

125 Singh, D. Astrocytic and microglial cells as the modulators of neuroinflammation in Alzheimer's disease. *J Neuroinflammation* **19**, 206 (2022). https://doi.org/10.1186/s12974-022-02565-0

126 Leng, F. & Edison, P. Neuroinflammation and microglial activation in Alzheimer disease: where do we go from here? *Nat Rev Neurol* **17**, 157-172 (2021). https://doi.org/10.1038/s41582-020-00435-y

127 Franco-Bocanegra, D. K. *et al*. Microglial morphology in Alzheimer's disease and after Abeta immunotherapy. *Sci Rep* **11**, 15955 (2021). https://doi.org/10.1038/s41598-021-95535-0

128 Nimmerjahn, A., Kirchhoff, F. & Helmchen, F. Resting microglial cells are highly dynamic surveillants of brain parenchyma in vivo. *Science* **308**, 1314-1318 (2005). https://doi.org/10.1126/science.1110647

129 Jin, J. J., Kim, H. D., Maxwell, J. A., Li, L. & Fukuchi, K. Toll-like receptor 4-dependent upregulation of cytokines in a transgenic mouse model of Alzheimer's disease. *J Neuroinflammation* **5**, 23 (2008). https://doi.org/10.1186/1742-2094-5-23

130 Tahara, K. *et al*. Role of toll-like receptor signalling in Abeta uptake and clearance. *Brain* **129**, 3006-3019 (2006). https://doi.org/10.1093/brain/awl249
131 Yan, S. D. *et al*. RAGE and amyloid-beta peptide neurotoxicity in Alzheimer's disease. *Nature* **382**, 685-691 (1996). https://doi.org/10.1038/382685a0
132 Heneka, M. T. *et al*. NLRP3 is activated in Alzheimer's disease and contributes to pathology in APP/PS1 mice. *Nature* **493**, 674-678 (2013). https://doi.org/10.1038/nature11729
133 Liddelow, S. A. *et al*. Neurotoxic reactive astrocytes are induced by activated microglia. *Nature* **541**, 481-487 (2017). https://doi.org/10.1038/nature21029
134 Keren-Shaul, H. *et al*. A Unique Microglia Type Associated with Restricting Development of Alzheimer's Disease. *Cell* **169**, 1276-1290 e1217 (2017). https://doi.org/10.1016/j.cell.2017.05.018
135 Olah, M. *et al*. Single cell RNA sequencing of human microglia uncovers a subset associated with Alzheimer's disease. *Nat Commun* **11**, 6129 (2020). https://doi.org/10.1038/s41467-020-19737-2
136 Guerreiro, R. *et al*. TREM2 variants in Alzheimer's disease. *N Engl J Med* **368**, 117-127 (2013). https://doi.org/10.1056/NEJMoa1211851
137 Jonsson, T. *et al*. Variant of TREM2 associated with the risk of Alzheimer's disease. *N Engl J Med* **368**, 107-116 (2013). https://doi.org/10.1056/NEJMoa1211103
138 Zhang, B. *et al*. Integrated systems approach identifies genetic nodes and networks in late-onset Alzheimer's disease. *Cell* **153**, 707-720 (2013). https://doi.org/10.1016/j.cell.2013.03.030
139 Yuan, P. *et al*. TREM2 Haplodeficiency in Mice and Humans Impairs the Microglia Barrier Function Leading to Decreased Amyloid Compaction and Severe Axonal Dystrophy. *Neuron* **90**, 724-739 (2016). https://doi.org/10.1016/j.neuron.2016.05.003
140 Condello, C., Yuan, P., Schain, A. & Grutzendler, J. Microglia constitute a barrier that prevents neurotoxic protofibrillar Abeta42 hotspots around plaques. *Nat Commun* **6**, 6176 (2015). https://doi.org/10.1038/ncomms7176
141 Akiyama, H. *et al*. Inflammation and Alzheimer's disease. *Neurobiol Aging* **21**, 383-421 (2000). https://doi.org/10.1016/s0197-4580(00)00124-x
142 Giovannoni, F. & Quintana, F. J. The Role of Astrocytes in CNS Inflammation. *Trends Immunol* **41**, 805-819 (2020). https://doi.org/10.1016/j.it.2020.07.007
143 Kriegstein, A. & Alvarez-Buylla, A. The glial nature of embryonic and adult neural stem cells. *Annu Rev Neurosci* **32**, 149-184 (2009). https://doi.org/10.1146/annurev.neuro.051508.135600
144 Prakash, P. *et al*. Proteomic profiling of interferon-responsive reactive astrocytes in rodent and human. *Glia* **72**, 625-642 (2024). https://doi.org/10.1002/glia.24494
145 Han, R. T., Kim, R. D., Molofsky, A. V. & Liddelow, S. A. Astrocyte-immune cell interactions in physiology and pathology. *Immunity* **54**, 211-224 (2021). https://doi.org/10.1016/j.immuni.2021.01.013
146 Liddelow, S. A. & Sofroniew, M. V. Astrocytes usurp neurons as a disease focus. *Nat Neurosci* **22**, 512-513 (2019). https://doi.org/10.1038/s41593-019-0367-6

147 Escartin, C. *et al.* Reactive astrocyte nomenclature, definitions, and future directions. *Nat Neurosci* **24**, 312-325 (2021). https://doi.org/10.1038/s41593-020-00783-4
148 Serrano-Pozo, A. *et al.* Astrocyte transcriptomic changes along the spatiotemporal progression of Alzheimer's disease. *Nat Neurosci* **27**, 2384-2400 (2024). https://doi.org/10.1038/s41593-024-01791-4
149 Guttenplan, K. A. *et al.* Neurotoxic reactive astrocytes induce cell death via saturated lipids. *Nature* **599**, 102-107 (2021). https://doi.org/10.1038/s41586-021-03960-y
150 Lian, H. *et al.* Astrocyte-Microglia Cross Talk through Complement Activation Modulates Amyloid Pathology in Mouse Models of Alzheimer's Disease. *J Neurosci* **36**, 577-589 (2016). https://doi.org/10.1523/JNEUROSCI.2117-15.2016
151 Lian, H. *et al.* NFkappaB-activated astroglial release of complement C3 compromises neuronal morphology and function associated with Alzheimer's disease. *Neuron* **85**, 101-115 (2015). https://doi.org/10.1016/j.neuron.2014.11.018
152 Emery, B. Regulation of oligodendrocyte differentiation and myelination. *Science* **330**, 779-782 (2010). https://doi.org/10.1126/science.1190927
153 Ettle, B., Schlachetzki, J. C. M. & Winkler, J. Oligodendroglia and Myelin in Neurodegenerative Diseases: More Than Just Bystanders? *Mol Neurobiol* **53**, 3046-3062 (2016). https://doi.org/10.1007/s12035-015-9205-3
154 Lubetzki, C., Sol-Foulon, N. & Desmazieres, A. Nodes of Ranvier during development and repair in the CNS. *Nat Rev Neurol* **16**, 426-439 (2020). https://doi.org/10.1038/s41582-020-0375-x
155 Nave, K. A. Myelination and support of axonal integrity by glia. *Nature* **468**, 244-252 (2010). https://doi.org/10.1038/nature09614
156 Greer, J. M. & Lees, M. B. Myelin proteolipid protein--the first 50 years. *Int J Biochem Cell Biol* **34**, 211-215 (2002). https://doi.org/10.1016/s1357-2725(01)00136-4
157 Mallucci, G., Peruzzotti-Jametti, L., Bernstock, J. D. & Pluchino, S. The role of immune cells, glia and neurons in white and gray matter pathology in multiple sclerosis. *Prog Neurobiol* **127-128**, 1-22 (2015). https://doi.org/10.1016/j.pneurobio.2015.02.003
158 Steinman, L. Multiple sclerosis: a coordinated immunological attack against myelin in the central nervous system. *Cell* **85**, 299-302 (1996). https://doi.org/10.1016/s0092-8674(00)81107-1
159 Braak, H. & Braak, E. Development of Alzheimer-related neurofibrillary changes in the neocortex inversely recapitulates cortical myelogenesis. *Acta Neuropathol* **92**, 197-201 (1996). https://doi.org/10.1007/s004010050508
160 Bartzokis, G. *et al.* White matter structural integrity in healthy aging adults and patients with Alzheimer disease: a magnetic resonance imaging study. *Arch Neurol* **60**, 393-398 (2003). https://doi.org/10.1001/archneur.60.3.393
161 Lee, S. *et al.* White matter hyperintensities are a core feature of Alzheimer's disease: Evidence from the dominantly inherited Alzheimer network. *Ann Neurol* **79**, 929-939 (2016). https://doi.org/10.1002/ana.24647

162 Mitew, S. *et al.* Focal demyelination in Alzheimer's disease and transgenic mouse models. *Acta Neuropathol* **119**, 567-577 (2010). https://doi.org/10.1007/s00401-010-0657-2

163 Rajani, R. M. *et al.* Selective suppression of oligodendrocyte-derived amyloid beta rescues neuronal dysfunction in Alzheimer's disease. *PLoS Biol* **22**, e3002727 (2024). https://doi.org/10.1371/journal.pbio.3002727

164 Sasmita, A. O. *et al.* Oligodendrocytes produce amyloid-beta and contribute to plaque formation alongside neurons in Alzheimer's disease model mice. *Nat Neurosci* **27**, 1668-1674 (2024). https://doi.org/10.1038/s41593-024-01730-3

165 Ip, C. W. *et al.* Immune cells contribute to myelin degeneration and axonopathic changes in mice overexpressing proteolipid protein in oligodendrocytes. *J Neurosci* **26**, 8206-8216 (2006). https://doi.org/10.1523/JNEUROSCI.1921-06.2006

166 Mayatepek, E., Baumann, M., Meissner, T., Hanefeld, F. & Korenke, G. C. Role of leukotrienes as indicators of the inflammatory demyelinating reaction in x-linked cerebral adrenoleukodystrophy. *J Neurol* **250**, 1259-1260 (2003). https://doi.org/10.1007/s00415-003-0189-y

167 Askenazi, M. *et al.* Compilation of reported protein changes in the brain in Alzheimer's disease. *Nat Commun* **14**, 4466 (2023). https://doi.org/10.1038/s41467-023-40208-x

168 Bai, B. *et al.* Proteomic landscape of Alzheimer's Disease: novel insights into pathogenesis and biomarker discovery. *Mol Neurodegener* **16**, 55 (2021). https://doi.org/10.1186/s13024-021-00474-z

169 Chen, W. T. *et al.* Spatial Transcriptomics and In Situ Sequencing to Study Alzheimer's Disease. *Cell* **182**, 976-991 e919 (2020). https://doi.org/10.1016/j.cell.2020.06.038

170 Johnson, E. C. B. *et al.* Large-scale deep multi-layer analysis of Alzheimer's disease brain reveals strong proteomic disease-related changes not observed at the RNA level. *Nat Neurosci* **25**, 213-225 (2022). https://doi.org/10.1038/s41593-021-00999-y

171 Leng, K. *et al.* Molecular characterization of selectively vulnerable neurons in Alzheimer's disease. *Nat Neurosci* **24**, 276-287 (2021). https://doi.org/10.1038/s41593-020-00764-7

172 Mathys, H. *et al.* Single-cell transcriptomic analysis of Alzheimer's disease. *Nature* **570**, 332-337 (2019). https://doi.org/10.1038/s41586-019-1195-2

173 Cai, Y. *et al.* Myelin-axon interface vulnerability in Alzheimer's disease revealed by subcellular proteomics and imaging of human and mouse brain. *Nat Neurosci* (2025). https://doi.org/10.1038/s41593-025-01973-8

174 Falcao, A. M. *et al.* Disease-specific oligodendrocyte lineage cells arise in multiple sclerosis. *Nat Med* **24**, 1837-1844 (2018). https://doi.org/10.1038/s41591-018-0236-y

175 Kaya, T. *et al.* CD8(+) T cells induce interferon-responsive oligodendrocytes and microglia in white matter aging. *Nat Neurosci* **25**, 1446-1457 (2022). https://doi.org/10.1038/s41593-022-01183-6

176 Kenigsbuch, M. *et al*. A shared disease-associated oligodendrocyte signature among multiple CNS pathologies. *Nat Neurosci* **25**, 876-886 (2022). https://doi.org/10.1038/s41593-022-01104-7

177 Zhou, Y. *et al*. Human and mouse single-nucleus transcriptomics reveal TREM2-dependent and TREM2-independent cellular responses in Alzheimer's disease. *Nat Med* **26**, 131-142 (2020). https://doi.org/10.1038/s41591-019-0695-9

178 Haile, Y. *et al*. Granzyme B-inhibitor serpina3n induces neuroprotection in vitro and in vivo. *J Neuroinflammation* **12**, 157 (2015). https://doi.org/10.1186/s12974-015-0376-7

179 Peng, L., Bestard-Lorigados, I. & Song, W. The synapse as a treatment avenue for Alzheimer's Disease. *Mol Psychiatry* **27**, 2940-2949 (2022). https://doi.org/10.1038/s41380-022-01565-z

180 Fein, J. A. *et al*. Co-localization of amyloid beta and tau pathology in Alzheimer's disease synaptosomes. *Am J Pathol* **172**, 1683-1692 (2008). https://doi.org/10.2353/ajpath.2008.070829

181 Tai, H. C. *et al*. The synaptic accumulation of hyperphosphorylated tau oligomers in Alzheimer disease is associated with dysfunction of the ubiquitin-proteasome system. *Am J Pathol* **181**, 1426-1435 (2012). https://doi.org/10.1016/j.ajpath.2012.06.033

182 Largo-Barrientos, P. *et al*. Lowering Synaptogyrin-3 expression rescues Tau-induced memory defects and synaptic loss in the presence of microglial activation. *Neuron* **109**, 767-777 e765 (2021). https://doi.org/10.1016/j.neuron.2020.12.016

183 McInnes, J. *et al*. Synaptogyrin-3 Mediates Presynaptic Dysfunction Induced by Tau. *Neuron* **97**, 823-835 e828 (2018). https://doi.org/10.1016/j.neuron.2018.01.022

184 Zhou, L. *et al*. Tau association with synaptic vesicles causes presynaptic dysfunction. *Nat Commun* **8**, 15295 (2017). https://doi.org/10.1038/ncomms15295

185 Lauren, J., Gimbel, D. A., Nygaard, H. B., Gilbert, J. W. & Strittmatter, S. M. Cellular prion protein mediates impairment of synaptic plasticity by amyloid-beta oligomers. *Nature* **457**, 1128-1132 (2009). https://doi.org/10.1038/nature07761

186 Renner, M. *et al*. Deleterious effects of amyloid beta oligomers acting as an extracellular scaffold for mGluR5. *Neuron* **66**, 739-754 (2010). https://doi.org/10.1016/j.neuron.2010.04.029

187 Ronicke, R. *et al*. Early neuronal dysfunction by amyloid beta oligomers depends on activation of NR2B-containing NMDA receptors. *Neurobiol Aging* **32**, 2219-2228 (2011). https://doi.org/10.1016/j.neurobiolaging.2010.01.011

188 Wei, W. *et al*. Amyloid beta from axons and dendrites reduces local spine number and plasticity. *Nat Neurosci* **13**, 190-196 (2010). https://doi.org/10.1038/nn.2476

189 Yin, Y. *et al*. Tau accumulation induces synaptic impairment and memory deficit by calcineurin-mediated inactivation of nuclear CaMKIV/CREB signaling. *Proc Natl Acad Sci U S A* **113**, E3773-3781 (2016). https://doi.org/10.1073/pnas.1604519113

190 Izzo, N. J. *et al*. Alzheimer's therapeutics targeting amyloid beta 1-42 oligomers II: Sigma-2/PGRMC1 receptors mediate Abeta 42 oligomer binding and synaptotoxicity. *PLoS One* **9**, e111899 (2014). https://doi.org/10.1371/journal.pone.0111899

191 Riad, A. *et al*. The Sigma-2 Receptor/TMEM97, PGRMC1, and LDL Receptor Complex Are Responsible for the Cellular Uptake of Abeta42 and Its Protein Aggregates. *Mol Neurobiol* **57**, 3803-3813 (2020). https://doi.org/10.1007/s12035-020-01988-1

192 Carmona, S., Hardy, J. & Guerreiro, R. The genetic landscape of Alzheimer disease. *Handb Clin Neurol* **148**, 395-408 (2018). https://doi.org/10.1016/B978-0-444-64076-5.00026-0

193 Zhang, X. X. *et al*. The Epidemiology of Alzheimer's Disease Modifiable Risk Factors and Prevention. *J Prev Alzheimers Dis* **8**, 313-321 (2021). https://doi.org/10.14283/jpad.2021.15

194 Karch, C. M. & Goate, A. M. Alzheimer's disease risk genes and mechanisms of disease pathogenesis. *Biol Psychiatry* **77**, 43-51 (2015). https://doi.org/10.1016/j.biopsych.2014.05.006

195 Gatz, M. *et al*. Role of genes and environments for explaining Alzheimer disease. *Arch Gen Psychiatry* **63**, 168-174 (2006). https://doi.org/10.1001/archpsyc.63.2.168

196 Bekris, L. M., Yu, C. E., Bird, T. D. & Tsuang, D. W. Genetics of Alzheimer disease. *J Geriatr Psychiatry Neurol* **23**, 213-227 (2010). https://doi.org/10.1177/0891988710383571

197 Goate, A. *et al*. Segregation of a missense mutation in the amyloid precursor protein gene with familial Alzheimer's disease. *Nature* **349**, 704-706 (1991). https://doi.org/10.1038/349704a0

198 Levy-Lahad, E. *et al*. Candidate gene for the chromosome 1 familial Alzheimer's disease locus. *Science* **269**, 973-977 (1995). https://doi.org/10.1126/science.7638622

199 Murrell, J., Farlow, M., Ghetti, B. & Benson, M. D. A mutation in the amyloid precursor protein associated with hereditary Alzheimer's disease. *Science* **254**, 97-99 (1991). https://doi.org/10.1126/science.1925564

200 Ryman, D. C. *et al*. Symptom onset in autosomal dominant Alzheimer disease: a systematic review and meta-analysis. *Neurology* **83**, 253-260 (2014). https://doi.org/10.1212/WNL.0000000000000596

201 Brase, L. *et al*. Single-nucleus RNA-sequencing of autosomal dominant Alzheimer disease and risk variant carriers. *Nat Commun* **14**, 2314 (2023). https://doi.org/10.1038/s41467-023-37437-5

202 Zhou, L. *et al*. Amyloid precursor protein mutation E682K at the alternative beta-secretase cleavage beta'-site increases Abeta generation. *EMBO Mol Med* **3**, 291-302 (2011). https://doi.org/10.1002/emmm.201100138

203 Tsubuki, S., Takaki, Y. & Saido, T. C. Dutch, Flemish, Italian, and Arctic mutations of APP and resistance of Abeta to physiologically relevant proteolytic degradation. *Lancet* **361**, 1957-1958 (2003). https://doi.org/10.1016/s0140-6736(03)13555-6

204 Cruchaga, C. *et al*. Rare variants in APP, PSEN1 and PSEN2 increase risk for AD in late-onset Alzheimer's disease families. *PLoS One* **7**, e31039 (2012). https://doi.org/10.1371/journal.pone.0031039

205 Corder, E. H. *et al*. Gene dose of apolipoprotein E type 4 allele and the risk of Alzheimer's disease in late onset families. *Science* **261**, 921-923 (1993). https://doi.org/10.1126/science.8346443

206 Kim, J., Basak, J. M. & Holtzman, D. M. The role of apolipoprotein E in Alzheimer's disease. *Neuron* **63**, 287-303 (2009). https://doi.org/10.1016/j.neuron.2009.06.026

207 Mishra, S. *et al*. Longitudinal brain imaging in preclinical Alzheimer disease: impact of APOE epsilon4 genotype. *Brain* **141**, 1828-1839 (2018). https://doi.org/10.1093/brain/awy103

208 Strittmatter, W. J. *et al*. Binding of human apolipoprotein E to synthetic amyloid beta peptide: isoform-specific effects and implications for late-onset Alzheimer disease. *Proc Natl Acad Sci U S A* **90**, 8098-8102 (1993). https://doi.org/10.1073/pnas.90.17.8098

209 Yamazaki, Y., Zhao, N., Caulfield, T. R., Liu, C. C. & Bu, G. Apolipoprotein E and Alzheimer disease: pathobiology and targeting strategies. *Nat Rev Neurol* **15**, 501-518 (2019). https://doi.org/10.1038/s41582-019-0228-7

210 Grehan, S., Tse, E. & Taylor, J. M. Two distal downstream enhancers direct expression of the human apolipoprotein E gene to astrocytes in the brain. *J Neurosci* **21**, 812-822 (2001). https://doi.org/10.1523/JNEUROSCI.21-03-00812.2001

211 Xu, Q. *et al*. Profile and regulation of apolipoprotein E (ApoE) expression in the CNS in mice with targeting of green fluorescent protein gene to the ApoE locus. *J Neurosci* **26**, 4985-4994 (2006). https://doi.org/10.1523/JNEUROSCI.5476-05.2006

212 Gong, J. S. *et al*. Apolipoprotein E (ApoE) isoform-dependent lipid release from astrocytes prepared from human ApoE3 and ApoE4 knock-in mice. *J Biol Chem* **277**, 29919-29926 (2002). https://doi.org/10.1074/jbc.M203934200

213 Morikawa, M. *et al*. Production and characterization of astrocyte-derived human apolipoprotein E isoforms from immortalized astrocytes and their interactions with amyloid-beta. *Neurobiol Dis* **19**, 66-76 (2005). https://doi.org/10.1016/j.nbd.2004.11.005

214 Wahrle, S. E. *et al*. Deletion of Abca1 increases Abeta deposition in the PDAPP transgenic mouse model of Alzheimer disease. *J Biol Chem* **280**, 43236-43242 (2005). https://doi.org/10.1074/jbc.M508780200

215 Wahrle, S. E. *et al*. Overexpression of ABCA1 reduces amyloid deposition in the PDAPP mouse model of Alzheimer disease. *J Clin Invest* **118**, 671-682 (2008). https://doi.org/10.1172/JCI33622

216 Castellano, J. M. *et al*. Low-density lipoprotein receptor overexpression enhances the rate of brain-to-blood Abeta clearance in a mouse model of beta-amyloidosis. *Proc Natl Acad Sci U S A* **109**, 15502-15507 (2012). https://doi.org/10.1073/pnas.1206446109

217 Fryer, J. D. *et al*. The low density lipoprotein receptor regulates the level of central nervous system human and murine apolipoprotein E but does not

modify amyloid plaque pathology in PDAPP mice. *J Biol Chem* **280**, 25754-25759 (2005). https://doi.org/10.1074/jbc.M502143200

218 Holtzman, D. M., Herz, J. & Bu, G. Apolipoprotein E and apolipoprotein E receptors: normal biology and roles in Alzheimer disease. *Cold Spring Harb Perspect Med* **2**, a006312 (2012). https://doi.org/10.1101/cshperspect.a006312

219 Christensen, D. Z., Schneider-Axmann, T., Lucassen, P. J., Bayer, T. A. & Wirths, O. Accumulation of intraneuronal Abeta correlates with ApoE4 genotype. *Acta Neuropathol* **119**, 555-566 (2010). https://doi.org/10.1007/s00401-010-0666-1

220 Naslund, J. *et al*. Characterization of stable complexes involving apolipoprotein E and the amyloid beta peptide in Alzheimer's disease brain. *Neuron* **15**, 219-228 (1995). https://doi.org/10.1016/0896-6273(95)90079-9

221 Wisniewski, T. & Frangione, B. Apolipoprotein E: a pathological chaperone protein in patients with cerebral and systemic amyloid. *Neurosci Lett* **135**, 235-238 (1992). https://doi.org/10.1016/0304-3940(92)90444-c

222 Kok, E. *et al*. Apolipoprotein E-dependent accumulation of Alzheimer disease-related lesions begins in middle age. *Ann Neurol* **65**, 650-657 (2009). https://doi.org/10.1002/ana.21696

223 Serrano-Pozo, A., Qian, J., Monsell, S. E., Betensky, R. A. & Hyman, B. T. APOEepsilon2 is associated with milder clinical and pathological Alzheimer disease. *Ann Neurol* **77**, 917-929 (2015). https://doi.org/10.1002/ana.24369

224 Tiraboschi, P. *et al*. Impact of APOE genotype on neuropathologic and neurochemical markers of Alzheimer disease. *Neurology* **62**, 1977-1983 (2004). https://doi.org/10.1212/01.wnl.0000128091.92139.0f

225 Fleisher, A. S. *et al*. Apolipoprotein E epsilon4 and age effects on florbetapir positron emission tomography in healthy aging and Alzheimer disease. *Neurobiol Aging* **34**, 1-12 (2013). https://doi.org/10.1016/j.neurobiolaging.2012.04.017

226 Gonneaud, J. *et al*. Relative effect of APOE epsilon4 on neuroimaging biomarker changes across the lifespan. *Neurology* **87**, 1696-1703 (2016). https://doi.org/10.1212/WNL.0000000000003234

227 Kantarci, K. *et al*. APOE modifies the association between Abeta load and cognition in cognitively normal older adults. *Neurology* **78**, 232-240 (2012). https://doi.org/10.1212/WNL.0b013e31824365ab

228 Murphy, K. R. *et al*. Mapping the effects of ApoE4, age and cognitive status on 18F-florbetapir PET measured regional cortical patterns of beta-amyloid density and growth. *Neuroimage* **78**, 474-480 (2013). https://doi.org/10.1016/j.neuroimage.2013.04.048

229 Harman, D. Alzheimer's disease pathogenesis: role of aging. *Ann N Y Acad Sci* **1067**, 454-460 (2006). https://doi.org/10.1196/annals.1354.065

230 Schrijvers, E. M., Koudstaal, P. J., Hofman, A. & Breteler, M. M. Plasma clusterin and the risk of Alzheimer disease. *JAMA* **305**, 1322-1326 (2011). https://doi.org/10.1001/jama.2011.381

231 Thambisetty, M. *et al*. Association of plasma clusterin concentration with severity, pathology, and progression in Alzheimer disease. *Arch Gen Psychiatry* **67**, 739-748 (2010). https://doi.org/10.1001/archgenpsychiatry.2010.78

232 Deming, Y. *et al.* A potential endophenotype for Alzheimer's disease: cerebrospinal fluid clusterin. *Neurobiol Aging* **37**, 208 e201-208 e209 (2016). https://doi.org/10.1016/j.neurobiolaging.2015.09.009

233 Kim, W. S., Guillemin, G. J., Glaros, E. N., Lim, C. K. & Garner, B. Quantitation of ATP-binding cassette subfamily-A transporter gene expression in primary human brain cells. *Neuroreport* **17**, 891-896 (2006). https://doi.org/10.1097/01.wnr.0000221833.41340.cd

234 Chan, S. L. *et al.* ATP-binding cassette transporter A7 regulates processing of amyloid precursor protein in vitro. *J Neurochem* **106**, 793-804 (2008). https://doi.org/10.1111/j.1471-4159.2008.05433.x

235 Jehle, A. W. *et al.* ATP-binding cassette transporter A7 enhances phagocytosis of apoptotic cells and associated ERK signaling in macrophages. *J Cell Biol* **174**, 547-556 (2006). https://doi.org/10.1083/jcb.200601030

236 Kim, W. S. *et al.* Abca7 null mice retain normal macrophage phosphatidylcholine and cholesterol efflux activity despite alterations in adipose mass and serum cholesterol levels. *J Biol Chem* **280**, 3989-3995 (2005). https://doi.org/10.1074/jbc.M412602200

237 Tanaka, N., Abe-Dohmae, S., Iwamoto, N. & Yokoyama, S. Roles of ATP-binding cassette transporter A7 in cholesterol homeostasis and host defense system. *J Atheroscler Thromb* **18**, 274-281 (2011). https://doi.org/10.5551/jat.6726

238 Kim, W. S. *et al.* Deletion of Abca7 increases cerebral amyloid-beta accumulation in the J20 mouse model of Alzheimer's disease. *J Neurosci* **33**, 4387-4394 (2013). https://doi.org/10.1523/JNEUROSCI.4165-12.2013

239 Shulman, J. M. *et al.* Genetic susceptibility for Alzheimer disease neuritic plaque pathology. *JAMA Neurol* **70**, 1150-1157 (2013). https://doi.org/10.1001/jamaneurol.2013.2815

240 Walker, D. G. *et al.* Association of CD33 polymorphism rs3865444 with Alzheimer's disease pathology and CD33 expression in human cerebral cortex. *Neurobiol Aging* **36**, 571-582 (2015). https://doi.org/10.1016/j.neurobiolaging.2014.09.023

241 Griciuc, A. *et al.* Alzheimer's disease risk gene CD33 inhibits microglial uptake of amyloid beta. *Neuron* **78**, 631-643 (2013). https://doi.org/10.1016/j.neuron.2013.04.014

242 Ulland, T. K. & Colonna, M. TREM2 - a key player in microglial biology and Alzheimer disease. *Nat Rev Neurol* **14**, 667-675 (2018). https://doi.org/10.1038/s41582-018-0072-1

243 Wang, Y. *et al.* TREM2 lipid sensing sustains the microglial response in an Alzheimer's disease model. *Cell* **160**, 1061-1071 (2015). https://doi.org/10.1016/j.cell.2015.01.049

244 Melchior, B. *et al.* Dual induction of TREM2 and tolerance-related transcript, Tmem176b, in amyloid transgenic mice: implications for vaccine-based therapies for Alzheimer's disease. *ASN Neuro* **2**, e00037 (2010). https://doi.org/10.1042/AN20100010

245 Chapuis, J. *et al.* Increased expression of BIN1 mediates Alzheimer genetic risk by modulating tau pathology. *Mol Psychiatry* **18**, 1225-1234 (2013). https://doi.org/10.1038/mp.2013.1

246 Harold, D. *et al*. Genome-wide association study identifies variants at CLU and PICALM associated with Alzheimer's disease. *Nat Genet* **41**, 1088-1093 (2009). https://doi.org/10.1038/ng.440

247 Xiao, Q. *et al*. Role of phosphatidylinositol clathrin assembly lymphoid-myeloid leukemia (PICALM) in intracellular amyloid precursor protein (APP) processing and amyloid plaque pathogenesis. *J Biol Chem* **287**, 21279-21289 (2012). https://doi.org/10.1074/jbc.M111.338376

248 Rogaeva, E. *et al*. The neuronal sortilin-related receptor SORL1 is genetically associated with Alzheimer disease. *Nat Genet* **39**, 168-177 (2007). https://doi.org/10.1038/ng1943

249 Dodson, S. E. *et al*. Loss of LR11/SORLA enhances early pathology in a mouse model of amyloidosis: evidence for a proximal role in Alzheimer's disease. *J Neurosci* **28**, 12877-12886 (2008). https://doi.org/10.1523/JNEUROSCI.4582-08.2008

250 Sager, K. L. *et al*. Neuronal LR11/sorLA expression is reduced in mild cognitive impairment. *Ann Neurol* **62**, 640-647 (2007). https://doi.org/10.1002/ana.21190

251 Lambert, J. C. *et al*. Meta-analysis of 74,046 individuals identifies 11 new susceptibility loci for Alzheimer's disease. *Nat Genet* **45**, 1452-1458 (2013). https://doi.org/10.1038/ng.2802

252 De Leon, M. J. *et al*. Frequency of hippocampal formation atrophy in normal aging and Alzheimer's disease. *Neurobiol Aging* **18**, 1-11 (1997). https://doi.org/10.1016/s0197-4580(96)00213-8

253 Jack, C. R., Jr. *et al*. Rate of medial temporal lobe atrophy in typical aging and Alzheimer's disease. *Neurology* **51**, 993-999 (1998). https://doi.org/10.1212/wnl.51.4.993

254 Koedam, E. L. *et al*. Early-versus late-onset Alzheimer's disease: more than age alone. *J Alzheimers Dis* **19**, 1401-1408 (2010). https://doi.org/10.3233/JAD-2010-1337

255 Barnes, J. *et al*. Alzheimer's disease first symptoms are age dependent: Evidence from the NACC dataset. *Alzheimers Dement* **11**, 1349-1357 (2015). https://doi.org/10.1016/j.jalz.2014.12.007

256 Suribhatla, S. *et al*. Neuropsychological performance in early and late onset Alzheimer's disease: comparisons in a memory clinic population. *Int J Geriatr Psychiatry* **19**, 1140-1147 (2004). https://doi.org/10.1002/gps.1196

257 Graff-Radford, J. *et al*. New insights into atypical Alzheimer's disease in the era of biomarkers. *Lancet Neurol* **20**, 222-234 (2021). https://doi.org/10.1016/S1474-4422(20)30440-3

258 Murray, M. E. *et al*. Neuropathologically defined subtypes of Alzheimer's disease with distinct clinical characteristics: a retrospective study. *Lancet Neurol* **10**, 785-796 (2011). https://doi.org/10.1016/S1474-4422(11)70156-9

259 Palasi, A. *et al*. Differentiated clinical presentation of early and late-onset Alzheimer's disease: is 65 years of age providing a reliable threshold? *J Neurol* **262**, 1238-1246 (2015). https://doi.org/10.1007/s00415-015-7698-3

260 Jellinger, K. A. Pathobiological Subtypes of Alzheimer Disease. *Dement Geriatr Cogn Disord* **49**, 321-333 (2020). https://doi.org/10.1159/000508625

261 Mann, U. M., Mohr, E. & Chase, T. N. Rapidly progressive Alzheimer's disease. *Lancet* **2**, 799 (1989). https://doi.org/10.1016/s0140-6736(89)90857-x
262 Mayeux, R., Stern, Y. & Spanton, S. Heterogeneity in dementia of the Alzheimer type: evidence of subgroups. *Neurology* **35**, 453-461 (1985). https://doi.org/10.1212/wnl.35.4.453
263 Chitravas, N. *et al*. Treatable neurological disorders misdiagnosed as Creutzfeldt-Jakob disease. *Ann Neurol* **70**, 437-444 (2011). https://doi.org/10.1002/ana.22454
264 Drummond, E. *et al*. Proteomic differences in amyloid plaques in rapidly progressive and sporadic Alzheimer's disease. *Acta Neuropathol* **133**, 933-954 (2017). https://doi.org/10.1007/s00401-017-1691-0
265 Cohen, M. L. *et al*. Rapidly progressive Alzheimer's disease features distinct structures of amyloid-beta. *Brain* **138**, 1009-1022 (2015). https://doi.org/10.1093/brain/awv006
266 Blennow, K., de Leon, M. J. & Zetterberg, H. Alzheimer's disease. *Lancet* **368**, 387-403 (2006). https://doi.org/10.1016/S0140-6736(06)69113-7
267 Wolfe, M. S. In search of pathogenic amyloid beta-peptide in familial Alzheimer's disease. *Prog Mol Biol Transl Sci* **168**, 71-78 (2019). https://doi.org/10.1016/bs.pmbts.2019.07.002
268 Wu, L. *et al*. Early-onset familial Alzheimer's disease (EOFAD). *Can J Neurol Sci* **39**, 436-445 (2012). https://doi.org/10.1017/s0317167100013949
269 Fortea, J., Quiroz, Y. T. & Ryan, N. S. Lessons from Down syndrome and autosomal dominant Alzheimer's disease. *Lancet Neurol* **22**, 5-6 (2023). https://doi.org/10.1016/S1474-4422(22)00437-9
270 Antonarakis, S. E. Down syndrome and the complexity of genome dosage imbalance. *Nat Rev Genet* **18**, 147-163 (2017). https://doi.org/10.1038/nrg.2016.154
271 Antonarakis, S. E. *et al*. Down syndrome. *Nat Rev Dis Primers* **6**, 9 (2020). https://doi.org/10.1038/s41572-019-0143-7
272 Satge, D. & Seidel, M. G. The Pattern of Malignancies in Down Syndrome and Its Potential Context With the Immune System. *Front Immunol* **9**, 3058 (2018). https://doi.org/10.3389/fimmu.2018.03058
273 Down, J. L. Observations on an ethnic classification of idiots. 1866. *Ment Retard* **33**, 54-56 (1995).
274 Jacobs, P. A., Baikie, A. G., Court Brown, W. M. & Strong, J. A. The somatic chromosomes in mongolism. *Lancet* **1**, 710 (1959). https://doi.org/10.1016/s0140-6736(59)91892-6
275 Lejeune, J., Gautier, M. & Turpin, R. [Study of somatic chromosomes from 9 mongoloid children]. *C R Hebd Seances Acad Sci* **248**, 1721-1722 (1959).
276 Russo, M. L., Sousa, A. M. M. & Bhattacharyya, A. Consequences of trisomy 21 for brain development in Down syndrome. *Nat Rev Neurosci* **25**, 740-755 (2024). https://doi.org/10.1038/s41583-024-00866-2
277 Becker, L., Mito, T., Takashima, S. & Onodera, K. Growth and development of the brain in Down syndrome. *Prog Clin Biol Res* **373**, 133-152 (1991).

278 Wisniewski, K. E. Down syndrome children often have brain with maturation delay, retardation of growth, and cortical dysgenesis. *Am J Med Genet Suppl* **7**, 274-281 (1990). https://doi.org/10.1002/ajmg.1320370755

279 Baumer, N. T. *et al*. Co-occurring conditions in Down syndrome: Findings from a clinical database. *Am J Med Genet C Semin Med Genet* **193**, e32072 (2023). https://doi.org/10.1002/ajmg.c.32072

280 Bull, M. J. Down Syndrome. *N Engl J Med* **382**, 2344-2352 (2020). https://doi.org/10.1056/NEJMra1706537

281 Patterson, D. Molecular genetic analysis of Down syndrome. *Hum Genet* **126**, 195-214 (2009). https://doi.org/10.1007/s00439-009-0696-8

282 National Down Syndrome Society. *About Down Syndrome*, <https://ndss.org/about> (n.d.).

283 Papavassiliou, P. *et al*. The phenotype of persons having mosaicism for trisomy 21/Down syndrome reflects the percentage of trisomic cells present in different tissues. *Am J Med Genet A* **149A**, 573-583 (2009). https://doi.org/10.1002/ajmg.a.32729

284 Moyer, A. J., Gardiner, K. & Reeves, R. H. All Creatures Great and Small: New Approaches for Understanding Down Syndrome Genetics. *Trends Genet* **37**, 444-459 (2021). https://doi.org/10.1016/j.tig.2020.09.017

285 Letourneau, A. & Antonarakis, S. E. Genomic determinants in the phenotypic variability of Down syndrome. *Prog Brain Res* **197**, 15-28 (2012). https://doi.org/10.1016/B978-0-444-54299-1.00002-9

286 Lockstone, H. E. *et al*. Gene expression profiling in the adult Down syndrome brain. *Genomics* **90**, 647-660 (2007). https://doi.org/10.1016/j.ygeno.2007.08.005

287 Bamburg, J. R. & Bloom, G. S. Cytoskeletal pathologies of Alzheimer disease. *Cell Motil Cytoskeleton* **66**, 635-649 (2009). https://doi.org/10.1002/cm.20388

288 Terry, R. D. The cytoskeleton in Alzheimer disease. *J Neural Transm Suppl* **53**, 141-145 (1998). https://doi.org/10.1007/978-3-7091-6467-9_12

289 De Vita, S. *et al*. Trisomic dose of several chromosome 21 genes perturbs haematopoietic stem and progenitor cell differentiation in Down's syndrome. *Oncogene* **29**, 6102-6114 (2010). https://doi.org/10.1038/onc.2010.351

290 Osato, M. & Ito, Y. Increased dosage of the RUNX1/AML1 gene: a third mode of RUNX leukemia? *Crit Rev Eukaryot Gene Expr* **15**, 217-228 (2005). https://doi.org/10.1615/critreveukargeneexpr.v15.i3.40

291 Pecze, L. & Szabo, C. Meta-analysis of gene expression patterns in Down syndrome highlights significant alterations in mitochondrial and bioenergetic pathways. *Mitochondrion* **57**, 163-172 (2021). https://doi.org/10.1016/j.mito.2020.12.017

292 Krivega, M. & Storchova, Z. Consequences of trisomy syndromes - 21 and beyond. *Trends Genet* **39**, 172-174 (2023). https://doi.org/10.1016/j.tig.2022.11.004

293 Pritchard, M. A. & Kola, I. The "gene dosage effect" hypothesis versus the "amplified developmental instability" hypothesis in Down syndrome. *J Neural Transm Suppl* **57**, 293-303 (1999).

294 Shapiro, B. L. Down syndrome--a disruption of homeostasis. *Am J Med Genet* **14**, 241-269 (1983). https://doi.org/10.1002/ajmg.1320140206
295 Epstein, C. J. *et al.* Protocols to establish genotype-phenotype correlations in Down syndrome. *Am J Hum Genet* **49**, 207-235 (1991).
296 Patterson, D. The causes of Down syndrome. *Sci Am* **257**, 52-57, 60 (1987). https://doi.org/10.1038/scientificamerican0887-52
297 Shapiro, B. L. The Down syndrome critical region. *J Neural Transm Suppl* **57**, 41-60 (1999). https://doi.org/10.1007/978-3-7091-6380-1_3
298 Pelleri, M. C. *et al.* Systematic reanalysis of partial trisomy 21 cases with or without Down syndrome suggests a small region on 21q22.13 as critical to the phenotype. *Hum Mol Genet* **25**, 2525-2538 (2016). https://doi.org/10.1093/hmg/ddw116
299 Cheon, M. S. *et al.* Protein levels of genes encoded on chromosome 21 in fetal Down syndrome brain: challenging the gene dosage effect hypothesis (Part I). *Amino Acids* **24**, 111-117 (2003). https://doi.org/10.1007/s00726-002-0336-2
300 Greber-Platzer, S., Schatzmann-Turhani, D., Wollenek, G. & Lubec, G. Evidence against the current hypothesis of "gene dosage effects" of trisomy 21: ets-2, encoded on chromosome 21" is not overexpressed in hearts of patients with Down Syndrome. *Biochem Biophys Res Commun* **254**, 395-399 (1999). https://doi.org/10.1006/bbrc.1998.9743
301 Hunter, S., Hendrix, J., Freeman, J., Dowell, R. D. & Allen, M. A. Transcription dosage compensation does not occur in Down syndrome. *BMC Biol* **21**, 228 (2023). https://doi.org/10.1186/s12915-023-01700-4
302 Lyle, R. *et al.* Genotype-phenotype correlations in Down syndrome identified by array CGH in 30 cases of partial trisomy and partial monosomy chromosome 21. *Eur J Hum Genet* **17**, 454-466 (2009). https://doi.org/10.1038/ejhg.2008.214
303 Olson, L. E., Richtsmeier, J. T., Leszl, J. & Reeves, R. H. A chromosome 21 critical region does not cause specific Down syndrome phenotypes. *Science* **306**, 687-690 (2004). https://doi.org/10.1126/science.1098992
304 Rastogi, M. *et al.* Integrative multi-omic analysis reveals conserved cell-projection deficits in human Down syndrome brains. *Neuron* **112**, 2503-2523 e2510 (2024). https://doi.org/10.1016/j.neuron.2024.05.002
305 Bittles, A. H., Bower, C., Hussain, R. & Glasson, E. J. The four ages of Down syndrome. *Eur J Public Health* **17**, 221-225 (2007). https://doi.org/10.1093/eurpub/ckl103
306 Capone, G. *et al.* Co-occurring medical conditions in adults with Down syndrome: A systematic review toward the development of health care guidelines. Part II. *Am J Med Genet A* **182**, 1832-1845 (2020). https://doi.org/10.1002/ajmg.a.61604
307 Glasson, E. J. *et al.* The changing survival profile of people with Down's syndrome: implications for genetic counselling. *Clin Genet* **62**, 390-393 (2002). https://doi.org/10.1034/j.1399-0004.2002.620506.x
308 Snyder, H. M. *et al.* Further understanding the connection between Alzheimer's disease and Down syndrome. *Alzheimers Dement* **16**, 1065-1077 (2020). https://doi.org/10.1002/alz.12112

309 Hithersay, R. *et al.* Association of Dementia With Mortality Among Adults With Down Syndrome Older Than 35 Years. *JAMA Neurol* **76**, 152-160 (2019). https://doi.org/10.1001/jamaneurol.2018.3616

310 Baburamani, A. A., Patkee, P. A., Arichi, T. & Rutherford, M. A. New approaches to studying early brain development in Down syndrome. *Dev Med Child Neurol* **61**, 867-879 (2019). https://doi.org/10.1111/dmcn.14260

311 Carmona-Iragui, M., Videla, L., Lleo, A. & Fortea, J. Down syndrome, Alzheimer disease, and cerebral amyloid angiopathy: The complex triangle of brain amyloidosis. *Dev Neurobiol* **79**, 716-737 (2019). https://doi.org/10.1002/dneu.22709

312 Dekker, A. D. *et al.* The Behavioral and Psychological Symptoms of Dementia in Down Syndrome (BPSD-DS) Scale: Comprehensive Assessment of Psychopathology in Down Syndrome. *J Alzheimers Dis* **63**, 797-819 (2018). https://doi.org/10.3233/JAD-170920

313 Glenner, G. G. & Wong, C. W. Alzheimer's disease and Down's syndrome: sharing of a unique cerebrovascular amyloid fibril protein. *Biochem Biophys Res Commun* **122**, 1131-1135 (1984). https://doi.org/10.1016/0006-291x(84)91209-9

314 Iulita, M. F. *et al.* Association of Alzheimer Disease With Life Expectancy in People With Down Syndrome. *JAMA Netw Open* **5**, e2212910 (2022). https://doi.org/10.1001/jamanetworkopen.2022.12910

315 Bateman, R. J. *et al.* Clinical and biomarker changes in dominantly inherited Alzheimer's disease. *N Engl J Med* **367**, 795-804 (2012). https://doi.org/10.1056/NEJMoa1202753

316 Silverman, W. *et al.* Individualized estimated years from onset of Alzheimer's disease- related decline for adults with Down syndrome. *Alzheimers Dement (Amst)* **15**, e12444 (2023). https://doi.org/10.1002/dad2.12444

317 Doran, E. *et al.* Down Syndrome, Partial Trisomy 21, and Absence of Alzheimer's Disease: The Role of APP. *J Alzheimers Dis* **56**, 459-470 (2017). https://doi.org/10.3233/JAD-160836

318 Gardiner, K. & Davisson, M. The sequence of human chromosome 21 and implications for research into Down syndrome. *Genome Biology* **1**, reviews0002.0001 (2000). https://doi.org/10.1186/gb-2000-1-2-reviews0002

319 Prasher, V. P. *et al.* Molecular mapping of Alzheimer-type dementia in Down's syndrome. *Ann Neurol* **43**, 380-383 (1998). https://doi.org/10.1002/ana.410430316

320 Fortea, J. *et al.* Clinical and biomarker changes of Alzheimer's disease in adults with Down syndrome: a cross-sectional study. *Lancet* **395**, 1988-1997 (2020). https://doi.org/10.1016/S0140-6736(20)30689-9

321 Cataldo, A. M. *et al.* Endocytic pathway abnormalities precede amyloid beta deposition in sporadic Alzheimer's disease and Down syndrome: differential effects of APOE genotype and presenilin mutations. *Am J Pathol* **157**, 277-286 (2000). https://doi.org/10.1016/s0002-9440(10)64538-5

322 Gyure, K. A., Durham, R., Stewart, W. F., Smialek, J. E. & Troncoso, J. C. Intraneuronal abeta-amyloid precedes development of amyloid plaques in

Down syndrome. *Arch Pathol Lab Med* **125**, 489-492 (2001). https://doi.org/10.5858/2001-125-0489-IAAPDO

323 Botte, A. *et al*. Ultrastructural and dynamic studies of the endosomal compartment in Down syndrome. *Acta Neuropathol Commun* **8**, 89 (2020). https://doi.org/10.1186/s40478-020-00956-z

324 Busciglio, J. *et al*. Altered metabolism of the amyloid beta precursor protein is associated with mitochondrial dysfunction in Down's syndrome. *Neuron* **33**, 677-688 (2002). https://doi.org/10.1016/s0896-6273(02)00604-9

325 Mann, D. M. The pathological association between Down syndrome and Alzheimer disease. *Mech Ageing Dev* **43**, 99-136 (1988). https://doi.org/10.1016/0047-6374(88)90041-3

326 Iwatsubo, T., Mann, D. M., Odaka, A., Suzuki, N. & Ihara, Y. Amyloid beta protein (A beta) deposition: A beta 42(43) precedes A beta 40 in Down syndrome. *Ann Neurol* **37**, 294-299 (1995). https://doi.org/10.1002/ana.410370305

327 Mann, D. M. & Iwatsubo, T. Diffuse plaques in the cerebellum and corpus striatum in Down's syndrome contain amyloid beta protein (A beta) only in the form of A beta 42(43). *Neurodegeneration* **5**, 115-120 (1996). https://doi.org/10.1006/neur.1996.0017

328 Azizeh, B. Y. *et al*. Molecular dating of senile plaques in the brains of individuals with Down syndrome and in aged dogs. *Exp Neurol* **163**, 111-122 (2000). https://doi.org/10.1006/exnr.2000.7359

329 Fonseca, M. I., Head, E., Velazquez, P., Cotman, C. W. & Tenner, A. J. The presence of isoaspartic acid in beta-amyloid plaques indicates plaque age. *Exp Neurol* **157**, 277-288 (1999). https://doi.org/10.1006/exnr.1999.7058

330 Head, E. *et al*. Oxidation of Abeta and plaque biogenesis in Alzheimer's disease and Down syndrome. *Neurobiol Dis* **8**, 792-806 (2001). https://doi.org/10.1006/nbdi.2001.0431

331 Head, E., Lott, I. T., Wilcock, D. M. & Lemere, C. A. Aging in Down Syndrome and the Development of Alzheimer's Disease Neuropathology. *Curr Alzheimer Res* **13**, 18-29 (2016). https://doi.org/10.2174/1567205012666151020114607

332 Iwatsubo, T., Saido, T. C., Mann, D. M., Lee, V. M. & Trojanowski, J. Q. Full-length amyloid-beta (1-42(43)) and amino-terminally modified and truncated amyloid-beta 42(43) deposit in diffuse plaques. *Am J Pathol* **149**, 1823-1830 (1996).

333 Liu, K. *et al*. Characterization of Abeta11-40/42 peptide deposition in Alzheimer's disease and young Down's syndrome brains: implication of N-terminally truncated Abeta species in the pathogenesis of Alzheimer's disease. *Acta Neuropathol* **112**, 163-174 (2006). https://doi.org/10.1007/s00401-006-0077-5

334 Drummond, E. *et al*. The amyloid plaque proteome in early onset Alzheimer's disease and Down syndrome. *Acta Neuropathologica Communications* **10**, 53 (2022). https://doi.org/10.1186/s40478-022-01356-1

335 Carmona-Iragui, M. *et al*. Cerebral amyloid angiopathy in Down syndrome and sporadic and autosomal-dominant Alzheimer's disease. *Alzheimers Dement* **13**, 1251-1260 (2017). https://doi.org/10.1016/j.jalz.2017.03.007

336 Head, E. *et al*. Parallel compensatory and pathological events associated with tau pathology in middle aged individuals with Down syndrome. *J Neuropathol Exp Neurol* **62**, 917-926 (2003). https://doi.org/10.1093/jnen/62.9.917

337 Hof, P. R. *et al*. Age-related distribution of neuropathologic changes in the cerebral cortex of patients with Down's syndrome. Quantitative regional analysis and comparison with Alzheimer's disease. *Arch Neurol* **52**, 379-391 (1995). https://doi.org/10.1001/archneur.1995.00540280065020

338 Harris, C. D., Ermak, G. & Davies, K. J. RCAN1-1L is overexpressed in neurons of Alzheimer's disease patients. *FEBS J* **274**, 1715-1724 (2007). https://doi.org/10.1111/j.1742-4658.2007.05717.x

339 Wegiel, J. *et al*. Link between DYRK1A overexpression and several-fold enhancement of neurofibrillary degeneration with 3-repeat tau protein in Down syndrome. *J Neuropathol Exp Neurol* **70**, 36-50 (2011). https://doi.org/10.1097/NEN.0b013e318202bfa1

340 Perluigi, M. & Butterfield, D. A. Oxidative Stress and Down Syndrome: A Route toward Alzheimer-Like Dementia. *Curr Gerontol Geriatr Res* **2012**, 724904 (2012). https://doi.org/10.1155/2012/724904

341 Potter, H., Granic, A. & Caneus, J. Role of Trisomy 21 Mosaicism in Sporadic and Familial Alzheimer's Disease. *Curr Alzheimer Res* **13**, 7-17 (2016). https://doi.org/10.2174/1567205013011512071006l6

342 Wiseman, F. K. *et al*. Trisomy of human chromosome 21 enhances amyloid-beta deposition independently of an extra copy of APP. *Brain* **141**, 2457-2474 (2018). https://doi.org/10.1093/brain/awy159

343 Cardenas, A. M., Ardiles, A. O., Barraza, N., Baez-Matus, X. & Caviedes, P. Role of tau protein in neuronal damage in Alzheimer's disease and Down syndrome. *Arch Med Res* **43**, 645-654 (2012). https://doi.org/10.1016/j.arcmed.2012.10.012

344 Kimura, R. *et al*. The DYRK1A gene, encoded in chromosome 21 Down syndrome critical region, bridges between beta-amyloid production and tau phosphorylation in Alzheimer disease. *Hum Mol Genet* **16**, 15-23 (2007). https://doi.org/10.1093/hmg/ddl437

345 Lloret, A. *et al*. Amyloid-beta toxicity and tau hyperphosphorylation are linked via RCAN1 in Alzheimer's disease. *J Alzheimers Dis* **27**, 701-709 (2011). https://doi.org/10.3233/JAD-2011-110890

346 Benzi, G. & Moretti, A. Are reactive oxygen species involved in Alzheimer's disease? *Neurobiol Aging* **16**, 661-674 (1995). https://doi.org/10.1016/0197-4580(95)00066-n

347 Gulesserian, T., Engidawork, E., Fountoulakis, M. & Lubec, G. Antioxidant proteins in fetal brain: superoxide dismutase-1 (SOD-1) protein is not overexpressed in fetal Down syndrome. *J Neural Transm Suppl*, 71-84 (2001). https://doi.org/10.1007/978-3-7091-6262-0_6

348 Cheon, M. S., Dierssen, M., Kim, S. H. & Lubec, G. Protein expression of BACE1, BACE2 and APP in Down syndrome brains. *Amino Acids* **35**, 339-343 (2008). https://doi.org/10.1007/s00726-007-0618-9

349 Abdul-Hay, S. O., Sahara, T., McBride, M., Kang, D. & Leissring, M. A. Identification of BACE2 as an avid ss-amyloid-degrading protease. *Mol Neurodegener* **7**, 46 (2012). https://doi.org/10.1186/1750-1326-7-46

350 Sun, X., He, G. & Song, W. BACE2, as a novel APP theta-secretase, is not responsible for the pathogenesis of Alzheimer's disease in Down syndrome. *FASEB J* **20**, 1369-1376 (2006). https://doi.org/10.1096/fj.05-5632com

351 Yan, R., Munzner, J. B., Shuck, M. E. & Bienkowski, M. J. BACE2 functions as an alternative alpha-secretase in cells. *J Biol Chem* **276**, 34019-34027 (2001). https://doi.org/10.1074/jbc.M105583200

352 Cremona, O. *et al*. Essential role of phosphoinositide metabolism in synaptic vesicle recycling. *Cell* **99**, 179-188 (1999). https://doi.org/10.1016/s0092-8674(00)81649-9

353 Martin, S. B. *et al*. Synaptophysin and synaptojanin-1 in Down syndrome are differentially affected by Alzheimer's disease. *J Alzheimers Dis* **42**, 767-775 (2014). https://doi.org/10.3233/JAD-140795

354 Kligman, D. & Marshak, D. R. Purification and characterization of a neurite extension factor from bovine brain. *Proc Natl Acad Sci U S A* **82**, 7136-7139 (1985). https://doi.org/10.1073/pnas.82.20.7136

355 Esposito, G. *et al*. Genomic and functional profiling of human Down syndrome neural progenitors implicates S100B and aquaporin 4 in cell injury. *Hum Mol Genet* **17**, 440-457 (2008). https://doi.org/10.1093/hmg/ddm322

356 Sharma, A. *et al*. Common genetic signatures of Alzheimer's disease in Down Syndrome. *F1000Res* **9**, 1299 (2020). https://doi.org/10.12688/f1000research.27096.2

357 Marshak, D. R., Pesce, S. A., Stanley, L. C. & Griffin, W. S. Increased S100 beta neurotrophic activity in Alzheimer's disease temporal lobe. *Neurobiol Aging* **13**, 1-7 (1992). https://doi.org/10.1016/0197-4580(92)90002-f

358 Araya, P. *et al*. Trisomy 21 dysregulates T cell lineages toward an autoimmunity-prone state associated with interferon hyperactivity. *Proc Natl Acad Sci U S A* **116**, 24231-24241 (2019). https://doi.org/10.1073/pnas.1908129116

359 Sullivan, K. D. *et al*. Trisomy 21 consistently activates the interferon response. *Elife* **5** (2016). https://doi.org/10.7554/eLife.16220

360 Wiseman, F. K. *et al*. A genetic cause of Alzheimer disease: mechanistic insights from Down syndrome. *Nat Rev Neurosci* **16**, 564-574 (2015). https://doi.org/10.1038/nrn3983

361 Wilcock, D. M. Neuroinflammation in the aging down syndrome brain; lessons from Alzheimer's disease. *Curr Gerontol Geriatr Res* **2012**, 170276 (2012). https://doi.org/10.1155/2012/170276

362 Wilcock, D. M. *et al*. Down syndrome individuals with Alzheimer's disease have a distinct neuroinflammatory phenotype compared to sporadic Alzheimer's disease. *Neurobiol Aging* **36**, 2468-2474 (2015). https://doi.org/10.1016/j.neurobiolaging.2015.05.016

363 Flores-Aguilar, L. *et al*. Evolution of neuroinflammation across the lifespan of individuals with Down syndrome. *Brain* **143**, 3653-3671 (2020). https://doi.org/10.1093/brain/awaa326

364 Xue, Q. S. & Streit, W. J. Microglial pathology in Down syndrome. *Acta Neuropathol* **122**, 455-466 (2011). https://doi.org/10.1007/s00401-011-0864-5
365 Adaikkan, C. *et al*. Gamma Entrainment Binds Higher-Order Brain Regions and Offers Neuroprotection. *Neuron* **102**, 929-943 e928 (2019). https://doi.org/10.1016/j.neuron.2019.04.011
366 Malcolm, J. C. *et al*. Neuropathological changes and cognitive deficits in rats transgenic for human mutant tau recapitulate human tauopathy. *Neurobiol Dis* **127**, 323-338 (2019). https://doi.org/10.1016/j.nbd.2019.03.018
367 Filippone, A. & Pratico, D. Endosome Dysregulation in Down Syndrome: A Potential Contributor to Alzheimer Disease Pathology. *Ann Neurol* **90**, 4-14 (2021). https://doi.org/10.1002/ana.26042
368 Wandinger-Ness, A. & Zerial, M. Rab proteins and the compartmentalization of the endosomal system. *Cold Spring Harb Perspect Biol* **6**, a022616 (2014). https://doi.org/10.1101/cshperspect.a022616
369 Huotari, J. & Helenius, A. Endosome maturation. *Embo j* **30**, 3481-3500 (2011). https://doi.org/10.1038/emboj.2011.286
370 Poteryaev, D., Fares, H., Bowerman, B. & Spang, A. Caenorhabditis elegans SAND-1 is essential for RAB-7 function in endosomal traffic. *Embo j* **26**, 301-312 (2007). https://doi.org/10.1038/sj.emboj.7601498
371 Rink, J., Ghigo, E., Kalaidzidis, Y. & Zerial, M. Rab conversion as a mechanism of progression from early to late endosomes. *Cell* **122**, 735-749 (2005). https://doi.org/10.1016/j.cell.2005.06.043
372 Ginsberg, S. D. *et al*. Microarray analysis of hippocampal CA1 neurons implicates early endosomal dysfunction during Alzheimer's disease progression. *Biol Psychiatry* **68**, 885-893 (2010). https://doi.org/10.1016/j.biopsych.2010.05.030
373 Vassar, R. *et al*. Beta-secretase cleavage of Alzheimer's amyloid precursor protein by the transmembrane aspartic protease BACE. *Science* **286**, 735-741 (1999). https://doi.org/10.1126/science.286.5440.735
374 Chen, X. Q., Zuo, X., Becker, A. & Mobley, W. C. Hyperactivation of RAB5 disrupts the endosomal Rab cascade leading to endolysosomal dysregulation in Down syndrome: A necessary role for increased APP gene dose. *Alzheimers Dement* **21**, e70046 (2025). https://doi.org/10.1002/alz.70046
375 Nixon, R. A. Amyloid precursor protein and endosomal-lysosomal dysfunction in Alzheimer's disease: inseparable partners in a multifactorial disease. *FASEB J* **31**, 2729-2743 (2017). https://doi.org/10.1096/fj.201700359
376 Jiang, Y. *et al*. Lysosomal Dysfunction in Down Syndrome Is APP-Dependent and Mediated by APP-betaCTF (C99). *J Neurosci* **39**, 5255-5268 (2019). https://doi.org/10.1523/JNEUROSCI.0578-19.2019
377 Lee, S., Sato, Y. & Nixon, R. A. Lysosomal proteolysis inhibition selectively disrupts axonal transport of degradative organelles and causes an Alzheimer's-like axonal dystrophy. *J Neurosci* **31**, 7817-7830 (2011). https://doi.org/10.1523/jneurosci.6412-10.2011
378 Perera, R. M. & Zoncu, R. The Lysosome as a Regulatory Hub. *Annu Rev Cell Dev Biol* **32**, 223-253 (2016). https://doi.org/10.1146/annurev-cellbio-111315-125125

379 Kedia, S. & Simons, M. Oligodendrocytes in Alzheimer's disease pathophysiology. *Nat Neurosci* **28**, 446-456 (2025). https://doi.org/10.1038/s41593-025-01873-x

380 Olmos-Serrano, J. L. *et al*. Down Syndrome Developmental Brain Transcriptome Reveals Defective Oligodendrocyte Differentiation and Myelination. *Neuron* **89**, 1208-1222 (2016). https://doi.org/10.1016/j.neuron.2016.01.042

381 Ikeda, S. *et al*. Variability of beta-amyloid protein deposited lesions in Down's syndrome brains. *Tohoku J Exp Med* **174**, 189-198 (1994). https://doi.org/10.1620/tjem.174.189

382 Tokuda, T., Tanaka, K., Kametani, F., Ikeda, S. & Yanagisawa, N. Secretory form of beta-amyloid precursor protein is much abundantly contained in the cerebral white matter in human brain. *Neurosci Lett* **175**, 33-36 (1994). https://doi.org/10.1016/0304-3940(94)91071-5

383 Rosas, H. D. *et al*. Alzheimer-related altered white matter microstructural integrity in Down syndrome: A model for sporadic AD? *Alzheimers Dement (Amst)* **12**, e12040 (2020). https://doi.org/10.1002/dad2.12040

384 Cavedo, E. *et al*. Disrupted white matter structural networks in healthy older adult APOE epsilon4 carriers - An international multicenter DTI study. *Neuroscience* **357**, 119-133 (2017). https://doi.org/10.1016/j.neuroscience.2017.05.048

385 Powell, D. *et al*. Frontal white matter integrity in adults with Down syndrome with and without dementia. *Neurobiol Aging* **35**, 1562-1569 (2014). https://doi.org/10.1016/j.neurobiolaging.2014.01.137

386 Hartley, D. *et al*. Down syndrome and Alzheimer's disease: Common pathways, common goals. *Alzheimers Dement* **11**, 700-709 (2015). https://doi.org/10.1016/j.jalz.2014.10.007

387 Hyman, B. T., West, H. L., Rebeck, G. W., Lai, F. & Mann, D. M. Neuropathological changes in Down's syndrome hippocampal formation. Effect of age and apolipoprotein E genotype. *Arch Neurol* **52**, 373-378 (1995). https://doi.org/10.1001/archneur.1995.00540280059019

388 Chartier-Harlin, M. C. *et al*. Early-onset Alzheimer's disease caused by mutations at codon 717 of the beta-amyloid precursor protein gene. *Nature* **353**, 844-846 (1991). https://doi.org/10.1038/353844a0

389 Szabo, M. P., Mishra, S., Knupp, A. & Young, J. E. The role of Alzheimer's disease risk genes in endolysosomal pathways. *Neurobiol Dis* **162**, 105576 (2022). https://doi.org/10.1016/j.nbd.2021.105576

390 Aldecoa, I. *et al*. Down Syndrome Biobank Consortium: A perspective. *Alzheimers Dement* (2024). https://doi.org/10.1002/alz.13692

391 Rafii, M. S. *et al*. Down syndrome and Alzheimer's disease: insights into biomarkers, clinical symptoms, and pathology. *Lancet Neurol* **24**, 753-762 (2025). https://doi.org/10.1016/S1474-4422(25)00237-6

392 Rachubinski, A. L. *et al*. JAK inhibition decreases the autoimmune burden in Down syndrome. *Elife* **13** (2024). https://doi.org/10.7554/eLife.99323

393 DeTure, M. A. & Dickson, D. W. The neuropathological diagnosis of Alzheimer's disease. *Mol Neurodegener* **14**, 32 (2019). https://doi.org/10.1186/s13024-019-0333-5

394 McGeer, P. L., Klegeris, A., Walker, D. G., Yasuhara, O. & McGeer, E. G. Pathological proteins in senile plaques. *Tohoku J Exp Med* **174**, 269-277 (1994). https://doi.org/10.1620/tjem.174.269
395 Drummond, E. & Wisniewski, T. in *Alzheimer's Disease* (ed T. Wisniewski) (2019).
396 Cummings, J. Lessons Learned from Alzheimer Disease: Clinical Trials with Negative Outcomes. *Clin Transl Sci* **11**, 147-152 (2018). https://doi.org/10.1111/cts.12491
397 Wisniewski, T. & Drummond, E. Developing therapeutic vaccines against Alzheimer's disease. *Expert Rev Vaccines* **15**, 401-415 (2016). https://doi.org/10.1586/14760584.2016.1121815
398 Namba, Y., Tomonaga, M., Kawasaki, H., Otomo, E. & Ikeda, K. Apolipoprotein E immunoreactivity in cerebral amyloid deposits and neurofibrillary tangles in Alzheimer's disease and kuru plaque amyloid in Creutzfeldt-Jakob disease. *Brain Res* **541**, 163-166 (1991). https://doi.org/10.1016/0006-8993(91)91092-f
399 Coon, K. D. *et al*. A high-density whole-genome association study reveals that APOE is the major susceptibility gene for sporadic late-onset Alzheimer's disease. *J Clin Psychiatry* **68**, 613-618 (2007). https://doi.org/10.4088/jcp.v68n0419
400 Lambert, J. C. *et al*. Genome-wide association study identifies variants at CLU and CR1 associated with Alzheimer's disease. *Nat Genet* **41**, 1094-1099 (2009). https://doi.org/10.1038/ng.439
401 Bellenguez, C. *et al*. New insights into the genetic etiology of Alzheimer's disease and related dementias. *Nat Genet* **54**, 412-436 (2022). https://doi.org/10.1038/s41588-022-01024-z
402 Seshadri, S. *et al*. Genome-wide analysis of genetic loci associated with Alzheimer disease. *JAMA* **303**, 1832-1840 (2010). https://doi.org/10.1001/jama.2010.574
403 Allen, M. *et al*. Conserved brain myelination networks are altered in Alzheimer's and other neurodegenerative diseases. *Alzheimers Dement* **14**, 352-366 (2018). https://doi.org/10.1016/j.jalz.2017.09.012
404 Mostafavi, S. *et al*. A molecular network of the aging human brain provides insights into the pathology and cognitive decline of Alzheimer's disease. *Nat Neurosci* **21**, 811-819 (2018). https://doi.org/10.1038/s41593-018-0154-9
405 Morabito, S., Miyoshi, E., Michael, N. & Swarup, V. Integrative genomics approach identifies conserved transcriptomic networks in Alzheimer's disease. *Hum Mol Genet* **29**, 2899-2919 (2020). https://doi.org/10.1093/hmg/ddaa182
406 Seyfried, N. T. *et al*. A Multi-network Approach Identifies Protein-Specific Co-expression in Asymptomatic and Symptomatic Alzheimer's Disease. *Cell Syst* **4**, 60-72 e64 (2017). https://doi.org/10.1016/j.cels.2016.11.006
407 Andreev, V. P. *et al*. Label-free quantitative LC-MS proteomics of Alzheimer's disease and normally aged human brains. *J Proteome Res* **11**, 3053-3067 (2012). https://doi.org/10.1021/pr3001546
408 Dai, J. *et al*. Effects of APOE Genotype on Brain Proteomic Network and Cell Type Changes in Alzheimer's Disease. *Front Mol Neurosci* **11**, 454 (2018). https://doi.org/10.3389/fnmol.2018.00454

409 Hales, C. M. *et al.* Changes in the detergent-insoluble brain proteome linked to amyloid and tau in Alzheimer's Disease progression. *Proteomics* **16**, 3042-3053 (2016). https://doi.org/10.1002/pmic.201600057

410 Ho Kim, J. *et al.* Proteome-wide characterization of signalling interactions in the hippocampal CA4/DG subfield of patients with Alzheimer's disease. *Sci Rep* **5**, 11138 (2015). https://doi.org/10.1038/srep11138

411 Hondius, D. C. *et al.* Profiling the human hippocampal proteome at all pathologic stages of Alzheimer's disease. *Alzheimers Dement* **12**, 654-668 (2016). https://doi.org/10.1016/j.jalz.2015.11.002

412 Johnson, E. C. B. *et al.* Deep proteomic network analysis of Alzheimer's disease brain reveals alterations in RNA binding proteins and RNA splicing associated with disease. *Mol Neurodegener* **13**, 52 (2018). https://doi.org/10.1186/s13024-018-0282-4

413 Zhang, Q. *et al.* Integrated proteomics and network analysis identifies protein hubs and network alterations in Alzheimer's disease. *Acta Neuropathol Commun* **6**, 19 (2018). https://doi.org/10.1186/s40478-018-0524-2

414 Tijms, B. M. *et al.* Cerebrospinal fluid proteomics in patients with Alzheimer's disease reveals five molecular subtypes with distinct genetic risk profiles. *Nat Aging* **4**, 33-47 (2024). https://doi.org/10.1038/s43587-023-00550-7

415 de Geus, M. B., Nairn, A. C., Arnold, S. E. & Carlyle, B. C. A compilation of reported alterations in the cerebrospinal fluid proteome in Alzheimer's disease. *Brain Commun* **7**, fcaf202 (2025). https://doi.org/10.1093/braincomms/fcaf202

416 Wik, L. *et al.* Proximity Extension Assay in Combination with Next-Generation Sequencing for High-throughput Proteome-wide Analysis. *Mol Cell Proteomics* **20**, 100168 (2021). https://doi.org/10.1016/j.mcpro.2021.100168

417 Gold, L. *et al.* Aptamer-based multiplexed proteomic technology for biomarker discovery. *PLoS One* **5**, e15004 (2010). https://doi.org/10.1371/journal.pone.0015004

418 Balcomb, K. *et al.* SMOC1 colocalizes with Alzheimer's disease neuropathology and delays Abeta aggregation. *Acta Neuropathol* **148**, 72 (2024). https://doi.org/10.1007/s00401-024-02819-6

419 Connolly, K. *et al.* Potential role of chitinase-3-like protein 1 (CHI3L1/YKL-40) in neurodegeneration and Alzheimer's disease. *Alzheimers Dement* **19**, 9-24 (2023). https://doi.org/10.1002/alz.12612

420 Drummond, E., Nayak, S., Pires, G., Ueberheide, B. & Wisniewski, T. Isolation of Amyloid Plaques and Neurofibrillary Tangles from Archived Alzheimer's Disease Tissue Using Laser-Capture Microdissection for Downstream Proteomics. *Methods Mol Biol* **1723**, 319-334 (2018). https://doi.org/10.1007/978-1-4939-7558-7_18

421 Drummond, E. S., Nayak, S., Ueberheide, B. & Wisniewski, T. Proteomic analysis of neurons microdissected from formalin-fixed, paraffin-embedded Alzheimer's disease brain tissue. *Sci Rep* **5**, 15456 (2015). https://doi.org/10.1038/srep15456

422 Drummond, E. & Wisniewski, T. The use of localized proteomics to identify the drivers of Alzheimer's disease pathogenesis. *Neural Regen Res* **12**, 912-913 (2017). https://doi.org/10.4103/1673-5374.208570

423 Marta-Ariza, M. *et al*. Comparison of the amyloid plaque proteome in Down syndrome, early-onset Alzheimer's disease, and late-onset Alzheimer's disease. *Acta Neuropathol* **149**, 9 (2025). https://doi.org/10.1007/s00401-025-02844-z

424 Drummond, E. *et al*. Phosphorylated tau interactome in the human Alzheimer's disease brain. *Brain* **143**, 2803-2817 (2020). https://doi.org/10.1093/brain/awaa223

425 Ayyadevara, S. *et al*. Proteins that mediate protein aggregation and cytotoxicity distinguish Alzheimer's hippocampus from normal controls. *Aging Cell* **15**, 924-939 (2016). https://doi.org/10.1111/acel.12501

426 Wang, H. *et al*. Somatostatin binds to the human amyloid beta peptide and favors the formation of distinct oligomers. *Elife* **6** (2017). https://doi.org/10.7554/eLife.28401

427 Meier, S. *et al*. Identification of Novel Tau Interactions with Endoplasmic Reticulum Proteins in Alzheimer's Disease Brain. *J Alzheimers Dis* **48**, 687-702 (2015). https://doi.org/10.3233/JAD-150298

428 Kavanagh, T. *et al*. The interactome of tau phosphorylated at T217 in Alzheimer's disease human brain tissue. *Acta Neuropathol* **149**, 44 (2025). https://doi.org/10.1007/s00401-025-02881-8

429 Thierry, M. *et al*. The influence of APOE(epsilon4) on the pTau interactome in sporadic Alzheimer's disease. *Acta Neuropathol* **147**, 91 (2024). https://doi.org/10.1007/s00401-024-02744-8

430 Hartley, D. *et al*. Down syndrome and Alzheimer's Disease: common pathways, common goals. *Alzheimer's and Dementia* **11**, 700-709 (2015).

431 Ferreira, D., Nordberg, A. & Westman, E. Biological subtypes of Alzheimer disease. *Neurology* **94**, 436-448 (2020). https://doi.org/10.1212/wnl.0000000000009058

432 Wisniewski, K. E., Wisniewski, H. M. & Wen, G. Y. Occurrence of neuropathological changes and dementia of Alzheimer's disease in Down's syndrome. *Ann Neurol* **17**, 278-282 (1985). https://doi.org/10.1002/ana.410170310

433 Zigman, W. B. *et al*. Alzheimer's Disease in Adults with Down Syndrome. *Int Rev Res Ment Retard* **36**, 103-145 (2008). https://doi.org/10.1016/S0074-7750(08)00004-9

434 Head, E., Mapstone, M. & Lott, I. T. in *The Neurobiology of Aging and Alzheimer Disease in Down Syndrome* (eds Elizabeth Head & Ira Lott) 1-10 (Academic Press, 2022).

435 Montoliu-Gaya, L. *et al*. Proteomic analysis of Down syndrome cerebrospinal fluid compared to late-onset and autosomal dominant Alzheimer s disease. *Nat Commun* **16**, 6003 (2025). https://doi.org/10.1038/s41467-025-61054-z

436 Levites, Y. *et al*. Integrative proteomics identifies a conserved Abeta amyloid responsome, novel plaque proteins, and pathology modifiers in Alzheimer's disease. *Cell Rep Med*, 101669 (2024). https://doi.org/10.1016/j.xcrm.2024.101669

437 Hashimoto, T. *et al.* Collagenous Alzheimer amyloid plaque component impacts on the compaction of amyloid-beta plaques. *Acta Neuropathol Commun* **8**, 212 (2020). https://doi.org/10.1186/s40478-020-01075-5

438 Tong, Y., Xu, Y., Scearce-Levie, K., Ptacek, L. J. & Fu, Y. H. COL25A1 triggers and promotes Alzheimer's disease-like pathology in vivo. *Neurogenetics* **11**, 41-52 (2010). https://doi.org/10.1007/s10048-009-0201-5

439 Kakuyama, H. *et al.* CLAC binds to aggregated Abeta and Abeta fragments, and attenuates fibril elongation. *Biochemistry* **44**, 15602-15609 (2005). https://doi.org/10.1021/bi051263e

440 Qiang, W., Yau, W. M., Lu, J. X., Collinge, J. & Tycko, R. Structural variation in amyloid-beta fibrils from Alzheimer's disease clinical subtypes. *Nature* **541**, 217-221 (2017). https://doi.org/10.1038/nature20814

441 Grau, S. *et al.* Implications of the serine protease HtrA1 in amyloid precursor protein processing. *Proc Natl Acad Sci U S A* **102**, 6021-6026 (2005). https://doi.org/10.1073/pnas.0501823102

442 Watanabe, N. *et al.* Glypican-1 as an Abeta binding HSPG in the human brain: its localization in DIG domains and possible roles in the pathogenesis of Alzheimer's disease. *FASEB J* **18**, 1013-1015 (2004). https://doi.org/10.1096/fj.03-1040fje

443 Levin, E. C. *et al.* Neuronal expression of vimentin in the Alzheimer's disease brain may be part of a generalized dendritic damage-response mechanism. *Brain Res* **1298**, 194-207 (2009). https://doi.org/10.1016/j.brainres.2009.08.072

444 Vagnoni, A. *et al.* Calsyntenin-1 mediates axonal transport of the amyloid precursor protein and regulates Abeta production. *Hum Mol Genet* **21**, 2845-2854 (2012). https://doi.org/10.1093/hmg/dds109

445 Bai, B. *et al.* Deep Multilayer Brain Proteomics Identifies Molecular Networks in Alzheimer's Disease Progression. *Neuron* **105**, 975-991 e977 (2020). https://doi.org/10.1016/j.neuron.2019.12.015

446 Lee, J. H. *et al.* Faulty autolysosome acidification in Alzheimer's disease mouse models induces autophagic build-up of Abeta in neurons, yielding senile plaques. *Nat Neurosci* **25**, 688-701 (2022). https://doi.org/10.1038/s41593-022-01084-8

447 Evans, H. T., Benetatos, J., van Roijen, M., Bodea, L. G. & Gotz, J. Decreased synthesis of ribosomal proteins in tauopathy revealed by non-canonical amino acid labelling. *EMBO J* **38**, e101174 (2019). https://doi.org/10.15252/embj.2018101174

448 Koren, S. A. *et al.* Tau drives translational selectivity by interacting with ribosomal proteins. *Acta Neuropathol* **137**, 571-583 (2019). https://doi.org/10.1007/s00401-019-01970-9

449 Itagaki, R. *et al.* Characteristics of PPT1 and TPP1 enzymes in neuronal ceroid lipofuscinosis (NCL) 1 and 2 by dried blood spots (DBS) and leukocytes and their application to newborn screening. *Mol Genet Metab* **124**, 64-70 (2018). https://doi.org/10.1016/j.ymgme.2018.03.007

450 Poet, M. *et al.* Lysosomal storage disease upon disruption of the neuronal chloride transport protein ClC-6. *Proc Natl Acad Sci U S A* **103**, 13854-13859 (2006). https://doi.org/10.1073/pnas.0606137103

451 Pressey, S. N. *et al.* Distinct neuropathologic phenotypes after disrupting the chloride transport proteins ClC-6 or ClC-7/Ostm1. *J Neuropathol Exp Neurol* **69**, 1228-1246 (2010). https://doi.org/10.1097/NEN.0b013e3181ffe742

452 Sassi, C. *et al.* Exploring dementia and neuronal ceroid lipofuscinosis genes in 100 FTD-like patients from 6 towns and rural villages on the Adriatic Sea cost of Apulia. *Sci Rep* **11**, 6353 (2021). https://doi.org/10.1038/s41598-021-85494-x

453 Hu, Y. B., Dammer, E. B., Ren, R. J. & Wang, G. The endosomal-lysosomal system: from acidification and cargo sorting to neurodegeneration. *Transl Neurodegener* **4**, 18 (2015). https://doi.org/10.1186/s40035-015-0041-1

454 He, H. *et al.* Mutations in CLCN6 as a Novel Genetic Cause of Neuronal Ceroid Lipofuscinosis in Patients and a Murine Model. *Ann Neurol* **96**, 608-624 (2024). https://doi.org/10.1002/ana.27002

455 Carcel-Trullols, J., Kovacs, A. D. & Pearce, D. A. Cell biology of the NCL proteins: What they do and don't do. *Biochim Biophys Acta* **1852**, 2242-2255 (2015). https://doi.org/10.1016/j.bbadis.2015.04.027

456 Sole-Domenech, S. *et al.* Lysosomal enzyme tripeptidyl peptidase 1 destabilizes fibrillar Abeta by multiple endoproteolytic cleavages within the beta-sheet domain. *Proc Natl Acad Sci U S A* **115**, 1493-1498 (2018). https://doi.org/10.1073/pnas.1719808115

457 Hassiotis, S. *et al.* Lysosomal LAMP1 immunoreactivity exists in both diffuse and neuritic amyloid plaques in the human hippocampus. *Eur J Neurosci* **47**, 1043-1053 (2018). https://doi.org/10.1111/ejn.13913

458 Cataldo, A. M., Hamilton, D. J. & Nixon, R. A. Lysosomal abnormalities in degenerating neurons link neuronal compromise to senile plaque development in Alzheimer disease. *Brain Res* **640**, 68-80 (1994). https://doi.org/10.1016/0006-8993(94)91858-9

459 Jiang, Y. *et al.* Alzheimer's-related endosome dysfunction in Down syndrome is Abeta-independent but requires APP and is reversed by BACE-1 inhibition. *Proc Natl Acad Sci U S A* **107**, 1630-1635 (2010). https://doi.org/10.1073/pnas.0908953107

460 Buser, D. P. & Spang, A. Protein sorting from endosomes to the TGN. *Front Cell Dev Biol* **11**, 1140605 (2023). https://doi.org/10.3389/fcell.2023.1140605

461 Gansa, W. *et al.* Dysregulation of the Immune System in a Natural History Study of 1299 Individuals with Down Syndrome. *J Clin Immunol* **44**, 130 (2024). https://doi.org/10.1007/s10875-024-01725-6

462 Hong, S. *et al.* Complement and microglia mediate early synapse loss in Alzheimer mouse models. *Science* **352**, 712-716 (2016). https://doi.org/10.1126/science.aad8373

463 Shi, Q. *et al.* Complement C3 deficiency protects against neurodegeneration in aged plaque-rich APP/PS1 mice. *Sci Transl Med* **9** (2017). https://doi.org/10.1126/scitranslmed.aaf6295

464 Batista, A. F., Khan, K. A., Papavergi, M. T. & Lemere, C. A. The Importance of Complement-Mediated Immune Signaling in Alzheimer's Disease Pathogenesis. *Int J Mol Sci* **25** (2024). https://doi.org/10.3390/ijms25020817

465 DeMattos, R. B. *et al.* Clusterin promotes amyloid plaque formation and is critical for neuritic toxicity in a mouse model of Alzheimer's disease. *Proc Natl*

Acad Sci U S A **99**, 10843-10848 (2002). https://doi.org/10.1073/pnas.162228299

466 Muramatsu, H. *et al*. Midkine as a factor to counteract the deposition of amyloid beta-peptide plaques: in vitro analysis and examination in knockout mice. *Int Arch Med* **4**, 1 (2011). https://doi.org/10.1186/1755-7682-4-1

467 Wang, Z. X., Wan, Q. & Xing, A. HLA in Alzheimer's Disease: Genetic Association and Possible Pathogenic Roles. *Neuromolecular Med* **22**, 464-473 (2020). https://doi.org/10.1007/s12017-020-08612-4

468 Silva, M. N. *et al*. Genetic markers involved in neuroinflammation in Down syndrome: a systematic review. *Dement Neuropsychol* **19**, e20240251 (2025). https://doi.org/10.1590/1980-5764-DN-2024-0251

469 Zhan, X. *et al*. Myelin basic protein associates with AbetaPP, Abeta1-42, and amyloid plaques in cortex of Alzheimer's disease brain. *J Alzheimers Dis* **44**, 1213-1229 (2015). https://doi.org/10.3233/JAD-142013

470 Depp, C. *et al*. Myelin dysfunction drives amyloid-beta deposition in models of Alzheimer's disease. *Nature* **618**, 349-357 (2023). https://doi.org/10.1038/s41586-023-06120-6

471 Franceschi, C. *et al*. Accelerated bio-cognitive aging in Down syndrome: State of the art and possible deceleration strategies. *Aging Cell* **18**, e12903 (2019). https://doi.org/10.1111/acel.12903

472 Morcillo-Nieto, A. O. *et al*. Characterization of white matter hyperintensities in Down syndrome. *Alzheimers Dement* **20**, 6527-6541 (2024). https://doi.org/10.1002/alz.14146

473 Rosas, H. D. *et al*. Association of plasma neurofilament light chain with microstructural white matter changes in Down syndrome. *Alzheimers Dement (Amst)* **16**, e70023 (2024). https://doi.org/10.1002/dad2.70023

474 Quiroz, Y. T. *et al*. Plasma neurofilament light chain in the presenilin 1 E280A autosomal dominant Alzheimer's disease kindred: a cross-sectional and longitudinal cohort study. *Lancet Neurol* **19**, 513-521 (2020). https://doi.org/10.1016/S1474-4422(20)30137-X

475 Kobayashi, K. *et al*. Cerebral cortical calbindin D28K and parvalbumin neurones in Down's syndrome. *Neurosci Lett* **113**, 17-22 (1990). https://doi.org/10.1016/0304-3940(90)90487-t

476 Sohal, V. S., Zhang, F., Yizhar, O. & Deisseroth, K. Parvalbumin neurons and gamma rhythms enhance cortical circuit performance. *Nature* **459**, 698-702 (2009). https://doi.org/10.1038/nature07991

477 Verret, L. *et al*. Inhibitory interneuron deficit links altered network activity and cognitive dysfunction in Alzheimer model. *Cell* **149**, 708-721 (2012). https://doi.org/10.1016/j.cell.2012.02.046

478 He, Q. *et al*. A feasibility trial of gamma sensory flicker for patients with prodromal Alzheimer's disease. *Alzheimers Dement (N Y)* **7**, e12178 (2021). https://doi.org/10.1002/trc2.12178

479 Martorell, A. J. *et al*. Multi-sensory Gamma Stimulation Ameliorates Alzheimer's-Associated Pathology and Improves Cognition. *Cell* **177**, 256-271 e222 (2019). https://doi.org/10.1016/j.cell.2019.02.014

480 Duits, F. H. *et al.* Matrix Metalloproteinases in Alzheimer's Disease and Concurrent Cerebral Microbleeds. *J Alzheimers Dis* **48**, 711-720 (2015). https://doi.org/10.3233/JAD-143186

481 Manousopoulou, A. *et al.* Systems proteomic analysis reveals that clusterin and tissue inhibitor of metalloproteinases 3 increase in leptomeningeal arteries affected by cerebral amyloid angiopathy. *Neuropathol Appl Neurobiol* **43**, 492-504 (2017). https://doi.org/10.1111/nan.12342

482 Bateman, R. J. *et al.* Safety and efficacy of long-term gantenerumab treatment in dominantly inherited Alzheimer's disease: an open-label extension of the phase 2/3 multicentre, randomised, double-blind, placebo-controlled platform DIAN-TU trial. *Lancet Neurol* **24**, 316-330 (2025). https://doi.org/10.1016/S1474-4422(25)00024-9

483 Calabrese, G., Molzahn, C. & Mayor, T. Protein interaction networks in neurodegenerative diseases: From physiological function to aggregation. *J Biol Chem* **298**, 102062 (2022). https://doi.org/10.1016/j.jbc.2022.102062

484 Ittner, L. M. *et al.* Dendritic function of tau mediates amyloid-beta toxicity in Alzheimer's disease mouse models. *Cell* **142**, 387-397 (2010). https://doi.org/10.1016/j.cell.2010.06.036

485 David, D. C. *et al.* Proteasomal degradation of tau protein. *J Neurochem* **83**, 176-185 (2002). https://doi.org/10.1046/j.1471-4159.2002.01137.x

486 Myeku, N. *et al.* Tau-driven 26S proteasome impairment and cognitive dysfunction can be prevented early in disease by activating cAMP-PKA signaling. *Nat Med* **22**, 46-53 (2016). https://doi.org/10.1038/nm.4011

487 Piatnitskaia, S. *et al.* USP10 is a critical factor for Tau-positive stress granule formation in neuronal cells. *Sci Rep* **9**, 10591 (2019). https://doi.org/10.1038/s41598-019-47033-7

488 Woo, J. A. *et al.* beta-arrestin1 promotes tauopathy by transducing GPCR signaling, disrupting microtubules and autophagy. *Life Sci Alliance* **5** (2022). https://doi.org/10.26508/lsa.202101183

489 Thierry, M. *et al.* Human subiculo-fornico-mamillary system in Alzheimer's disease: Tau seeding by the pillar of the fornix. *Acta Neuropathol* **139**, 443-461 (2020). https://doi.org/10.1007/s00401-019-02108-7

490 Wu, J. W. *et al.* Neuronal activity enhances tau propagation and tau pathology in vivo. *Nat Neurosci* **19**, 1085-1092 (2016). https://doi.org/10.1038/nn.4328